STRATIGRAPHY, LITHOFACIES AND ENVIRONMENTAL ANALYSIS OF THE BAHI FORMATION (LATE CRETACEOUS) IN THE NORTHWESTERN SIRTE BASIN, LIBYA.

by

Abdussalam Mohamed Abdussalam Sghair, B. Sc.

A thesis submitted for the degree of Master of Science

at

University of Glasgow

Department of Geology & Applied Geology

University of Glasgow.

March 1990

ProQuest LLC.
789 East Eisenhower Parkway
P.O. Box 1346
Ann Arbor, MI 48106 – 1346

I wish to express my sincere thanks and gratitude to my late father "Mr. Mohamed Sghair" whom I lost during my sojourn stay in the city of Glasgow, Scotland. His understanding and compassion in times of crisis and difficulty, which gave me confidence that I would one day finish my project. His hope was that I will finish this study and I am very glad to fullfill his ambition.

CONTENTS

LIST OF FIGURES

LIST OF PLATES

LIST OF TABLES

ACKNOWLEDGEMENTS

I particularly wish to thank Dr J. K. Ingham, who supervised this study, for his help, interest, enthusiasm and constant advice, especially in connection with the general improvement of this thesis.

I am specially grateful to Professor B. E. Leake for his helpful support in supervising the part of the study dealing with geochemistry and for clarifying many doubts and problems. I should also like to thank him for providing the facilities that enabling the work to be done.

I am grateful to Professor B. J. Bluck for his help and for many fruitful discussions.

I gratefully acknowledge the Petroleum Research Centre, Tripoli, Libya for financial support allowing completion of this study. The National Oil Corporation and the Oasis Oil Company, Tripoli, Libya, for permission to take rock samples from well and borehole cores for analysis.

I would like to thank Dr C. Farrow for his expert help and advice with XRF technicalities and for clarifying problems with geochemical statistics and general computing, Mr R. Morrison, the Departmental Superintendent, for his constant support and helpful advice, Mr D. Maclean for his skills and instruction in photomicrography and Mr G. Bruce and Mr J. Gallagher for their help with geochemical and XRD analyses. I am thankful to Mr P. Ainsworth who offered much help in connection with the use of SEM equipment and Mr K. Roberts who produced excellent finished thin sections from my rock slices.

I am grateful particularly to my friend Lifta Kadem for fruitful discussions, but this work has involved many people in one way or another, and I wish to thank them all even through I do not cite them specifically.

Finally, I am very grateful to my wife, Amna for her continuous encouragement and to my daughters, Jadis, Ariss and Salsabeel for their unending patience, even during the frustrating moments of this project of which there were many.

ABSTRACT

The Bahi Formation forms the diachronous lower part of the Upper Cretaceous succession where it is known only from subsurface data in the western part of the Sirte Basin in north central Libya. It consist of interbedded sandstone, siltstone, conglomerate and shale. Core logs indicate that the formation overlies Palaeozoic sediments and occasionally Precambrian basement rocks with profound unconformity and is overlain by marine Upper Cretaceous sediments. It forms the basal unit of a late Cretaceous transgressive sequence which eventually affected virtually all of the country: the marine invasion was from the north or north-west. The thickness of the formation is variable and largely controlled by contemporaneous faulting. The lower part of the formation consists of fine red, silty sandstone with coarse unit at its base. The upper part is mostly with a coarse to very coarse-grained, cross-bedded sandstone and contains glauconite only in its uppermost part.

Petrographically, the formation is classified as a subarkosic quartz arenite in composition with carbonate (dolomite and calcite), anhydrite and clay mineral (illite, kaolinite and chlorite) cements. Zircon, tourmaline and rutile are the most abundant heavy minerals throughout the formation. Geochemical studies of the major and trace elements indicate that K_2O, Al_2O_3 and most of the trace elements are associated with feldspar and/or clay minerals. The relationship between the various trace elements shows that the Bahi sediment was derived largely from pre-existing sedimentary sources. The framework mineralogy and the discriminant function analyses of the major elements suggests that the Bahi Formation was derived from a craton interior and/or a passive continental margin. The mineralogy of the uppermost part indicates shallow marine deposition, probably in an oscillating shoreline situation whereas the sedimentological analyses strongly suggest that the bulk of the formation accumulated in fluvial systems which became established prior to the marine incursion.

DECLARATION

The material presented herein is the result of independent research by the author undertaken between March 1988 and March 1990 at the Department of Geology & Applied Geology, University of Glasgow. Any published or unpublished results of other works have been given full acknowldgement in the text.

Abdussalam M. Sghair

CHAPTER 1

INTRODUCTION

1.1 Definition

The Bahi Formation is defined as a heterogeneous clastic rock succession known only from boreholes. The term Bahi Sandstone has been used widely and rather loosely in the central and western part of the Sirte Basin. Sandstones are recognised as "Bahi' especially when they rest on Palaeozoic or Precambrian strata. They commonly underlie distinctly marine Upper Cretaceous beds ranging in age from Cenomanian to Maastrichtian.

The Bahi Formation is barren of mega-fossils and consequently its age is uncertain spores have not been researched for. Nevertheless, the formation occurs at the base of marine Upper Cretaceous formations. Cenomanian marine sediments have been recorded from the area of the A-32 boreholes. Maastrichtian strata occur above the Bahi in concession 11 and 16. The Bahi Formation lies unconfomably upon either igneous and metamorphic Precambrian rocks, the Cambro-Ordovician Hofra Formation or the Devonian Tadrart Formation.

Over much of the area, the base of the Bahi is taken at the contact of the mainly conglomeratic sandstone with the quartizitic sandstone of the Hofra Formation. Over part of the region the Bahi Formation becomes dolomitic or calcareous towards the top where it also becomes glauconitic. It grades upward through sandy carbonate into the pure carbonates of the overlying units. The top of the formation is placed at the top of the dominantly clastic sequence.

1.2 Geographical and tectonic location

Libya lies along the northern coast of Africa between Egypt and the Sudan to the east, Tunisia and Algeria to the west, with Niger and Chad situated directly to the south. It covers about 1,800,000 km^2 and extends about 1,925 kms from east to west and 1,450 kms from north to south. Except for the northernmost parts, the country is substantially Saharan in aspect. The Sirte Basin is located on the Libyan part of the north Africa. Its orientation is

generally NW-SE and is defined more or less by the Hun graben to the west, whilst its eastern boundary is limited by the Antalat Fault which separates the Sirte Basin from the Cyrenaican Platform and the Western Desert Basin. To the north is the Mediterranean Sea (Sirte Gulf) and to the south is the beginning of the major Tibesti-Sirte Uplift. The surface area of the basin is about 300,000 km^2 (Figure 1.1)

The area studied is located in the western part of the Sirte Basin, between 29° 30' to 30° 30' N and 16° 45' to 28° 30'E, and covers the area of concessions 32, 17, 16, 11 and NC29, where the Bahi Field (A-32 area) and the type section of the Bahi Formation (borehole A3-32) are located. Exploration activities in this area have stimulated interest in the detailed stratigraphical record of the Bahi Formation and its structural context. Such detailed information as is available derives from cores and well-log records.

1.3 Previous work

The Bahi Formation has been given various names. In the northeastern part of the Sirte Basin, it has been known as the Maragh Formation (Fig. 1.2) and as the Basal Upper Cretaceous Sandstone in the eastern part (Al Hamiemat Trough).

There is very limited previous published or unpublished work concerned with the Bahi Formation and what is available is mostly brief and cursory. Baird (1964, unpublished report, Oasis Oil Co.) had limited subsurface data from the boreholes in the western part of the Sirte Basin but he noted that the Bahi Sandstone consisted essentially of two units, the lower one composed of argillaceous sandstone and the upper being subdivisible into two tongues of coarse to very coarse sandstone with crossed bedding and coarse-grained sandstone respectively, separated by a thin sequence of argillaceous red sandstone. He also recognised glauconite in the uppermost part of the formation.

Barr & Weegar (1972) published a general stratigraphical summary of the Bahi Formation. They pointed out that it consists largely of interbedded sandstone, siltstone, conglomerate and shale, the sandstone being medium to coarse-grained with subangular to angular quartz grains. They also commented on the occurence of glauconite in the uppermost

part and its apparent absence lower down. They reported that the siltstones and shales are mainly red and sometimes mottled and that the conglomerate contains rounded quartz pebbles with a sand or sand and shale matrix, often with red staining. They remarked on the regular presence of a 3-6m basal conglomerate.

1.4 Aims of the study

The aims of the research project are:

1. Detailed stratigraphical studies to document as far as possible the diachronous nature of the Bahi Formation with respect to the overlying marine formations of Cenomanian-Maastrichtian ages. Detailed lithological description of local successions and the nature of any lateral variation.
2. Palaeogeographical studies based on all available subsurface data such as well-log records, core samples, facies distribution and tectonic framework.
3. Petrographical and mineralogical investigations to identify the mineralogical composition of the formation and its lateral and vertical variation thus providing information about the provenance of the sediment.
4. Geochemical studies of the major and trace elements to indicate the character of the provenance and to throw light on the gross tectonic regimes involved.
5. Grain-size analysis to determine textural variations and to give a clearer picture of depositional environments and nature of the transporting agents of the sediment.

1.5 Methods

The top of the Bahi Formation lies mostly between 1500 and 2500m below sea level. To construct various maps (isopach, structure) and the stratigraphical cross-sections, subsurface data were collected from log records in ninty-five wells and boreholes.

The detailed investigations concentrate on the A2-32, A3-32, A4-32, D1-32, and F6-32 boreholes, where thick sequences have a good coverage in terms of core available for study. Samples were selected according to the following criteria:

1. Substantial vertical variation in lithology within the Bahi Formation in the same borehole.
2. The possibility of recording the detailed lateral variation patterns between the five boreholes.

Slabbed Bahi Formation cores (Table 1.1) from the five boreholes were examined for texture, colour, sedimentary structures, etc. Samples were selected from these cores for petrographical, geochemical and grain-size studies for which established standard techniques have been employed.

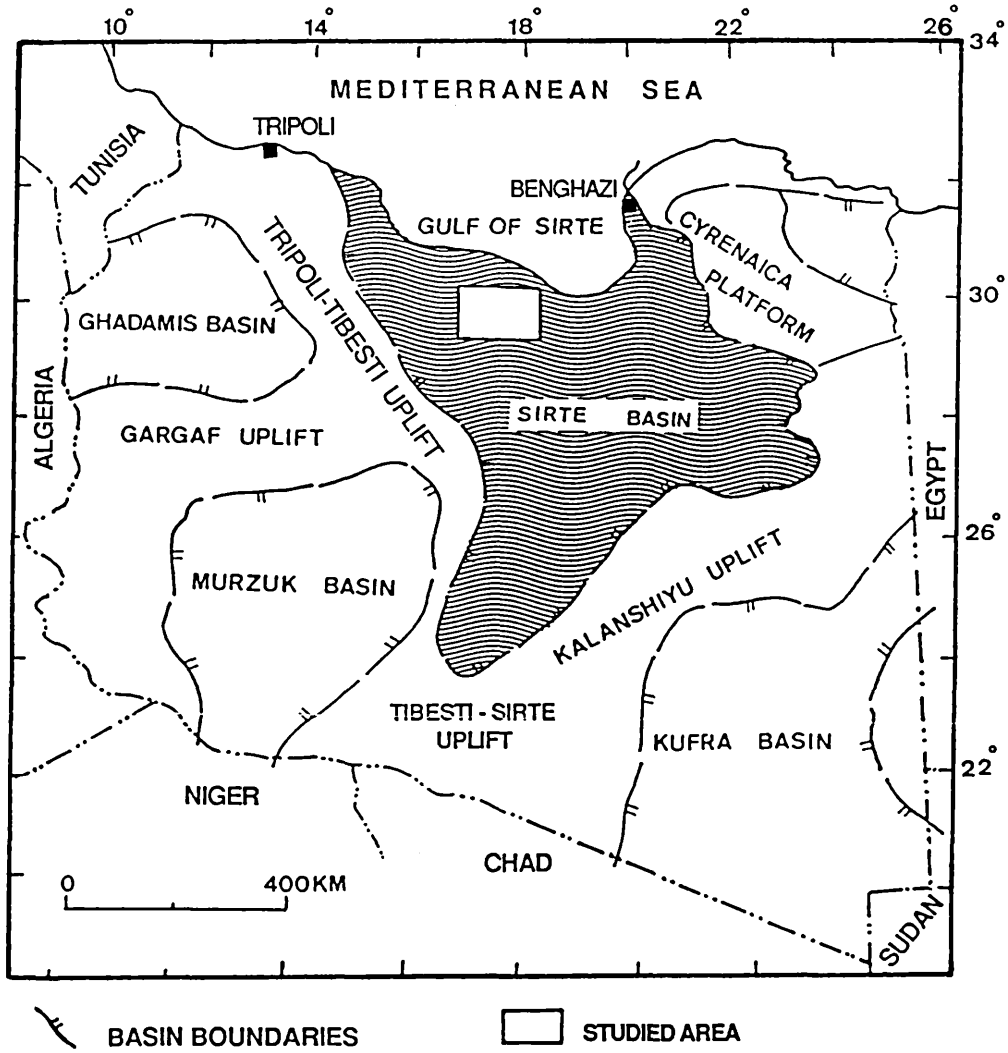

Fig. 1.1 Geographical location map of the area studied within the Sirte Basin, Libya.

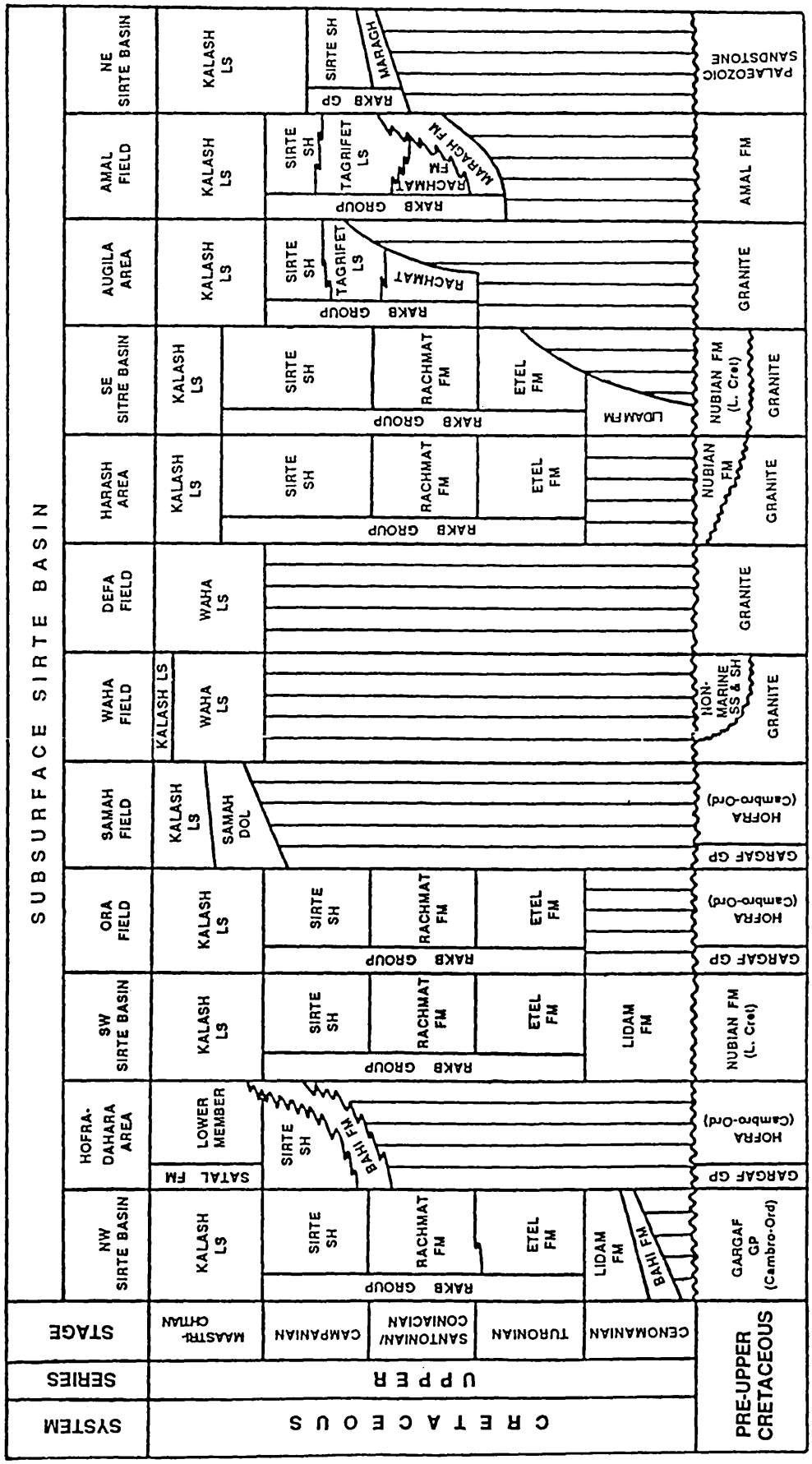

Fig. 1.2 Correlation chart of the Upper Cretaceous formations within the Sirte Basin, after Barr & Weegar, 1972.

Table 1.1 Core number, position and total thickness within the Bahi Formation in the studied boreholes.

Borehole	Core No.	Core interval (M)		Thickness (total) (M)
		Top	Bottom	
A2-32	5,6	1898.26	1929.20	30.94
A3-32	5	1043.40	1055.60	12.00
A4-32	2	1825.46	1831.53	51.24
	3	1833.65	1839.72	
	4	1841.23	1848.82	
	5,6,7	1850.33	1874.60	
	8	1880.06	1887.34	
D1-32	18	2198.56	2203.72	14.26
	19	2208.87	2217.97	
F6-32	2	1432.34	1449.93	17.59

CHAPTER 2

STRATIGRAPHY

2.1 Introduction

Libya is on the Mediterranean foreland of the African shield. Since Early Palaeozoic times it has been the site of deposition of extensive sheets of continental clastic sediments, and several transgressions and regressions by the sea with consequent accumulation of a wide variety of marine sedimentary rocks (Fig. 2.1). Several tectonic cycles have affected the area and shaped the geological setting of the country. Six sedimentary basins, namely the Ghadamis or Hamra, Murzuk, Kufra, Western Desert and Sirte were formed, separated by intervening uplifted arches (Conant & Goudarzi,1967). All the above-mentioned basins have been active since Early Palaeozoic times except the Sirte Basin and several thousands of metres of marine and continental sediments have accumulated in them. During Carboniferous times, Variscan tectonism in Europe relates to a general regression of the sea over most of Libya. The two southern basins (i.e. Kufra and Murzuk) were never covered by the sea again, so that late Palaeozoic sediments were deposited there under continental conditions. During the Triassic, only the northwestern and northeastern corners of Libya (Nefusah Uplift, Ghadamis Basin and nothern Cyrenaica) were covered by the sea. Terrigenous clastics, carbonates and evaporites were deposited unconformably over the Palaeozoic rocks. During the Jurassic, marine areas did not change very much in the north-west, whilst in northern Cyrenaica the sea extended farther to the south. Shallow water carbonates and clastics were deposited to the south and deeper marine sediments accumulated in the north. In Lower Cretaceous times, a regression took place in northwestern Libya, where only continental sediments are recorded whilst northern Cyrenaica was still covered by a shallow sea.

The beginning of the Upper Cretaceous (Cenomanian) was characterised by major tensional events, which created the Sirte Basin. Consequently, the sea spread southward over the northern half of the country. Only the major horsts in the Sirte Basin and the Cyrenaica Platform remained emergent. Throughout the Upper Cretaceous, the sea continued to

advance southwards: by the end of Maastrichtian time only a few scattered horst crests remained above the sea as isolated islands (Duronio & Colombi,1983)

2.2 Stratigraphical succession in the Sirte Basin

The stratigraphical sequence of the Sirte Basin is characterised by much reduced or completely absent Palaeozoic rocks. The Cambro-Ordovician is the only Palaeozoic sequence with a wide distribution in the Sirte Basin, except in some palaeo-high areas were it is absent as at the western edge of the Beda and Zelten platforms. The Silurian and Devonian is present in scattered areas in the western part of the basin, whereas the Carboniferous and Permian are completely unrepresented. The pre-Cretaceous Mesozoic (Triassic and Jurassic) is characterised by a thin succession of rocks (where present) located in the northeastern part of the basin where it is associated with a very thin Lower Cretaceous sequence. The Lower Cretaceous is however thicker and more widespread in the south-eastern part of the basin (Sarir Trough).

The thickness of the Upper Cretaceous marine sequence ranging from Cenomanian to Maastrichtian age, is largely dependent on structural position, and appears to be largely structurally controlled. The simple nature of the tectonics accompanying the initial development of the basin and the movements that followed, which further emphasised the topographic relief of the newly formed horsts against the structurally low intervening grabens, restricted the distribution of the stratigraphical units throughout the basin. The high areas received the coarse fractions of sediments that were being deposited there to form the shelves and platforms and continued to build outward, while the low areas, further deepened by renewed movement along basement faults, received only the fine and very fine silts and clays. Such distribution is clearly evident in the Sirte Basin in general and in the western part of the basin in particular.

Many previous studies have been made of the stratigraphical succession in the Sirte basin (Conent & Goudarzi,1967; Pomeyrol, 1968; Williams,1968; Conely,1971; Barr & Weegar, 1972; Clifford, Grund & Musrati, 1980; Hammuda, 1980; Van Houten,1980; Massa & Delort,

1984; Gumati & Kanes, 1985; Butt, 1986 and others). The stratigraphical details given below are adapted from Barr and Weegar, 1972 with additional information (Fig. 2.2):

2.2.1 Precambrian rocks

Precambrian basement rocks are present in the subsurface of the Sirte Basin, except in the Dorel Gussa area, where the Precambrian is exposed at the surface. Both igneous and metamorphic rocks are present.

2.2.2 Cambro-Ordovician rocks

The Precambrian basement rocks are overlain by Palaeozoic sequences most of them belonging to the Cambro-Ordovician Hofra Formation. These sediments are widely distributed in the basin. In certain areas, the Hofra Formation was greatly eroded during Lower Cretaceous times and at Zelten and Beda and in a few other places it is completely absent. Nevertheless, the formation has a widespread distribution throughout the western part of the basin, where it is equivalent to the Amal Formation in the eastern part of the basin. Thicknesses vary from place to place. Where the distribution is controlled by structural lows in the Sirte Basin, the maximum thickness reaches 1300m as in the area of the Dahra-Hofra Platform (A1-11 borehole). The formation comprises primarily a sequence of quartz sandstones with minor amounts of shale, siltstone, and conglomerate. The sandstones are normally white to grey in colour, firmly cemented with silica. Quartz overgrowths are common and quartz is the dominant detrital component, moderately sorted, and fine to coarse in texture. The grains are occasionally frosted, and subrounded. Accessory constituents are pyrite, biotite, micas, sericite, chlorite and rare feldspars. The shales and siltstones occur throughout in thin beds and laminae, and are grey to brown-grey, rarely red in colour, moderately to very micaceous, varying from blocky to fissile and sometimes soft, waxy and lustrous. Diagnostic fossils have not been recovered from the formation and the age is thus uncertain. However, in the D1-32 borehole, it underlies undoubted Lower Silurian graptolitic shales, and in the A1-11 borehole it rests on a phyllite supposedly metamophosed during the Cambrian (Barr & Weegar, 1972, 98). The Hofra

Formation is therefore tentatively assessed as Cambro-Ordovician in age.

2.2.3 Silurian System

Two Silurian formations are recognised, the Tanezzuft Shale and Acacus Sandstone. The Tanezzuft Shale passes gradually upward into the Acacus Sandstone (type area in the Wadi Tanezzuft, in southwestern Libya). The Silurian rocks are richly graptolitic. The Tanezzuft Shale rests directly on and is transgressive over Cambro-Ordovician rocks. It is overlain unconformably by the Devonian Tadrart Formation. The Tanezzuft Formation In the D1-32 borehole is made up of black graptolitic shales, which become more sandy toward the base and have a thickness of up to 175m. The assemblage of graptolites (species of *Diplograptus* & *Climacograptus*) together with mollusca, brachiopoda and trilobites all indicate a Llandovery age. The sandy basal beds have been dated as Early Llandovery, while the shales are known to range in age from Middle to Late Llandovery (Desio, 1959).

Massa & Delort (1984), have indicated that Silurian strata were undoubtedly widespread in northern Libya and that late or end Silurian epeirogenetic movements associated with the north Atlantic Caledonian orogeny was responsible for the present scattered distribution.

2.2.4 Devonian System

The Devonian strata overlie the Silurian unconformably and also have a scattered distribution. They have been divided into three formations in the type locality (Murzuk Basin). There is predominantly sandstone at the base (Aouinet Ouenine Formation) followed upward by shale and sandstone units (Ouan-Kasa and Tadrart Formations). The sedimentary cycles making up the Devonian total more than 1000m of strata (Bellini & Massa, 1980). In the type area (Jabal Tadrart, south-western Libya) the Tadrart Formation is considered to be of Early Devonian (Siegenian) age (Desio, 1959). In the northwestern part of the Sirte Basin, the Tadrart Formation is seen in the D1-32 borehole where it consists of a sequence of grey coarse-grained, unsorted, massive cross-bedded sandstone. It ranges in thickness up to 80m, rests on Lower Silurian and is unconformably overlain by the Upper Cretaceous Bahi Formation.

2.2.5 Cretaceous System

The Cretaceous rock succession of the Sirte Basin is divided into two parts. The Lower Cretaceous is represented by a non-marine clastic unit (Nubian Sandstone). The Upper Cretaceous consists largely of a sequence of sandstones, shales and carbonates.

1. Lower Cretaceous Series

The Lower Cretaceous Nubian Sandstone is found along the eastern side of the Sirte Basin where it unconformably overlies the Cambro-Ordovician or Precambrian basement rocks. Here it reaches a thickness of 1200m. It is completely absent in the western part of the basin. The Nubian Sandstone consists of a variety of interbedded non-marine lithofacies including sandstones, siltstones, shales, and conglomerates.

2. Upper Cretaceous Series

Upper Cretaceous sediments are widely distributed in the Sirte Basin, the various formations ranging in age from Cenomanian to Maastrichtian. They unconformably overlie the Lower Cretaceous, Palaeozoic and Precambrian rocks. The beginning of deposition took place during Cenomanian times in a major transgression. The sequence consists mainly of marine sediments (shales and limestones) with largely non-marine sandstone at the base. It is divided into the following lithostratigraphical units (Barr & Weegar, 1972), none of which is seen at surface outcrop.

A. Bahi Formation

At the beginning of the Cenomanian and continuing into the Maastrichtian, a transgressive sandy base is recognised which has been given various formational names in the Sirte Basin (Bahi, Maragh, Basal Sandstones, etc.). During this time span a major transgression took place in northern Libya. The Bahi Formation at the base of the succession is made up of interbedded sandstone, siltstone, conglomerate and shale. Sandstone is the most common lithology: it is usually medium to coarse in texture with subangular to angular quartz grains.

Glauconite is common in the uppermost part ,3 to 6m, thick, but seems to be absent in the lower part. The siltstone and shale are red or mottled. Usually there is a basal conglomerate (3 to 6m), thick consisting of rounded quartzitic pebbles with a sandy or shaley matrix. This formation is found in the northwestern part of the Sirte Basin and attains a maximum thickness of about 110m. In various places, the Bahi Formation is overlain by the Lidam Formation or other younger Upper Cretaceous formations (Argub, Rachmat, Sirte, Kalash, etc.), ranging in age from Cenomanian to Maastrichtian, and it is seen to unconformably overlie the Cambro-Ordovician Hofra Formation: in the D1-32 borehole, it rests unconformably on Devonian sediments. It can be concluded, then, that the Bahi Formation is a diachronous unit, considered to range in age from Cenomanian to Maastrichtian. The Bahi Formation appears to be palaeontologically barren and consequently its precise age from place to place is uncertain.

B. Lidam Formation

The Lidam Formation consists of a light brown to light grey sucrosic dolomite or packstone/ grainstone with abundant pellets. Sand grains are common in the lower part of the formation. Molluscan, algal and echinoid debris are sometimes common. Rare benthonic microfossils are also present. This indicates that the formation was deposited in a very shallow marine environment, in part lagoonal or intertidal. It is usually found in the main trough areas where it overlies the Bahi Formation and is in turn overlain by the Argub Formation. It may reach a maximum thickness of about 200m. In the type section (G1-57 borehole, in the western part of the basin), the presence of macrofossil fragments and microfossils, consisting mainly of ostracodes, miliolids and the large benthonic foraminifer, *Ovalveolina ovum* shows the Lidam Formation to be of Cenomanian age there. The formation may be slightly diachronous and have a slightly different age range elsewhere.

C. Argub Formation

In Turonian times, the Argub Formation was deposited in the central and western part of the Sirte Basin: It passes laterally into the Etel Formation toward the east. The Argub

Formation consists mainly of a hard, tan, finely crystalline and slightly glauconitic dolomite with subordinate interbeds of white to grey, argillaceous, glauconitic limestone and very rare, thin sandstone. The Argub Formation has an average thickness of 65m. No diagnostic fossils have been recovered. However, its stratigraphical position (D1-32 borehole) indicates that it is from the early part of the Upper Cretaceous and is probably at least in part of Turonian age.

D. Rachmat Formation

In Santonian-Coniacian times, the Rachmat Formation was deposited widely in the Sirte Basin. It is typically a shale sequence with minor limestone, sandstone and occasional dolomite interbeds. It is overlain by the Sirte Shale Formation. Depending on its position within the basin, the Rachmat Formation may conformably overlie the Argub Carbonate, Bahi Sandstone (as in the area of the Dahra-Hofra platform), or it may rest unconformably on the Hofra Formation or basement rocks. The shales are often grey, becoming sometimes green or brown, being frequently glauconitic and pyritic. Limestone is more frequent in the lower part of the formation: it is tan to brown in colour, microcrystalline and anhydritic indicating deposition in hypo conditions. The formation attains its maximum thickness (over 700m) in the major troughs. It is absent or very thin on regional palaeo-highs such as the Dahra-Hofra platform. It disappears through facies change over the palaeo-highs (platforms) where the Bahi Formation is present (there is a facies change relationship to the Bahi Formation as well as to the overlying Kalash Formation in such areas). In the type section (O2-59 borehole, in the central part of the Sirte Basin) the Rachmat Formation contains the common foraminifera *Globotruncana concavata*, *G. coronata* and *G. angusticarinata*, which indicate that here it is of Santonian to Coniacian age but this could well vary somewhat from place to place.

E. Sirte Formation

In its type development in the central Sirte Basin, the Sirte Formation is dominantly a shale sequence with thin limestone interbeds. The shale is a dark grey to dark brown, fissile calcareous rock and is occasionally silty and sandy at its base. The formation is conformably

overlain by the Kalash Formation, and it commonly disconformably overlies the Rachmat Formation depending on basin position. The Sirte Shale probably began to be deposited in a shallow restricted marine environment which became rapidly deeper.

In the type section (O2-59 borehole) the Sirte Formation contains abundant foraminifera. Planktonic species which are present throughout include: *Globotruncana fornicata, G. arca, G tricarinata, G. linneiana* and *G. obliqua* which indicate that the formation ranges in age from lowermost Campanian or even Santonian to Lower Maastrichtian there.

F. Kalash Formation

The Kalash Formation consists predominantly of argillaceous calcilutite, with some calcareous shale interbeds. It often conformably overlies the Sirte, Bahi, and other Upper Cretaceous units. It may also unconformably overlie older rocks such as the Lower Cretaceous Nubian Sandstone (in the eastern part of the Sirte Basin), or the Cambro-Ordovician Hofra Formation, or igneous and metamorphic basement rocks. It is most often conformably overlain by the Paleocene Hagfa Shale, its lateral equivalent, the Upper Satal Formation, and it is laterally equivalent to the Lower Satal Formation (as in the area of the Dahra-Hofra platform), and the Waha Formation (Beda platform). The Kalash Formation consists predominantly of a white, tan or grey argillaceous mudstone with some calcareous shale interbeds. Its thickness various from a few metres to over 200m. This formation is widespread in the Sirte Basin. Only in some palaeo-high areas it is replaced by its lateral equivalents. In the type section (E1-57, in the western part of the basin) the Kalash Formation contains abundant foraminifera including common planktonic species belonging to the genera *Globotruncana, Rugoglobigerina* and *Heterohelix*. These assemblages indicate that the Kalash Formation was deposited in an open, probably neritic sea during Maastrichtian times.

2.2.6 Paleogene System

Paleogene formations in the Sirte Basin fall naturally into two groups which equate with the Paleocene and Eocene Series respectively.

1. Paleocene Series

As general subsidence continued, a thick sequence of shales and limestones was deposited throughout the Paleocene during which time almost all topographic highs were buried. The Danian, Montian and Landenian stages are all represented and lithologies consist of alternating open marine calcareous shales and shallow water carbonates. The total thickness and lithology of the sediments are a function of the sea level changes controlled by the basin's major structural elements.

A. Hagfa Formation

During the Danian times, the maximum marine transgression took place. The Paleocene basal shale unit, the Hagfa Formation, infilled the trough areas, where it was deposited in moderately deep water surrounding shallower water environments, which covered the Dahra-Hofra, Beda, Jahama and Zelten platforms and also the part of the eastern Sirte Basin where the Upper Satal Formation was deposited. The Hagfa Formation consists mainly of shale which is predominantly grey, soft to moderately hard, calcareous, fissile and fossiliferous. It conformably overlies the Kalash Formation, and is conformably overlain by the Beda Formation. It contains a diverse foraminiferal assemblage. Planktonic Danian species are common especially in its lower part and include *Globoconusa daubjergensis, Globorotalia compressa, Globigerina pseudobulloides and G. triloculinoides.* The Upper Satal Formation on the highs has yielded rare Danian benthonic foraminifera together with molluscs, corals, echinoderms, ostracodes and algae.

B. Beda Formation

During Montian times, a carbonate sequence was deposited in the western part of the Sirte basin. The Beda Formation, which consists mainly of limestone interbedded with dolomite and calcareous shale in turn conformably overlies the Hagfa Formation with abrupt contact and it is conformably overlain by the Dahra Formation. Fossil assemblages consist largely of dasycladacean algae, benthonic foraminifera including miliolids, molluscs, echinoids

and corals indicating a variety of shallow marine environments.

C. Dahara, Zelten, Harash and Kheir formations

During Landenian times, a thick sequence of carbonates was deposited. The Dahara Formation consists mainly of white to light grey, chalky, calcarenite and calcilutite which are sometimes slightly argillaceous. There are subordinate tan to brown microcrystalline dolomites and thin interbeds of dark shale. Benthonic foraminifera consisting of miliolids and texturids are common. The Zelten Formation which consists mainly of tan to brown, very fossiliferous, arenaceous and glauconitic, calcilutite and calcarenite also with subordinate amounts of white to brown, finely to medium-grained crystalline dolomite. The Harash Formation consists mainly of soft, chalky, white to brown, argillaceous calcilutite and muddy calcarenite with thin interbeds of grey to green, calcareous fissile shale. The foraminifer *Operculina*, bryozoans and algae are common. The Kheir Formation is predominately a grey to dark grey and green fissile and calcareous shale with some grey, argillaceous marl and grey calcilutite. Microfossils, including *Operculina* and other smaller benthonic and planktonic foraminifera occur. Important forms such as *Globorotalia velascoenis*, known from the lower part of the formation, and *G. subbotinae* from its uppermost part indicate that the Kheir Formation straddles the Paleocene- Eocene boundary (i.e. Landenian-Ypresian stages).

2. Eocene Series

A variety of sediments of Eocene age was deposited in the Sirte Basin.

A. Gir Formation

Following the upper Kheir Formation, a thick interbedded sequence of Ypresian dolomites, dolomitic limestones and evaporites was laid down with a thickness reaching more than 1000m in the Zellah Trough. Dolomites and limestones below the Hon Anhydrite Member are known as the Facha Dolomite Member. The Gir Formation is overlain by the Gialo Formation. It contains very few fossils but benthonic foraminifera including nummulites occur.

B. Gialo Formation

The largely Lutetian Gialo Formation varies in thickness from a few metres on the palaeo-high areas to more than 1000m in the lows (e.g. the Ajdabiya Trough in the eastern part of the Sirte Basin) where it consists of a thick sequence of grey or tan to brown highly fossiliferous limestone deposited under shoaling marine environments. These are concentrations of several species of nummulite and molluscan, echinoid and bryozoan debris is locally common. The nummulite concentrations include *Nummulites gizehensis, N. cuvispira, N. discorbina, N. bullatus* and *N. partischi tauricus* which occur at different stratigraphical levels within the formation. There is evidence that the uppermost part of the Gialo Formation is of upper Eocene (Bartonian) age.

C. Augila Formation

This formation consists of a sequence of green sandy glauconitic shales, which lie disconformably on the Gialo Limestone. In the eastern part of the Sirte Basin the shales are replaced by calcilutites and calcarenites. In the southeastern and south central Sirte Basin the Augila Formation has been subdivided. The lowest member consists of a light grey to green shale with thin argillaceous limestone or dolomite interbeds. The middle member is a soft, friable, glauconitic sandstone, while the upper member consists of a light to dark grey, hard sandy and slightly glauconitic limestone. The Augila Formation contains both benthonic and planktonic foraminiferal assemblages indicative of a Bartonian age. Whilst the shales are probably open sea, neritic deposits, the arenaceous and carbonate rocks were probably laid down in more restricted, shallower environments.

2.3 General lithological description of the Bahi Formation

From all the available subsurface data, but in particular a thick sequence with good core coverage in the A4-32 borehole (51.24m), the A2-32 borehole (31m) and the F6-32 borehole (17.6m), the Bahi Formation can easily be divided into two parts. The upper part consists of coarse-grained and pebble-bearing sandstone which dominates the succession to the south of

the A1-32 borehole (e.g. A4-32 borehole) while the lower part consists of argillaceous, fine-grained red sandstone and siltstone with some conglomerate and this facies dominates sequences to the north (e.g. A2-32 borehole). The uppermost part of the formation is characterised by glauconite-bearing sandstone representing the intiation of a marine cycle (Figs. 2.3-2.5).

Representative slabbed cores photographs from the Bahi Formation in the A2-32 and A4-32 boreholes are shown in plates 2.6 & 2.7.

1. Basal Conglomerate

The lowermost part of the Bahi Formation is a basal conglomerate, composed of a sequence of 5 to 10m of coarse to very coarse pebbly sandstone. This unit marks the base of the Bahi Sandstone Formation, where It unconformably overlies the Cambro-Ordovician Hofra Formation, the Devonian Tadrart Formation and Precambrian rocks. There is a transitional contact with overlying red silty-sandstones.

2. Fine sandstone to siltstone

This unit ranges up to the middle part of the Bahi Formation. Fine red argillaceous sandstone and siltstone are the main lithologies of this lower part. It is only 14.6m thick in the A4-32 borehole, thins further to the north (<1m, A1-32), then thickness markedly over a contemporaneous fault to c. 36m in the A2-32 borehole. It is characterised by reddish-brown, very fine sandstone and siltstone. These are horizontally laminated with a variable degree of fissility, occasionally homogenised by bioturbation and sometimes associated with mottling which probably results from the migration of manganese and iron ions in solutions, leading to the patchy accumulation of their oxides and hydroxides as grain coatings (Reading, 1978, 52). Some samples show evidence of mud cracks. The degree of bioturbation varies from a few isolated burrows to total destruction locally of sedimentary structures. Massive and laminated beds occur. Minor structures include lenses of rippled siltstone and interclasts of clay. Trace fossils (escape structures) are present, *Cylindrichnus* is the main burrow type, characterised by

an elongated, slightly curving subconical form.

3. Coarse Sandstone

The upper part of the Bahi Formation varies greatly in thickness and local detail. To the south of the A1-32 borehole, two 22.5 to 30m thick coarse to very coarse, pale pink pebbly sandstones are seen. They vary from being tightly cemented to loose and friable and are separated by a red argillaceous and silty interval (A4-32 borehole). Here the upper unit can be divided into two tongues, the upper tongue being characterised by cross bedding, where foresets are often emphasised by lines of green and occasionally red shale interclasts. Higher angle foresets are most common in the basal portion of the upper tongue. The upper and middle portions of the lower tongue have finer textures with interclasts of dark brown clay. The lower part of this unit is a massive, light grey, medium to very coarse sandstone with scattered greenish grey mud interaclasts.

4. Glauconitic Sandstone

The uppermost part of the formation is a 3-6m thick light grey, white and clear quartz sandstone with small developments of grey and occasionally red shale. The sandstone is mainly fine to medium-grained but occasionally coarse, having moderately sorted subangular to rounded quartz grains. Glauconite is present throughout. It rest on a thin, locally persistent, richly glauconitic green shale which is usually less than 2m thick.

2.4 Depositional environment

The depositional environment of the Bahi Formation can be summarised as follows:

1: The lower part of the formation is almost certainly of terrestrial origin. This assessment is based primarily on its prevailing red colour, the ill-sorted, diverse nature of the sediments, the apparent absence of remains of marine organisms and the detailed sedimentological analyses presented in this thesis.

2: The presence of thick sequences of coarse to very coarse sandstone in the upper

part of the formation, characterised by graded-bedding and cross-bedding, where foresets are often emphasised by lines of green and occasionally red shale interaclasts is suggestive of fluvial, channel-fill deposits - an assessment which is supported by sedimentological work presented herein.

3: The presence of glauconite in the sandstone and shale of the uppermost part of the formation indicates a shallow marine environment. Glauconite being an indicator of submarine discontinuities and renewed transgressions, its accumulation in large quantities usually implies a low rate of sedimentation.

It appears therefore that the marine transgression began to the north or northwest of the Sirte Basin and progressed southeastwards over a continental platform of low relief on which an alluvial plain had established itself in Cenomanian times. Regardless of local structural controls, the Bahi Formation everywhere reflects the same sequence of events but its relationship with overlying marine formations across the basin shows it to be extremely diachronous, as is to be expected.

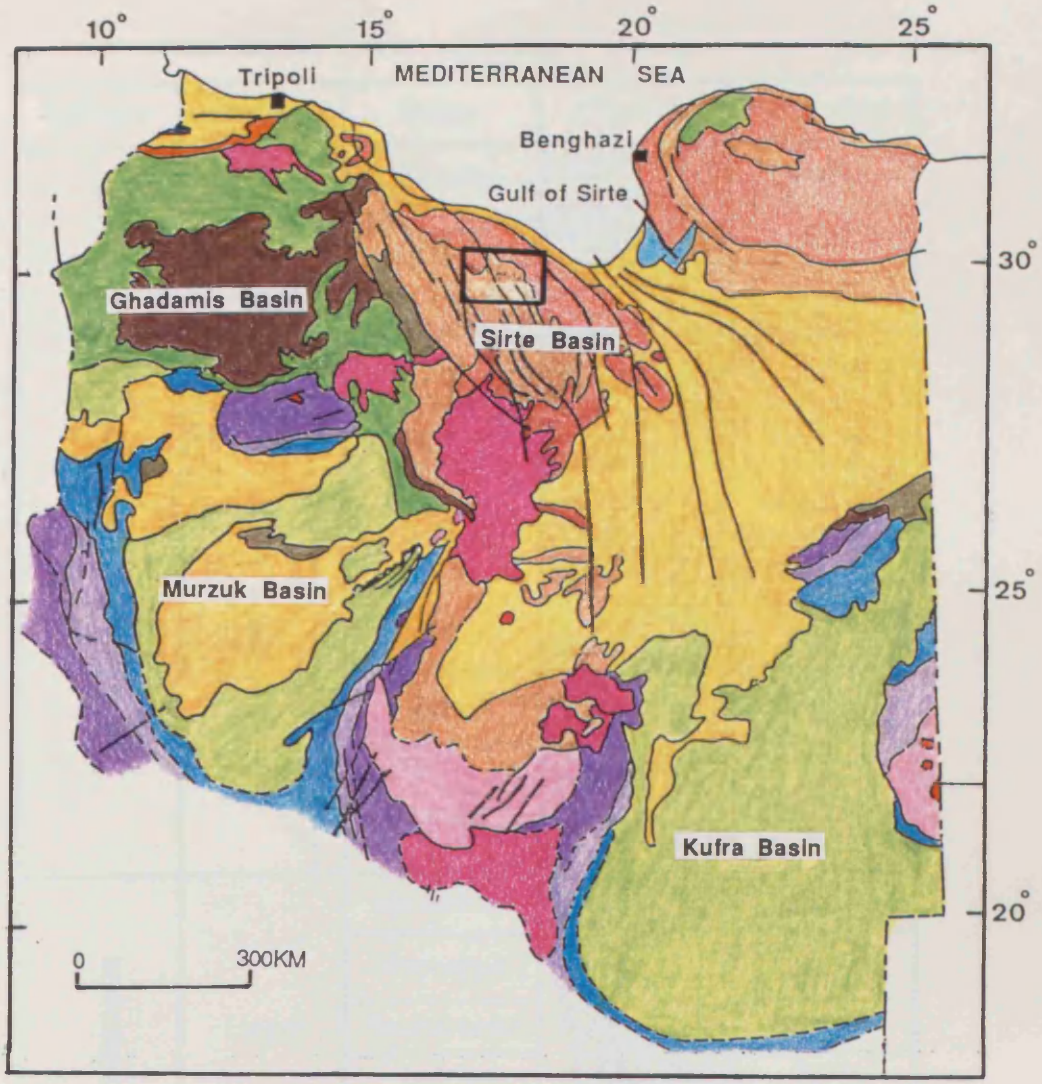

EXPLANATION

QUATERNARY
Pleistocene & Holocene
NEOGENE
Pliocene
Miocene
PALEOGENE
Eocene & Oligocene
Continental beds
(precise age uncertain)
Paleocene
CENOZOIC VOLCANIC ROCKS

CRETACEOUS
Upper Cretaceous
Lower Cretaceous
JURASSIC
TRIASSIC
CARBONIFEROUS
SILURIAN & DEVONIAN
CAMBRO-ORDOVICIAN
PRECAMBRIAN
GRANITE
Fault
Area studied (Sirte Basin)

Fig. 2.1 Geological map of Libya and areas to the south, after Conant & Goudarzi (1967).

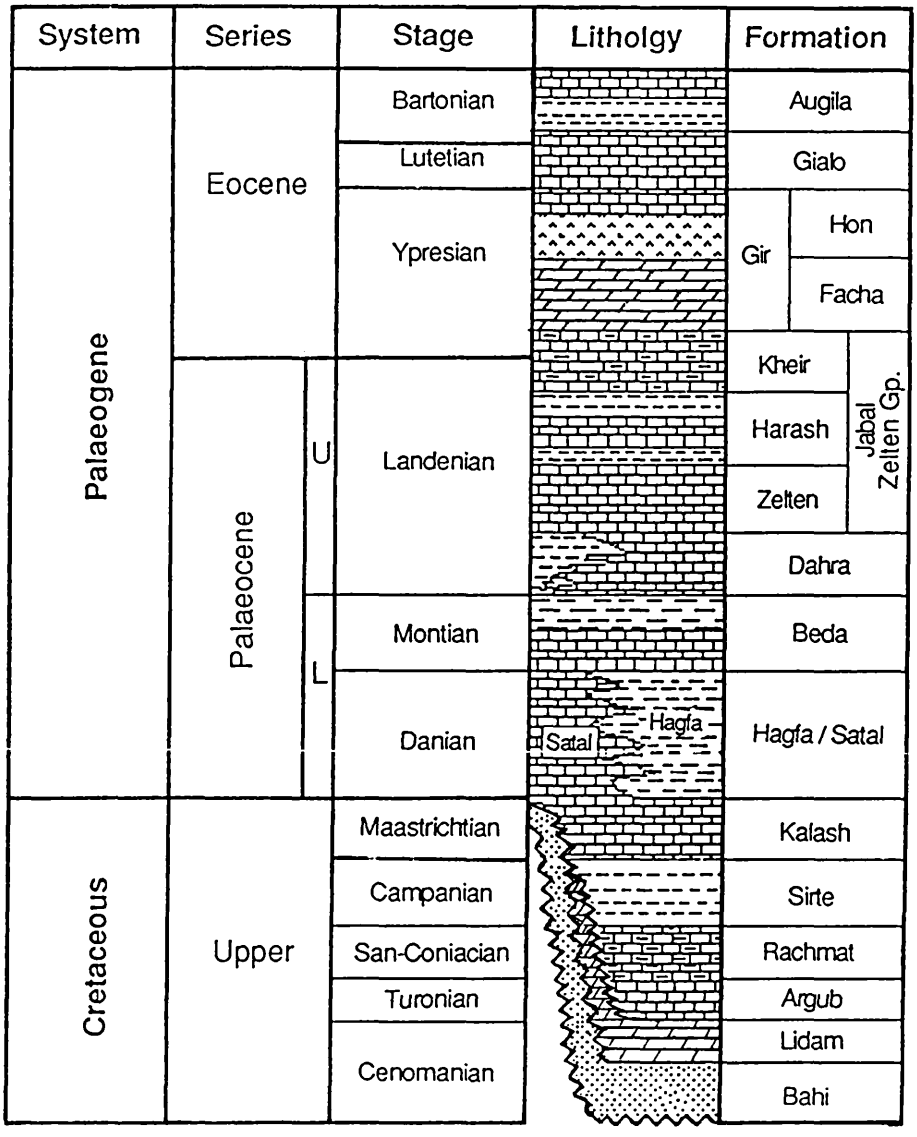

major stratigraphical break

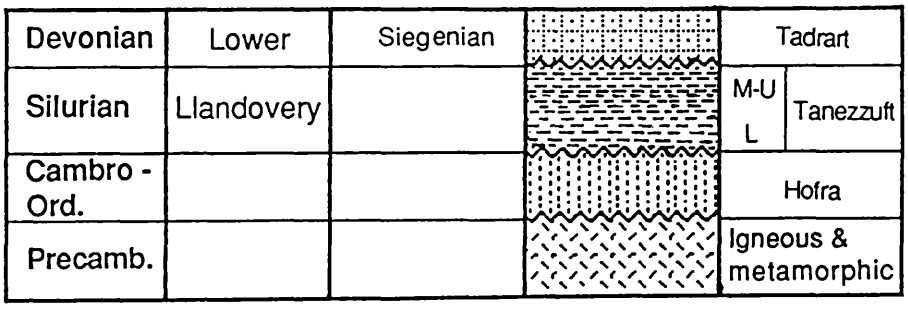

Fig. 2.2 Columnar section showing general lithology and stratigraphy of the area studied, modified from Barr & Weegar (1972).

Symbol key for Figures 2.3-2.5


Sandstone.


Pebbly sandstone.


Silty sandstone.


Fissile shale.


Cross-bedded sandstone.


Ripple-bedded sandstone.


Bioturbated sandstone.


Glauconite.


Trace fossils (escape structures).


Mud clasts.


Concretions.


Unconformity.

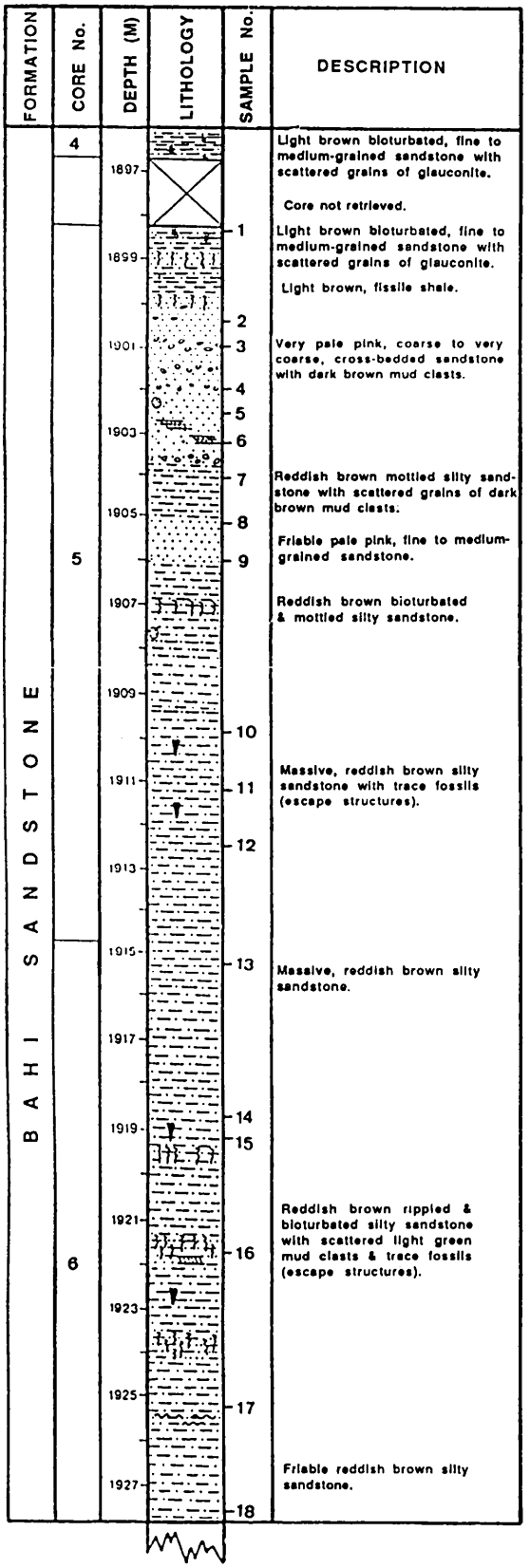

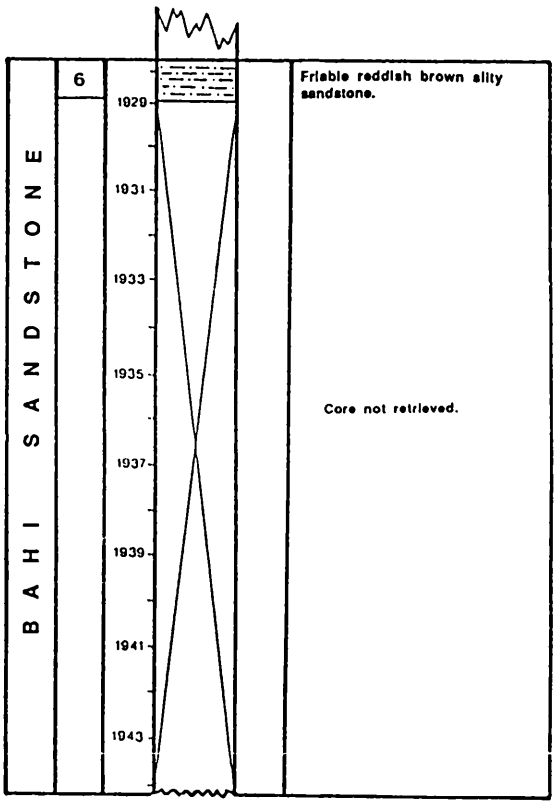

Fig. 2.3 Section through the Bahi Formation, information derived from the available cores in the A2-32 borehole.

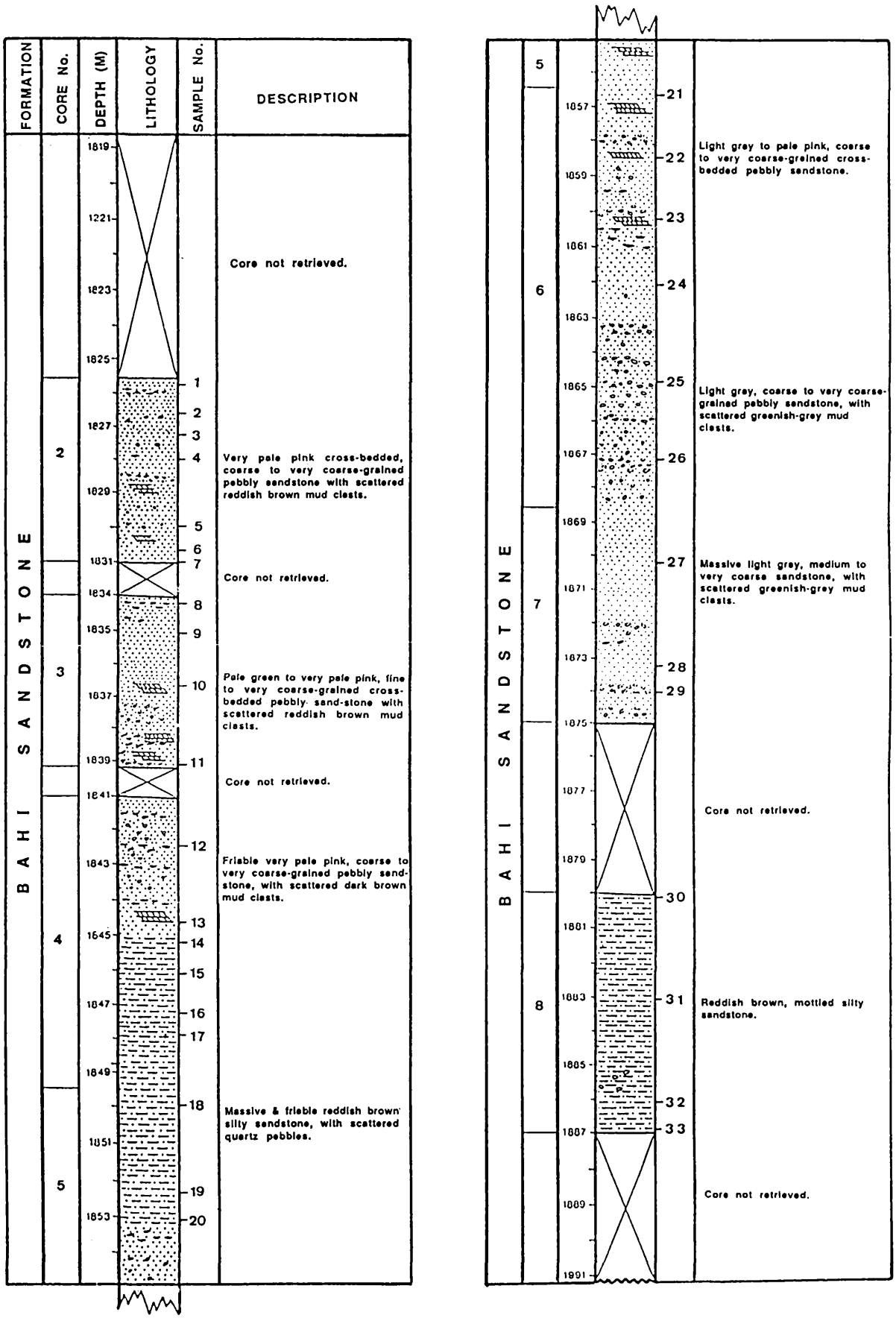

Fig. 2.4 Section through the Bahi Formation, information derived from the available cores in the A4-32 borehole.

D1-32

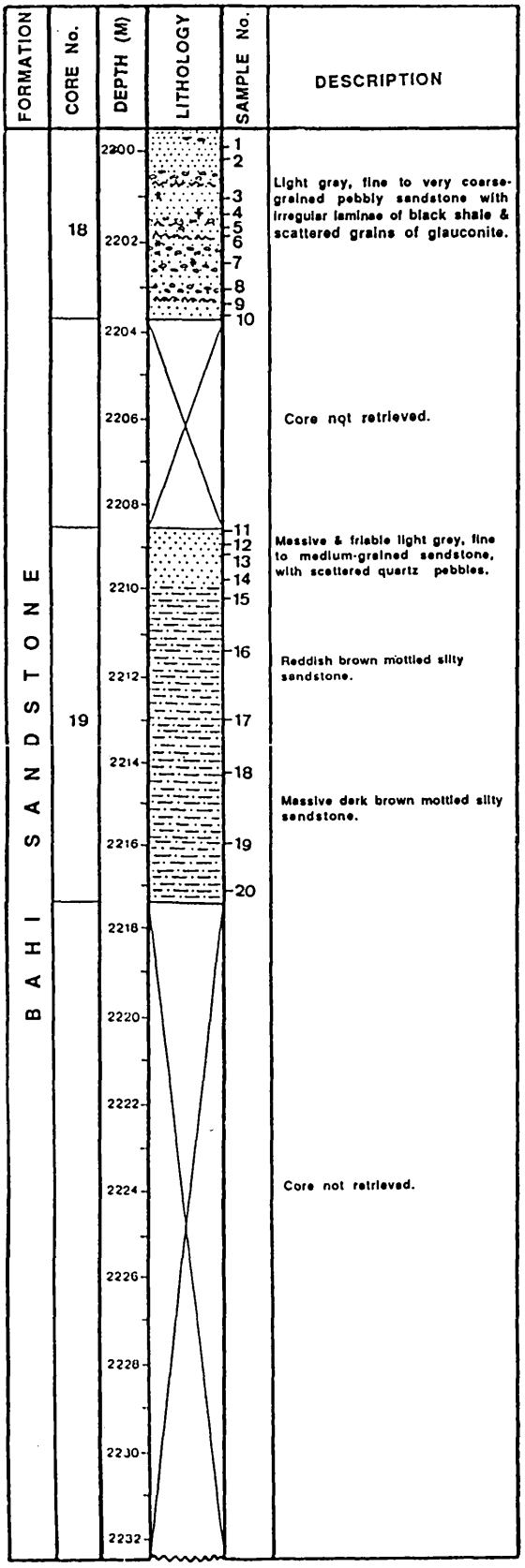

F6-32

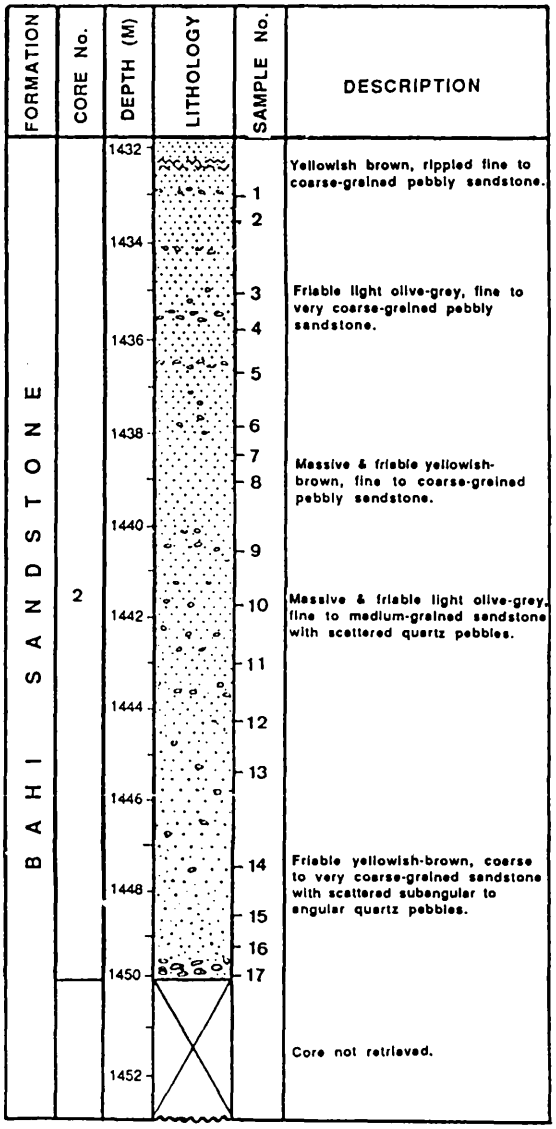

Fig. 2.5 Section through the Bahi Formation, information derived from the available cores in the D1-32 & F6-32 boreholes.

Plate 2.6 Representative slabbed cores from the Bahi Sandstone in the A2-32 boreholes.

A. Bioturbated sandstone and shale with scattered grains of glauconite. Sample from the uppermost part of the formation, depth=1.8m below top of formation.

B. Massive medium to coarse-grained sandstone with scattered pebbles of quartz, Anhydrite and a dolomitic cement is present. Sample from the upper part of the formation, depth=7.0m below top of formation.

C. Massive friable silty sandstone. Sample from the lower part of the formation, depth=13.0m below top of formation.

D. Trace fossils (escape structures) produced by organism acitvity, vertical type. Sample from the lower part of the formation, depth= 13.6m below top of formation.

E. Trace fossils (escape structures), produced by organism activity, *Cylindrichnnus* type, characterised by elongated, slightly curving subconical form. Sample from the lower part of the formation, depth=15.2m below top of formation.

F. Reddish brown rippled silty sandstone. Sample from the lower part of the formation, depth=29.1m below top of formation.

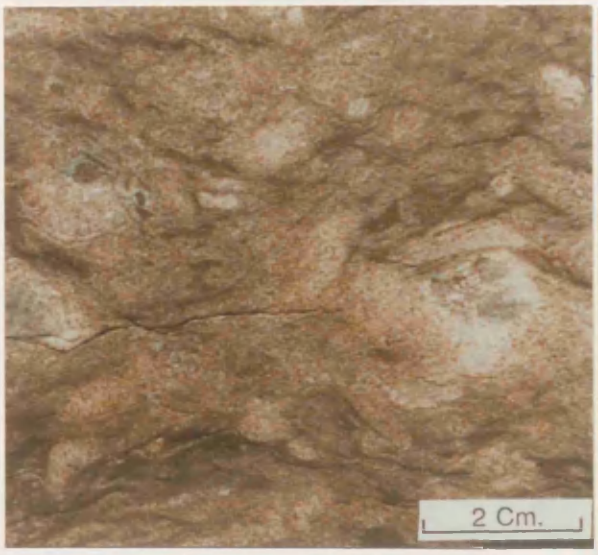

A

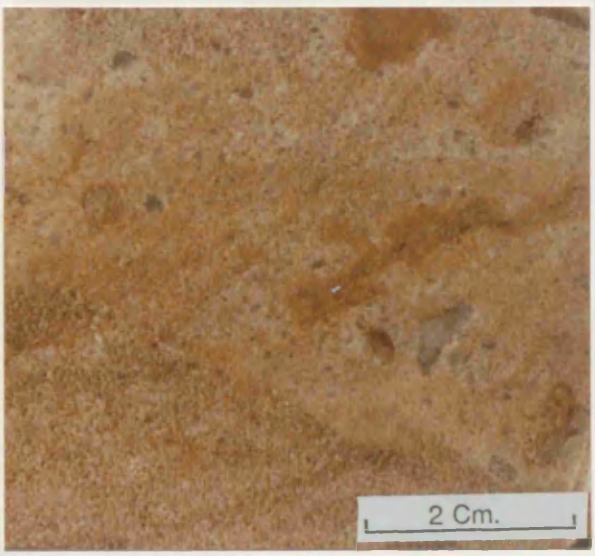

B

C

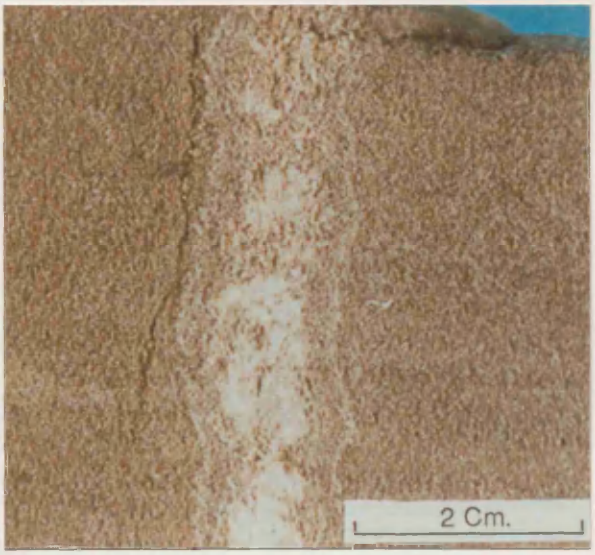

D

E

F

Plate 2.7 Representative slabbed cores from the Bahi Sandstone in the A432 boreholes.

A. Pale pink coarse to very coarse-grained pebbly sandstone with scattered quartz pebbles. Sample from the middle part of the formation, depth=28.2m below top of formation.

B. Very pale pink cross-bedded sandstone. Sample from the middle part of the formation, depth=36.7m below top of formation.

C. Pale pink coarse to very coarse-grained, cross-bedded pebbly sandstone. Sample from the middle part of the formation, depth= 39.1m below top of formation.

D. Pale green to very pale pink fine to coarse-grained cross-bedded pebbly sandstone with scattered dark brown mud clasts. Sample from the middle part of the formation, depth= 41.0m below top of formation.

E. Very pale pink coarse to very coarse-grained pebbly sandstone with scattered greenish-grey mud clasts. Sample from the middle part of the formation, depth=47.6m below top of formation.

F. Reddish brown mottled silty sandstone. Sample from the lower part of the formation, depth=67.3m below top of formation.

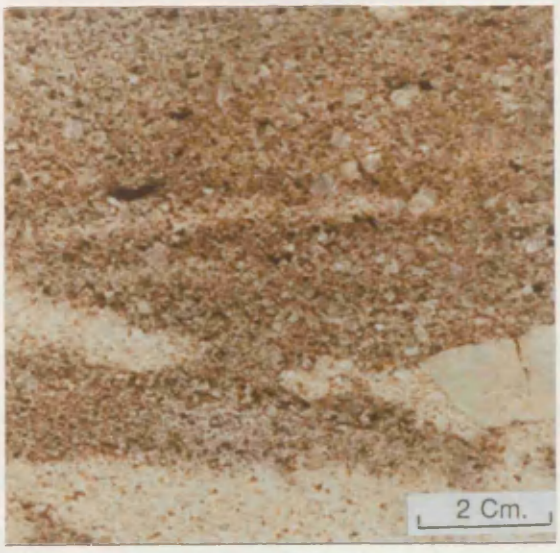

A

B

C

D

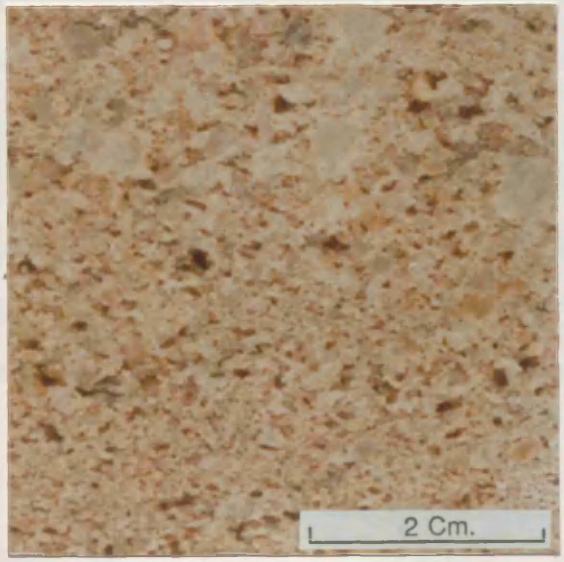

E

F

CHAPTER 3

TECTONIC SETTING

3.1 Tectonic setting of Libya

Libya is situated on the northern flank of the African shield. Several Europe-West African based orogenies appear to have affected the table-and and formed the present major structural and tectonic features. The major diastrophic disturbances recognised relate to the distant Caledonian and Variscian orogenies in Palaeozoic times, and caused uplifts, subsidence, tilting, faulting, and intrusions. However the effects of these diastrophic events were generally broad, and compressional folds are very few. East-west and north-south trending faults are present, but the major fault systems (NW-SE) broadly parallel the Red Sea and African rifts (Goudarzi, 1967).

Many workers have discussed the tectonic setting of Libya in general and the Sirte Basin in particular (Conant & Goudarzi, 1967; Klitzsch, 1968,1971, 1981; Sanford, 1970; Hea, 1971; Mikbel, 1977, 1979; Goudarzi, 1980; Kogbe, 1980; Mouzughi & Taleb, 1980; Kumati & Anketell, 1982; Harding, 1983; Van Houten, 1983; Gumati & Kanes, 1985; Reyment & Dingle, 1987 and others).

Klitzsch (1971) recognised three major periods of structural development which characterised the central part of north Africa: folding and consolidation in Precambrian times, formation of NW to NNW striking horsts during Cambrian times, which became the cores of uplifts (separated by troughs) in Silurian and Devonian times (Fig. 3.1), formation of uplifts and troughs striking NE, during Late Palaeozoic and Mesozoic times (Fig.3.2), and block faulting which occurred along the edge of some uplifts during the Jurassic or at the Jurassic-Cretaceous transition (Fig.3.3).

Three major north-west to south-east trending axes of uplift are recognised. In the southwest is the Tihembika Uplift of the Hoggar Massif. Toward the north-west, the Tripoli-Tibesti uplift and Haruj uplift define the small and narrow Dorel Gussa Trough. Further to the north-east lies the Calanshio-Uweinat Uplift. Crossing these north-west to south-east trending

structures in the south-east is the Ennedi-Uweinat Uplift, which together with the Tibesti-Sirte Uplift, and the Calanshio Uplift define the Kufra Basin. Further to the north-west, the Gargaf Uplift, where it crosses the Tihembika and Tripoli-Tibesti uplifts, defines the northern flank of the Murzuk basin and the southern flank of the Hamra basin. The northern flank of the Hamra basin is in turn defined by the Nefusa uplift, north of which lies the Jefarah Trough. To the east, in Cyrenaica the Calanshio uplift is followed to the north-east by the Western Desert Basin (see Fig. 3.3).

3.2 Tectonic setting of the Sirte Basin

The Sirte basin does not conform to the pattern noted above, a pattern in which individual basins appear to be bounded by well defined axes of uplift. Instead, it cuts at an angle across the north-eastward extension of the Tibesti-Sirte Uplift and the north-westward extension of the Calanshio Uplift. At the same time it displays a feature not common in the other basins. Hea (1971), stated that the structure of the Sirte Basin is controlled by four major feature systems: Rift, Atlan, Mediterranean and Meridian. The Rift and Atlan systems have NW and NE alignments, the Meridian system has N-S directions and is probably genetically related to the Rift system and the Mediterranean system has E-W alignments. The structural deformation of Libya from Precambrian to the present is essentially defined by differential uplift, subsidence, block faulting and tilting relative to these fracture systems.

Massa and Delort (1984) noted that at the beginning of the Late Cretaceous the northern crest of the Tibesti-Sirte Uplift collapsed to form the Sirte Basin. A number of tilted horsts (platforms) and grabens (troughs) of the rift fracture system were formed. Subsidence of the Sirte basin continued from Late Cretaceous through the Cenozoic. The Sirte Basin is tectonically a northwesterly aligned structure in which all the major features trend similarly. It is nevertheless to be considered as an intracratonic basin comparable to the other basins. It is divided into mobile and stable parts. The mobile part is the ridge-and-trough basin formed by the Rift faulting while the stable part in that part of the African foreland transgressed in Upper Cretaceous times. Several northwest trending faults in the basin probably reflect subsequent

movements along earlier basement lines. Some of the faults have large displacements. In the southern part of the basin, the faults trend almost northwards. The Sirte area generally remained a fairly positive region until Late Cretaceous tmie at which time movements and deformation took place in western Libya, and the Sirte Basin gradually submerged. Large scale subsidence and block faulting which began in late Cretaceous times continued intermittently until the Miocene.

The platforms were characterised by thin or absent of Palaeozoic (Cambro-Ordovician) sediments, while troughs contain thick sequences unconformably overlain by a Lower Cretaceous sequence (e.g in the eastern part of the basin) which is in turn unconformably overlain by Upper Cretaceous and Cenozoic sediments having a total thickness of up to more than 6000m as in the northern part of the Ajedabiya Trough (Fig. 3.4).

3.3 Subsurface analysis

The Bahi Formation has a wide distribution in the Sirte Basin, where it is known only from subsurface data. The regional stratigraphical relationships control the distribution and thickness of the formation. It lies unconformably on an irregular surface of Precambrian, Cambro- Ordovician and Devonian rocks. Younger Upper Cretaceous formations overly the Bahi Formation: the junction is both gradational and diachronous. These relationships are partly reflected in the considerable thickness variation of the formation and its local absence .

The structural configuration and thickness distribution of the Bahi Formation has been compiled on the basis of subsurface data from different sources including lithological well logs, electrical log (sp., resistivity), tectonic data and geological maps. Isopach and structural maps with 25m and 50m contour intervals respectively at a scale of 1:250,000 have been constructed in order to demonstrate the detailed pattern of thickness distribution, probable structural controls and suspected chrono-stratigraphical correlations of the Bahi Formation. These maps are based both on lithological characteristics, stratigraphical relationships, and local structural context. In order to compile these maps, more than 90 logs from deep wells and boreholes have been evaluated (Fig. 3.5). These wells and boreholes were drilled by various oil

companies (Oasis, Sirte, Mobil and Oxydental) during the intensive exploration activity of the last thirty years. Nearly 73 wells and boreholes penetrated the Bahi Formation and have been used as control points. Other wells and boreholes have been used to calculate the depth and thickness of the formation, taking into consideration the regional paleogeographical context and the local stratigraphical situation.

Figures 3.6-3.7 shows the thickness, topography of the Bahi Formation and structural controls on its attitude and distribution. The zero contour of the formation can only assessed in general terms and local pockets of deposition possibly existed within the zero isopach.

The structural-stratigraphical relationships of the formation, can best be displayed by constructing structural and stratigraphical cross-sections along significant transects. For example a stratigraphical section has been drawn with the top of the Bahi Formation as datum along a line passing through the D1-, A2-, A5-, A1-, A4-, and A3-32 boreholes. This clearly demonstrates lithological variation within the formation and the local structural controls which were active probably before, and perhaps, deposition of Bahi Formation (Fig.3.8).

Two structural cross-sections have been constructed, one below -1000m SL, the other with Mediterranean sea level as datum. These have northwest-southeast and east-west directions respectively and show the relationships and diachronous nature of the Bahi Formation, and also the pre-Bahi topography and structural development during the geological history of the area (Fig.3.9-3.10). Structural elements recognised in the study have previously been mentioned in the literature (e.g. Mouzughi & Taleb, 1980) and some have appeared on tectonic maps. Their existence is herein confirmed.

The general distribution and thickness variation of all the Upper Cretaceous formations in the area studied, the local structural controls and the diachronous relationships of the Bahi and Lidam Formations in particular are shown in a fence diagram (Fig. 3.11). Over much of the area, the Bahi Formation directly underlies the Lidam (e.g. A-32 area). In the deep troughs such as Zellah Trough (H1-32) and northern part of Hagfa Trough (F1-16), it directly underlies the Sirte Formation and here The Lidam, Argub and Rachmat Formations are absent. This probably relates to late subsidence during Campanian times in these structural lows and thus here the

Sirte Shale is itself probably diachronous and its lower part is locally equivalent to the Lidam-Rachmate formations inclusive. In the southeastern part of the area, the Bahi Formation directly underlies the even younger Kalash Formation (Maastrichtian). This almost certainly reflects the persistent paleo-high in this sector which prevented the sea from advancing southwards until latest Cretaceous times.

The local well and borehole density together with depth of penetration allows general regional conclusions to be drawn. The distribution of the Bahi Formation is irregular and it varies greatly in thickness. On the Dahra-Hofra Platform, it is characterised by thin to moderate sedimentation but also local non-deposition (0-100m), probably controlled by the palaeotopography of the pre-Upper Cretaceous surface. Locally contemporaneous faulting as in the A1-32 area was responsible for striking short distance variation. In the palaeo-lows, such as the Zellah Trough (H1-32 borehole), there was greater topographic relief and/or greater relative subsidence which provided sites for the accumulation of more than 350m of sediments. The major faults which bound such depressions are probably responsible for the thicker development of the Bahi Formation in them.

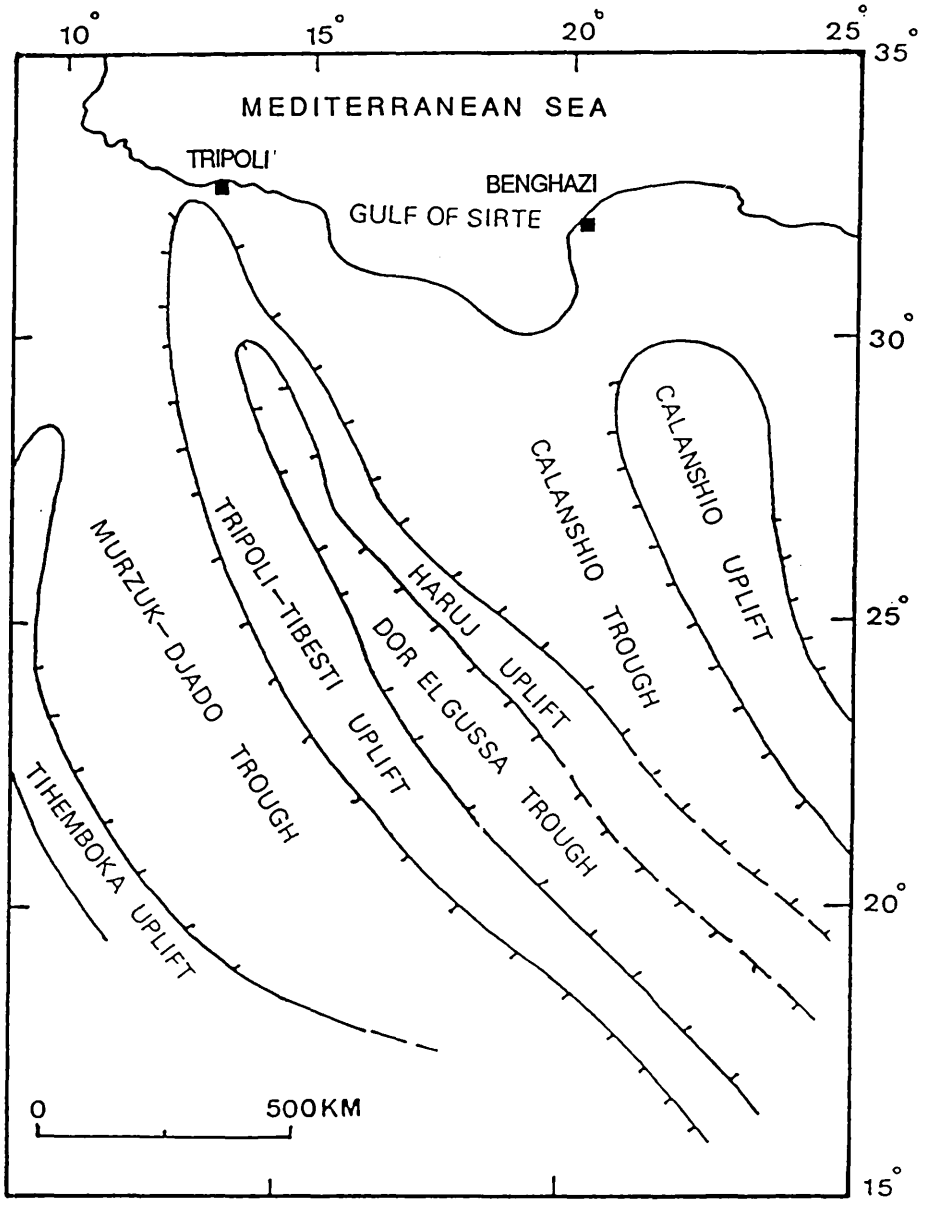

Fig.3.1 Map showing the major structural elements of the central Sahara in Early Palaeozoic times, after Klitzsch (1971).

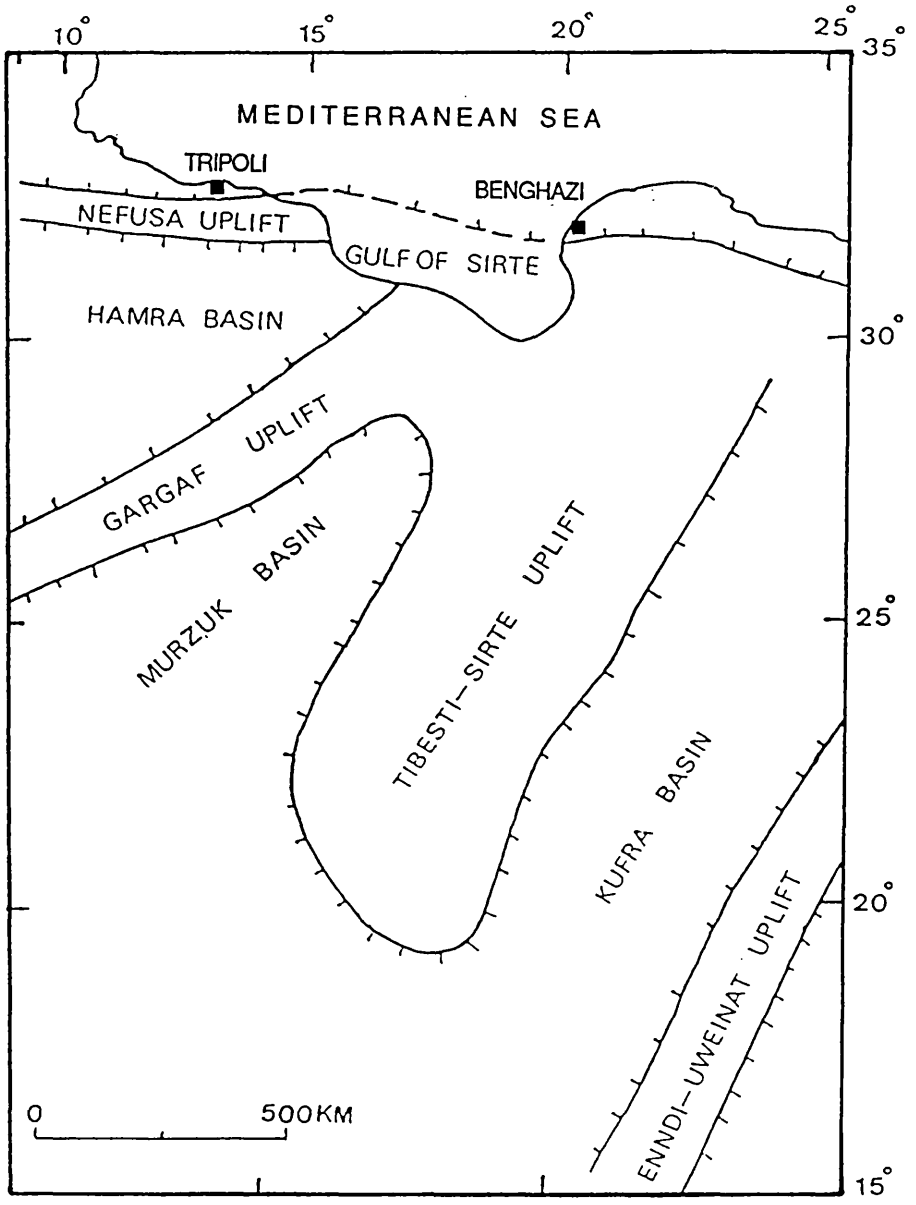

Fig. 3.2 Map showing the major structural elements of the central Sahara in Late Palaeozoic and Mesozoic times, after Klitzsch (1971).

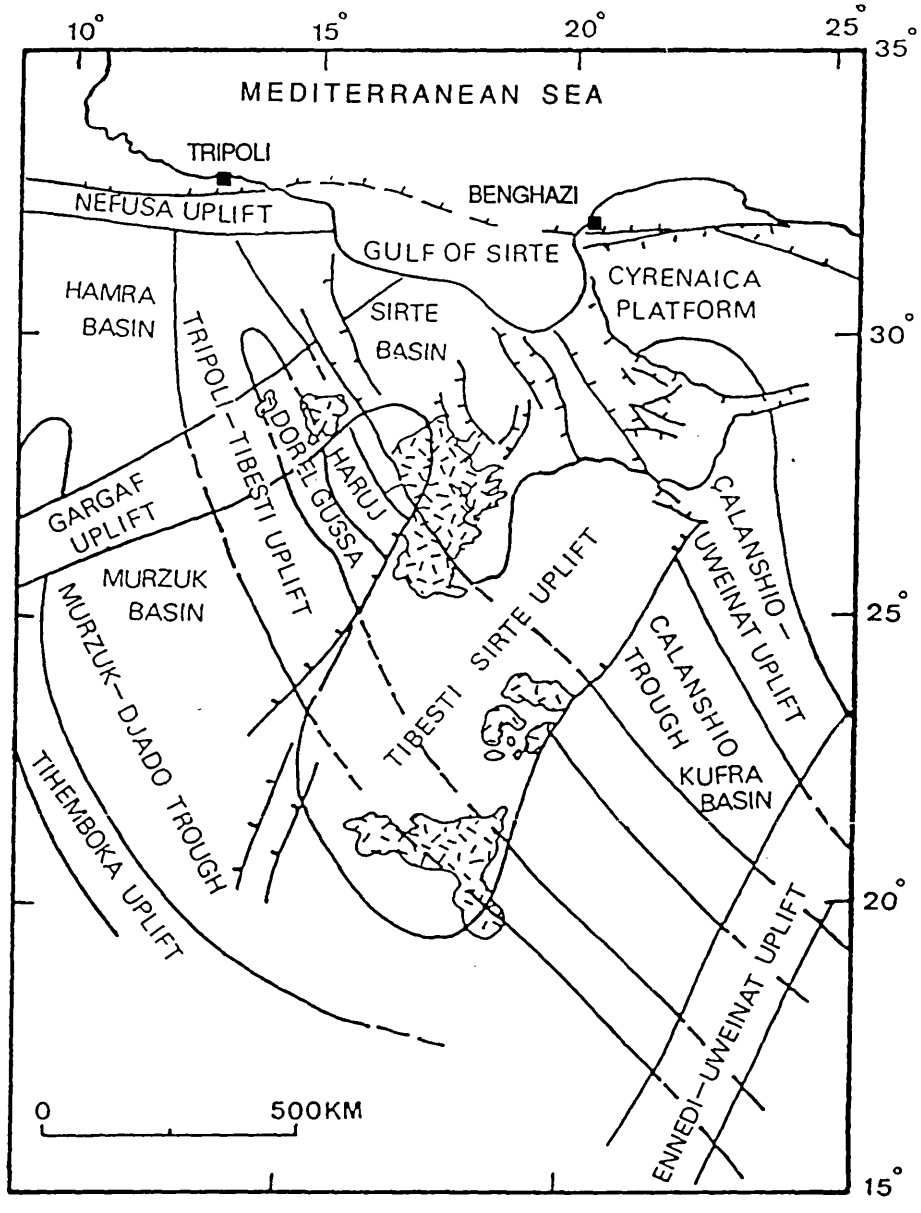

Fig. 3.3 Schematic map of major structural elements, showing the present day basins and uplifts of the central Sahara, resulting from a combination of the effects of two structural regimes, after Klitzsch (1971).

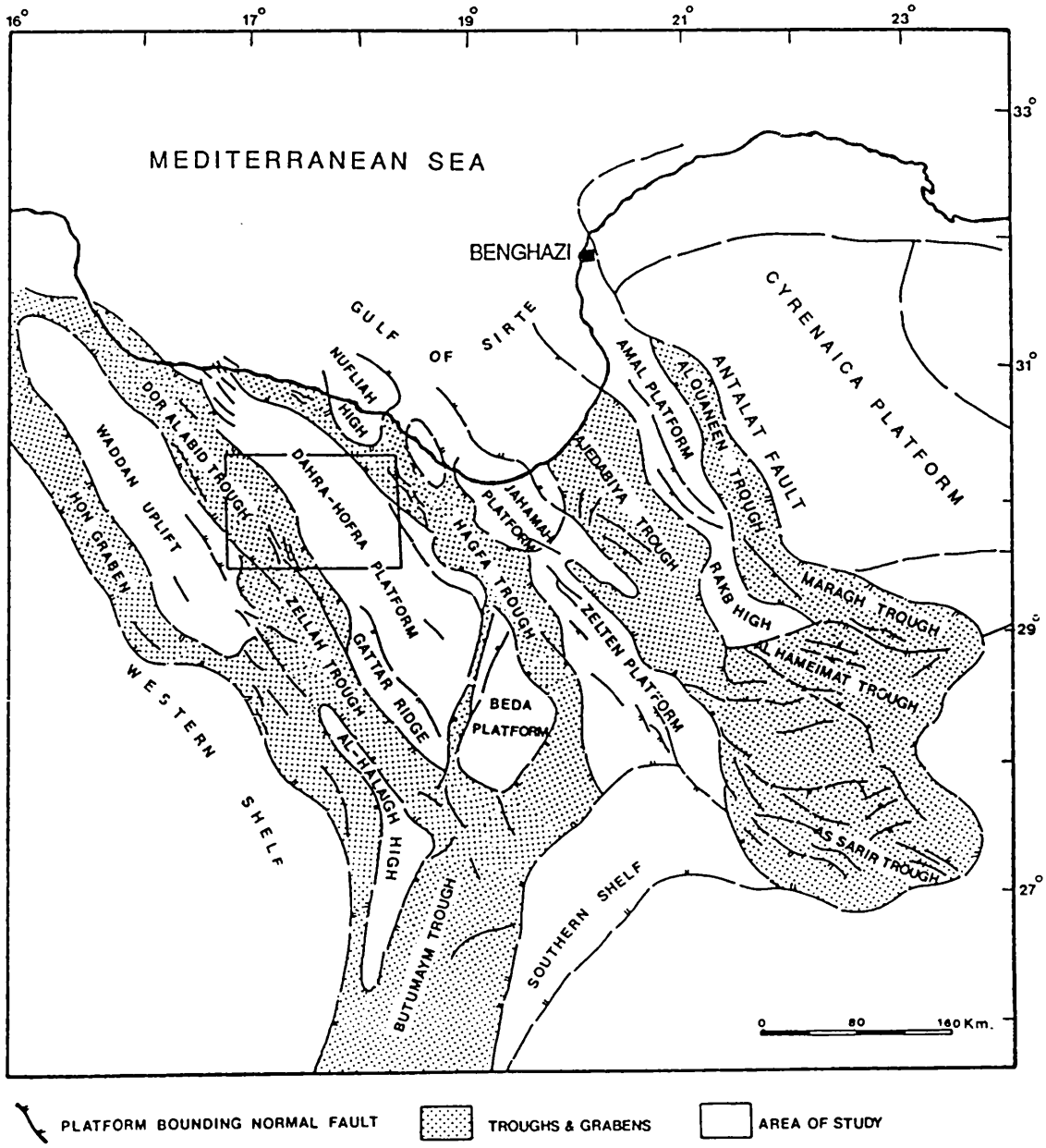

Fig. 3.4 Map showing structural elements of the Sirte Basin, after Mouzoghi & Taleb (1980).

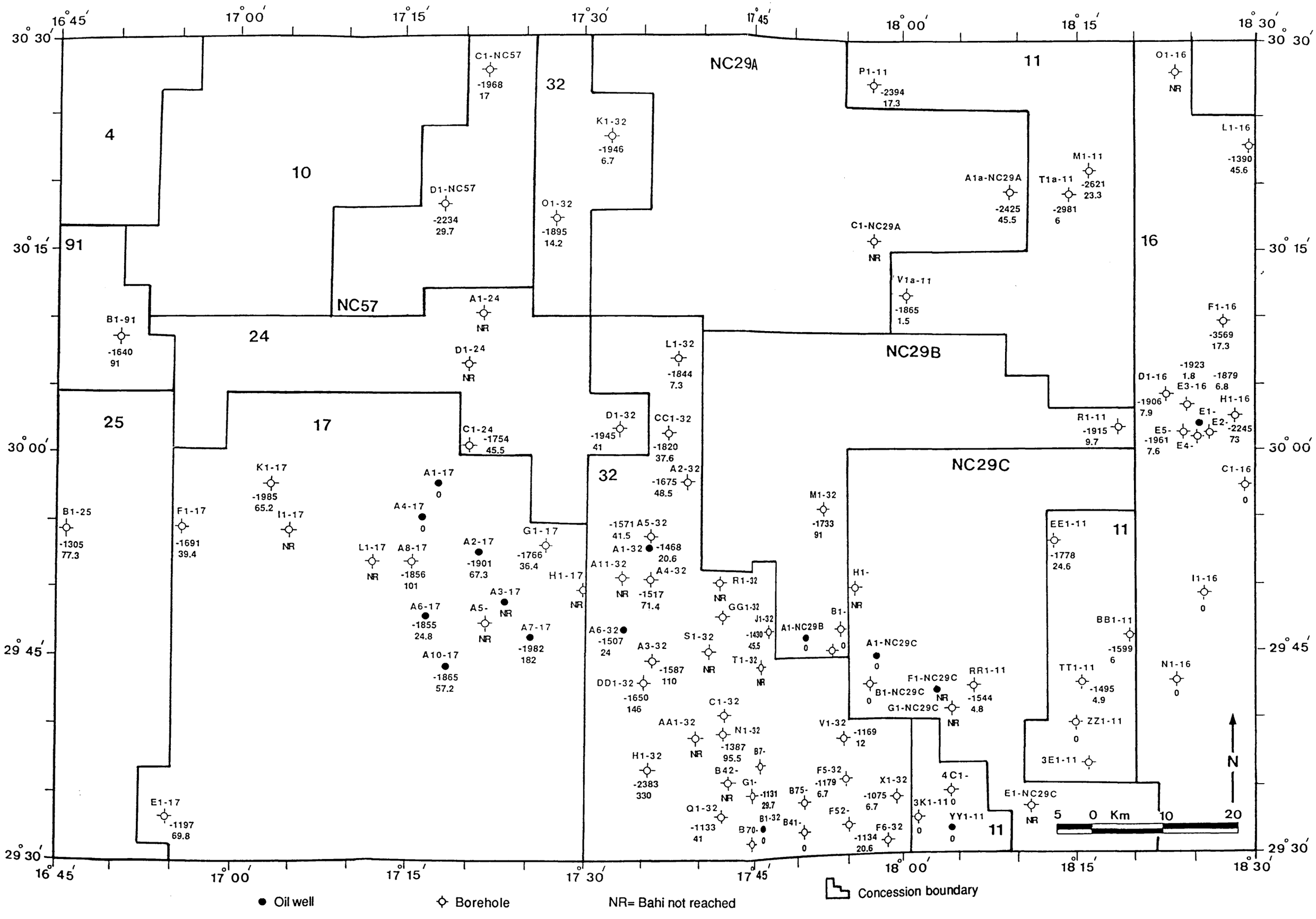

Fig. 3.5 Map showing the concession boundaries in the area studied together with location, depth from sea level and thickness of the Bahi Formation (all in metres).

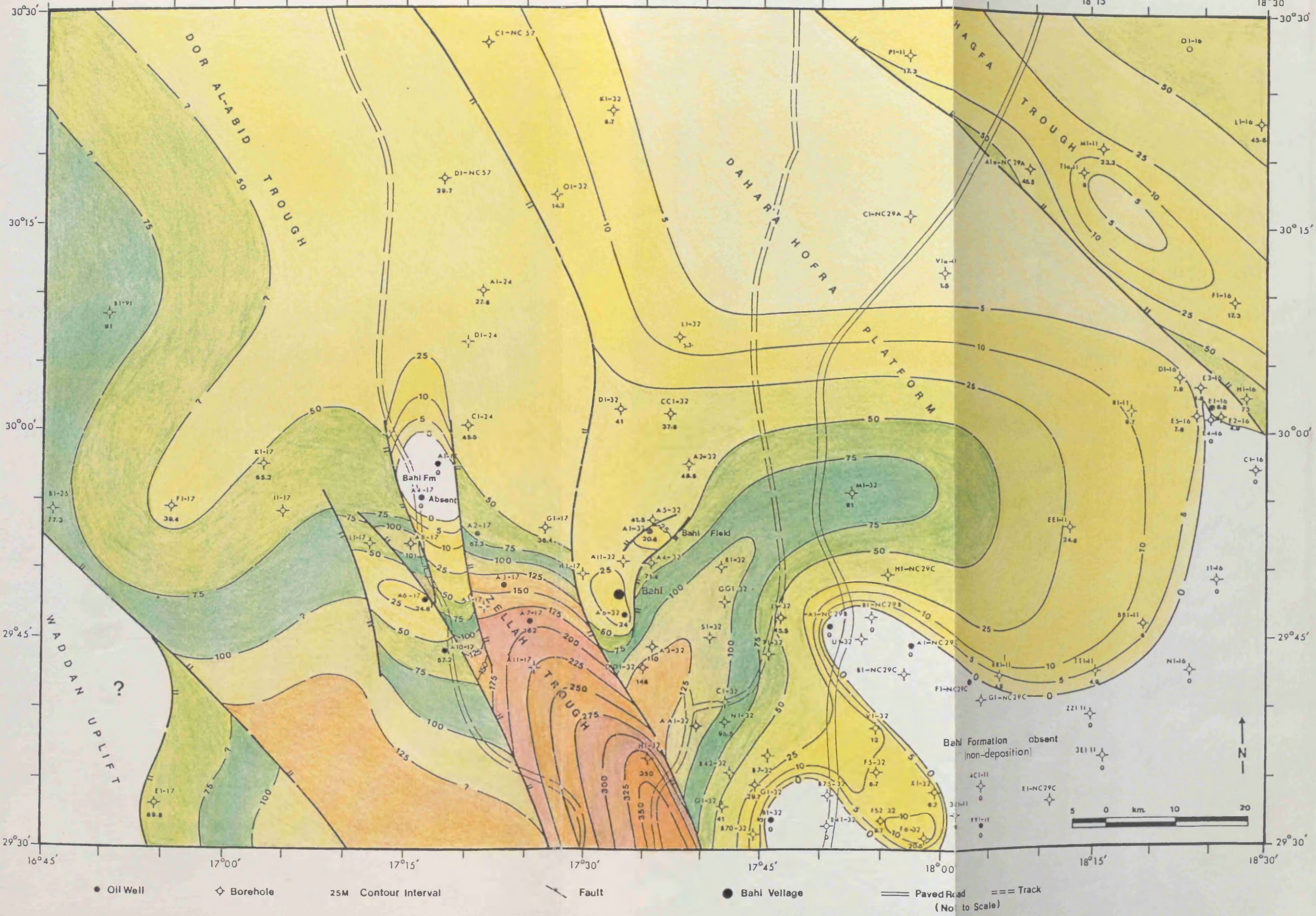

Fig. 3.6 Isopach map of the Bahi Formation showing the structural controls on its thickness distribution.

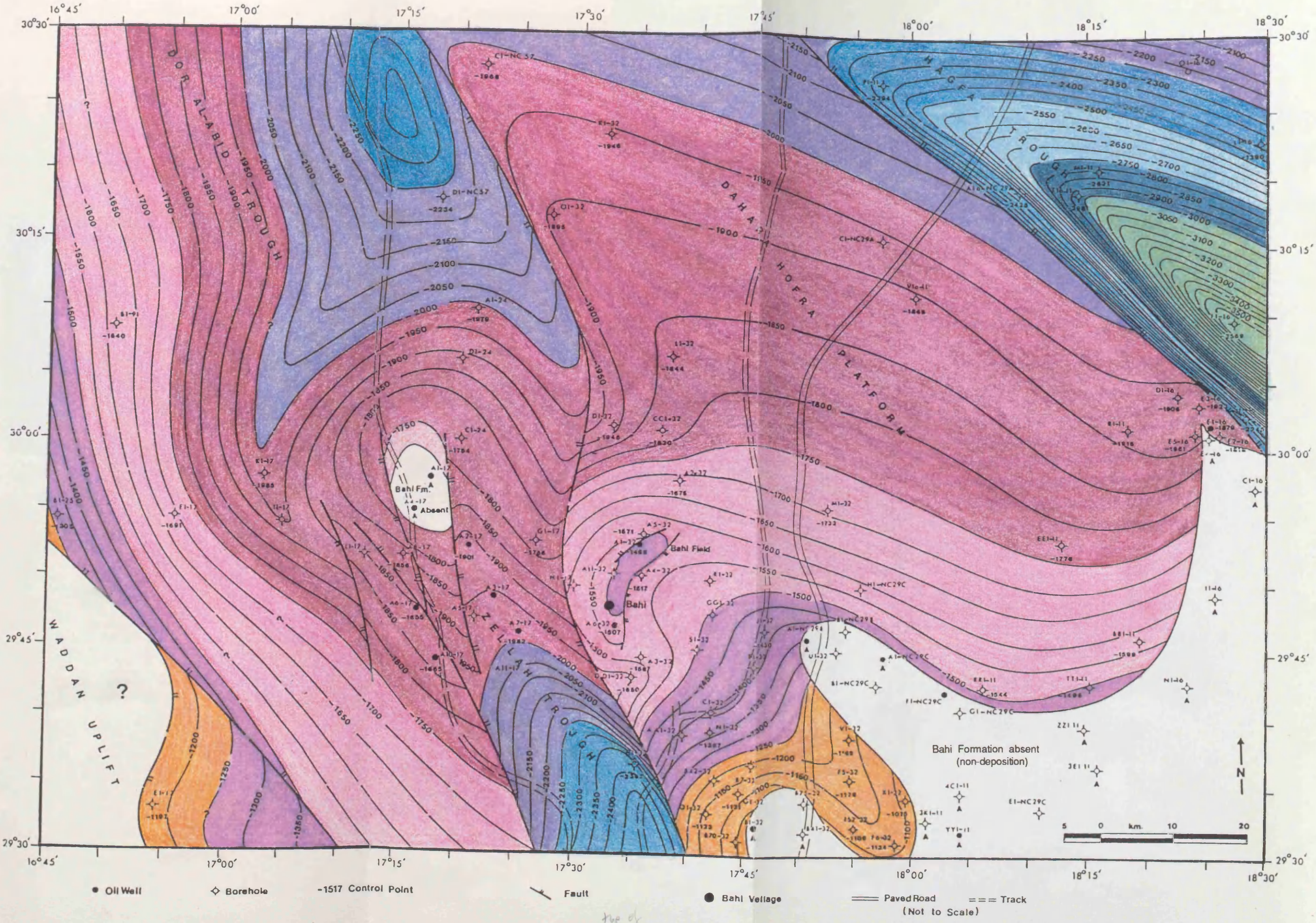

Fig. 3.7 Structure contour map, showing the present topography of the Bahi Formation and the structural controls on its attitude and distribution.

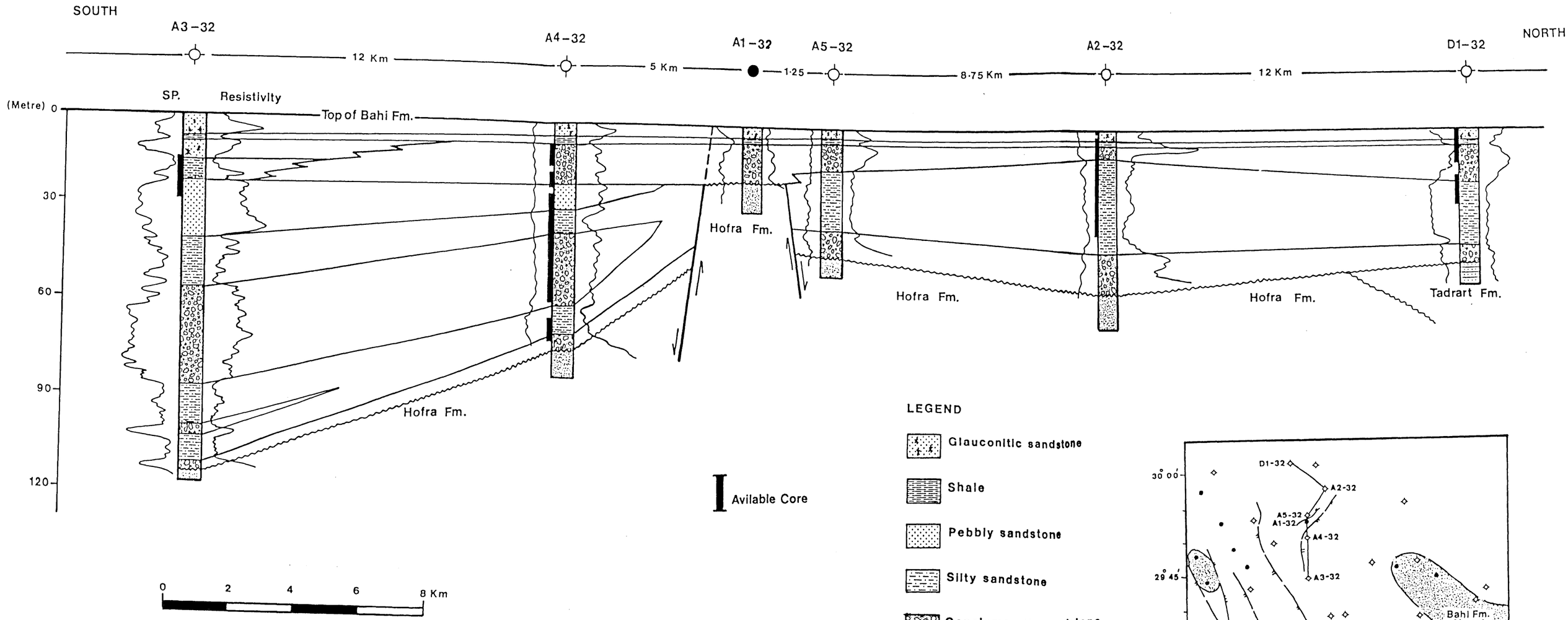

Avilable Core

LEGEND

- Glauconitic sandstone
- Shale
- Pebbly sandstone
- Silty sandstone
- Conglomeratic sandstone
- Massive sandstone
- Quartizitic sandstone

Fig. 3.8 Lithological correlation of the Bahi Formation and its sub units along the line shown on the inset map. Datum at the top of the Bahi Formation. Shows local fault control during deposition of the lower part of the Bahi Formation.

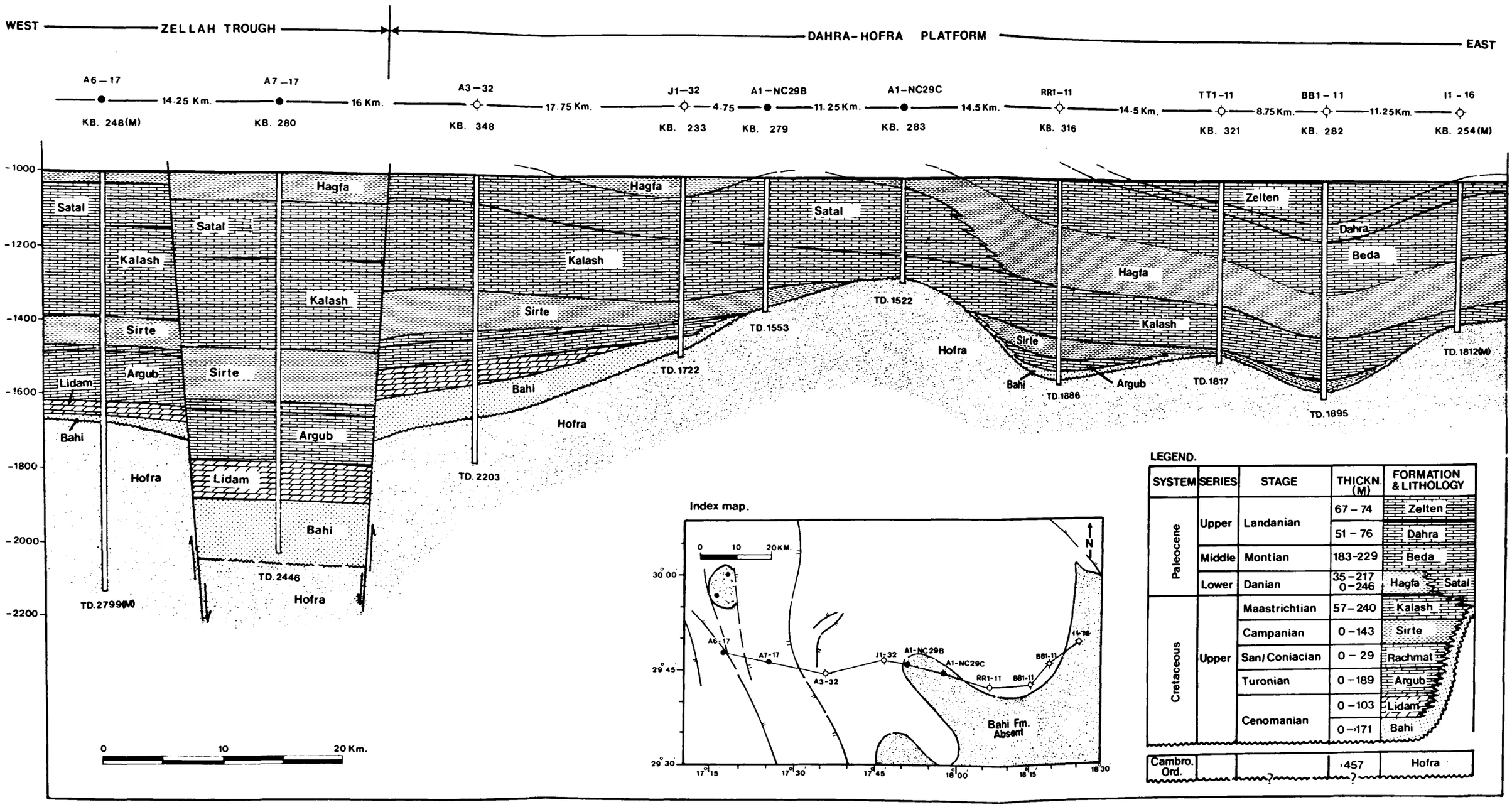

Fig. 3.9 Detailed scale section across a small area of the Sirte Basin, incorporating boreholes and wells I1-16, BB1-11, TT1-11, RR1-11, A1-NC29C, A1-NC29B, J1-32, A3-32, A7-17 and A6-17 shown on the inset map. This shows typical small-scale structural and topographical controls which have affected the thickness distribution of the Bahi Formation and some younger formations.

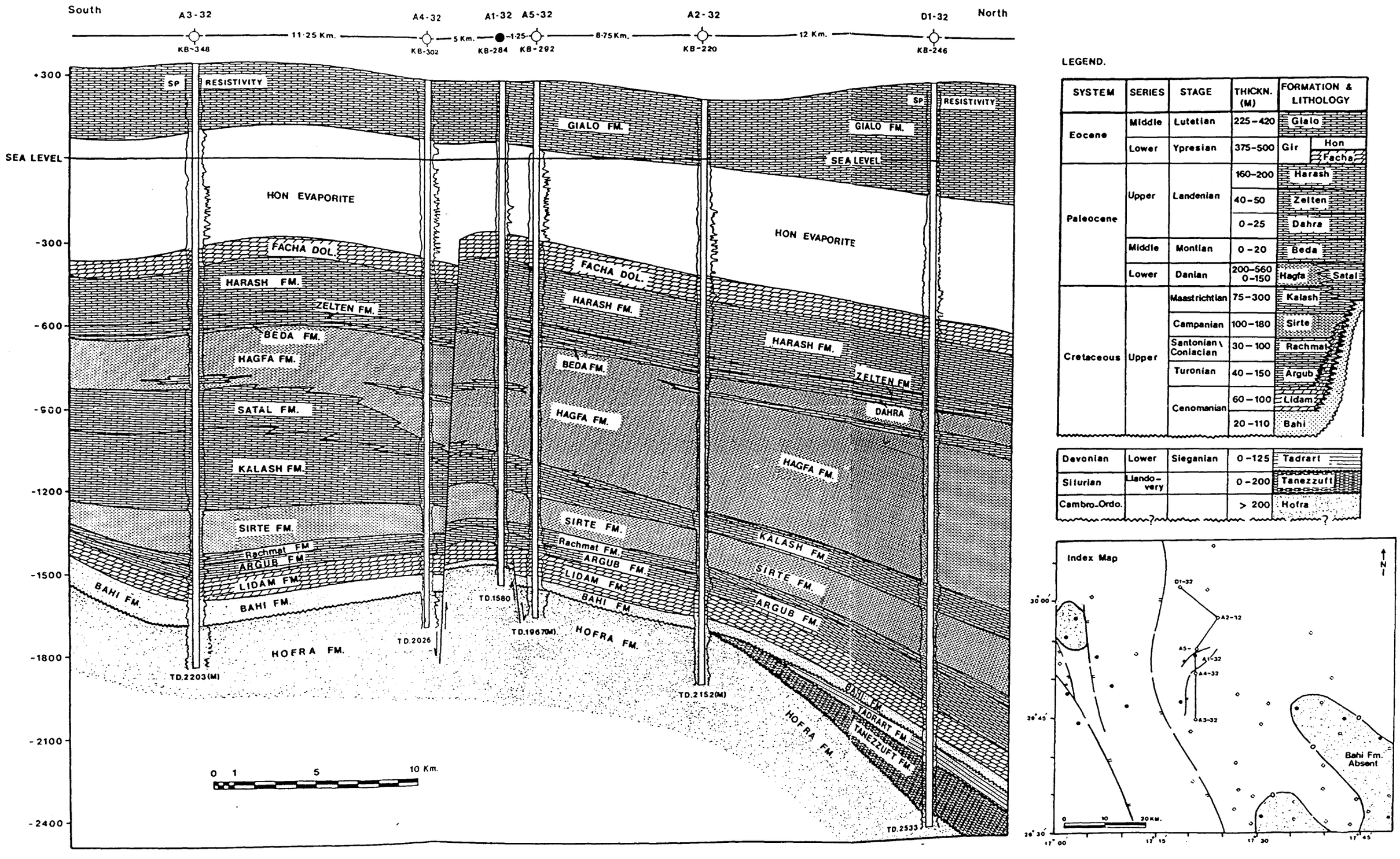

LEGEND.

SYSTEM	SERIES	STAGE	THICKN. (M)	FORMATION & LITHOLOGY
Eocene	Middle	Lutetian	225–420	Gialo
	Lower	Ypresian	375–500	Gir / Hon / Facha
Paleocene	Upper	Landenian	160–200	Harash
			40–50	Zelten
			0–25	Dahra
	Middle	Montian	0–20	Beda
	Lower	Danian	200–560 0–150	Hagfa / Satal
Cretaceous	Upper	Maastrichtian	75–300	Kalash
		Campanian	100–180	Sirte
		Santonian \ Coniacian	30–100	Rachmat
		Turonian	40–150	Argub
		Cenomanian	60–100	Lidam
			20–110	Bahi
Devonian	Lower	Sieganian	0–125	Tadrart
Silurian	Llando-very		0–200	Tanezzuft
Cambro-Ordo.			> 200	Hofra

Fig. 3.10 Geological section along the line shown on the inset map, to show structural controls on the distribution of the Bahi Formation and overlying formations of Late and post Cretaceous age.

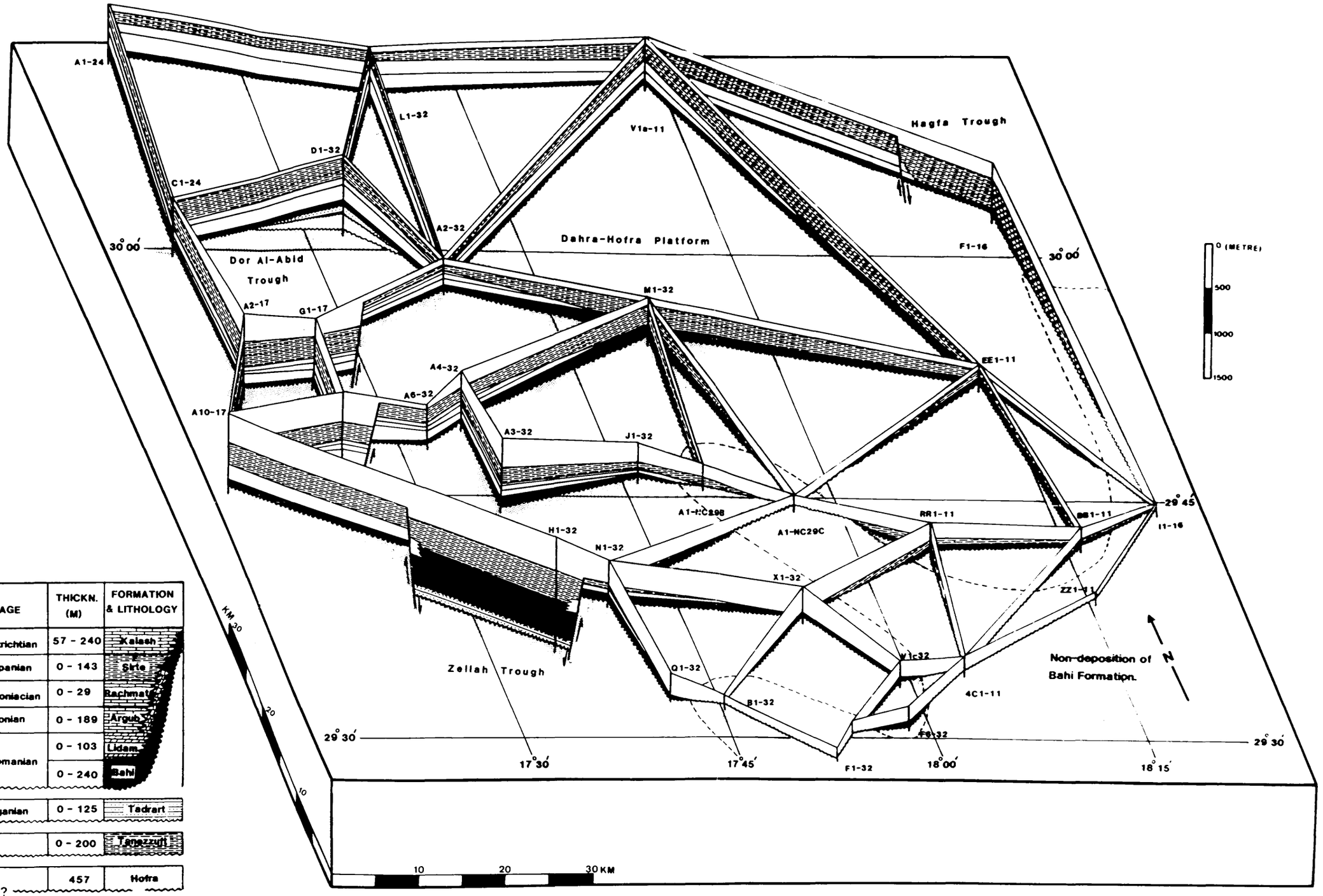

SYSTEM	SERIES	STAGE	THICKN. (M)	FORMATION & LITHOLOGY
Cretaceous	Upper	Maastrichtian	57 - 240	Kalash
		Campanian	0 - 143	Sirte
		San/Coniacian	0 - 29	Rachmat
		Turonian	0 - 189	Argub
		Cenomanian	0 - 103	Lidam
			0 - 240	Bahi
Devonian	Lower	Siegenian	0 - 125	Tadrart
Silurian	Llandovery		0 - 200	Tanezzuft
Cambro-Ord. ?	?	?	457	Hofra

Fig. 3.11 Fence diagram showing the general distribution of thr various Upper Cretaceous formations in the western part of the Sirte Basin, and their structural controls. N.B. The Bahi Formation and locally overlying Lidam Formation are clearly very diachronous. For clarity, only certain formations are indicated with shading. 1. Cambro-Ordovician 2. Devonian 3. Bahi (black) 4. Sirte.

CHAPTER 4

PETROGRAPHY

4.1 Introduction

The subsurface sediments of the Bahi Formation in the Sirte Basin are entirely clastic. Clastics are the insoluble materials left after the chemical breakdown and disintegration of pre-existing rocks and their mineralogical composition depends in part on the nature of the parent rock and in part on its maturity (Pettijohn, 1957, 498). Although some minerals may be lost or modified by weathering in the source area, by transportation to the site of sedimentation and by diagenesis (Pettijohn *et al.* 1973, 298), the remaining minerals are commonly the only guide to provenance (Carver,1971).

The mineralogy of the Bahi Sandstone has been examined by Baird,1967; Barr & Weegar,1972. No data of any substance has been formally published.

The aims of these petrographical studies are:

- To identify the petrographical composition of the Bahi Formation, to show the mineralogical abundance distribution throughout the formation, to identify the heavy and clay minerals within it and to identify any changes through time.
- To provide information about the provenance of the Bahi sediment from the accumulated data.

A detailed petrographic study of the Bahi Sandstone was carried out using a petrographic microscope fitted with a Swift automatic point counter. Ninety-two samples from the A2-32, A3-32, A4-32, D1-32, and F6-32 boreholes were mineralogically analysed, with 300 grains counted from each slide using the area count technique described by Galehouse (*In* Carver, 1971) without individual grains being counted more than once.

Table. 4.1 records the results of such a point count analysis of the 92 thin sections.

4.2 Mineralogical Classification

Many classifications are concerned mainly with the mineralogy and texture of sandstones (e.g. Pettijohn,1957; Mc Bride,1963; Pettijohn *et al.* 1973; Folk,1974, and others).

The mineralogical composition of the Bahi Sandstone Formation has been classified according to McBride (1963); which depend on the following framework mineral groups:

Q - Total quartzose grains of both poly- and monocrystalline varieties. Chert, orthoquartzite and metaquartzite lithic fragments are included.

F - Monocrystalline feldspar grains (plagioclase & K-feldspar).

L - Lithic fragments of sedimentary, igneous & metamorphic rocks.

These framework minerals are recalculated to 100% and are plotted on ternary diagrams (Fig. 4.1). All the points for the Bahi Sandstone in the five boreholes fall in the subarkosic quartz arenite fields (Fig. 4.2).

4.3 Mineralogical Framework

Microscopic examination of the Bahi samples shows that the sandstone is essentially composed of detrital grains of monocrystalline and polycrystalline quartz and both feldspar (plagioclase & K-feldspar) with illite, kaolinite, chlorite, dolomite, anhydrite and rock fragments also variably present. A little glauconite is present in the uppermost part (marine cycle) of the formation.

4.3.1 Quartz

Quartz is the most abundant constituent of most sands and sandstones because of its hardness, lack of good cleavage and lack of metallic cations. Quartz grains in the Bahi Formation show slight to strong undulatory extinction, with the majority of grains showing single outgrowth enlargement. Grain margins sometimes exhibit a corroded intergrowth with clay minerals or carbonates. The predominance of subangular and subrounded, poorly sorted, coarse to very

coarse quartz grains are related to diagenetic overgrowths. Haematite films show the original grains to have been well-rounded. (see e.g. Plts 4.6, 4.11 cf. with Plt 4.17). They dominate particularly the upper part of the formation.

Several different types of quartz are found in the Bahi Sandstone including grains of metamorphic, plutonic, and polycrystalline varieties. Abundant mineral inclusions of minute zircon, rutile, tourmaline and opaques have been seen in many grains. Monocrystalline quartz is probably largely of plutonic origin and polycrystalline quartz is largely metamorphic (Folk,1974, 67-77).

1. Monocrystalline quartz grains

Monocrystalline quartz grains with extinction varying from even and slightly undulose to highly undulose with abundant mineral inclusions are the most abundant minerals in the Bahi Sandstone. Such grains constitute an average of 66.28, 73.65, 73.43, 62.84 and 80.88% of the total rock volume, and 90.25, 89.42, 86.95, 87.61 and 94.38% of the total quartz in the A2-32, A3-32, A4-32, D1-32 and F6-32 boreholes respectively. Both non-undulatory and undulatory monocrystalline quartz grains are present throughout the formation.

Non-undulatory quartz is defined as a quartz crystal unit which is completely extinguished upon very slight (less than one degree) rotation of the flat microscope stage (Blatt & Christie, 1963). It is the end process of the breakdown of polycrystalline quartz. Non-undulose monocrystalline quartz grains throughout the formation generally are more common than the undulose variety (Plate 4.1).

Undulatory monocrystalline quartz is defined as any single quartz crystal unit which is not completely extinguished upon a very slight rotation of the flat microscope stage. Quartz which has been subjected to considerable pressure shows strain shadows or undulatory extinction. It occurs when quartz crystals have been deformed by stresses during or after their crystallisation in their original igneous or metamorphic context (Blatt *et al.* 1972). Quartz from metamorphic sources shows a marked wavy extinction (Plate 4.2). The presence of undulatory quartz grains is the result of the breakdown of polycrystalline undulatory quartz grains (Blatt &

Christie,1963). The zones of undulatory extinction may be gradational or may be separated by more or less well-defined planes (Blatt, 1967).

The predominance of monocrystalline quartz grains suggests that the Bahi Sandstone is derived largely from older pre-existing sedimentary sources, but significant amounts of polycrystalline quartz and feldspar suggest an additional contribution from metamorphic or igneous sources.

2. Polycrystalline quartz grains

Polycrystalline quartz grains are those which consist of two or more quartz crystal units of different optical orientation, each of which may be either strained or unstrained. The boundaries between adjacent crystal units may be either planar, curved, or sutured (Blatt, 1967). Where they have been subdivided into two groups, they comprise either composite quartz grains which make up an aggregate grain of two or more discrete extinguishing units separated by smooth, non-sutured boundaries or they are metaquartzite fragments consisting of two or more units that are separated by sutural boundaries.

Polycrystalline quartz grains constitute an average of 6.45, 8.25, 10.63, 8.65 and 4.82% of the total rock volume and 8.78, 10.02, 12.59, 12.06 and 5.62% of the total quartz in the five boreholes studied. The two main types of polycrystalline quartz grains which have been found in the Bahi Sandstone with sutured boundaries and more than three subcrystals, probably indicate a metamorphic origin or stressed granite (Plate 4.3), those with straight boundaries between subcrystals, indicating a plutonic origin (Folk, 1974, 73). Well rounded grains of polycrystalline quartz are likely to have undergone weathering and abrasion for long periods (Plate 4.4).

A number of attempts have been made to utilise the polycrystalline quartz grains as a guide to provenance (Blatt & Christie, 1963; Conolly, 1965; Blatt, 1967; Folk, 1974; Basu *et al.* 1975, Young, 1976; Mack *et al.* 1981, 1983). Mack *et al.* (1981) used polycrystalline quartz as a provenance indicator, employing a minor modification of Young's method (1976) but retaining the three original stability fields: low grade metamorphic, high grade metamorphic and

plutonic polycrystalline quartz. A polycrystalline index versus instability index was used. The polycrystalline index is the ratio of polycrystalline quartz to total quartz and the instability index is the ratio of unstable to total polycrystalline quartz. Unstable polycrystalline quartz is characterised by elongated crystal units, sutured margins between crystal units, undulosity of crystal units, and bimodal size distribution of these units. A high instability index is commonly related to low grade metamorphic source rocks, which provide a large amount of unstable polycrystalline quartz, whereas a low polycrystalline index is the result of the dilution of a quartz population with monocrystalline quartz from sedimentary sources (Mack *et al.* 1983).

The average number of crystal units in sand size grains of polycrystalline quartz varies depending on the source rock (Blatt *et al.* 1972, 270-273), these authors noted that in general, plutonic polycrystalline quartz is more coarsely crystalline (2-5 crystal units per grain), and that gneissic polycrystalline quartz is more finely crystalline (>5 crystal units per grain) for a given grain size. Crystal units in polycrystalline quartz from schist have an intermediate number.

The presence of stable and unstable varieties of polycrystalline quartz in the Bahi Formation shows that the sandstone has probably received a contribution from several rock sources, such as plutonic and metamorphic and including schists.

4.3.2 Feldspars

Feldspars including both potash and plagioclase varieties have been found in the Bahi Formation. Plagioclase feldspars are mainly altered and there are a few colourless fresh grains (Plate 4.5), whereas potash feldspar grains are invariably represented by microcline which is sometimes fresh (Plate 4.6). The plagioclase is twinned according to the albite laws whereas microcline displays the typical "cross hatching" structure. The stratigraphical distribution of the feldspars indicates that fresh plagioclase feldspars exceed fresh potash feldspars throughout the formation but this itself may have little significance. The average abundance of total (altered and unaltered) feldspars is 5.59, 9.43, 6.57, 5.34 and 3.88%, of the total rock volume and 7.02, 10.22, 7.15, 6.9 and 4.33% of the framework grains in the five boreholes studied.

Feldspar grains are sometimes extremely vacuolised. Much of the plagioclase feldspar

shows replacement by calcite, dolomite, anhydrite and iron oxide: kaolinitization is common. Skeletal grains of feldspar that have not been completely replaced by calcite or haematite or which have undergone direct dissolution are quite common in many samples: they have rugged boundaries and corroded interiors (Plate 4.5).

4.3.3 Lithic Fragments

Rock fragments comprise an average of 0.60, 0.49, 0.88, 0.33 and 0.03% of the total rock volume and 0.75, 0.53, 0.96, 0.39 and 0.03% of the total framework grains respectively in the A2-32, A3-32, A4-32, D1-32 and F6-32 boreholes. Fragments of sedimentary rocks are the principal types present and include quartz siltstone and very few metamorphic fragments. Some factors which influence the abundance of rock fragment in the sediments, are the nature of the source area, the maturity of the sediments and the mean grain size.

4.3.4 Accessory Minerals

Accessory minerals are represented by green glauconite, muscovite and heavy minerals such as zircon, rutile, tourmaline and opaques.

Glauconite is defined as a variety of illite with a high content of iron (Brust, 1958). Glauconite pellets are so named for any heterogeneous green earthy pellet that contains the mineral glauconite (iron-rich illite/montmorillonite) together with other minerals (James *et al.* 1974). The distribution of glauconite in the Bahi Sandstone is confined to the uppermost part. Grains are rounded to subrounded and occur in two modes - a scattering of green pellets between quartz grains (Plate 4.7-4.8) and a concentration of fine green pellets in seams. The presence of glauconite indicates a shallow marine environment such as is found mainly where marine continental shelf sediments are deposited, particularly where there is some turbulence, low rates of sedimentation and some organic matter (Reineck & Singh, 1980,151).

4.4 Heavy minerals

Heavy minerals have been studied by many workers (e.g. Brammall, 1928; Krynine,

1946; Vitanage, 1957; Heimlich *et al.* 1975; Smale, 1987; Mezzadri & Saccani, 1989 and others) as a guide to source rock lithologies and dispersal patterns. Heavy minerals are also useful in evaluating diagenetic history as well as the tectonic, weathering and erosional histories of the source area.

Twenty-one samples of the Bahi Sandstone have been analysed from three of the boreholes (A2-32, A4-32 and F6-32). Samples were crushed using a jaw crusher and a mortar and pestle. The heavy minerals were extracted from that portion of the sand fraction of each sample which remained on the 0.125mm sieve (0.25mm to 0.125mm) and on the 0.062mm sieve (0.125mm to 0.062mm). Separation of the heavy minerals was carried out by settling using Tribromomethane (S.G. 2.81), as outline by Carver (1971). After separation, the heavy minerals were mounted on microscope slides for petrographic study.

Figure 4.3 shows the mean percentages of the heavy minerals in the Bahi Sandstone in the three boreholes studied. Heavy minerals assemblages are similar in all samples indicating similar sources throughout, originally plutonic and metamorphic but degrees of rounding indicates that the assemblages are largely recycled. The heavy-mineral assemblages from the Bahi Formation consist of two classes: opaque and non-opaque heavy minerals:

4.4.1 Opaque Minerals

Opaque minerals such as haematite, limonite and magnetite are present in all samples. All have a high specific gravity due to their iron content. They survive because of their stability in the kind of oxidising environments created when leaching of rocks under tropical conditions is prevalent. The average of mean percentages of the opaque minerals is 15.75, 12.69, and 11.25% of the total heavy minerals in the three boreholes investigated.

4.4.2 Non Opaque Minerals

Three types of non-opaque heavy minerals - zircon, tourmaline and rutile - have been recognised.

1. Zircon

Zircon is an ultra-stable mineral: it is very hard, inert and can survive much recycling (Folk,1974,97). Zircon crystals formed initially by crystallisation from a magma and they develop typically as euhedral or subhedral, sharply-faceted crystals (Heimlich *et al.* 1975). The latter workers pointed out that weathering of igneous rocks normally causes little or no change in the morphology of zircons. However, when subjected to aqueous transport, however, such zircons become rounded to varying degrees due to attrition.

The average of mean percentages of zircon in the A2-32, A4-32 and F6-32 boreholes is 41.86, 50.51, and 58.0% of the total heavy minerals in the samples. The zircon grains recognised in the Bahi sediment are mainly well rounded to subrounded with few subhedral grains (Plate 4.9). They are colourless, commonly worn and contain a variety of minute inclusions. This suggests that most of the Bahi zircons are likely either to have undergone weathering and abrasion for long periods or they are recycled and derive from a pre-existing sedimentary source such as the Hofra Formation. A very few zircons may be first cycle grains having been derived directly from a distant plutonic source

2. Tourmaline

Tourmaline is one of the most widespread of the non-opaque heavy accessory constituents in sediments.

The average of mean percentages of the Bahi tourmalines in samples from three boreholes is 30.93, 24.49, and 21.20% of the total heavy minerals present (Plate 4.10). All are well-rounded to sub-rounded. Tourmaline occurs in the Bahi Formation with a variety of colours. Brown predominates, in shades ranging from red-brown, through yellow-brown to strong yellow and pale yellow to almost colourless. Blue tourmaline is uncommon, the shade ranging from deep indigo-blue to pale lavender-blue and sometimes almost colourless. The brown and yellow-brown varieties are the most common and probably originally derive from a metamorphic source (Blatt *et al.* 1972, 294) but are probably recycled. The relatively rare blue varieties may have come originally from a plutonic source and may also have been recycled. The overall

pattern suggests a derivation from a reworked sediment containing several tourmaline varieties from different, largely metamorphic, original sources.

3. Rutile

The third most abundant of the non-opaque heavy minerals is rutile. The average mean percentages of rutile in the three boreholes is 13.54, 12.29, and 9.60% of the total heavy minerals present (Plate 4.9-4.10). It is present in the Bahi Sandstone as mainly reddish-brown to dark red, rounded to subrounded crystals, with a few elongated grains, all reddish-brown. This again suggests a predominantly reworked source rock, with most of the grains deriving originally from plutonic and metamorphic terranes. A few may be first cycle grains.

4.5 Diagenesis

Diagenetic processes have produced different effects for each of the Bahi Sandstone lithologies. These have been controlled by local properties such as texture, chemical composition, biological activity, compaction of the sediments, type and movement of pore water and also regional properties such as the burial depth of the sandstone and its structural setting.

The Bahi Sandstone has undergone through compaction involving pressure solution, cementation, replacement and dissolution. The relative order of diagenetic processes can be determined by the textural relationships between the authigenic minerals and the framework-grains. The following diagenetic processes and minerals have been recognised:

4.5.1 Compaction

Mechanical compaction of sandstone and shale reduce the bulk volume of the sediment by decreasing the size of the pore spaces. Compaction of sandstone results in loss of porosity by mechanical rotation and slippage of grains leading to tighter packing. This involves deformation of ductile grains, pressure solution, breakage of brittle grains and mechanical pressure solution. The probable major mechanism of compaction has been grain

slippage. Sutured contacts resulting from pressure solution (Plate 4.11) and breakage of brittle grains, such as quartz, distortion and bending of micas between sand grains are common locally.

4.5.2 Cementation

Sands with open spaces are normally first lithified by the introduction of a cement, deposited from circulating solutions, or formed by redistribution of some original constituent such as $CaCO_3$ or colloidal silica. However, petrographic examination of the Bahi Formation has revealed quartz, haematite, calcite, dolomite, anhydrite and clay minerals as important elements in various combinations as cementing or binding materials in the sandstone. A sequence of deposition has been established for these minerals. In some samples, secondary quartz is the only precipitated mineral (see Plate 4.11) but in others, a combination of two or three minerals is present.

1. Quartz

Quartz as an overgrowth to the original quartz grains is the dominant authigenic mineral in the Bahi Sandstone (Plates 4.6, 4.11 & 4.17). The lower part of the formation, composed mainly of fine sand and silt-sized grains has less quartz cement because of the development of early haematite and illite deposits (Plates 4.13-4.14), whereas the middle part of the formation, composed mainly of coarse to very coarse sand size grains, contains the highest proportion of quartz overgrowths. The upper part of the formation, however, although relatively coarse-grained, has less secondary silica cement. This could relate to the presence of early carbonate cements, anhydrite and clay mineral accumulations in the interstices. Pittman (1972), indicated that much of the secondary quartz in sandstones is probably derived from pressure solution, but other possible sources of silica are: (1) solution of siliceous shales; (2) devitrification of volcanic glass; (3) decomposition of feldspars; (4) solution of silica secreting organisms, such as diatoms, radiolaria, and sponges; (5) precipitation from river waters; (6) solubilising effects of

certain naturally occurring organic complexes on silica, which can lead to precipitation of quartz overgrowths; (7) precipitation directly from sea water.

2. Haematite

Early haematite occurs in the Bahi Sandstone as a grain coating, the mineral being usually present as an investing pellicle around each detrital quartz grain and is most clearly evident where secondary silicification has taken place (Plates 4.1, 4.4 & 4.6), this iron oxide coating becoming enclosed by the new crystal growth. Late haematite cement occurs as pigment in red beds, usually in the lower part of the formation, as randomly distributed authigenic crystals filling pore spaces (Plates 4.5 & 4.6). In most cases haematite coating together with the pore filling crystals also preceded the deposition of calcite, dolomite and anhydrite. Haematite is occasionally found as a replacement material of such unstable minerals as feldspar.

3. Calcite

Calcite cement is present in the upper part of the Bahi Sandstone and may originally have filled all pore spaces in this part of the formation. Calcite cement commonly coats the surface of corroded quartz grains resulting in an irregular, patchy distribution. Almost certainly it originates from percolating solutions deriving from overlying formations.

4. Dolomite

Dolomite cement is present occasionally and is usually associated with anhydrite in the upper part of the formation. It varies from pore-filling microcrystalline rhombs to coarse anhedral mosaics and large poikilotopic crystals (Plate 4.12 & 4.15). Early dolomite precipitation may originate from percolating solutions deriving from the overlying Lidam Formation or other dolomite-rich formations.

5. Anhydrite

Anhydrite cement is present in the upper part of the formation and is most abundant in the A2-32 borehole, (Plate 4.12-4.16). It is completely absent in the middle and lower parts of the formation. The association of dolomite with the anhydrite, could also result from the sinking of a denser evaporite brine from the overlying formation (Pettijohn *et al.*, 1973). Thus the occurrence of anhydrite as a cement is probably either related to evaporite conditions at the time of sedimentation or to movement of hypersaline pore waters from an overlying evaporite-bearing formation (Murray, 1964). The Lidam Formation could be the source rock.

6. Clays

There are no published data concerning the clay mineralogy of the Bahi Sandstone Formation. Two methods (XRD & SEM) have been used to identify the clay minerals and their nature.

A) X - ray diffraction (XRD)

The clay fractions from twenty-four samples from the A2-32, A4-32 and F6-32 boreholes have been X-rayed. Several different methods of extraction and preparation of the clay minerals prior to the application X-ray diffraction techniques have been published (e.g. Johns *et al.* 1954; Weaver,1958; Villumsen & Nielson,1971, and others). The method used here in that known as oriented samples preparation. The sand fraction was separated from the clay and silt fraction by wet-sieving through a 63μ sieve, the clay fraction (<2μ) was separated from the silt fraction (2-63μ) by repeated decanting from aqueous suspension. Oriented preparations, 28x48mm in size, were made of the untreated clay fraction, allowing the clay-water suspension to dry on the glass slides overnight. These preparations were run on a Phillips X-ray diffractometer. The untreated preparations were then glycolated with ethylene glycol vapour for 24 hours. After this treatment the preparations were again run on the diffractometer, then heated to 550 ^{o}C for one hour and X-rayed again.

Clay minerals can be identified more easily by diffraction analysis of their basal (001)

crystallographic planes, so the oriented aggregates prepared as indicated above give the best possible diffraction data. The following criteria have been used to identify the various clay minerals present (Thorez, 1976, Carroll, 1970, Schultz,1964):

A) Illite is characterised by a series of X-ray diffraction peaks at 10Å, 5Å, 3.3Å, etc., that are not appreciably affected by either glycolation or heat treatment.

B) Chlorite is characterised by a series of basal X-ray diffraction peaks at about 14Å, 7Å, 4.8Å, 3.5Å, etc., but heating at 550 ^{o}C for 30 mins causes a change in chlorite structure, increasing the 14Å reflection greatly in size: the other peaks virtually disappear.

C) Kaolinite is characterised by a series of basal X-ray diffraction peaks at about 7Å, 3.5Å, etc., which remain unchanged upon glycolation or thermal heating to 450^{o}C, but the structure collapses to an X-ray amorphous mineral on heating to 550^{o}C.

In this study, identification of the peaks have been made using the standard table of Chen (1977) and Carroll (1970). All of the samples exhibit similar patterns, but there are different peak intensities from sample to sample reflecting different relative abundances.

A representative pattern shows illite, kaolinite and chlorite (Figs. 4.4-4.6). Chlorite is present in two samples in the uppermost, glauconite-bearing sandstone of the formation (A2-32 borehole), whilst illite is the dominant clay mineral in all other samples from the three boreholes. Kaolinite is the next most abundant clay mineral in the formation.

B. Scanning Electronic Microscope (SEM)

Many recent studies have made use of the Scanning Electronic Microscope to identify and interpret the type, nature and origin of clay minerals (e.g. Sarkisyan, 1970, 1971; Pittman, 1974; Wilson & Pittman, 1977; Kantorowicz, 1984 and others).

Twenty-four samples from the Bahi Sandstone in the studied boreholes have been examined using Cambridge Instruments S360 Scanning Electronic Microscope with integrated link analytical A N 10,000 series EDX. techniques. Samples were coated with a gold palladium alloy. Three types of authigenic clay minerals were again investigated in the Bahi Formation.

1. Chlorite:

Chlorite is developed locally around most framework grains. Pore-filling chlorite is the dominant authigenic clay mineral to form in the uppermost part of the formation. In thin section chlorite rims are not detectable in most samples because of the extensive staining by haematite.

SEM investigation, however, reveals various crystal morphologies of this mineral but face-to-edge oriented flakes are most common (Plate 4.18). Such grains occur as dense rims around framework grains. Chlorite formed mainly from other clay minerals such as kaolinite or smectite in the presence of Fe^{2+} and/or Mg^{2+} in the basin of deposition.

2. Illite:

Authigenic illite is common throughout the Bahi Sandstone. It is found in the form of radially-arranged flakes and filaments growing into pore spaces between framework grains (Plate 4.19). Mostly the illite formed by the reaction of a pre-existing clay mineral with a potassium-bearing solution and/or reaction with a mineral such as K-feldspar (Macchi,1987).

3. Kaolinite:

Kaolinite is common in the middle part of the formation and is present as a partial replacement of feldspar. It forms 'books' or 'concertinas' consisting of stacked pseudo-hexagonal platy crystals, between framework grains (Plate 4.20). It probably formed by the kaolinitization of K-feldspar and commonly extends as a 'cement' into pore spaces.

4.6 Provenance

The term provenance has been used to embrace all the factors relating to production of a sediment. Most often it refers to the source rock from which sedimentary detritus was derived. Each type of source rock tends to yield a distinctive suite of minerals which therefore constitutes a guide to the character of that rock (Pettijohn, 1975, 484). Mineral associations in sandstone suites from different basins are a function of provenance types governed by their

plate tectonic settings. Many previous studies have documented the relationship between the framework mineralogy of sandstones, the provenance type and the tectonic setting of sedimentary basins (e.g. Dickinson, 1970; Reading,1978; Schwab, 1981, 1981; Garaham *et al.* 1976; Dickinson & Suczek, 1979; Dickinson & Valloni, 1980; Dickinson *et al.* 1983; Mack, 1984; Dutta & Suttner, 1986; DeCelles & Hertel, 1989 and others). Dickinson and Suczek (1979) showed that the mean composition of sandstone suites from different provenance terranes controlled by plate tectonics tends to form discrete and separate fields on QFL and QmFLt diagrams (see below). Proportions of key categories of grain types are determined by modal point counts. Two alternate sets of poles (QFL and QmFLt) are useful in this analysis (Graham *et al.* 1976)

A - For QFL diagrams, the poles are:

Q - total quartzose grains including lithic fragments such as chert and quartizite.

F - monocrystalline feldspar grains.

L- unstable polycrystalline lithic fragments of either igneous or sedimentary origin including metamorphic types.

B - For QmFLt diagram, the poles are:

Qm- Monocrystalline quartz grains.

F - Feldspar grains.

Lt - Total polycrystalline lithic fragments, including quartzose varieties.

The results of such modal point-count studies for the Bahi Sandstone Formation are shown in figures 4.7-4.8. As can be seen, the sandstone is to be classified as a subarkosic quartz arenite The majority of the samples lie in the craton interior and quartzose recycled sector. This observation suggests that the Bahi Sandstone was derived from a stable craton interior probably having a low relief and that much material derives from pre-existing and recycled quartzose sedimentary suites.

4.7 Conclusions

The significance of a mineralogical assessment of the Bahi Sandstone Formation leads to the following conclusions:

1: The Bahi Sandstone is to be classified as a subarkosic quartz arenite.

2: The most abundant minerals in the Bahi Sandstone are detrital grains of mono- and poly-crystalline quartz and feldspar. The former were originally well-rounded but have developed diagenetic overgrowths.

3: Glauconite is found only in the uppermost part of the formation. Its presence indicates the initiation of a truly marine cycle there.

4: The carbonate fraction (calcite, dolomite) and anhydrite cements are present only in the upper part the formation and probably originate from downward percolating solutions, whereas quartz overgrowth and haematite cements are present throughout the formation.

5: Radially-arranged flakes and filaments of illite which grow into the pore spaces is the dominant clay mineral throughout the Bahi Formation. 'Books' consisting of stacked pseudo-hexagonal platy crystals of kaolinite between framework grains is the second dominant clay mineral, whereas face-to-edge oriented flakes of chlorite are present in the uppermost part but seem to be absent lower down. They originate either directly from dissolution of K-feldspar or through reaction of pre-existing clay minerals with potassium-rich solution or directly with the K-feldspar itself.

6: Zircon, tourmaline, rutile and opaques are the dominant heavy minerals. There is a gross similarity in heavy minerals assemblages throughout the formation indicating a common source or sources. It is a mature assemblage and consists largely of recycled grains originally deriving from metamorphic and plutonic terranes.

7: The framework mineralogy suggests that the Bahi Sandstone was derived largely from a craton interior possessing pre-existing and recycled quartzose sedimentary rocks such as the Cambro-Ordovician Hofra Formation. The mature heavy mineral fraction also suggests a multi-cycled input originating from igneous and metamorphic terranes as does the presence of significant amounts of polycrystalline quartz and feldspar.

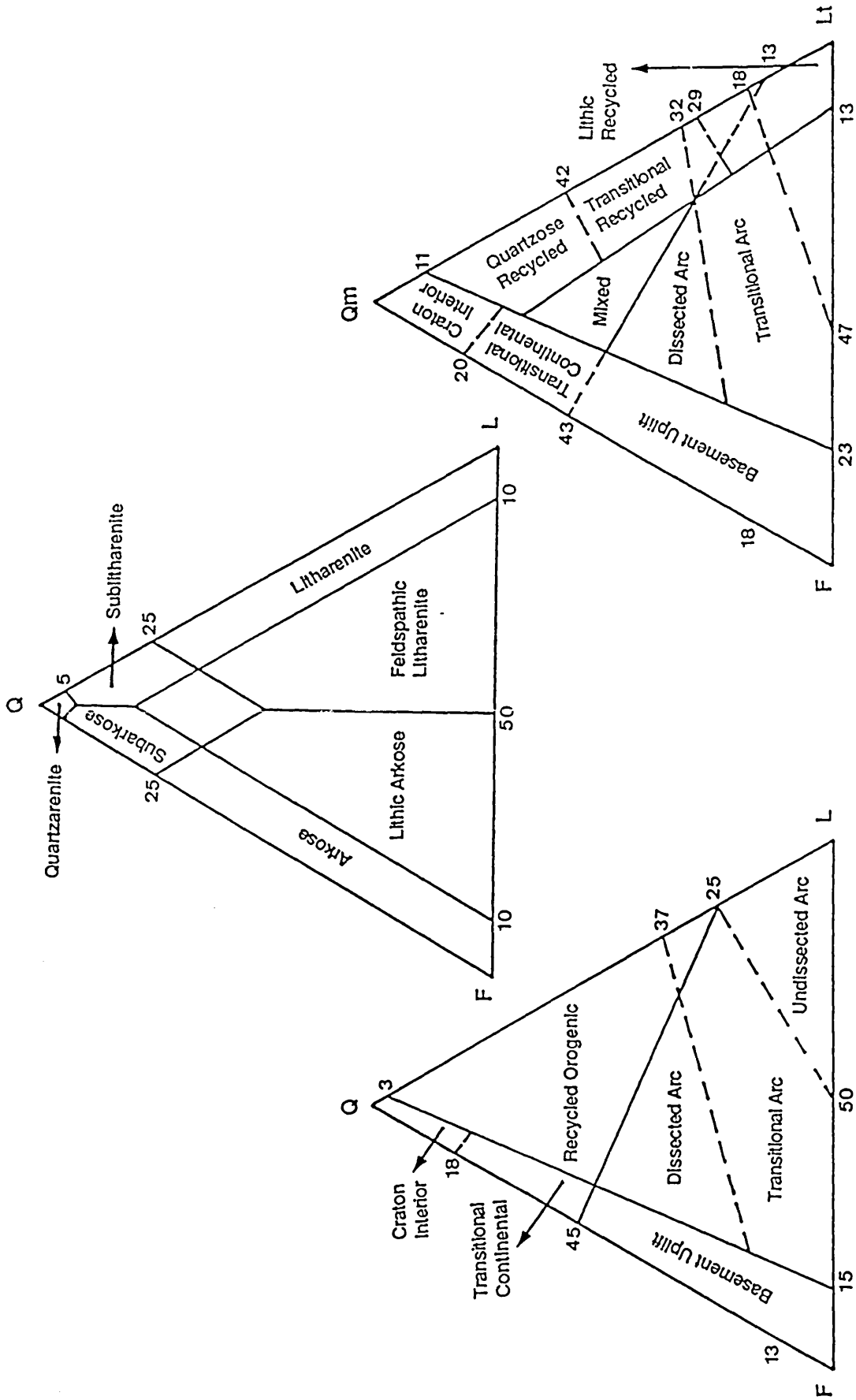

Fig. 4.1 Reference diagrams for petrographic data (1) QFL diagram (after Mc Bride, 1963) for classification of sandstones; (2) QFL diagram and (3) QmFLt diagram (after Dickinson *et al*, 1983) for indication of the sediment provenance.

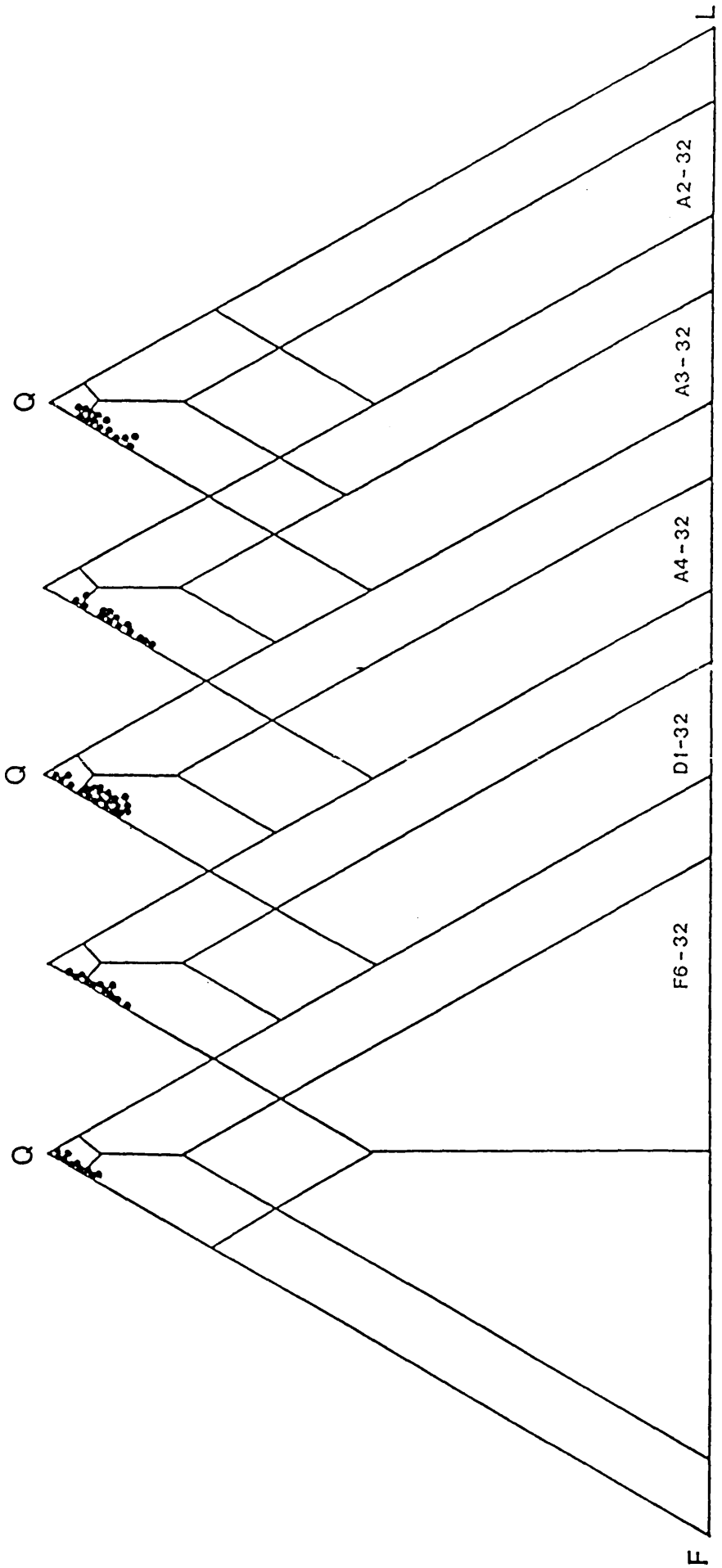

Fig. 4.2 QFL diagram showing the composition of the Bahi Sandstone in the five boreholes, indicating that the sandstone is a subarkosic quartzarenite.

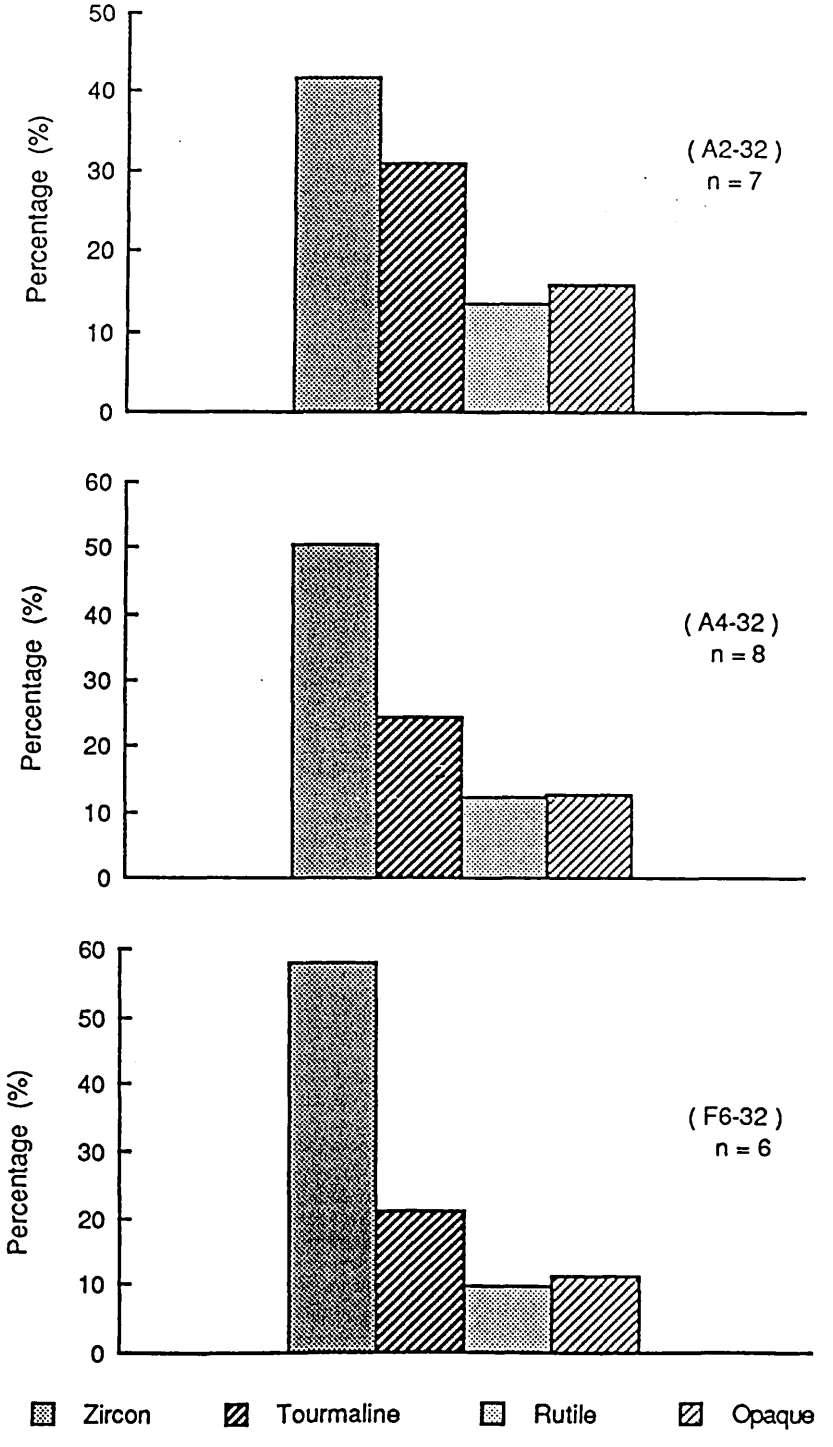

Fig. 4.3 Distribution of mean percentages of the heavy minerals of the Bahi Sandstone in three of the studied boreholes showing the gross similarity of the suites throughout.

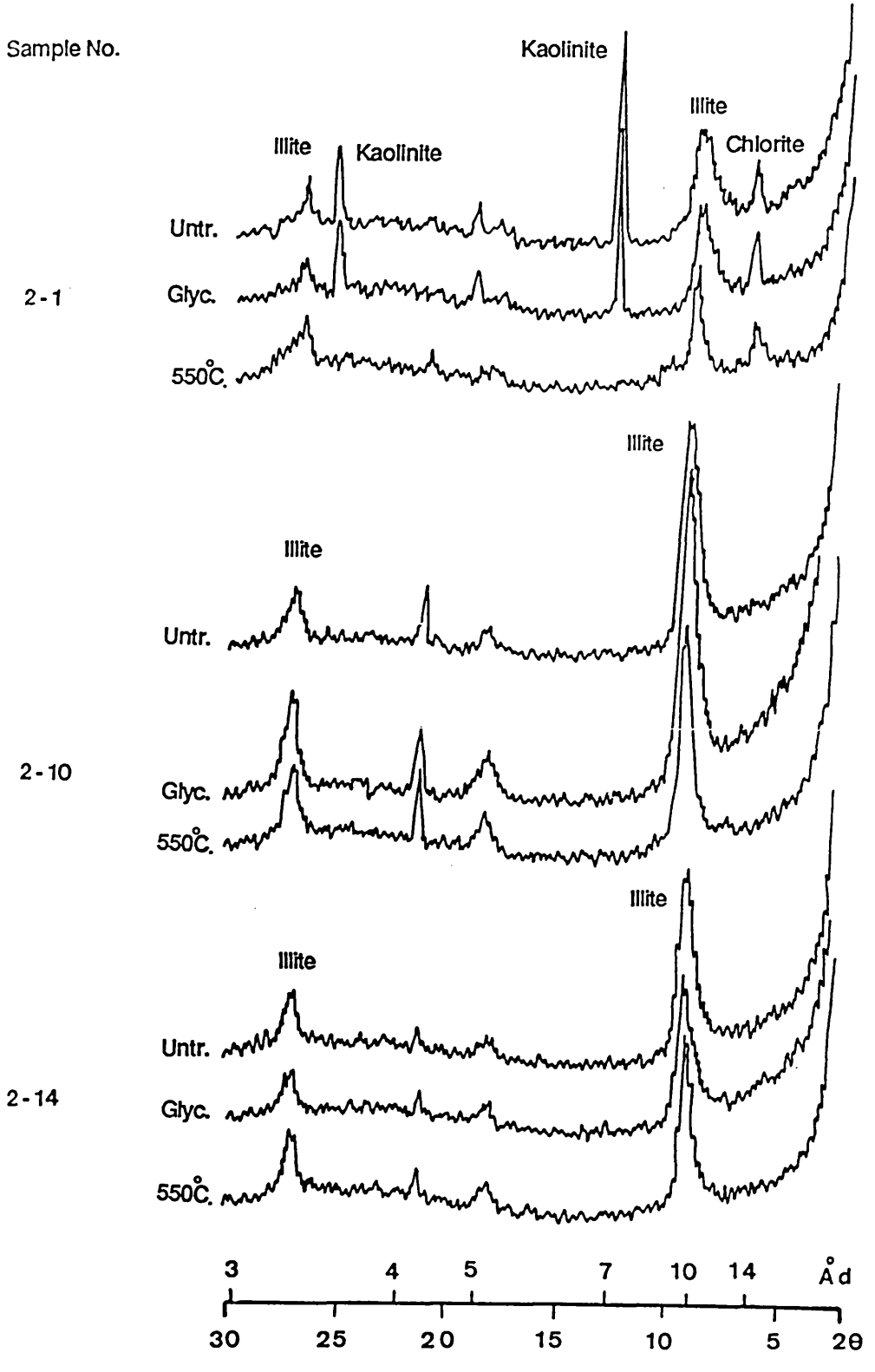

Fig. 4.4 X - ray diffractogram of the oriented clay fraction (<2 μm) in the Bahi Sandstone (A2-32 borehole). Three traces were run for these samples: Untreated (Untr.), samples that were glycolated with ethylene glycol (Glyc.), and samples that were heated to 550 °C for one hour (550 °C).

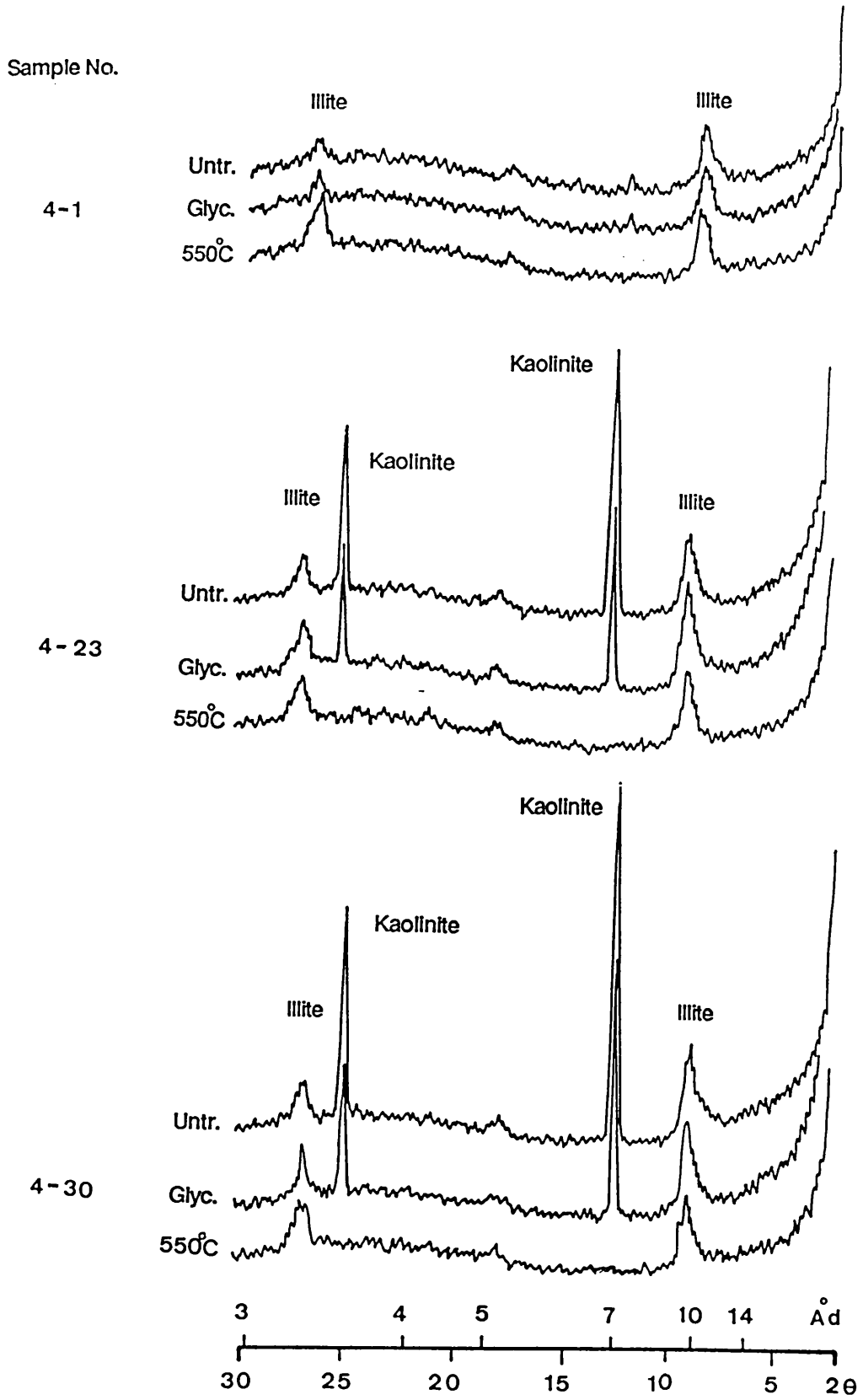

Fig. 4.5 X - ray diffractogram of the oriented clay fraction (<2 μm) in the Bahi Sandstone (A4-32 borehole). Three traces were run for these samples: Untreated (Untr.), samples that were glycolated with ethylene glycol (Glyc.), and samples that were heated to 550 °C for one hour (550 °C).

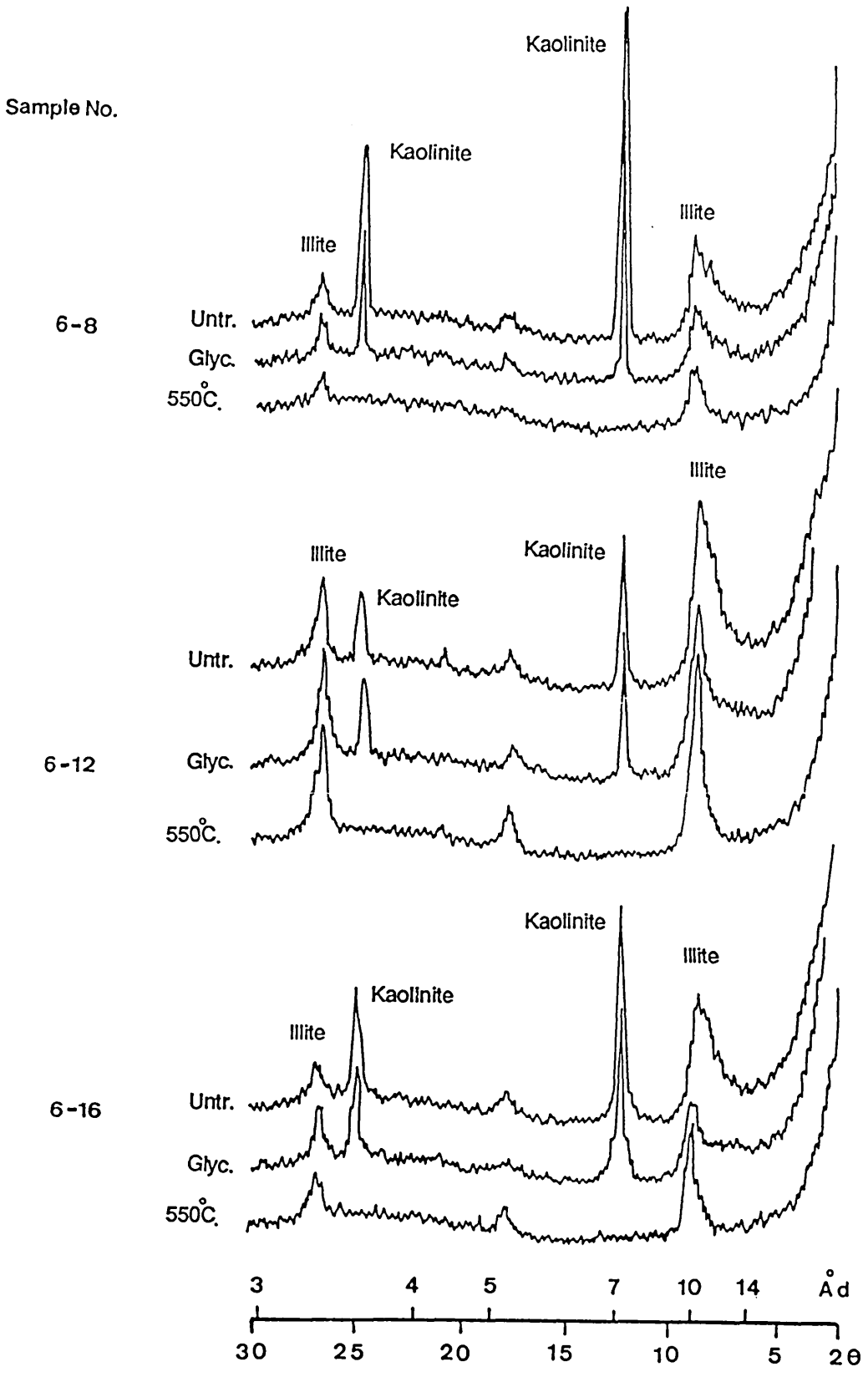

Fig. 4.6 X - ray diffractogram of the oriented clay fraction (<2 μm) in the Bahi Sandstone (F6-32 borehole). Three traces were run for these samples: Untreated (Untr.), samples that were glycolated with ethylene glycol (Glyc.), and samples that were heated to 550 °C for one hour (550 °C).

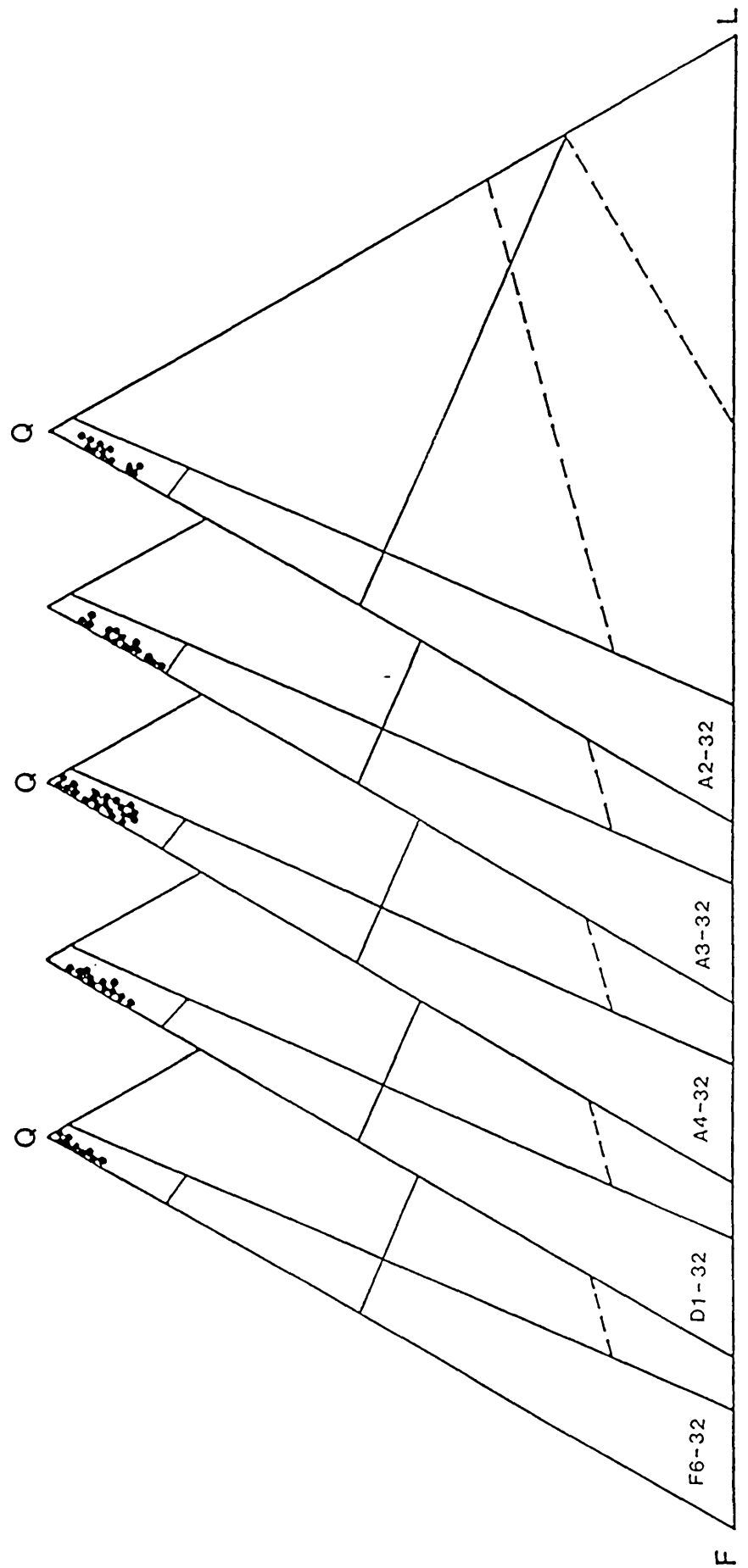

Fig. 4.7 QFL diagram to decipher the provenance of the Bahi Sandstone in the five boreholes, indicating that the sandstone was derived from a stable craton interior (see fig. 4.1).

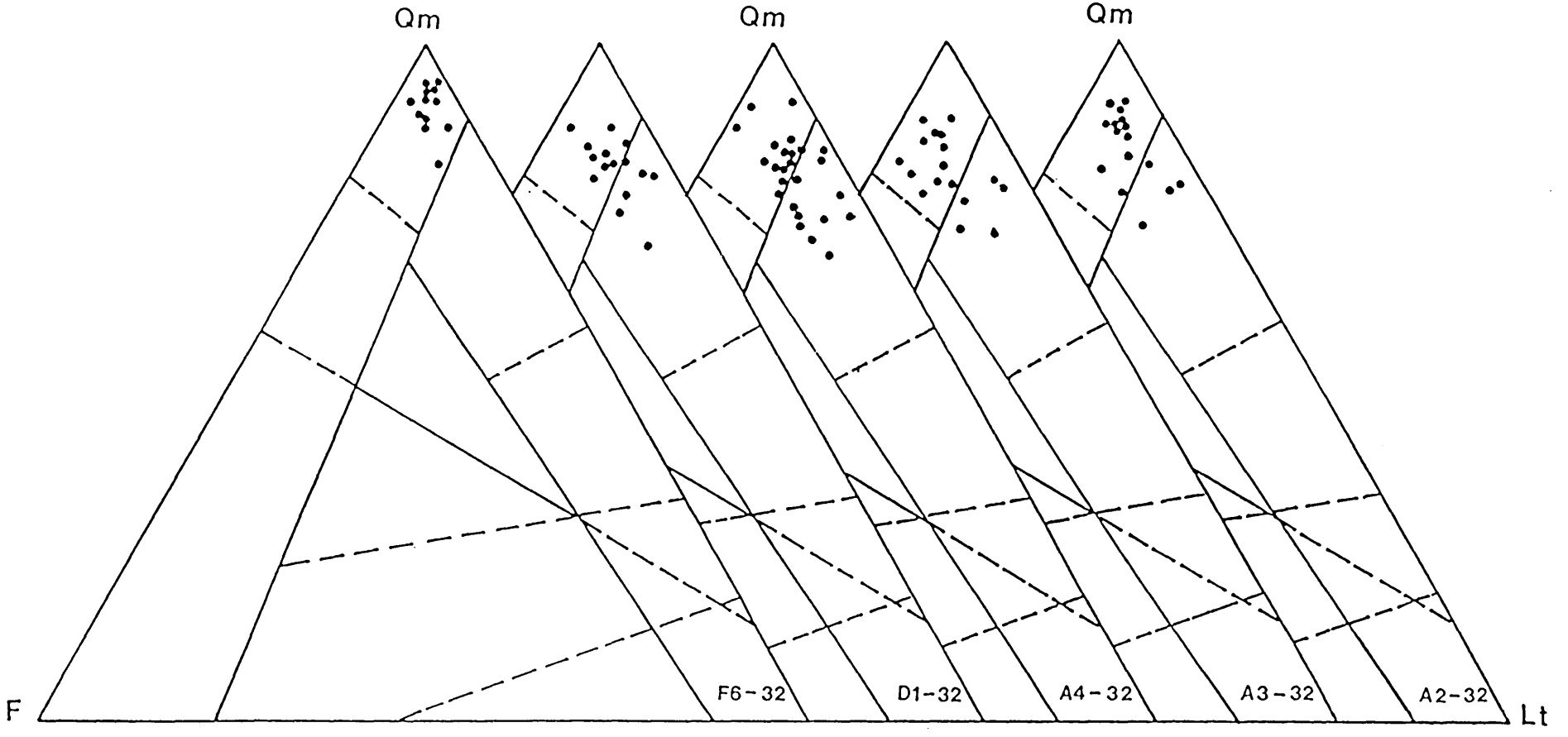

Fig. 4.8 QmFLt diagram to decipher the provenance of the Bahi Sandstone in the five boreholes, indicating that the sandstone was derived from a stable craton interior and also from a recycled quartzose sedimentary source or sources (see fig. 4.1).

Plate 4.1 Photomicrograph, XN. Well rounded quartz grain with authigenic overgrowth. The original grain is outlined by a thin layer of inclusions (probably clay or iron oxide). Sample from the upper part of the formation. F6-32 borehole, depth=9.7m below top of formation.

Plate 4.2 Photomicrograph, XN. A single-crystal quartz grain with strongly undulose extinction indicate of metamorphic origin. Sample from the upper part of the formation, D1-32 borehole, depth= 2.0m below top of formation.

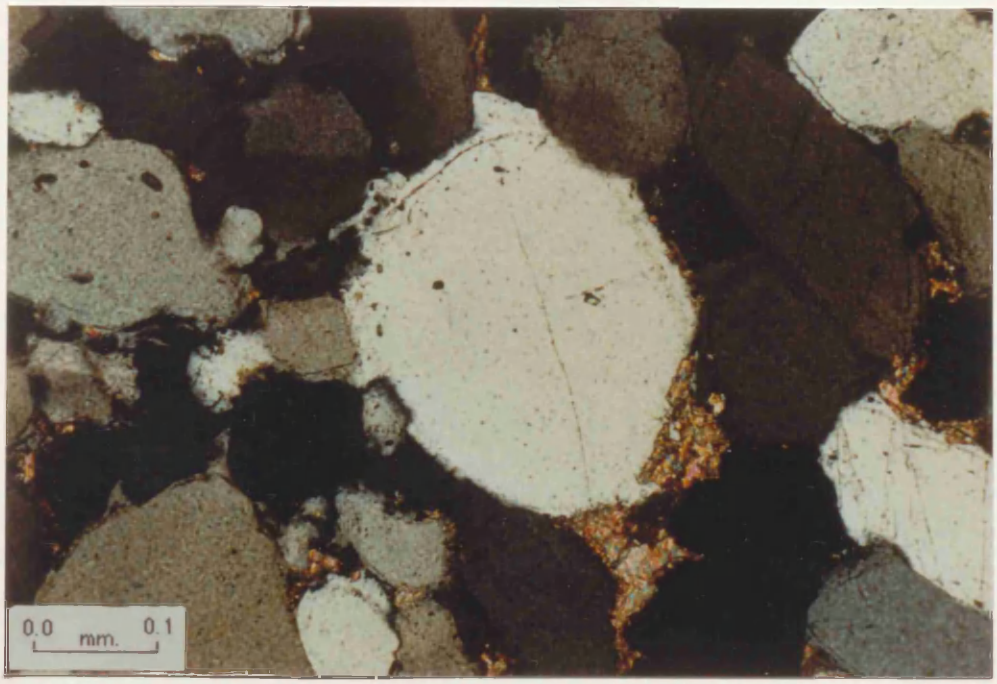
0.0 mm. 0.1

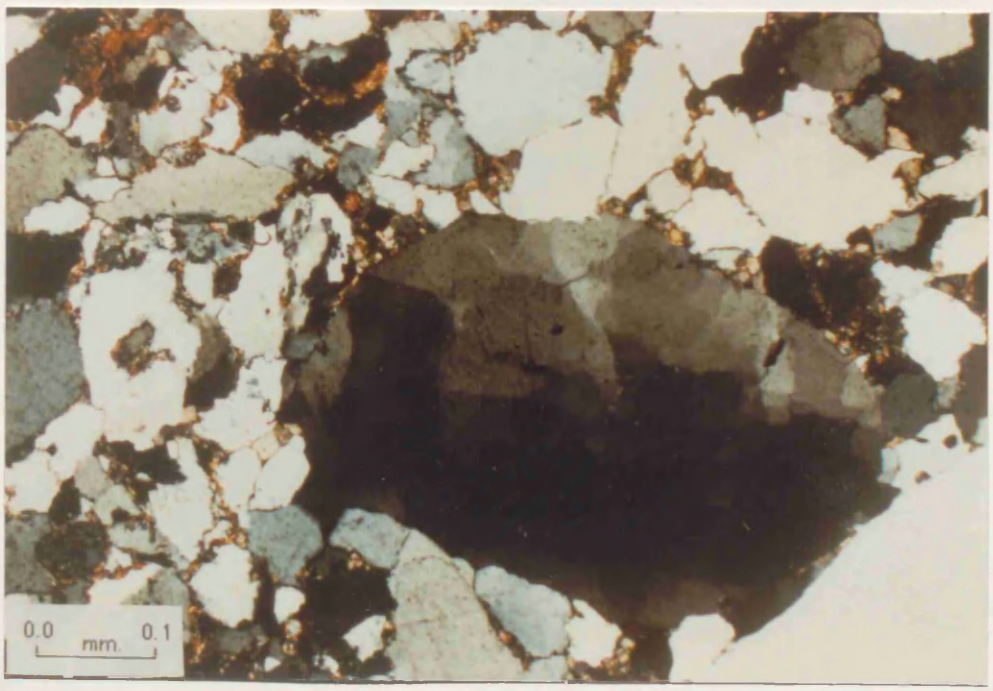
0.0 mm. 0.1

Plate 4.3 Photomicrograph, XN. Metaquartzite polycrystalline quartz grain of metamorphic origin, showing strongly sutured intercrystalline boundaries, elongation of contained quartz crystals and bimodal size distribution of these crystals. Sample from the upper part of the formation. A3-32 borehole, depth=23.7m below top of formation.

Plate 4.4 Photomicrograph, XN. Well rounded grain showing composite nature of a typical detrital quartzite with optical continuity of the overgrowth defined by the haematite-rich substrate (arrowed). This defines the original detrital grain surface. Sample from the middle part of the formation, A4-32 borehole, depth=41.5m below top of formation.

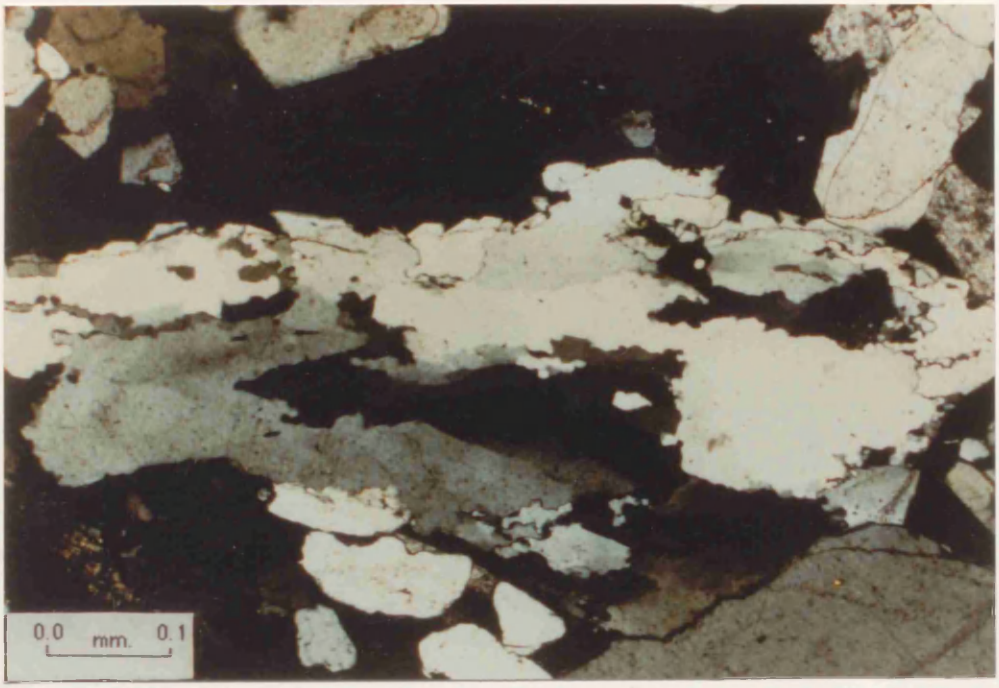
0.0 mm. 0.1

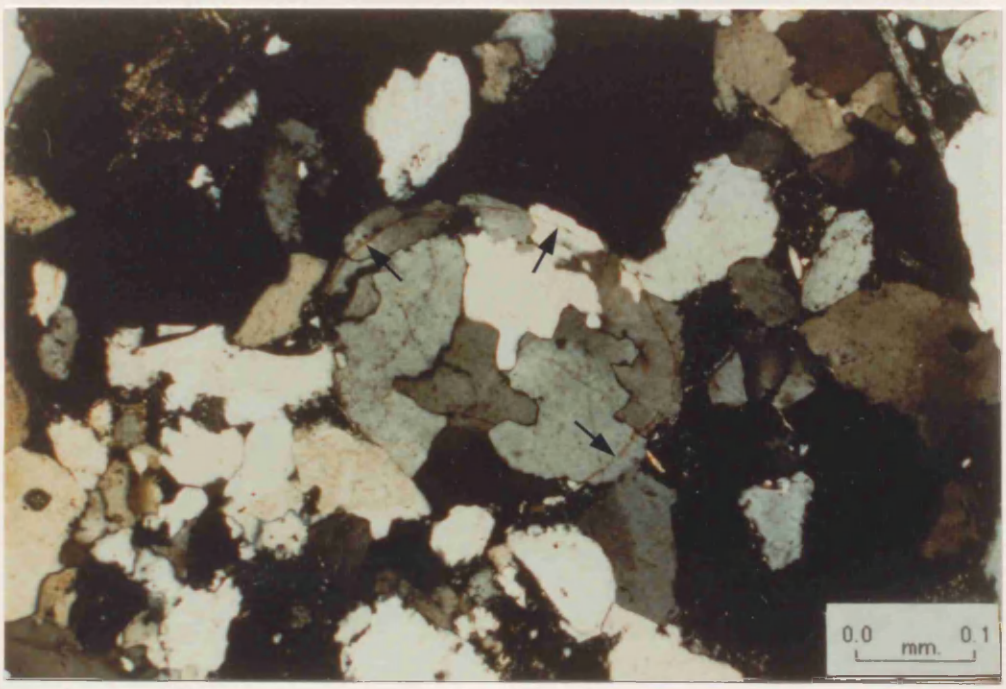
0.0 mm. 0.1

Plate 4.5 Photomicrograph, XN. Plagioclase feldspar grain largely replaced by diagenetic haematite, also shows pore-filling haematite, providing a 'pigment' to the rock. Sample from the upper part of the formation. D1-32 borehole, depth=12.6m below top of formation.

Plate 4.6 Photomicrograph, XN. Microcline grain surrounded by replacement haematite. Quartz overgrowths are also visible on almost all the quartz grains, the original surfaces of which are outlined by a layer of orpbably clay and/or haematite inclusions. Sample from the upper part of the formation. A3-32 borehole, depth=20.7m below top of formation.

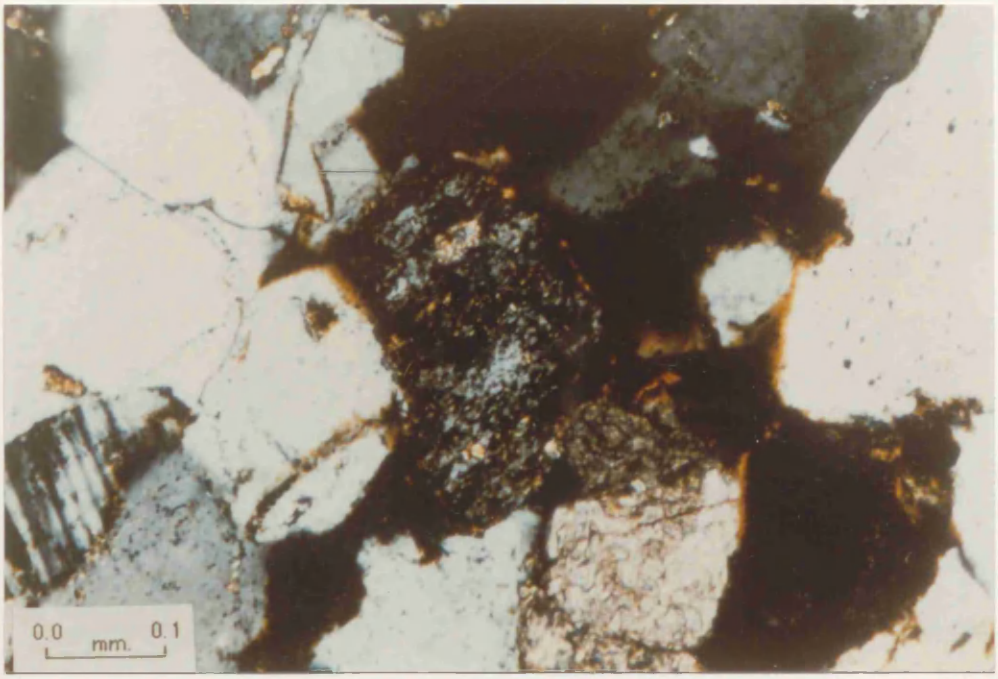
0.0
mm.
0.1

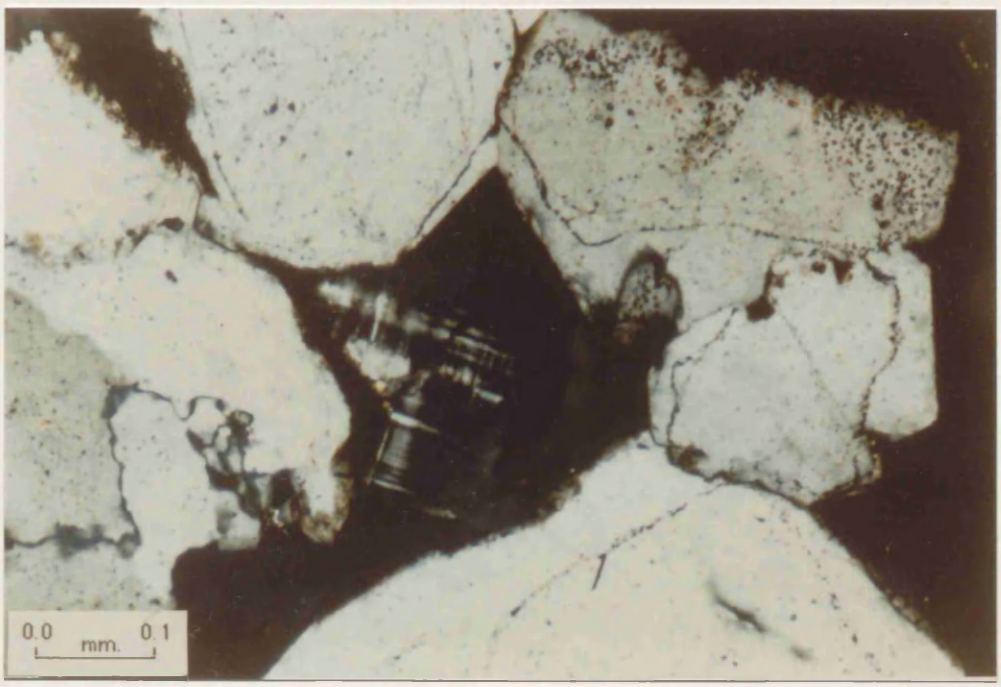
0.0
mm.
0.1

Plate 4.7 Photomicrograph, XN. Scattered rounded grains of glauconite (green). Most of the quartz grains have irrequlars boundaries where they have been partly replaced by clay minerals. Large crystal of secondary calcite also present. Sample from the uppermost part of the formation. A2-32 borehole, depth=1.8m below top of formation.

Plate 4.8 Photomicrograph, XN. Scattered small grains of glauconite amongst angular to subangular poorly sorted quartz grains showing pressure solution. Sample from the uppermost part of the formation, D1-32 borehole, depth=18.0m below top of formation.

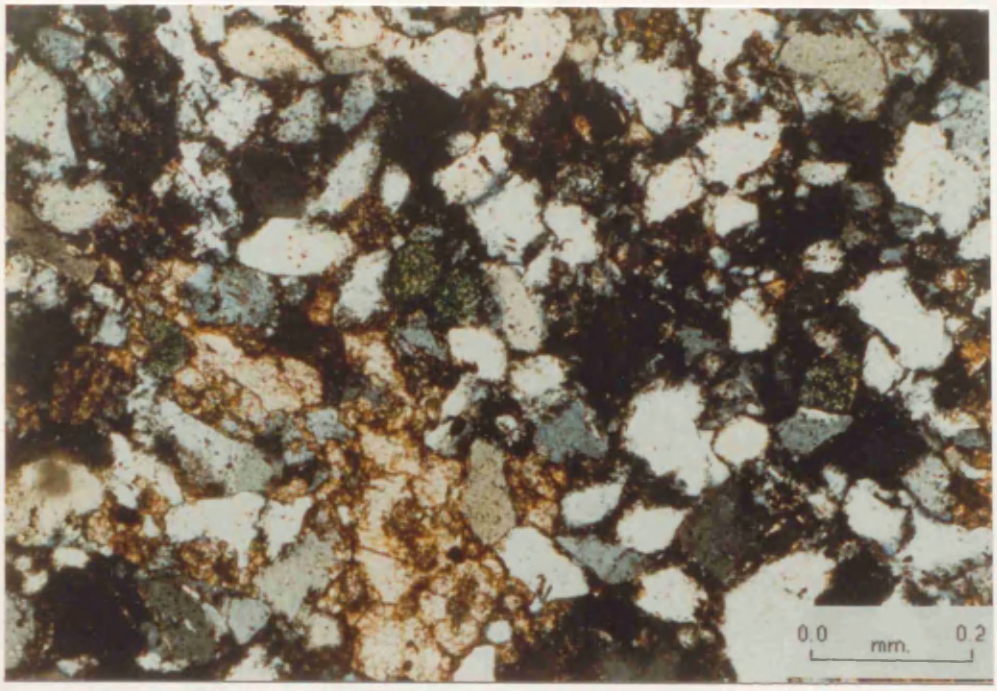
0.0 mm. 0.2

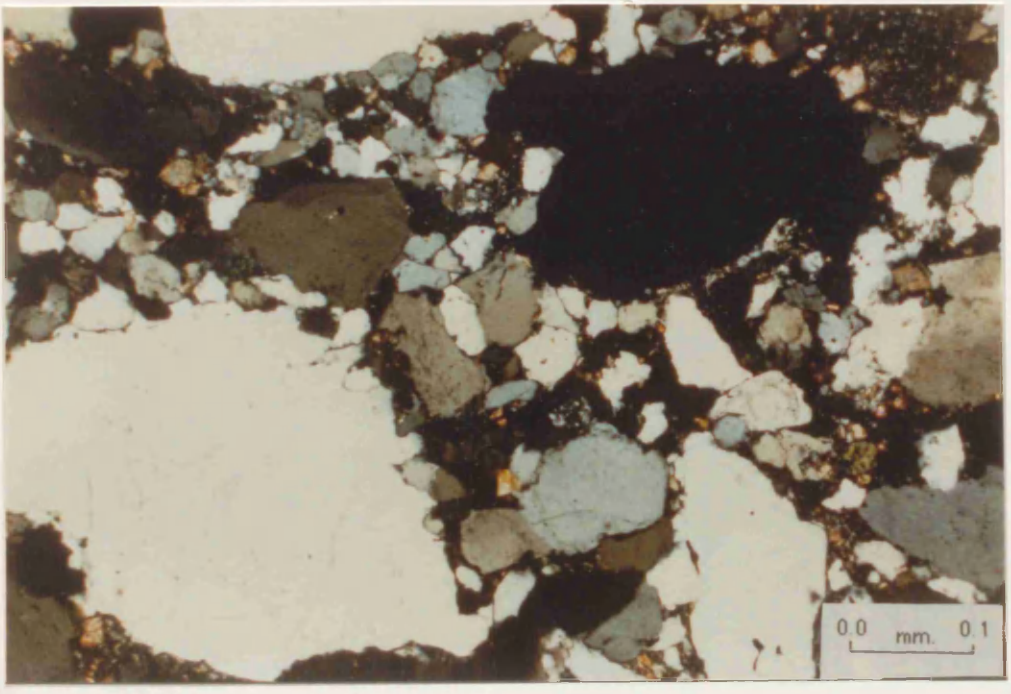
0.0 mm. 0.1

Plate 4.9 Grain mount photomicrograph. PPL. Bahi Sandstone heavy mineral separation, showing different shapes (rounded, subhedral) and broken zircon (Z), rounded rutile (R), tourmaline (T) and opaques (O). Sample from the upper part of the formation. F6-32 borehole, depth=9.6m below top of formation.

Plate 4.10 Grain mount photomicrograph. PPL. Bahi Sandstone heavy mineral separation, showing rounded zircon with different types of inclusions (Z), elongated rutile (R), tourmaline (T) and opaques (O). Sample from the lower part of the formation. A4-32 borehole, depth= 49.5m below top of formation.

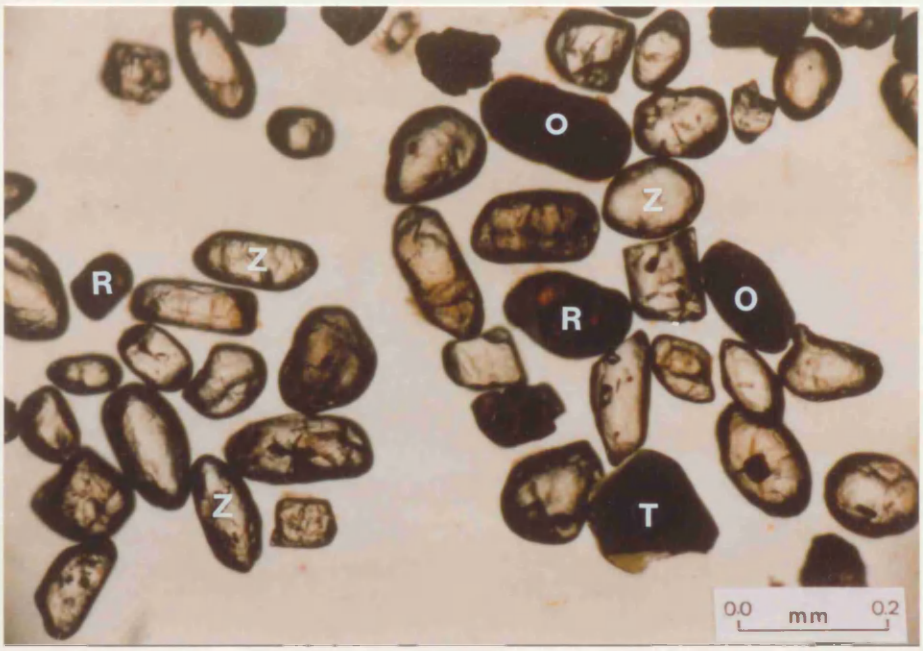
O
Z
R
Z
R
O
Z
T
0.0 mm 0.2

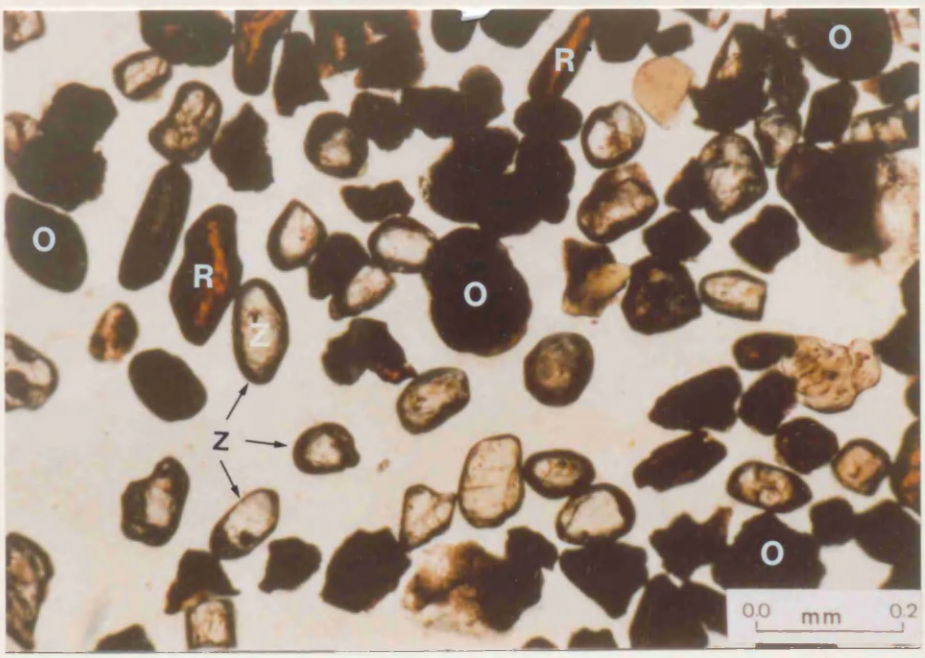
R
O
O
R
Z
O
Z
O
0.0 mm 0.2

Plate 4.11 Photomicrograph, XN. Quartz grains, all showing authigenic overgrowth throughout. Their angularity results entirely from this process. Scattered grains of glauconite are also present (G). Sample from the uppermost part of the formation. A3-32 borehole, depth=13.7m below top of formation.

Plate 4.12 Photomicrograph, XN. Large anhydrite crystals (A1, A2) surrounding framework grains. Dolomite (D) fills the pores paces between some quartz grains. The feldspar and quartz grains have irregular boundaries in part caused by dolomite and anhydrite replacement. Sample from the upper part of the formation. A2-32 borehole, depth=6.9m below top of formation.

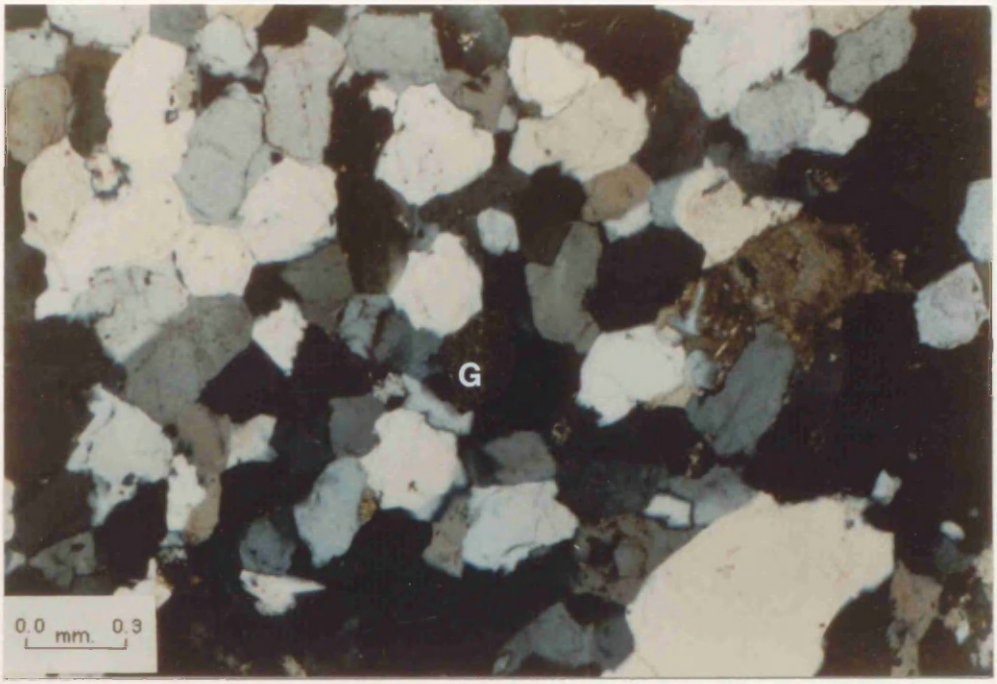
G
0.0 mm. 0.3

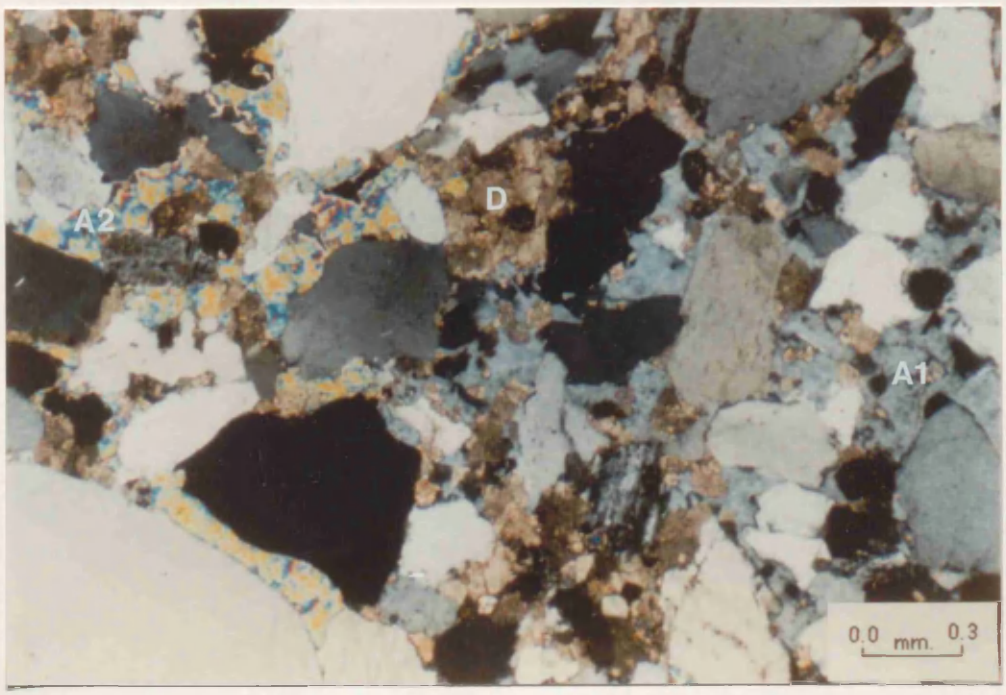
A2
D
A1
0.0 mm. 0.3

Plate 4.13 Photomicrograph, XN. Angular to subangular fine quartz grains with red-brown ferruginous clay mineral surrounds. Sample from the lower part of the formation. A2-32 borehole, depth=24.5m below top of formation.

Plate 4.14 Photomicrograph, XN. Angular to subangular fine sand grains floating in a large haematite crystal. Sample from the lower part of the formation, A4-32 borehole, depth=68.2m below top of formation.

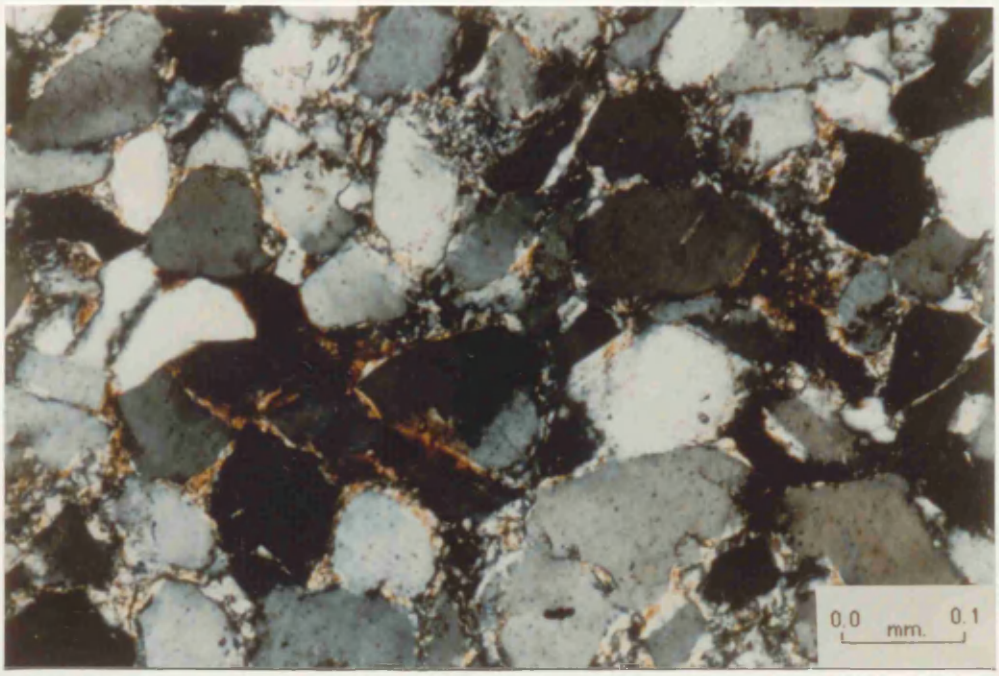
0.0 mm. 0.1

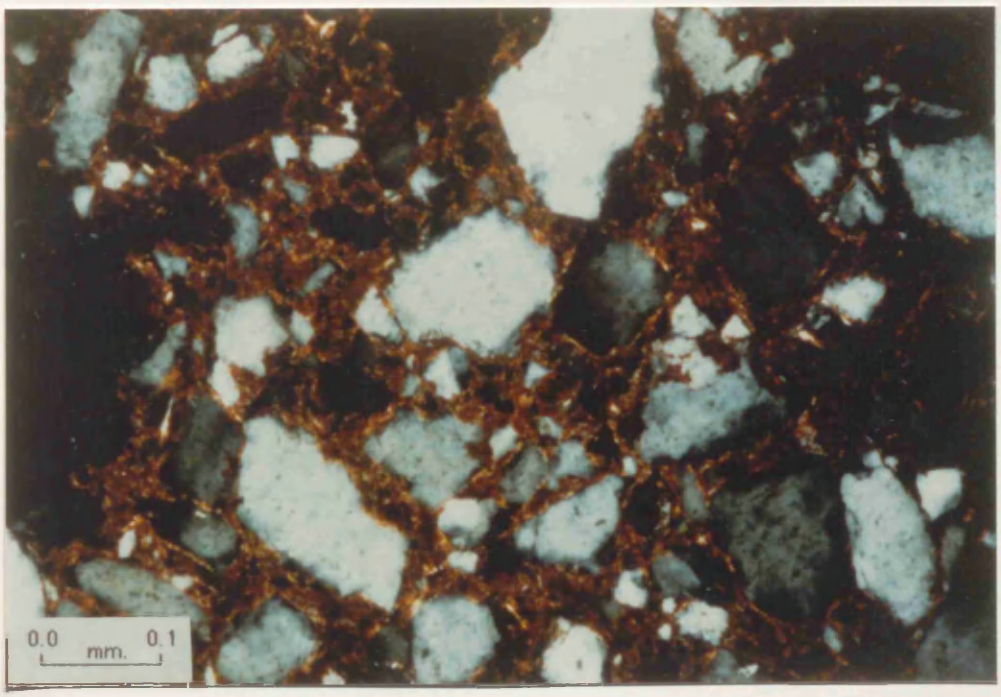
0.0 mm. 0.1

Plate 4.15 Photomicrograph, XN. Quartz grains floating in a dolomite cement (D). The quartz grains have irregular boundaries, in part caused by dolomite replacement. The darker fine-grained material (dolomicrite) was produced by organic activity (burrows). Sample from the upper part of the formation. A2-32 borehole, depth=6.9m below top of formation.

Plate 4.16 Photomicrograph, XN. Large anhydrite crystals (A1-3) between quartz grains and filling the intervening pore spaces. Note the absence of anhydrite between pressure solution contact quartz grains suggesting that the anhydrite is a late diagenetic addition. Sample from the upper part of the formation. A2-32 borehole, depth=5.1m below top of formation.

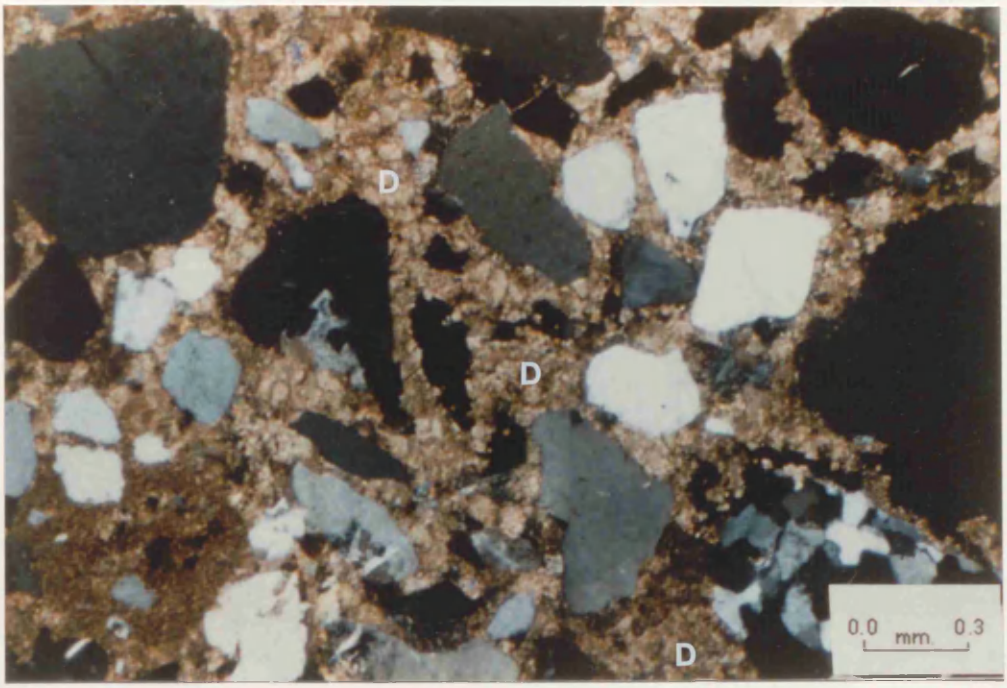
D
D
D
0.0 mm. 0.3

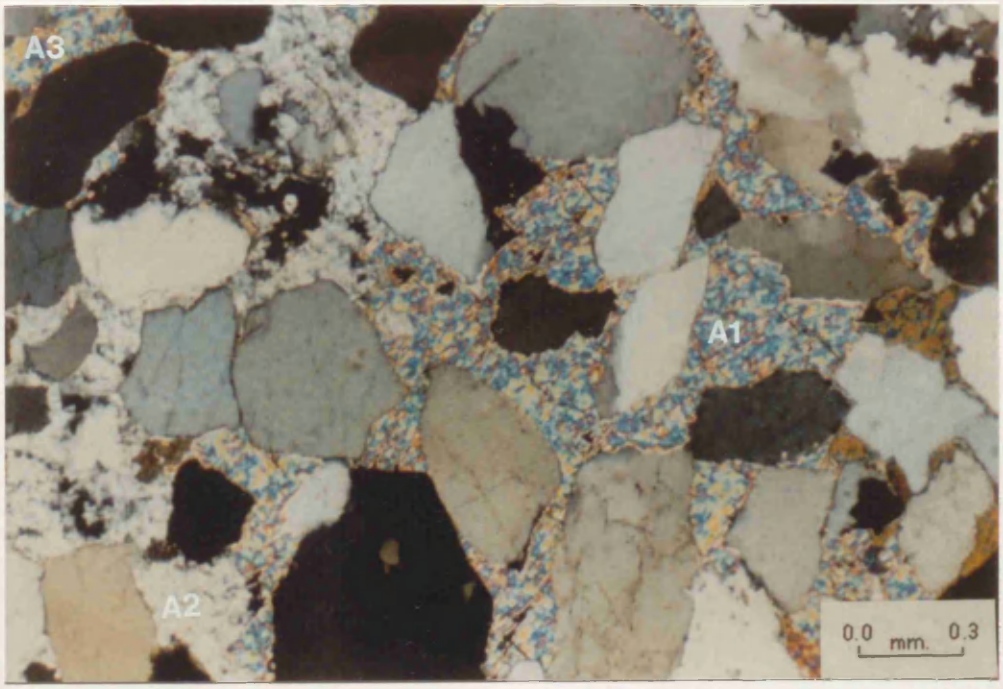
A3
A1
A2
0.0 mm. 0.3

Plate 4.17 SEM. photomicrograph showing well-developed euhedral quartz overgrowths. A subsequent thin illitic clay coating is also present. Sample from the middle part of the formation. A4-32 borehole, depth=42.1m below top of formation.

Magnification = X180.

Plate 4.18 SEM. photomicrograph showing pore-filling authigenic chlorite. Individual crystals are oriented edge-wise with respect to the concealed framework grains. Individual chlorite crystals are largely perpendicular to each other. Sample from the upper part of the formation. A2-32 borehole, depth=1.8m below top of formation.

Magnification = X10,500.

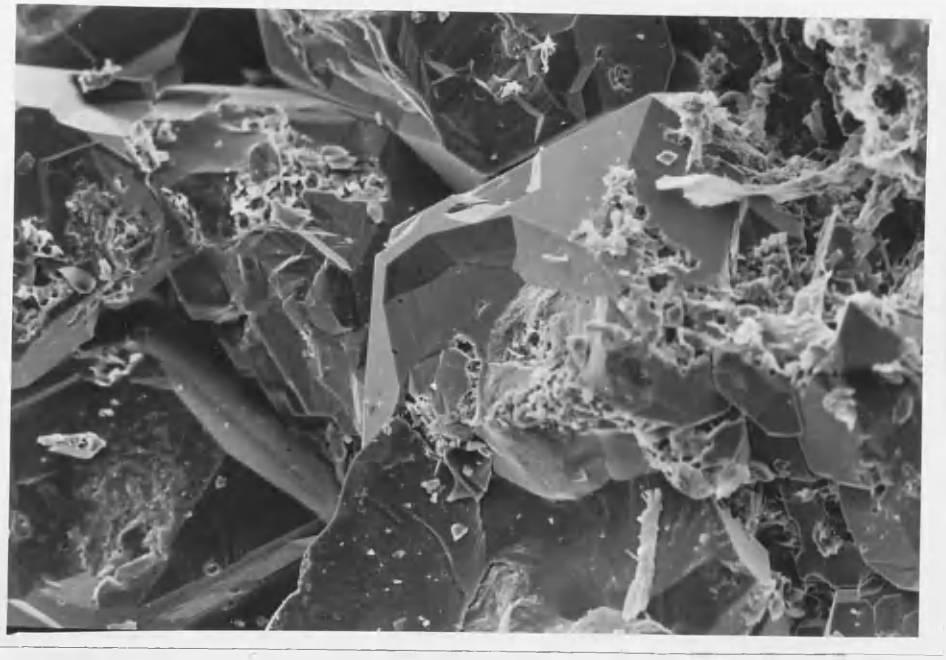

200 μm

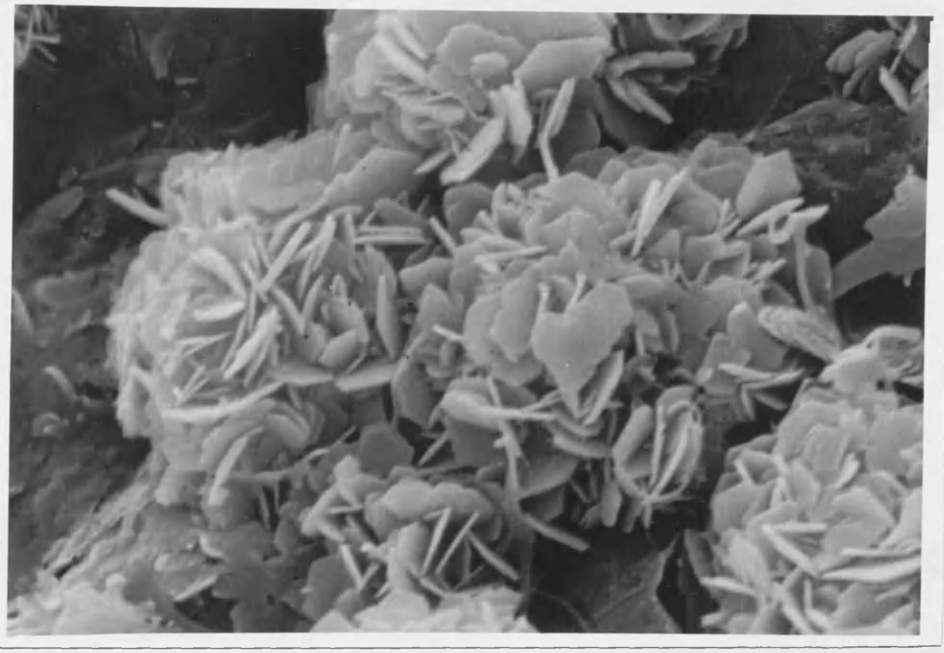

2.0 μm

Plate 4.19 SEM. photomicrograph showing filamentous pore-filling and pore-bridging authigenic illite. Open, interconnected pores are lined with such filaments forming a mat which coats the detrital grain surfaces. Sample from the upper part of the formation. A2-32 borehole, depth=12.8m below top of formation.
Magnification = X3,000.

Plate 4.20 SEM. photomicrograph showing well-crystallised, authigenic kaolinite occurring as face-to-face stacks of pseudohexagonal plates deriving from local feldspar decomposition. Sample from the middle part of the formation. A4-32 borehole, depth=41.8m below top of formation.
Magnification = X10,000.

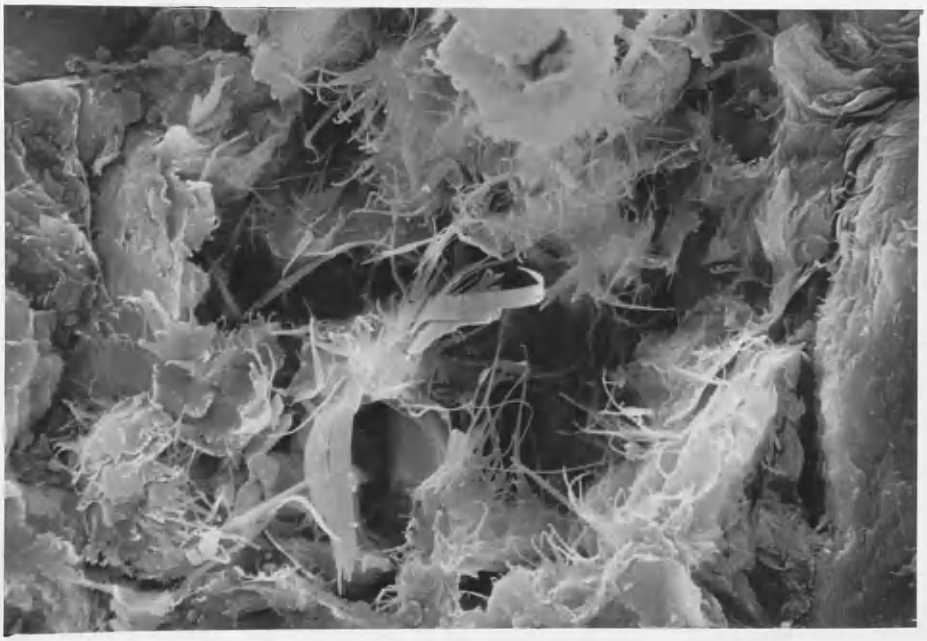

10.0 μm

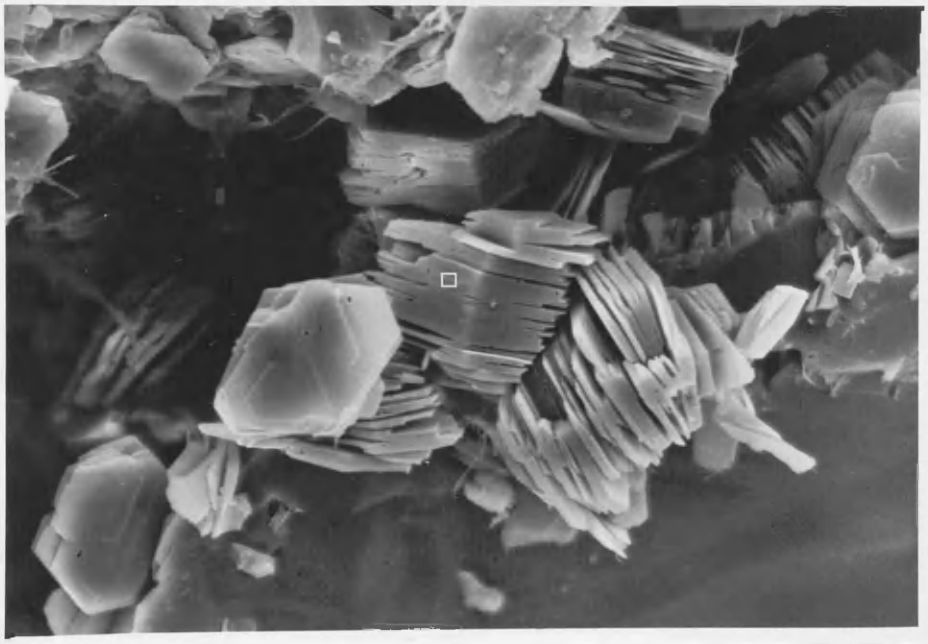

20.0 μm

Table 4.1 Mineralogy of the Bahi Sandstone in the boreholes investigated (given in percentages).

Borehole	Sample	Quartz			Feldspar	Lithic Fragment	Mica	Cement			Acce. Minerals
		Mono.	Poly.	Chert				Clay	Carbonate	Iron-oxide	
A2-32	2-1	61.6	2.0	2.0	3.9	0.0	0.6	11.0	6.3	14.0	8.3
	2-2	56.3	12.0	0.0	2.3	1.3	0.3	2.0	23.6	4.0	0.0
	2-3	52.6	10.6	1.6	3.3	1.3	0.0	4.0	24.6	4.0	0.3
	2-4	57.0	5.0	0.5	8.5	0.0	0.0	1.0	27.5	0.0	0.0
	2-5	55.6	12.6	0.6	8.6	0.6	0.3	0.0	19.6	0.0	0.0
	2-6	59.6	7.3	0.6	8.6	1.6	0.0	1.0	21.0	0.6	0.0
	2-7	70.3	7.0	0.6	8.3	0.0	0.6	6.6	3.0	6.9	0.6
	2-8	72.3	4.3	0.0	6.3	0.3	0.0	3.0	13.0	1.9	0.7
	2-9	68.3	4.3	0.0	4.6	0.3	2.3	5.0	8.6	8.6	1.0
	2-10	70.3	5.3	1.3	6.0	0.0	0.6	4.0	0.3	15.6	0.3
	2-11	64.0	10.6	0.3	4.6	0.0	0.0	6.0	5.0	12.2	1.6
	2-12	76.0	4.0	1.0	4.3	0.6	0.0	5.0	1.3	9.9	1.6
	2-13	75.0	5.6	0.3	5.6	1.6	1.6	4.0	5.0	2.6	1.0
	2-14	77.2	2.3	0.6	4.6	1.3	1.2	6.9	0.6	4.3	1.0
	2-15	69.3	8.0	1.3	6.3	0.0	2.0	8.0	1.3	3.3	0.5
	2-16	74.0	3.0	0.7	3.3	1.3	1.3	2.0	2.2	11.3	0.5
	2-17	67.3	4.0	0.6	6.0	0.0	2.6	11.0	0.6	14.0	1.0
A3-32	3-1	67.0	14.0	0.0	4.0	1.3	0.0	11.0	2.6	2.0	6.6
	3-2	79.0	5.6	1.3	5.3	0.0	0.0	1.0	2.6	3.3	1.6
	3-3	79.0	5.3	0.6	8.0	0.0	0.3	2.3	2.0	0.6	1.6
	3-4	77.0	5.0	2.0	8.0	0.3	0.0	3.6	2.3	1.0	0.6
	3-5	79.6	6.6	0.0	8.3	0.6	0.3	1.0	2.0	0.6	0.6
	3-6	76.6	3.6	0.3	10.0	0.3	0.0	3.6	3.6	1.0	0.6
	3-7	60.3	1.6	0.0	11.6	0.3	1.0	1.6	0.0	22.3	0.3
	3-8	86.0	2.3	0.0	9.3	0.0	0.0	0.6	0.0	1.6	0.0
	3-9	76.0	5.0	0.0	14.3	0.0	0.3	1.3	1.0	2.0	0.0
	3-10	78.8	7.6	0.4	10.0	0.8	0.0	1.6	0.8	0.0	0.0
	3-11	74.0	10.0	0.4	12.0	1.2	0.0	1.2	0.8	0.0	0.0
	3-12	70.0	12.6	1.0	9.6	0.3	0.0	12.0	0.6	1.6	0.0
	3-13	66.0	14.0	1.6	12.0	0.4	0.8	2.4	1.6	3.0	0.0
	3-14	72.3	14.3	0.0	4.3	0.6	0.3	4.0	1.6	5.0	0.0

Table 4.1 continued

Borehole	Sample	Quartz			Feldspar	Lithic Fragment	Mica	Cement			Acce. Minerals
		Mono.	Poly.	Chert				Clay	Carbonate	Iron-oxide	
A3-32	3-15	72.8	7.6	0.3	14.3	0.3	0.3	1.3	1.6	1.3	0.0
	3-16	65.0	17.6	0.0	8.0	1.3	0.6	9.0	1.0	3.3	0.0
	3-17	72.6	7.6	0.0	11.3	0.6	0.0	2.0	1.6	4.0	0.0
A4-32	4-1	60.5	16.0	2.0	2.0	0.0	1.5	11.5	5.5	0.5	0.5
	4-2	75.6	8.0	0.0	6.0	0.8	0.8	6.8	2.0	7.0	0.0
	4-3	61.5	19.5	1.0	2.5	0.0	0.0	12.0	2.5	0.5	0.5
	4-4	75.6	11.6	0.4	7.2	0.4	0.8	2.0	1.6	11.0	0.0
	4-5	79.2	6.8	0.0	10.0	0.0	1.2	2.8	0.0	9.0	0.0
	4-6	71.0	14.0	0.0	9.5	0.0	1.0	3.5	0.0	2.0	0.0
	4-7	74.5	8.0	0.5	4.5	0.0	0.0	9.5	0.0	9.0	0.5
	4-8	77.0	13.0	0.6	1.0	0.0	0.0	8.0	3.3	1.6	0.0
	4-9	75.2	10.4	0.0	10.4	1.2	0.0	2.0	0.0	1.0	0.4
	4-10	79.2	10.0	0.0	5.6	0.8	0.0	2.8	0.0	3.0	0.4
	4-11	80.6	8.4	0.0	9.0	0.8	0.0	1.2	0.0	0.0	0.0
	4-12	77.0	9.5	2.0	6.0	0.0	1.0	2.5	0.0	4.0	0.0
	4-13	79.2	10.0	0.0	6.4	0.4	0.4	2.4	0.4	2.0	0.0
	4-14	70.3	17.6	0.6	6.3	1.6	0.3	3.0	0.0	1.3	0.6
	4-15	72.0	11.0	0.5	6.0	0.0	0.0	5.5	0.0	4.0	0.5
	4-16	77.6	11.8	0.0	7.2	0.8	0.4	1.2	0.0	1.0	0.6
	4-17	71.6	0.8	0.0	6.4	0.4	0.0	7.6	0.0	31.0	0.8
	4-18	72.9	7.7	0.0	6.8	0.0	0.0	7.2	0.0	4.8	0.6
	4-19	70.0	7.6	0.0	8.4	2.4	0.0	6.2	1.2	14.0	0.4
	4-20	72.3	13.0	0.6	10.0	2.3	0.3	4.0	0.0	0.0	0.0
	4-21	80.0	7.6	0.0	6.4	0.4	0.0	4.8	0.0	4.0	0.8
	4-22	67.6	10.0	0.0	8.0	0.8	0.0	7.6	0.0	13.0	0.8
	4-23	66.0	15.6	2.0	9.0	3.0	0.0	10.0	0.0	0.0	0.6
	4-24	75.8	11.6	0.0	2.5	1.7	0.8	7.5	0.0	0.0	0.0
	4-25	82.0	6.8	0.0	7.6	0.4	0.0	2.0	0.0	2.0	0.4
	4-26	80.0	10.8	0.0	4.4	0.4	0.0	2.8	0.0	0.0	0.0
	4-27	65.0	19.3	0.3	6.3	4.3	1.6	5.0	0.3	0.0	0.9
	4-28	66.6	14.6	1.0	9.6	1.0	1.6	12.0	0.0	0.8	0.5

Table 4.1 continued

Borehole	Sample	Quartz			Feldspar	Lithic Fragment	Mica		Cement		Acce. Minerals
		Mono.	Poly.	Chert				Clay	Carbonate	Iron-oxide	
A4-32	4-29	78.8	1.2	0.0	10.4	0.0	0.0	8.4	0.0	1.2	0.0
	4-30	66.3	4.0	0.0	1.3	0.6	3.0	5.0	0.0	21.0	1.6
D1-32	1-1	60.0	6.3	0.3	5.3	0.3	2.0	12.0	6.6	10.2	3.6
	1-2	51.0	4.6	0.0	3.3	0.3	0.0	3.0	27.0	2.0	0.0
	1-3	49.0	3.2	0.4	5.2	0.4	0.0	0.0	37.8	1.0	1.2
	1-5	50.3	5.3	0.3	5.0	1.0	0.0	2.0	33.6	0.0	2.3
	1-6	75.6	9.3	0.3	3.6	0.6	0.0	2.0	2.6	4.3	2.6
	1-7	61.3	18.8	0.0	7.6	0.0	0.0	0.8	7.2	2.0	4.0
	1-8	67.0	13.6	0.0	2.6	0.3	0.3	4.0	8.6	2.6	3.0
	1-9	78.4	11.6	0.0	5.2	0.0	0.0	1.2	3.6	0.0	0.0
	1-10	74.0	13.6	0.6	3.6	0.6	0.0	3.0	3.6	2.0	0.0
	1-11	54.8	11.2	0.0	7.2	0.0	0.0	0.8	24.8	2.0	0.0
	1-12	55.8	6.4	1.2	7.6	0.0	0.0	0.4	27.4	3.0	1.2
	1-13	62.8	7.6	0.4	5.6	0.4	0.0	0.0	22.9	3.0	0.0
	1.15	72.0	13.0	0.0	7.3	0.6	0.6	2.0	3.6	0.3	1.0
	1-16	80.8	7.6	0.4	4.0	0.0	0.0	1.2	6.0	0.0	0.0
	1.17	58.0	5.0	0.0	6.3	0.3	0.0	14.0	11.3	4.3	0.6
	1-18	54.6	1.6	0.0	6.0	0.0	0.0	12.4	25.3	18.0	0.6
F6-32	6-1	87.6	4.6	0.0	6.0	0.0	0.0	1.0	0.0	0.0	0.6
	6-3	86.3	2.3	0.0	6.0	0.0	1.0	8.0	0.0	1.0	0.3
	6-4	74.3	10.0	0.0	6.6	0.0	0.0	1.0	0.0	8.0	0.0
	6-5	40.3	2.6	0.0	2.6	0.0	0.0	0.0	54.0	1.0	0.0
	6-6	80.0	4.0	0.0	3.6	0.0	0.0	7.0	0.0	5.0	1.6
	6-7	87.3	3.0	0.0	2.6	0.0	0.0	4.7	0.0	5.0	1.0
	6-8	90.6	4.5	0.0	1.3	0.0	0.0	3.0	0.0	0.0	0.0
	6-9	81.3	5.6	0.0	6.0	0.0	0.6	4.3	0.0	4.0	0.0
	6-11	89.0	4.0	0.0	2.3	0.3	0.0	1.2	2.6	0.3	0.3
	6-12	89.3	3.6	0.0	3.6	0.0	0.0	1.6	0.0	3.0	0.6
	6-16	78.6	8.3	0.0	3.0	0.0	1.3	6.3	1.6	0.0	0.6
	6-17	86.0	5.3	0.0	3.0	0.0	0.0	3.6	0.0	5.0	0.3

CHAPTER 5

GEOCHEMISTRY

5.1 Introduction

The geochemical composition of terrigenous sedimentary rocks is a function of the complex interplay of variables, such as provenance, weathering, transportation and diagenesis (Pettijohn & *et al.* 1973, 237-244).

Chemical analysis of sediments has been used by many workers to indicate the relationship between sandstone suites and their tectonic setting, to determine their depositional environments, the nature of their provenance and also to determine the relationships between grain size and trace element distribution (Pettijohn, 1963; Dennen, 1967; Fenner & Hagner,1967; Van de Kamp, Leake & Senior, 1976; Senior & Leake, 1978; Loring, 1981; Hickman & Wright, 1983; Bhatia 1983; Bhatia & Crook 1983; Van de Kamp & Leake, 1985; Argast, 1987; Roser & Korsch, 1986,1988).

There have been no geochemical studies hitherto of the Bahi Sandstone Formation. In this study, a detailed investigation of major and trace elements has been carried out. On the basis of vertical and lateral lithological variation of the formation a total of seventy-three samples were selected, 13, 27, 20 and 13 from cores in the A2-32, A4-32, D1-32 and F6-32 boreholes respectively. These have been analysed using an X-ray fluorescence spectrometer (Leake *et al.* 1969; Harvey *et al.* 1973).

Ten major oxides were determined using XRF (SiO_2, TiO_2, Al_2O_3, $Fe^*_2O_3$ (total), MnO, MgO, CaO, Na_2O, K_2O, P_2O_5), and 16 trace elements (Ba, Ce, Co, Cr, Cu, Ga, La, Ni, Pb, Sr, Th, Y, Zn, Zr, U)

The major oxides FeO, H_2O, CO_2, were determined by wet chemical analysis. The FeO was determined by titration of standard dichromate solution with rock solution made by dissolving a measured a mount of whole rock powder (0.5 grams) in sulphuric and hydrofluoric acids. The FeO percentage, determined by titration, was used to calculate the amount of Fe_2O_3 present. The amounts of H_2O and CO_2 in the samples was determined using the

Penfield method of combustion, adsorption and gravimetry. The amount of total sulphate (SO_3) was determined by using the gravimetric method.

Geochemical results (major and trace elements) are given in tables 5.1-5.4, major oxides by percentage and the trace elements in parts per million (ppm).

The aims of these geochemical studies are:

- To indicate the geochemical signature of the Bahi Sandstone Formation.
- To check the petrographic investigations, by relating the major and trace elements to the original minerals.
- To show how the major and trace elements vary both laterally and vertically within the formation.
- To give some indication of the provenance and depositional environment of the Bahi Sandstone Formation.
- To throw light on the tectonic setting of the formation.

5.2 Major elements

Several recent studies have investigated the sedimentary geochemistry of clastic rocks in order to indicate their provenance and geotectonic setting by using variable discriminate functions based on major- element data. Bhatia (1983) used the major oxides Fe_2O_3+MgO, Al_2O_3/SiO_2, K_2O/Na_2O, $Al_2O_3/(CaO+Na_2O)$ and TiO_2 as discriminating parameters to indicate the relationship between the geochemical composition of sandstones and the geotectonic settings of their sedimentary basins. He showed that the nature of continental margins and ocean basins can be deciphered on the basis of the major element compositions of sandstones.

In this study, the lateral and vertical geochemical variation within the Bahi Sandstone Formation in the four selected boreholes reflects different mineralogical composition resulting from changes in environmental conditions at the time of deposition and/or different sources for the Bahi sediments. The average weight percentage of the major oxides in the four boreholes

are shown in table 5.5.

Major oxides of the Bahi samples from the four boreholes, were plotted against each other on scatter plot diagrams to show the inter-relationships between these elements.

5.2.1 SiO_2

The major oxides results show a high content of SiO_2 at the expense of other oxides in most of the studied samples. This suggests a more mature sediment in these samples, whereas in the upper part of the formation at A2-32, D1-32 and F6-32 boreholes, the SiO_2 content is low due to an abundance of evaporites and carbonate as a cement or matrix. In the lower part of the formation the SiO_2 content varies inversely with the clay mineral and feldspar content.

5.2.2 Al_2O_3 Versus K_2O

The sources of both Al_2O_3 and K_2O in the sedimentary rocks are feldspars and sheet silicates such as micas and clays. As a result the abundance of Al_2O_3 can be directly related to the abundance of feldspar, mica and clay minerals.

A plot of Al_2O_3 against K_2O (Fig. 5.1), shows a strong positive correlation. This suggests the same source for minerals containing these oxides.

5.2.3 TiO_2 versus Al_2O_3 and K_2O

TiO_2 content in the sediments is due to terrigenous material consisting of (1) weathering residue in the form of chemically unaltered grains like rutile, or in the form of partly decomposed minerals like mica, (2) new products of weathering such as anatase and clay minerals, (3) diagenetic minerals (Wedepohl, 1978, 22-k-1).

A plot of TiO_2 against Al_2O_3 and K_2O (Figs. 5.2-5.3), shows a poor positive correlation in some studied samples. This suggests that the TiO_2 content is associated with the clay minerals and/or K-feldspar, whereas the majority of the studied samples shows very low content

of TiO_2, suggesting that the titanium content may be concentrated in oxides or non-layer silicates, opaques and rutile minerals which have been detected in the Bahi sediment.

5.2.4 Fe_2*O_3 (total) versus Al_2O_3 and K_2O

In most of the samples from the Bahi Sandstone Formation in the four boreholes, a plot of Al_2O_3 and K_2O against Fe_2*O_3 (total) (Figs. 4.5-5.5), shows a positive correlation suggesting that the Fe_2*O_3 content is concentrated in clay minerals and/or feldspar. However, iron oxide is present in replacement minerals in the weathered feldspar and in cement materials.

5.2.5 CO_2 versus CaO

Most of the calcium in sedimentary rocks occurs in the carbonate fraction (Wedepohl, 1978, 20-k-1). The detrital components in the form of Ca-plagioclase and accessory minerals such as apatites contain significant amounts of CaO in their crystal structure. The presence of a positive correlation between CaO and CO_2 (Fig. 5.6), is related to enrichment of the Bahi sediment by carbonate cement composed of varying proportions of calcite and dolomite, whereas some studied samples show high CaO content with very low CO_2. This is undoubtedly related to presence of evaporites ($CaSO_4$) in the uppermost part of the formation (petrographic observations).

5.2.6 CO_2 versus MgO

Magnesium is present in the sediments mainly as dolomite and phyllosilicates such as chlorite and glauconite. Phyllosilicates are mostly present in shales and to a smaller extent in sandstones, graywackes and arkoses (Wedepohl,1978, 12-k-1).

A plot of MgO against CO_2 in the four boreholes (Fig. 5.7), shows a positive correlation in most studied samples, suggesting that the amount of MgO is present mainly in a somewhat dolomitic carbonate cement, whereas small amounts of magnesium may indicate the presence of a phyllosilicate (glauconite). The uppermost part of the formation is rich in glauconite

(petrographic studies).

5.2.7 CaO versus MgO

A plot of CaO with MgO (Fig. 5.8), shows two trends which in some samples show a good positive correlation. This suggests that a high content of both oxides is related to an abundance of dolomite whereas in other samples there is a lack of correlation between MgO and CaO. High content of CaO is related to the presence of calcite and anhydrite.

5.3 Niggli Numbers

The use of Niggli numbers can be very useful in distinguishing between K which is derived from detrital feldspar and K from detrital illite, mica or other sheet silicate minerals. The Niggli numbers are based on taking the percentage of the sum of the molecular content of Al_2O_3 (al), CaO (c), FeO + Fe_2O_3 + MgO (fm) and Na_2O + K_2O (alk). k=K_2O/Na2O+K2O (Niggli, 1954, 13-15).

5.3.1 al - alk versus Niggli k

A plot of al - alk against Niggli k has been used to distinguish between K in feldspar and K in sheet silicates such as micas and clay minerals. High al - alk (>30), indicates clay-rich rocks (shale), whereas low al - alk (<30) indicates a high feldspar content, supported by negative correlation with Niggli k if the K was largely in potassium feldspar or positive correlation if the K was largely in sheet silicates. The absence of negative or positive correlations suggests that a mixture of the two minerals (Van de Kamp & Leake, 1985).

A plot of al - alk against Niggli k in the Bahi Sandstone (Fig. 5.9), shows absence of negative or positive correlation suggesting that the K occurs in a mixture of both feldspar and clay minerals is present. Some of the studied samples, shows al - alk >30. This suggests that most of K may be related to the sheet silicates whereas the majority of the samples have al-alk <30 suggesting that K is represented in a mixture of both feldspars and clay minerals.

5.3.2 Niggli c versus al - alk

A plot of Niggli c against al - alk (Fig. 5.10), shows three well-defined trends. The dominant trend shows that C is largely related to dolomite (c=50). Another trend shows that C is largely related to calcium carbonate (c=100), whereas some samples show very low content of C (c nearly 0), and this may be related to clay minerals.

5.3.3 al - alk versus $Fe_2^*O_3$ (total)

A plot of al - alk against $Fe^*_2O_3$ (total) (Fig. 5.11), shows two main separate fields. One trend shows a positive correlation suggesting that the $Fe_2^*O_3$ content is largely associated with clay minerals, whereas the other field shows low $Fe_2^*O_3$ content suggesting that Fe may be related to detrital iron oxides.

5.3.4 al - alk versus TiO_2

In a plot of al - alk versus TiO_2 (Fig. 5.12), most of the studied samples show very low content of TiO_2 and an undefined relationship with al - alk. This suggests that the titanium may be present in detrital minerals such as rutile and opaques and to a limited extent in a few samples it is associated with clay minerals giving a poor positive correlation.

5.4 Trace elements

Many attempts have been made by many workers to differentiate similar lithological units and to determine the depositional environments of the sediments and their provenance on the basis of trace element distributions. Van de Kamp & Leake (1985) stated that the trace elements are useful for provenance determination. They noted that the high values of cobalt, chromium and nickel indicate detritus from mafic and ultramafic sources; barium is a good indicator of a potassium feldspar-rich provenance and high barium content in arkoses suggests granites and monzonite in the source area. They also showed that most trace elements are concentrated in sheet silicates such as mica and clay minerals; Bhatia & Crook (1983) used the

La, Ce, Nd, Th, Zr, Nb, Y, Sc and Co trace elements to distinguish provenance types and tectonic settings; Hickman and Wright (1983) used rare earth elements to determine the provenance of sediments by plotting Y+La+Ce, Ni+Cr and Sr on a triangular diagram; Loring (1981) noted that the concentration of Zn, Cu, Pb, Co, Ni, Cr, V, Se, Hg and Be is low in sands, and increases with reduction in the grain size of sediments; Fenner & Hagner (1967) established a criterion to distinguish between stratigraphical units of similar lithology on the basis of trace element variations. Trace elements have been determined in the analysed samples from the four selected boreholes, in an attempt to understand the characteristics of these elements and their distribution, and to give some indication of the provenance and depositional environment of the Bahi Formation. The following plots of trace elements against each other and versus al - alk may help in this respect.

5.4.1 K_2O versus trace elemets

Most rubidium in sedimentary rocks resides in the feldspar and sheet silicates. Arkose and feldspathic sandstones and sandstones with an argillitic matrix contain more rubidium than do pure quartz sandstones (Weldepohl, 1978, 37-k-2). Rubidium occurs in abundance in both K-feldspar and K-rich sheet silicates (Van de Kamp & Leake,1985). Trace elements like lead, barium, and rubidium are frequently found in potassium-rich minerals because these elements have ionic radii close to that of potassium and may thus easily replace it (Krauskopf, 1967), while gallium may also show a positive correlation with K as it replaces aluminium which is abundant in feldspars, micas and sheet minerals.

A plot of K_2O against gallium, rubidium, lanthanium and cerium in the Bahi samples (Figs.5.15-5.18), shows a positive correlation. This suggests that these trace elements are concentrated in the K-feldspar and/or in the clay minerals, whereas plots of barium, strontium, cobalt, nickel, lead, thorium, uranium, chromium, copper, zinc and yttrium against K_2O do not show any clear correlation. This suggests that they are not concentrated in sheet silicate or K-feldspar.

5.4.2 Al_2O_3 versus Ga & Rb

A plot of Al_2O_3 against Ga and Rb in the Bahi samples (Figs. 5.13-5.14), shows a positive correlation suggesting that gallium and rubidium are mainly concentrated in the clay minerals or in the K-feldspar or in both.

5.4.3 al - alk versus trace elements

The parameter al - alk provides a measure of the aluminium contained in the clay minerals and micas rather than in the feldspar (Van de Kamp & Leake,1985).

Plots of al - alk against the trace elements lanthanium, cerium, zinc, gallium, zirconium, yttrium, rubidium, barium, strontium, cobalt, nickel, lead, thorium, uranium, copper and chromium (Figs. 5.19-5.26), show no positive or negative correlation. This suggests that these trace elements are neither concentrated mainly in feldspar nor clay minerals.

5.4.4 La versus Ce, Rb, Y and Ga

The presence of lanthanium in the sediments is related to an increase in the alkalinity of weathering solutions. It is precipitated and fixed like aluminium, gallium and titanium (Wedepohl, 1978, 39-57-71-G-1). Cerium content in the sediments could also be due to increase in alkalinity of weathering solutions. The presence of a positive correlation between lanthanium and cerium in the Bahi Formation (Fig. 5.28) suggests that these elements are contributed by the same sedimentary processes, from a source characterised by highly alkaline weathering.

A plot of rubidium, yttrium, and gallium against lanthanium (Figs. 5.27-5.30), shows a positive correlation. This suggests that these trace elements are largely concentrated in the clay minerals and/or in the feldspar.

5.4.5 Y+La+Ce versus Ni+Cr versus Sr

Hickman and Wright (1983) used this relationship for Appin Group slates (late Precambrian Dalradian Supergroup of Scotland) to suggest their provenance. The Ni and Cr end of the diagram represents provenances composed of basic rocks, the Y+La+Ce end

represents a provenance composed of granitic rocks whereas the Sr end represents a provenance containing the highest proportion of sedimentary rocks.

A plot of Y+La+Ce versus Ni+Cr versus Sr for the Bahi Sandstone samples in the four boreholes (Fig. 5.31), shows a very distinct trend. Virtually all the samples fall in the Sr sector indicating that the Bahi Sandstone is largely derived from a pre-existing sedimentary source.

5.5 Vertical variation of Bahi geochemistry

The vertical variation in major element composition, Al_2O_3, Na_2O, K_2O and $Fe_2{}^*O_3$ (total) of the Bahi Sandstone in the four boreholes, is related to changes in grain size and composition. This may indicate changes in the depositional environment and/or change in sediment provenance. Figures 5.32a-c, show the vertical distribution of the major and trace elements of the Bahi Sandstone in the A2-, A4- and F6-32 boreholes respectively.

In the A2-32 borehole, the uppermost part of the Bahi Sandstone Formation is characterised by large amounts of clay minerals including chlorite, illite and kaolinite together with glauconite, low silica content, and high proportion of the major elements (sample 2-1). The upper part of the formation is also characterised by a high CaO content in the form of carbonate and evaporite (samples from 2-2 to 2-6) and poor silica content, whereas the lower part of the formation (below 1904m) is characterised by smaller grain size, low silica content and also a high proportion of major elements. This reflects a less mature sediment. The high concentration of the trace elements varies inversely with the grain size and thus the maturity of this sediment. However, the concentration of trace elements is high in the samples which show a high proportion of feldspar and clay minerals (Fig. 5.32a).

In the A4-32 borehole, for a thickness of 7.6m down to 1845m (samples14-16) and for a thickness of 7m down to 1880m (samples 25-27), there is a reduction in grain size and a compositional change of the Bahi Sandstone. There is also a decrease in silica content and an increase in other major elements and hence increase in the amount of feldspar and clay minerals. This reflects variation in major elements distribution and indicates relative mineralogical maturity of the Bahi sediment for these intervals (Fig.5.32b). There is also a

change in the trace elements distribution particularly with respect to lanthanium, cerium, rubidium and yttrium, which shows increasing concentration with reduction in grain size.

In the F6-32 borehole, variation in major and trace elements is related to the low silica content and high CaO and MgO content particularly in the upper part of the section whereas the lower part is characterised by high silica content reflecting increase in quartz. This indicates a more mature sediment (Fig. 5.32c).

5.6 Discriminant function analysis and tectonic settings

In the past, several attempts have been made to use discriminant function analysis for sandstone geochemistry to classify individual sandstone samples into pre-defined groups on the basis of multiple variables in order to identify the tectonic setting of the provenance. Bhatia (1983) used discriminant function analysis to classify sandstone suites using eleven major element oxides as variables and chose five sandstone suites in eastern Australia to represent his pre-defined groups. Discriminant scores for the analysed Bahi samples from the four boreholes have been calculated (table 5.6) using the unstandardised function coefficient (Bhatia, 1983). In table 5.7, the results are plotted with respect to function I versus function II (Fig. 5.33).

All the studied samples in the Bahi Sandstone Formation in the four boreholes fall into the passive margin field except for two samples from the F6-32 borehole which fall into oceanic island arc and one from the A4-32 and two from the D1-32 boreholes which fall into the active continental margin field.

Passive margins are characterised by mineralogically mature sediments deposited in plate interiors, at stable continental margins or in intracratonic basins. Derived sediments are characterised by recycled quartz-rich sediments originating in older adjacent continental terranes (Bhatia, 1983).

5.7 Conclusions

The significance of the major and trace element distribution within the Bahi Formation leads to the following conclusions:

1: The high amount of SiO_2 in most of the Bahi Sandstone samples is considered to indicate a high degree of maturity, whilst in some samples showing a low content of SiO_2, the cause is probably due to enrichment of the sediment with carbonate, anhydrite and clay minerals.

2: Variation of K_2O and Al_2O_3 is probably due to variation of feldspar and clay mineral content both laterally and vertically.

3: High content of CaO and MgO in some of the studied samples, particularly in the upper part of the formation is related to enrichment with cement composed of varying proportions of calcite, dolomite and anhydrite.

4: Most of the trace elements - La, Rb, Ce, Zn, Ga and Y- show a positive correlation with Al_2O_3 and K_2O but a lack of correlation with al - alk. This may be related to the presence of these trace elements in both K-feldspar and clay minerals.

5: The relationships between Y+La+Ce, Ni+Cr and Sr, show that the Bahi sediment is derived primarily from a pre-existing sedimentary source.

6: The discriminant function analysis technique shows that the Bahi Sandstone is derived from a passive continental margin with a mature sandstone cover.

7: Lateral and vertical distribution of the Bahi Formation shows considerable variation in major and trace elements. This is related to specific lithofacies probably resulting from variation in the environmental conditions at the time of deposition of the unit. It is clear from the various geochemical plots there is variation from borehole to borehole involving clear correlation, particularly in borehole D1-32 and A2-32, but which are not evident in boreholes A4-32 and F6-32. This implies slightly different depositional controls and local diagenetic variations.

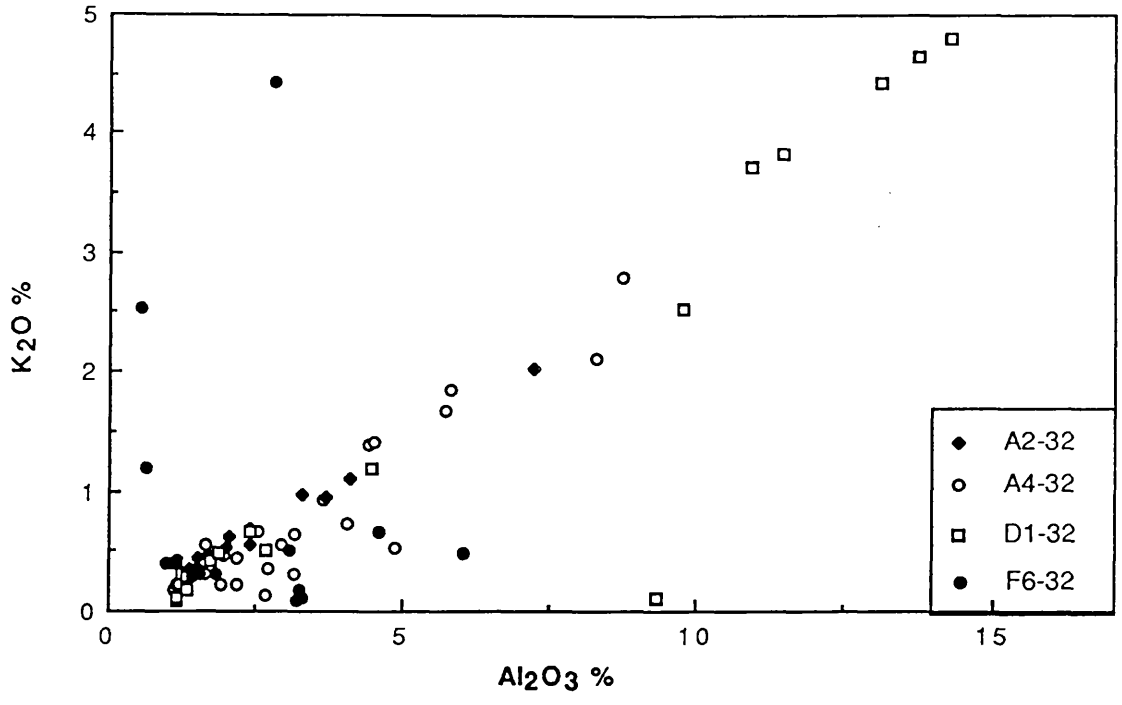

Fig. 5.1 Plot of Al_2O_3 against K_2O in the four boreholes, showing a positive correlation. This suggests that the same source for minerals containing these oxides.

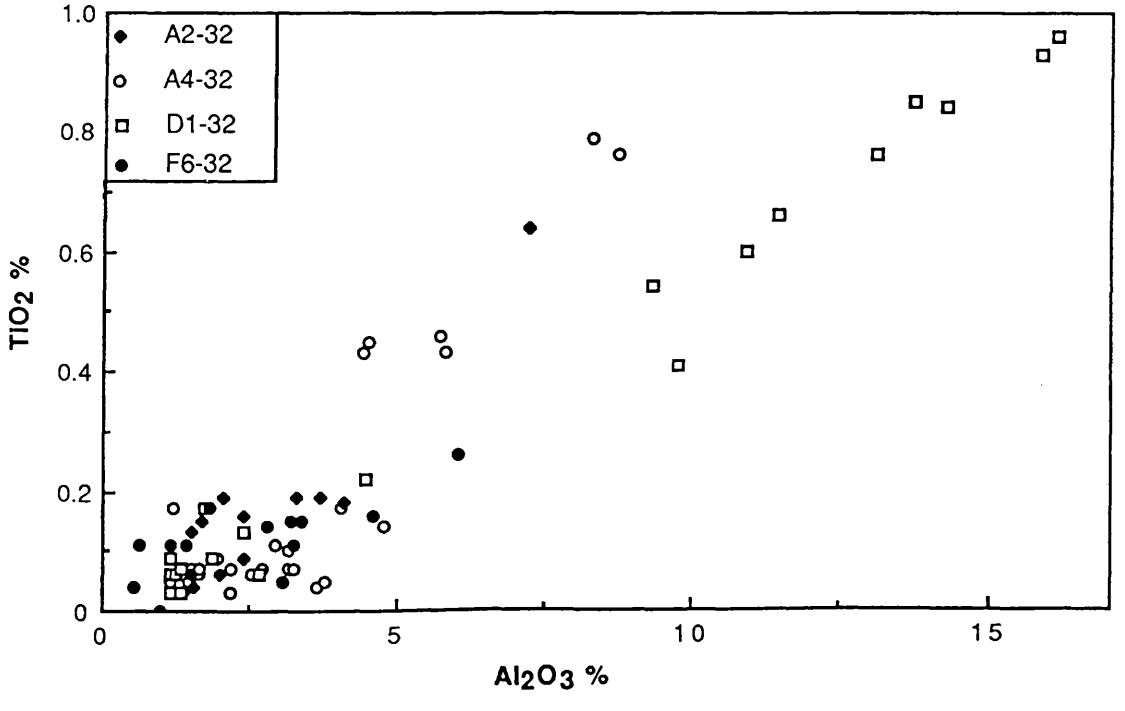

Fig. 5.2 Plot of Al_2O_3 against TiO_2 in the four boreholes, showing a positive correlation. This suggests that titanium is present in the feldspar or in the clay minerals and in detrital grains such as rutile.

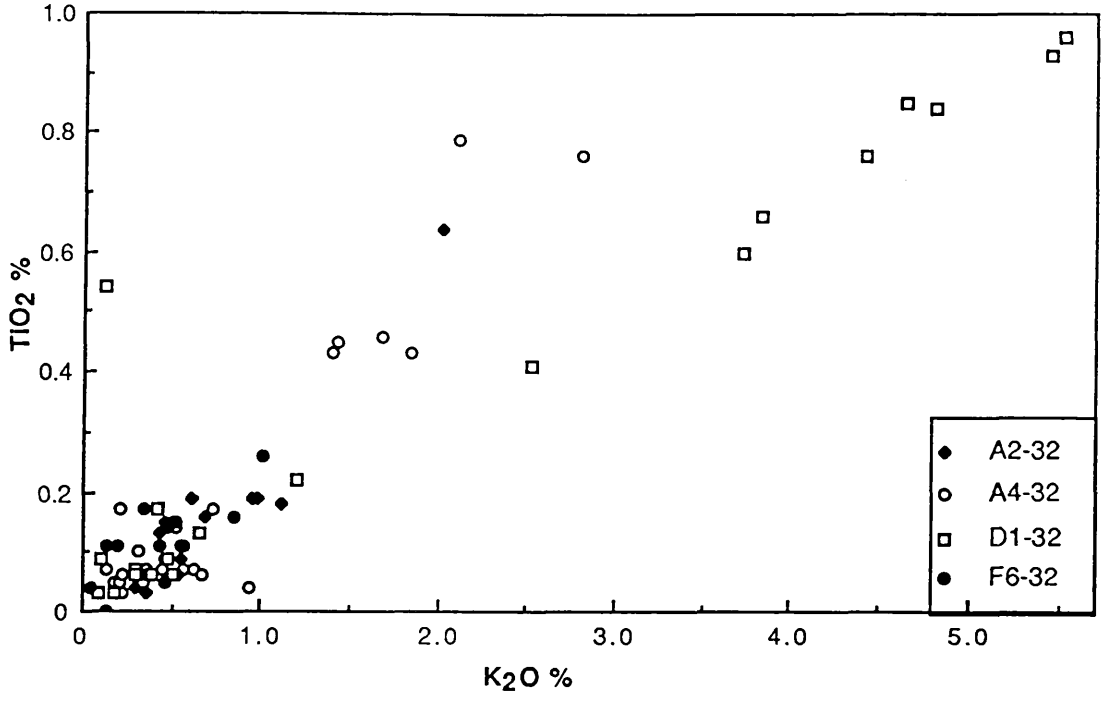

Fig. 5.3 Plot of K_2O against TiO_2 in the four boreholes, suggesting that titanium is concentrated in K-feldspar or in the clay minerals and in detrital grains such as rutile.

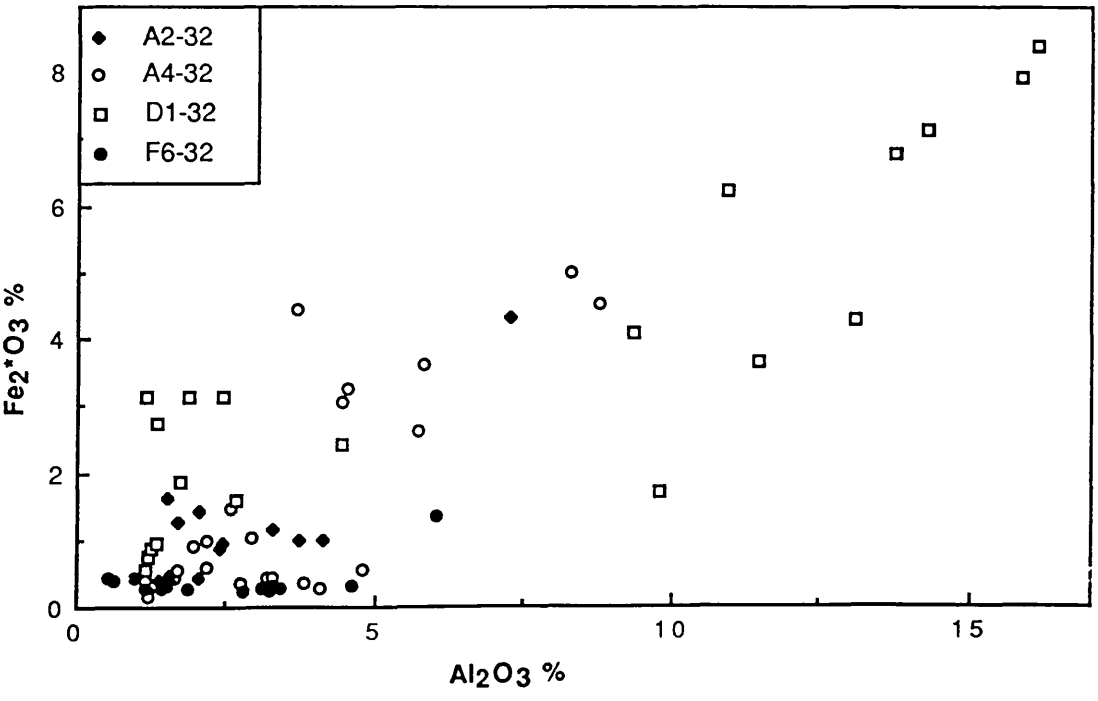

Fig. 5.4 Plot of Al_2O_3 against $Fe_2{}^*O_3$ (total) in the four boreholes, suggesting that iron oxide is present in the feldspar and/or the clay minerals.

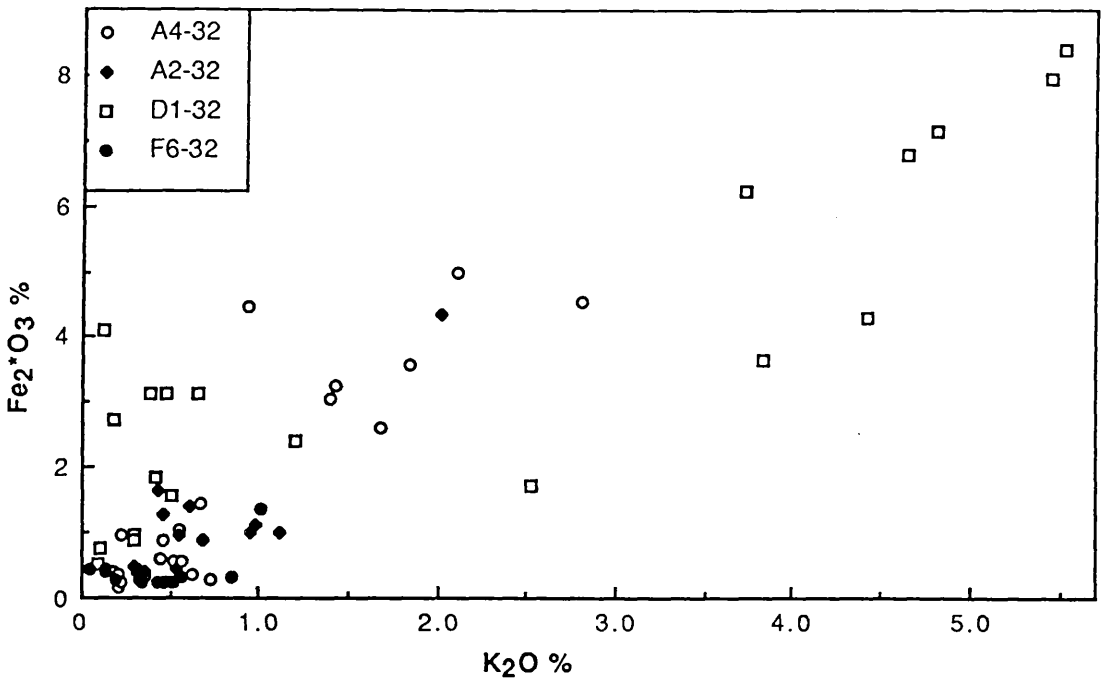

Fig. 5.5 Plot of K_2O against $Fe_2{}^*O_3$ (total) in the four boreholes, suggesting that iron oxide is present in both the K-feldspar and the clay minerals.

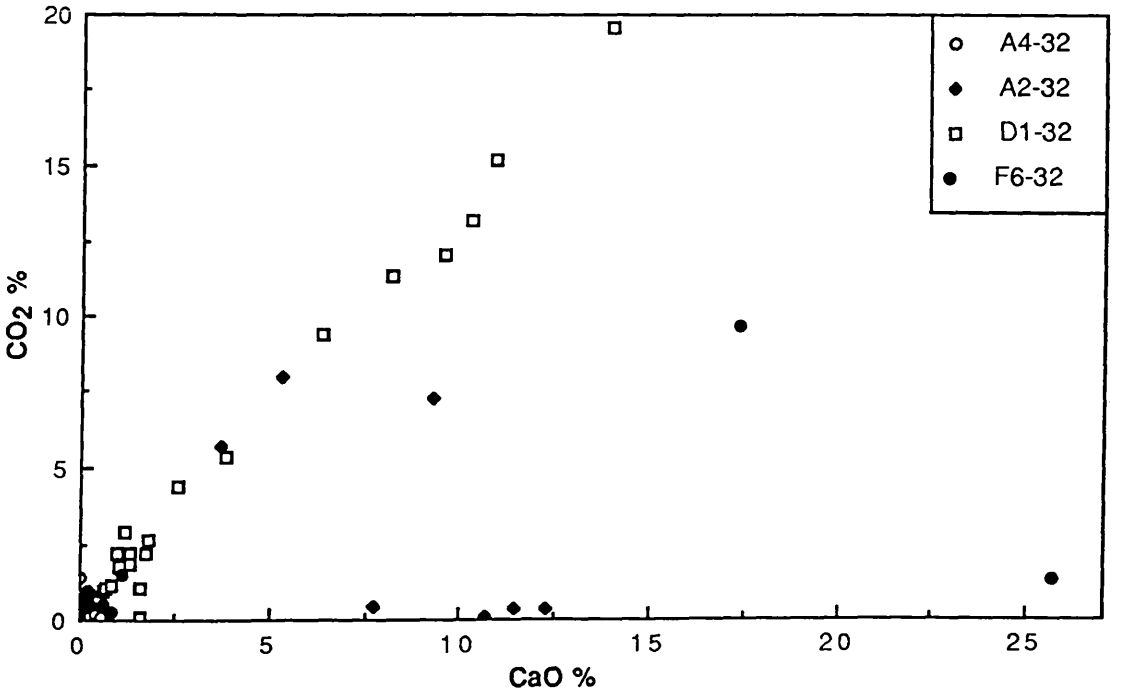

Fig. 5.6 Plot of CaO against CO_2 in the four boreholes, showing a positive correlation. This suggests that a somewhat calcitic cement is present in the Bahi Sandstone.

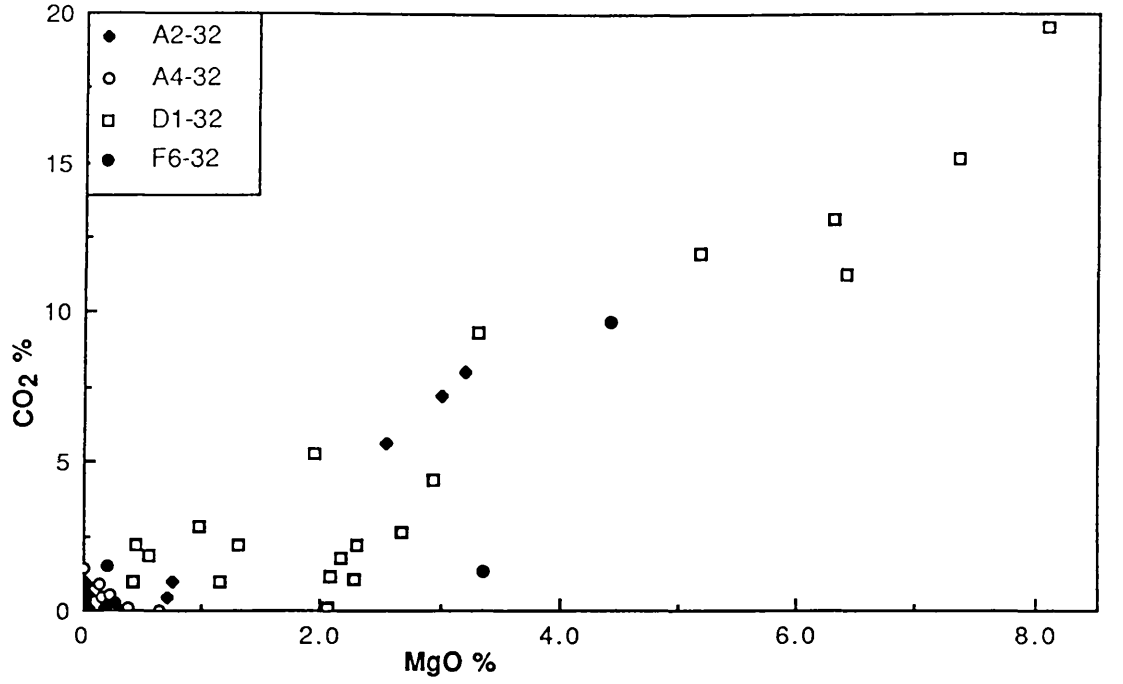

Fig. 5.7 Plot of MgO against CO_2 in the four boreholes, showing a positive correlation. This suggests that a somewhat dolomitic carbonate cement is present in the Bahi sediment.

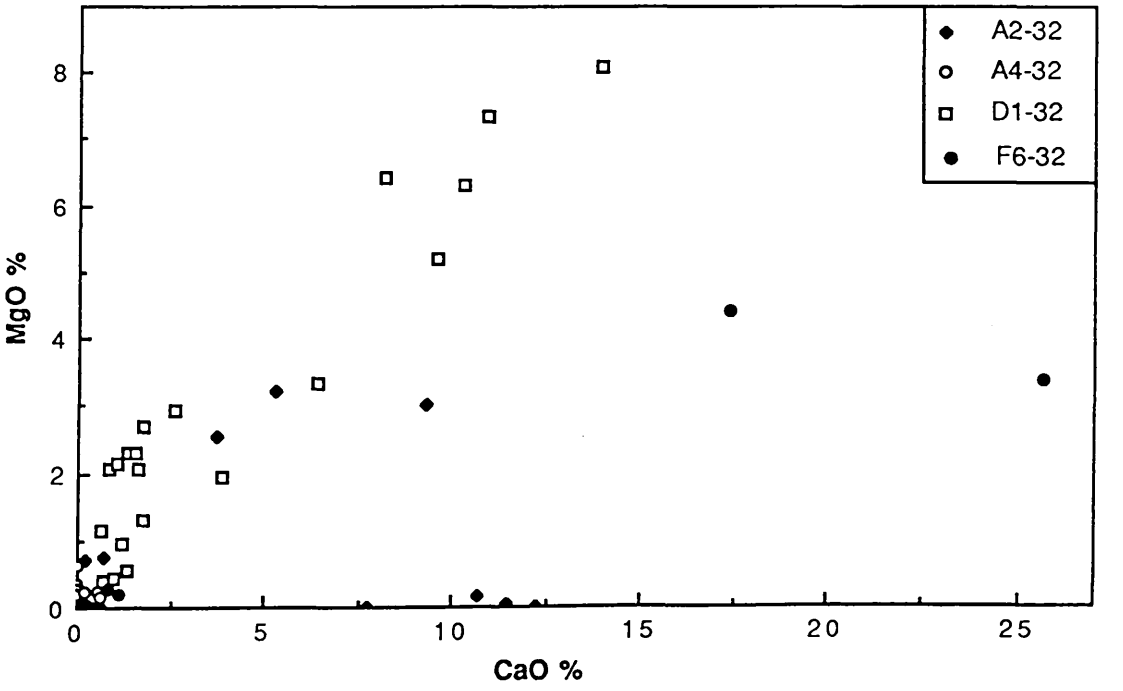

Fig. 5.8 Plot of CaO against MgO in the four boreholes, showing a positive correlation. This suggests that a somewhat calcitic, dolomitic carbonate cement and phyllosilicate minerals are present in the Bahi sediment.

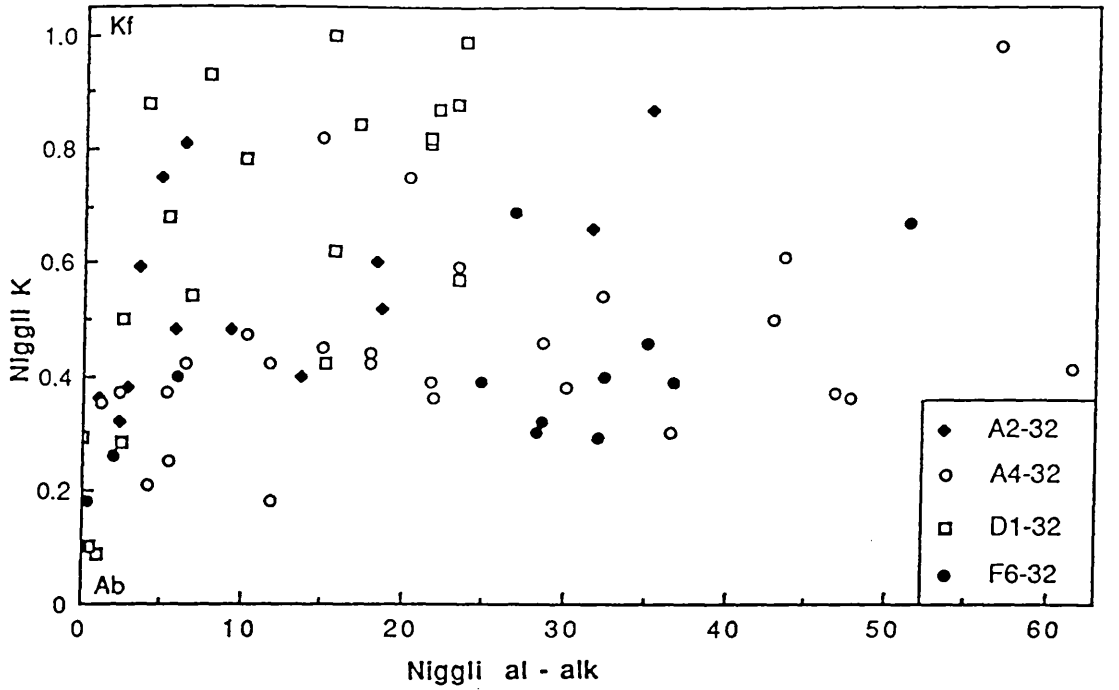

Fig. 5.9 Plot of al - alk against Niggli k in the four boreholes, showing total lack of correlation. This suggests that a mixture of both the feldspar and the clay minerals is present in the Bahi sedment; Al and Kf show the position where albite and potassium feldspar plot.

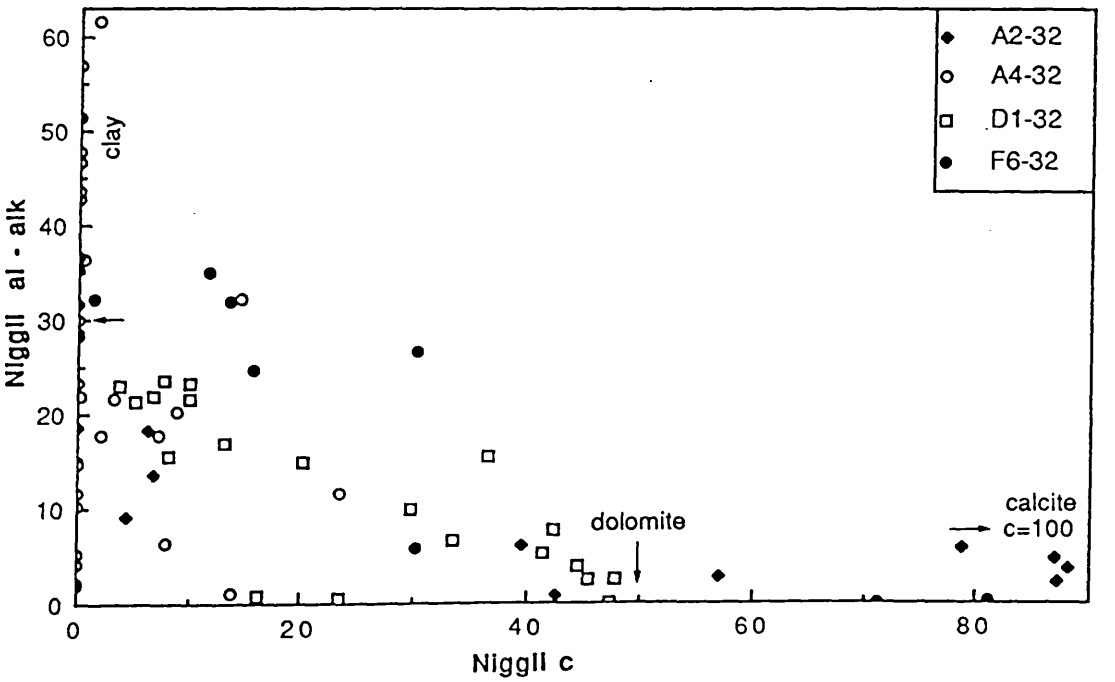

Fig. 5.10 Plot of Niggli c against al - alk in the four boreholes, showing three well defined trends. This suggests that calcite, dolomite and clay minerals are present in the Bahi sediment.

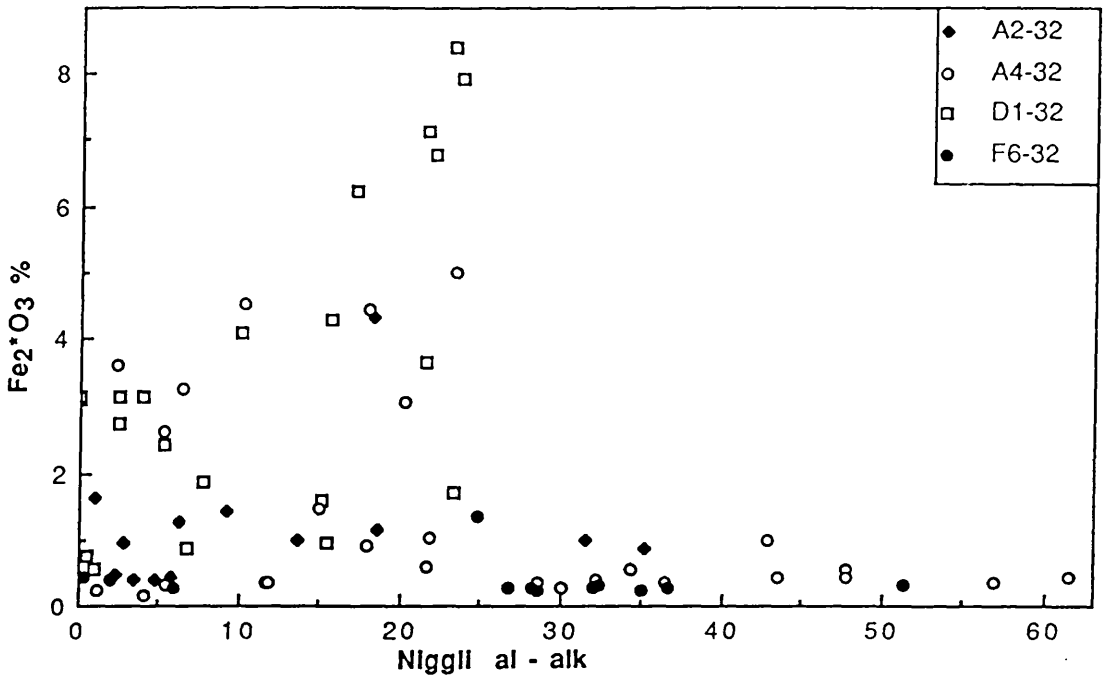

Fig. 5.11 Plot of al - alk against $Fe_2{}^*O_3$ (total) in the four boreholes, showing two trends. One of these trends shows $Fe_2{}^*O_3$ associated with clay minerals, the other shows no such correlation and may be related to detrital iron oxides.

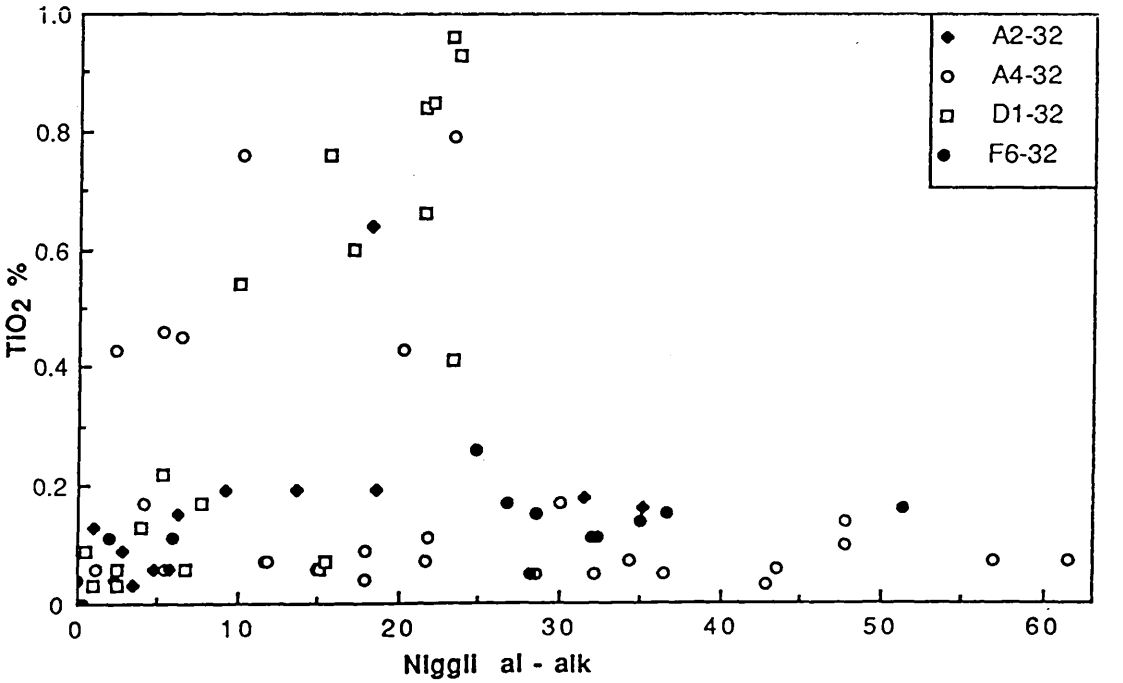

Fig. 5.12 Plot of al - alk against TiO_2 in the four boreholes, showing two trends. One trend suggests that titanium is present mainly in the clay minerals, the other suggests titanium in detrital oxides such as rutile or iron oxides.

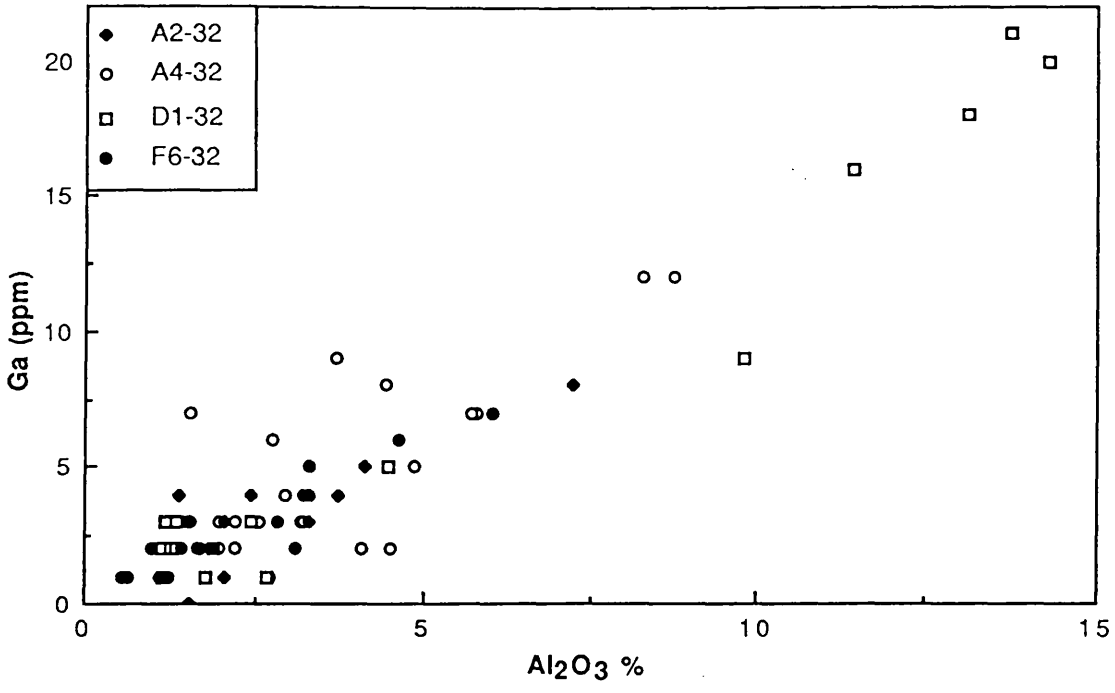

Fig. 5.13 Plot of Al_2O_3 against Ga in the four boreholes, showing a positive correlation. This suggests that gallium is associated with feldspar and/ or clay minerals.

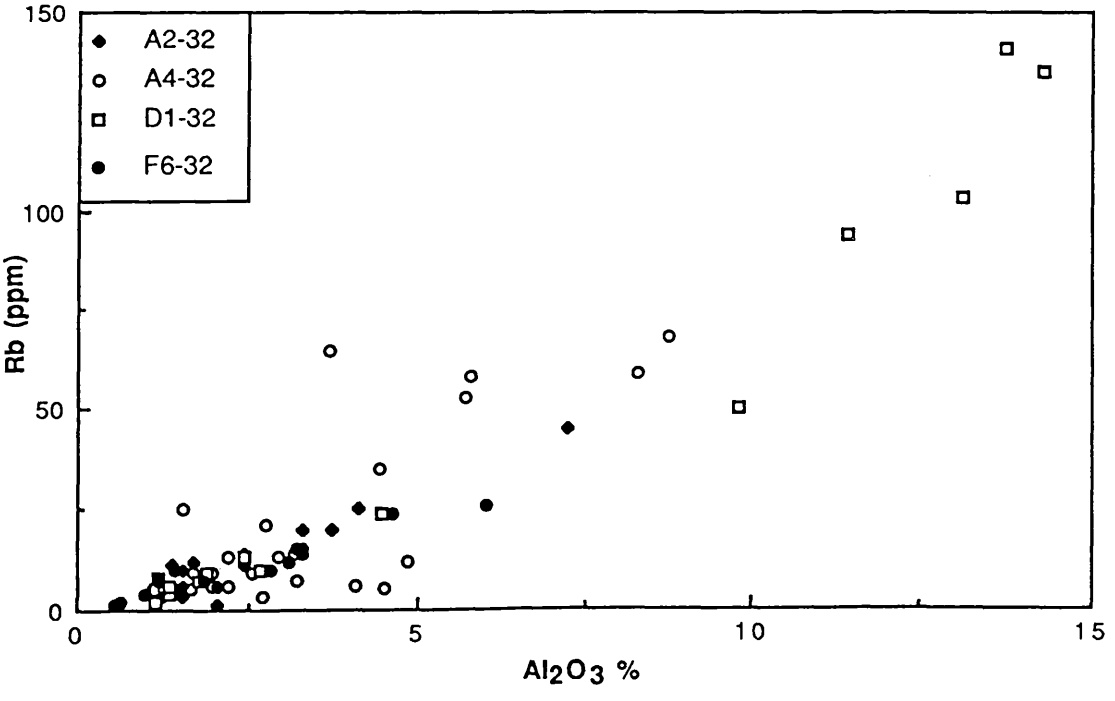

Fig. 5.14 Plot of Al_2O_3 against Rb in the four boreholes, showing a positive correlation. This suggests that rubidium is concentrated in the feldspar and the clay minerals.

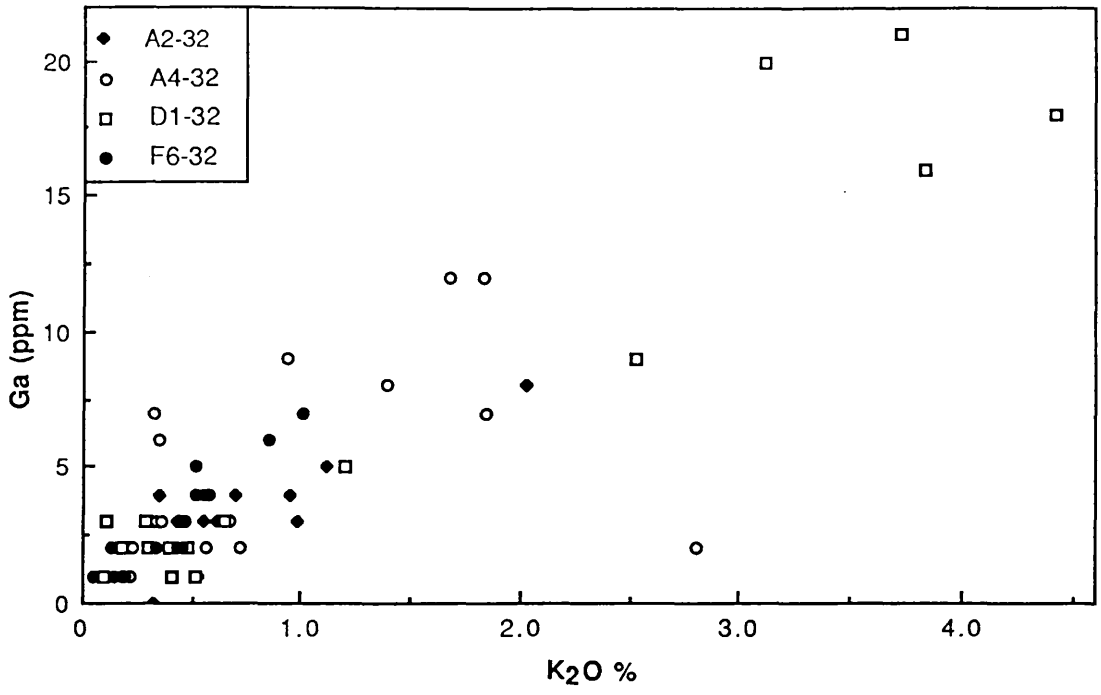

Fig. 5.15 Plot of K_2O against Ga in the four boreholes, showing a positive correlation. This suggests that gallium is concentrated in the K-feldspar and/or the clay minerals.

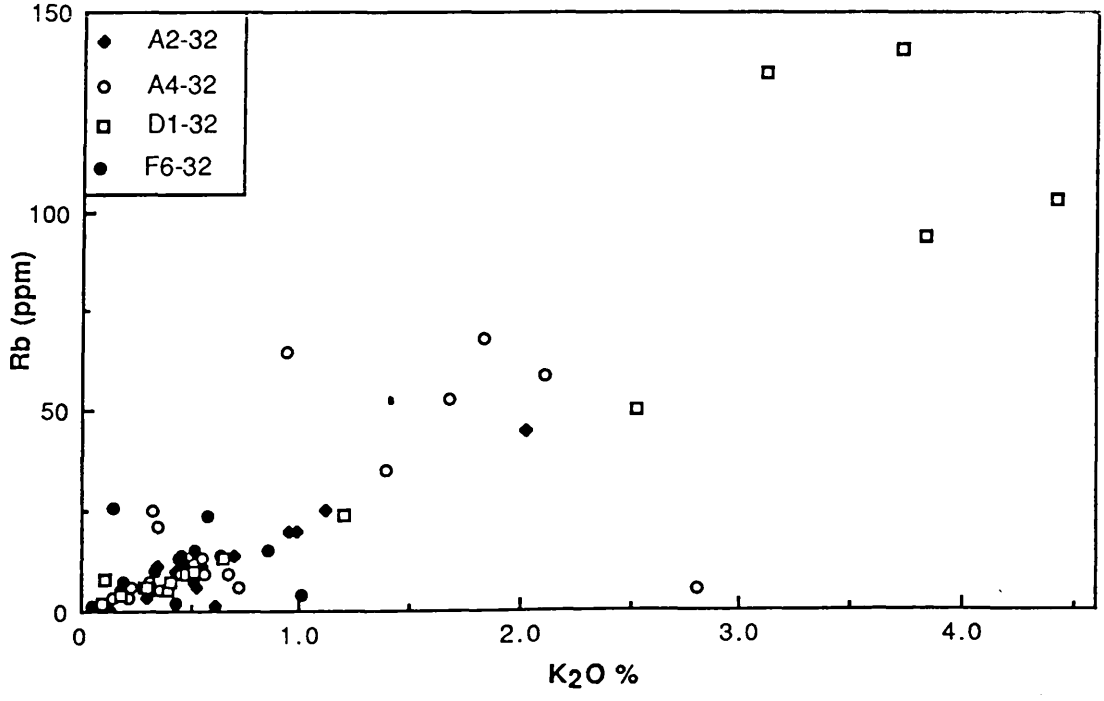

Fig. 5.16 Plot of K_2O against Rb in the four boreholes, showing a positive correlation. This suggests that rubidium is present in the K-feldspar and/or in the clay minerals.

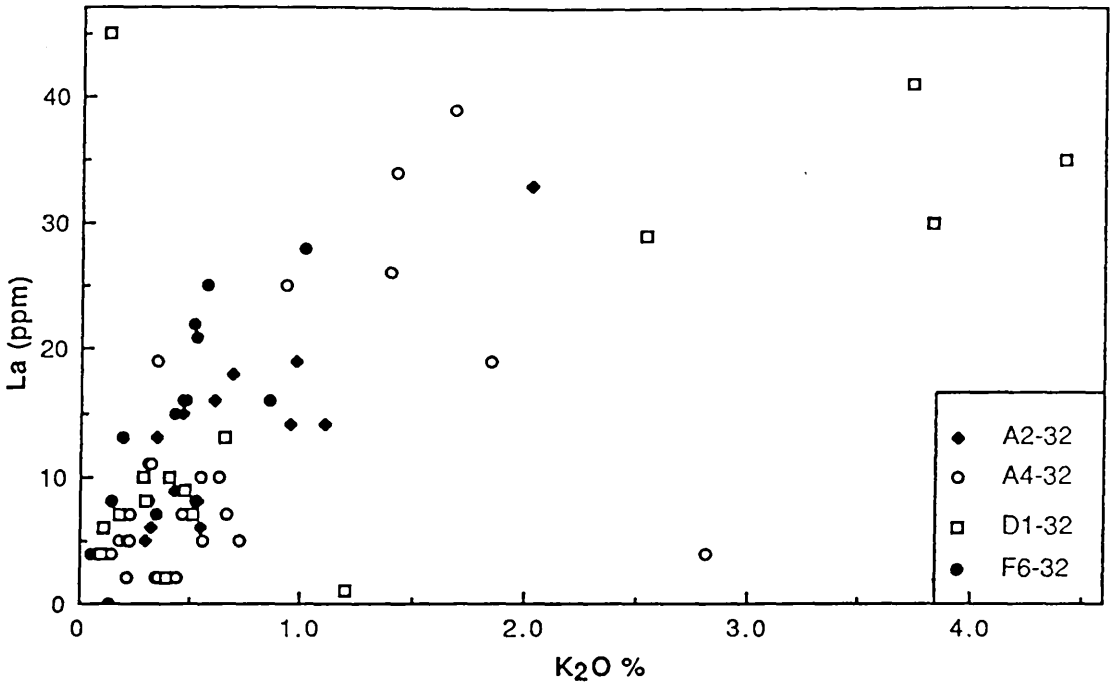

Fig. 5.17 Plot of K_2O agianst La in the four boreholes, showing a positive correlation. This suggests that the lanthanium is associated with K-feldspar and/or clay minerals.

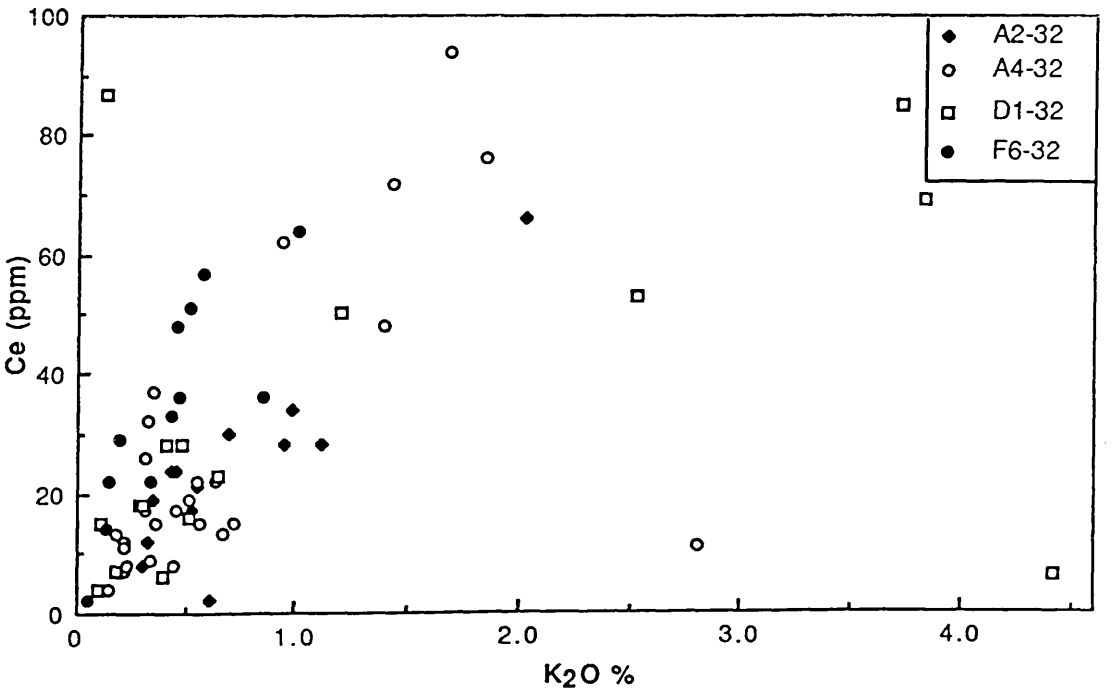

Fig. 5.18 Plot of K_2O agianst Ce in the four boreholes, showing a positive correlation. This suggests that the cerium is concentrated in the K-feldspar and/or in the clay minerals.

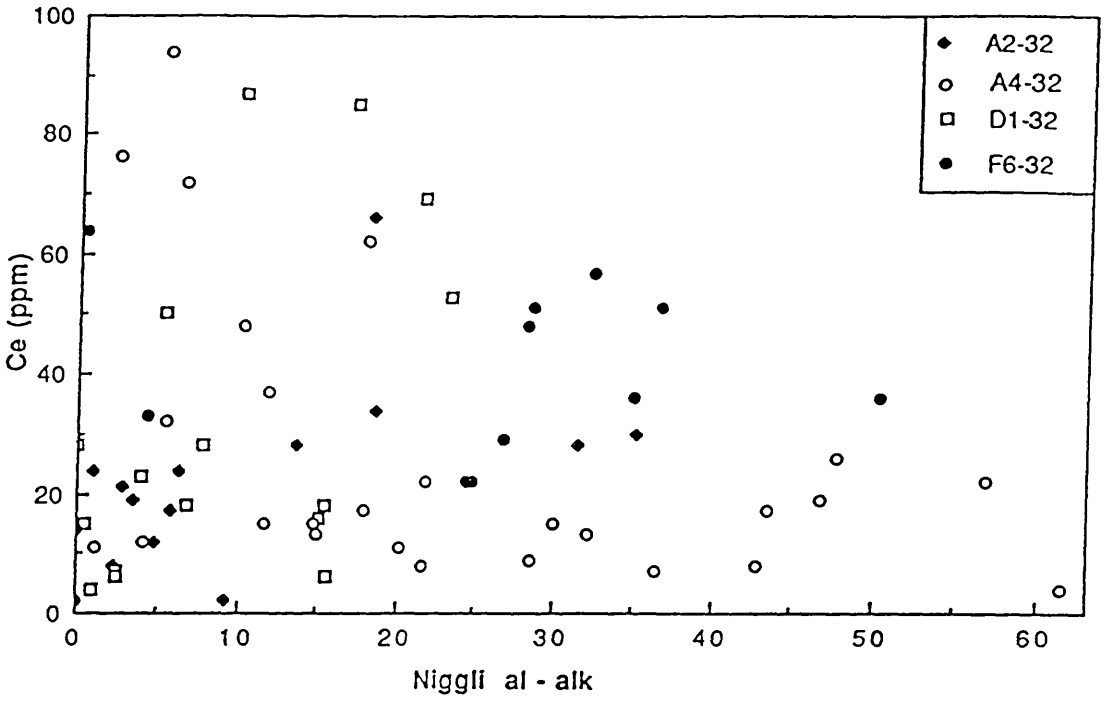

Fig. 5.19 Plot of al - alk against Ce in the four boreholes, showing lack of correlation. This suggests that cerium is neither associated solely with feldspar nor clay minerals.

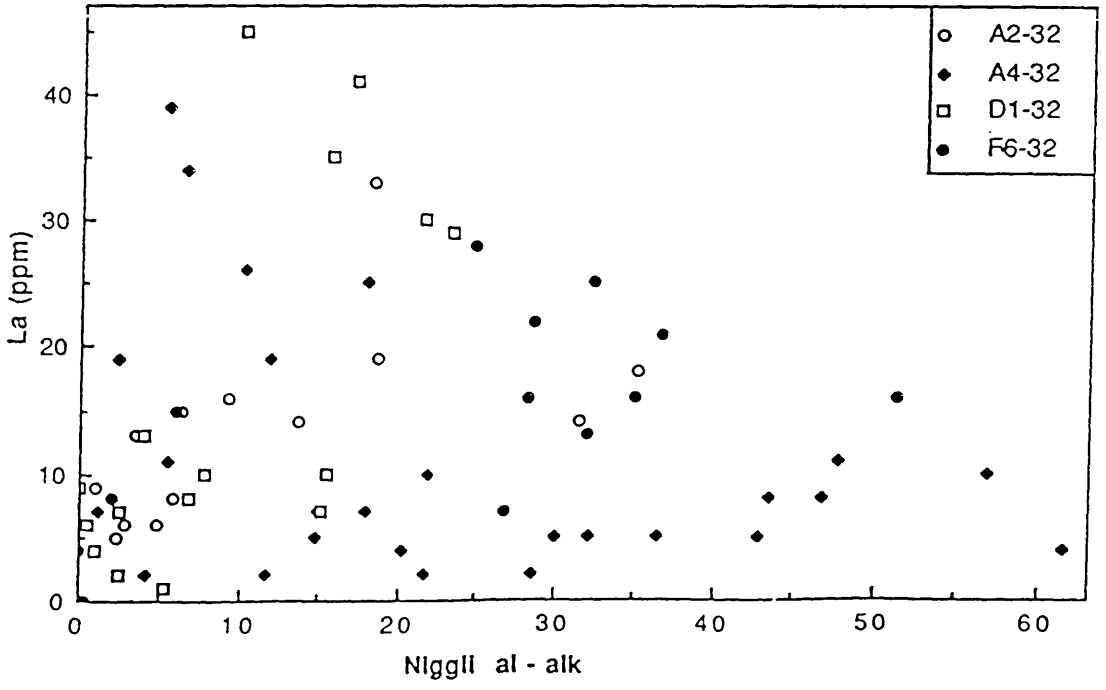

Fig. 5.20 Plot of al - alk against La in the four boreholes, showing lack of correlation. This suggests that lanthanium is neither associated solely with feldspar nor clay minerals.

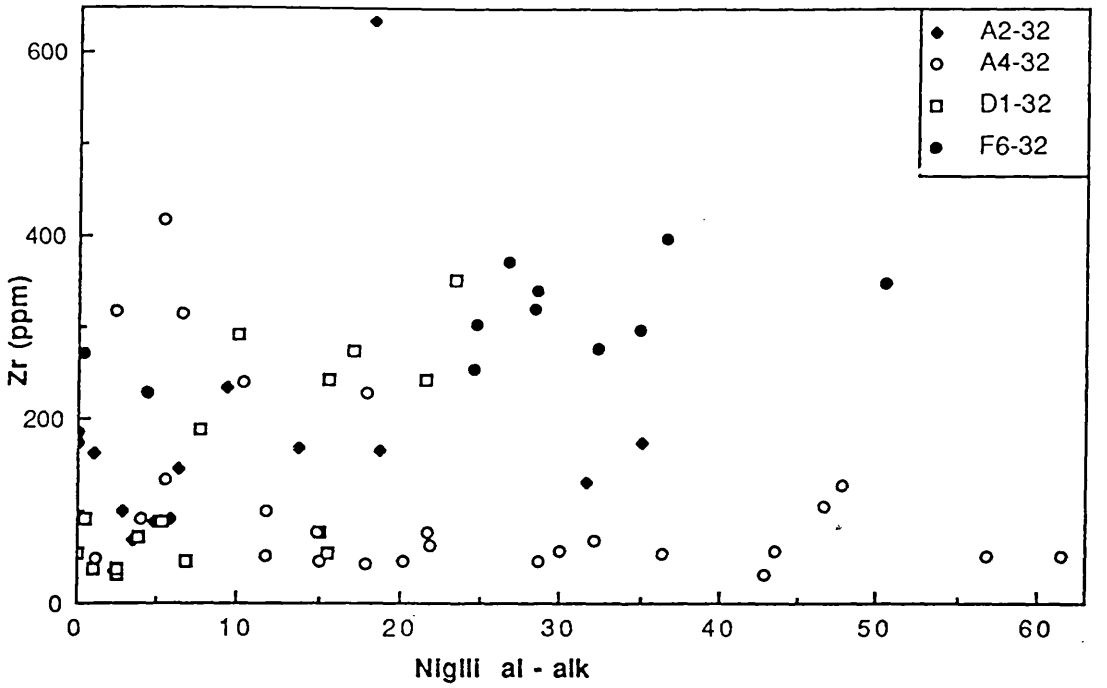

Fig. 5.21 Plot of al - alk against Zr in the four boreholes, showing lack of correlation. This suggests that zirconium is neither associated solely with feldspar nor clay minerals.

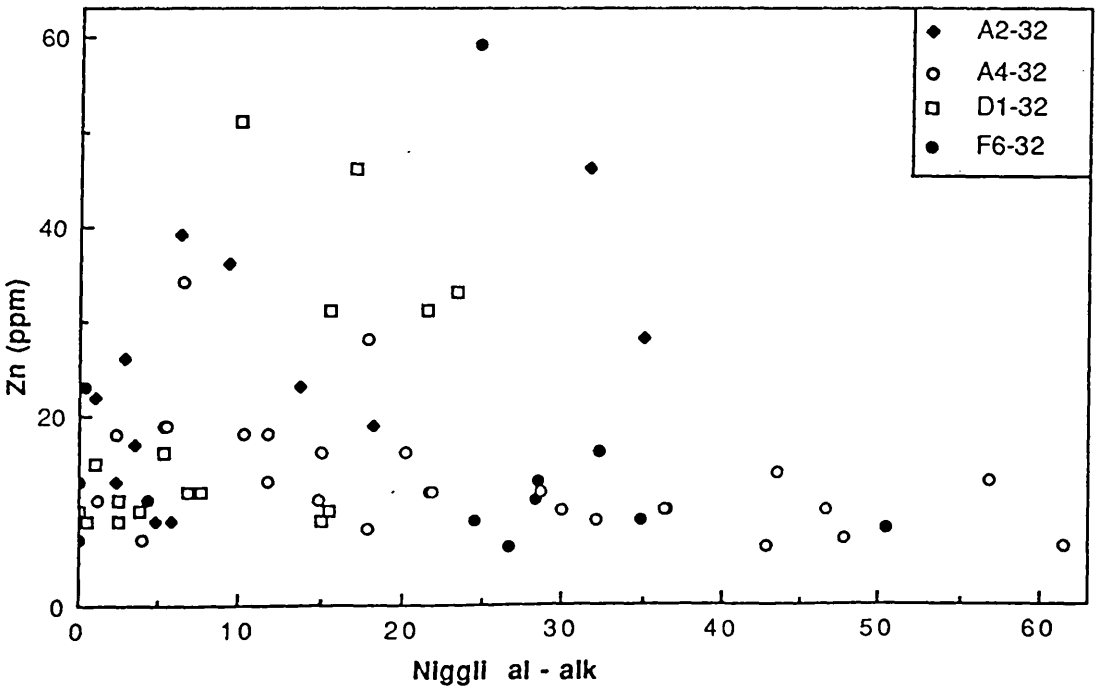

Fig. 5.22 Plot of al - alk against Zn in the four boreholes, showing lack of correlation. This suggests that zinc is neither associated solely with feldspar nor clay minerals.

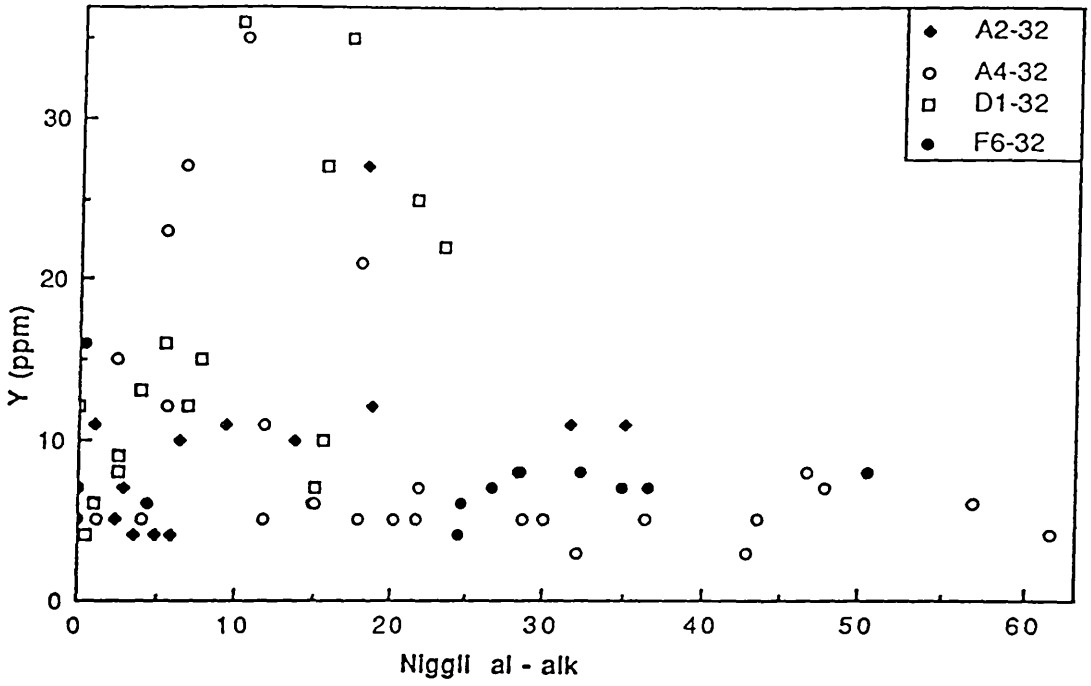

Fig. 5.23 Plot of al - alk against Y in the four boreholes, showing lack of correlation. This suggests that yttrium is neither associated solely with feldspar nor clay minerals.

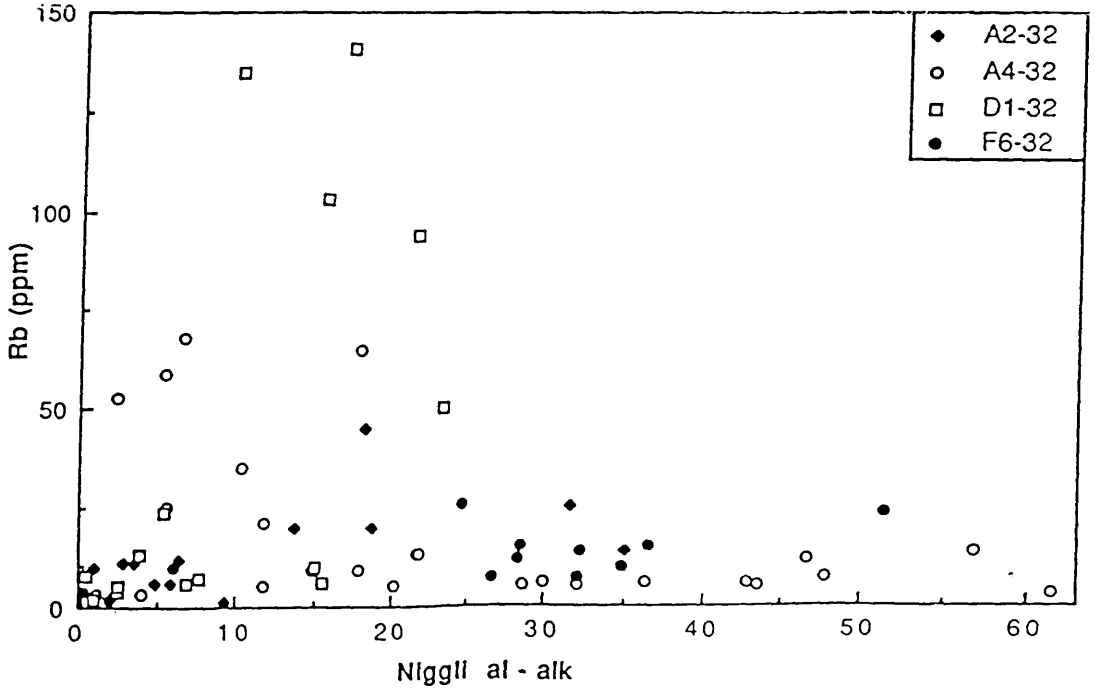

Fig. 5.24 Plot of al - alk against Rb in the four boreholes, showing lack of correlation. This suggests that rubidium is neither associated solely with feldspar nor clay minerals.

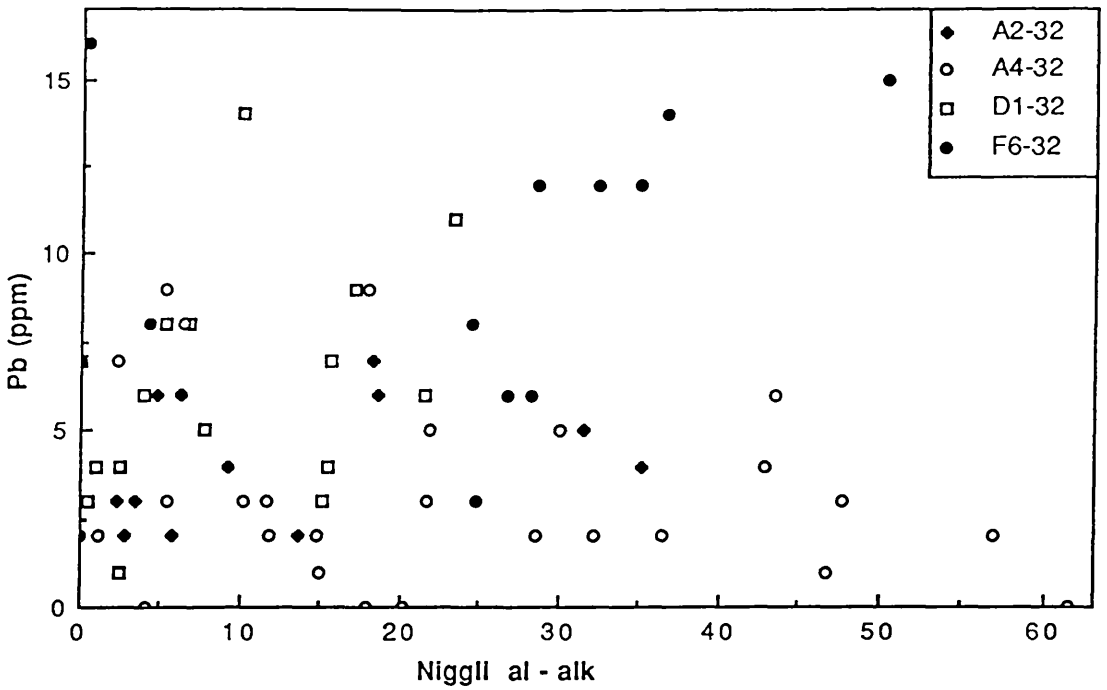

Fig. 5.25 Plot of al - alk against Pb in the four boreholes, showing lack of correlation. This suggests that lead is neither associated solely with feldspar nor clay minerals.

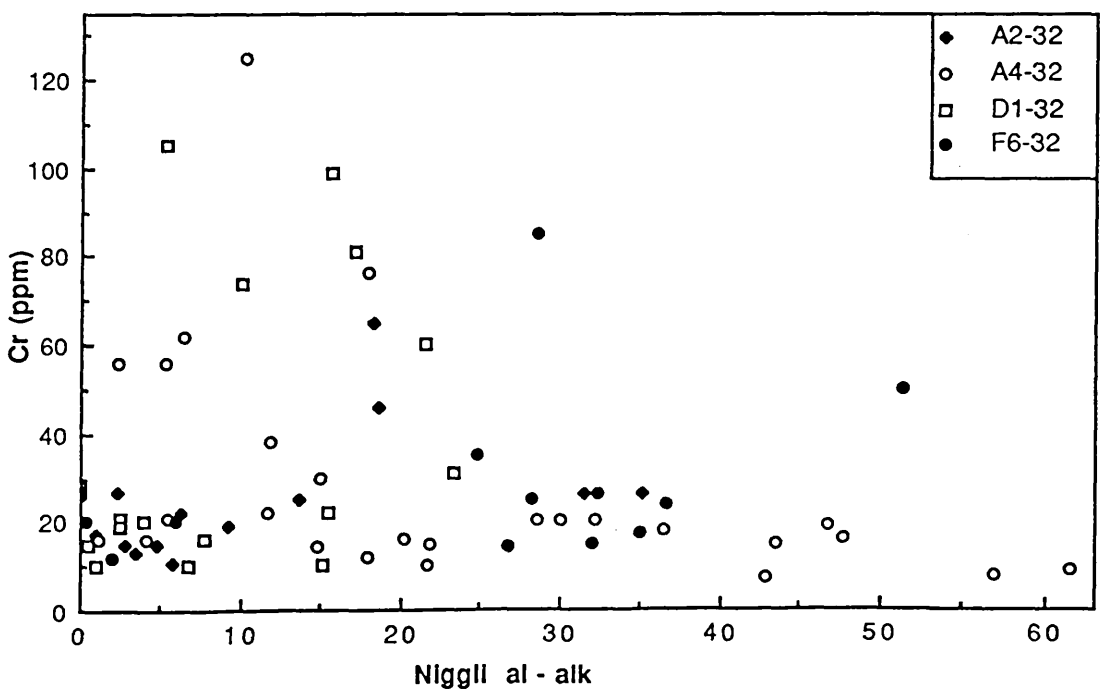

Fig. 5.26 Plot of al - alk against Cr in the four boreholes, showing lack of correlation. This suggests that chromium is neither associated solely with feldspar nor clay minerals.

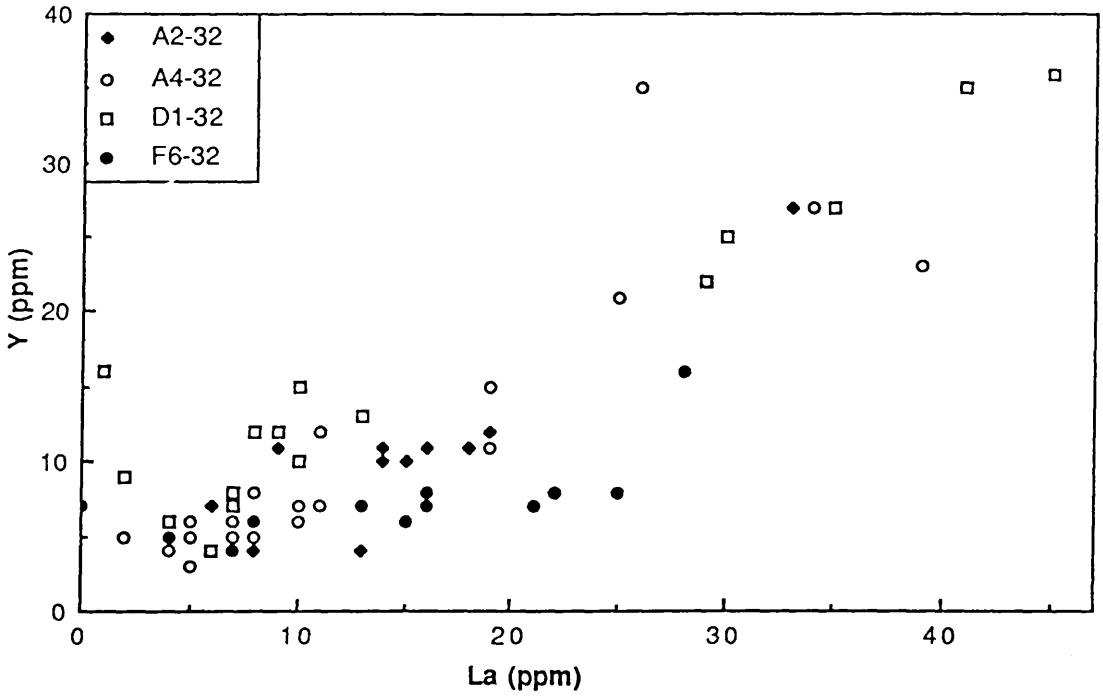

Fig. 5.27 Plot of La against Y in the four boreholes, showing a positive correlation. This suggests that both elements are associated in the same detrital minerals.

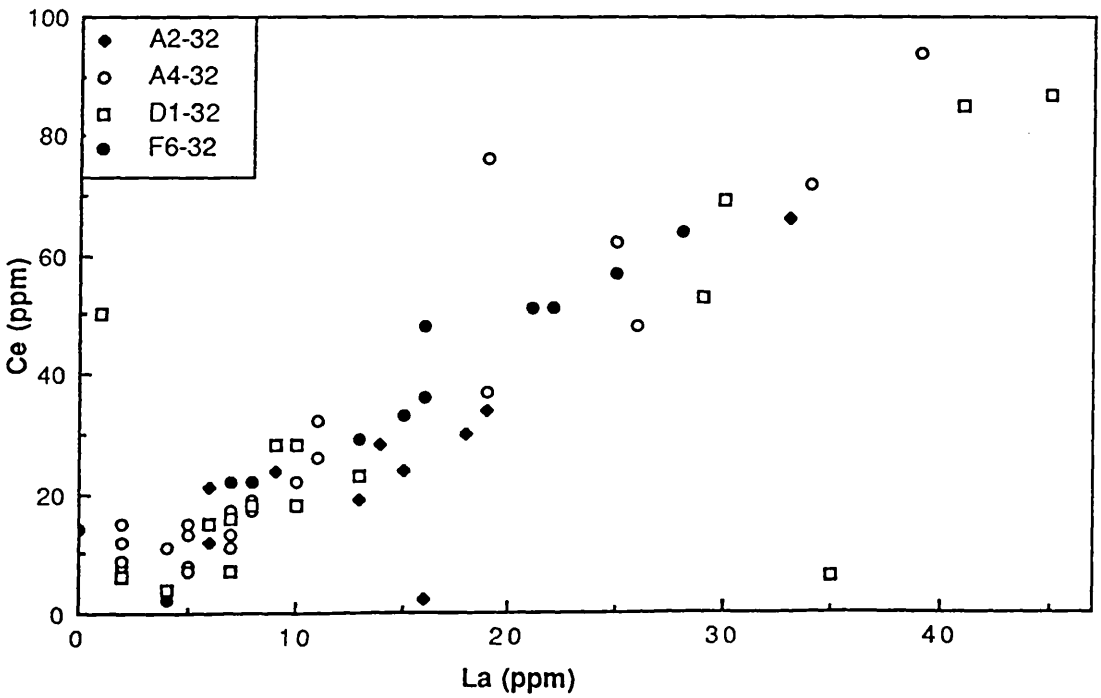

Fig. 5.28 Plot of La against Ce in the four boreholes, showing a positive correlation. This suggests that both elements are associated in the same detrital minerals.

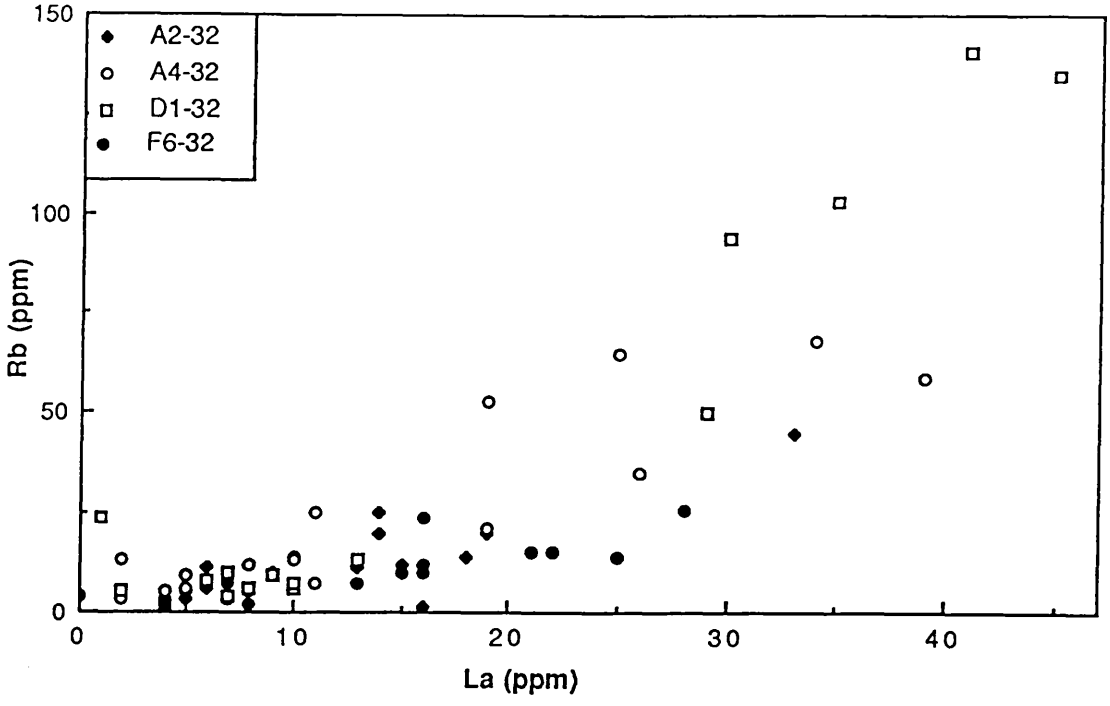

Fig. 5.29 Plot of La against Rb in the four boreholes, showing a poor positive correlation. Since rubidium is present in the K-feldspar and/or the clay minerals, this shows that lanthanium is probably also largely in these minerals.

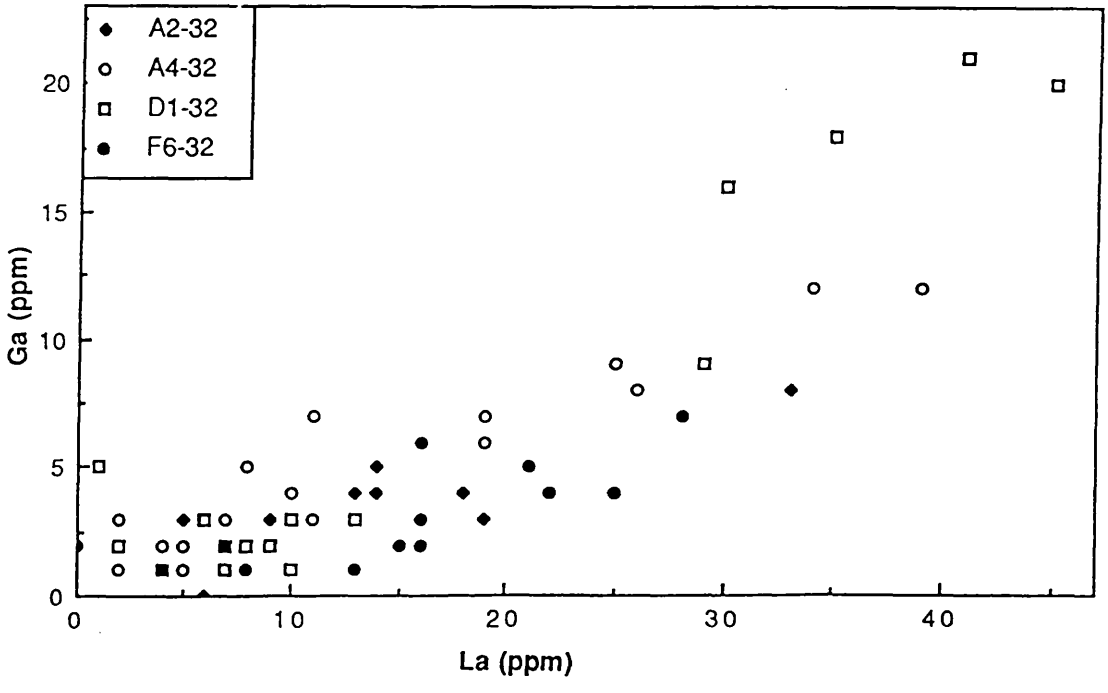

Fig. 5.30 Plot of La against Ga in the four boreholes, showing a poor positive correlation. This suggests that gallium is concentrated in the K-feldspar and/or clay minerals.

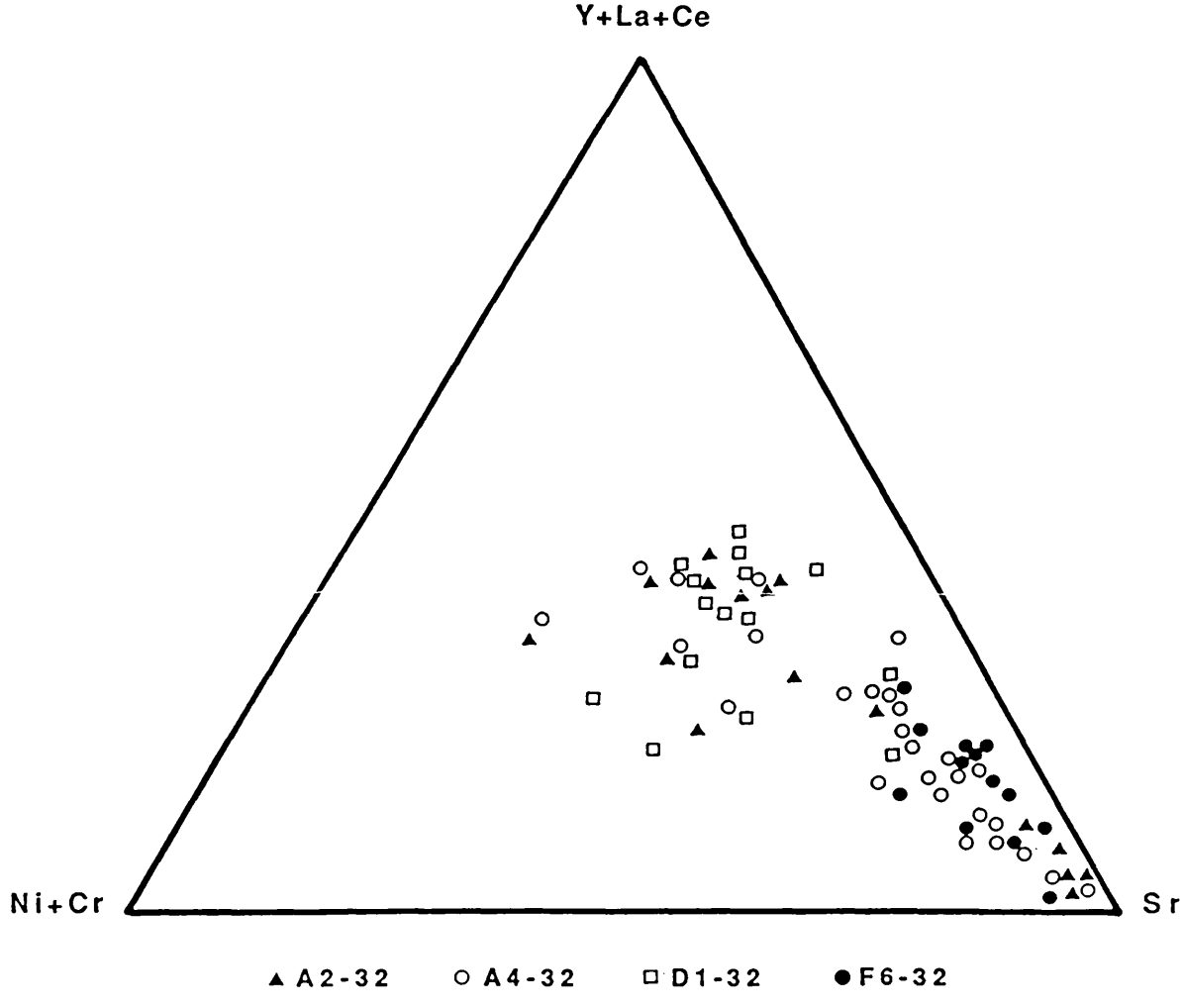

Fig. 5.31 Plot of Ni+Cr versus Y+La+Ce versus Sr in the four boreholes, suggesting that the Bahi Sandstone Formation is derived from a pre-existing sedimentary source or sources.

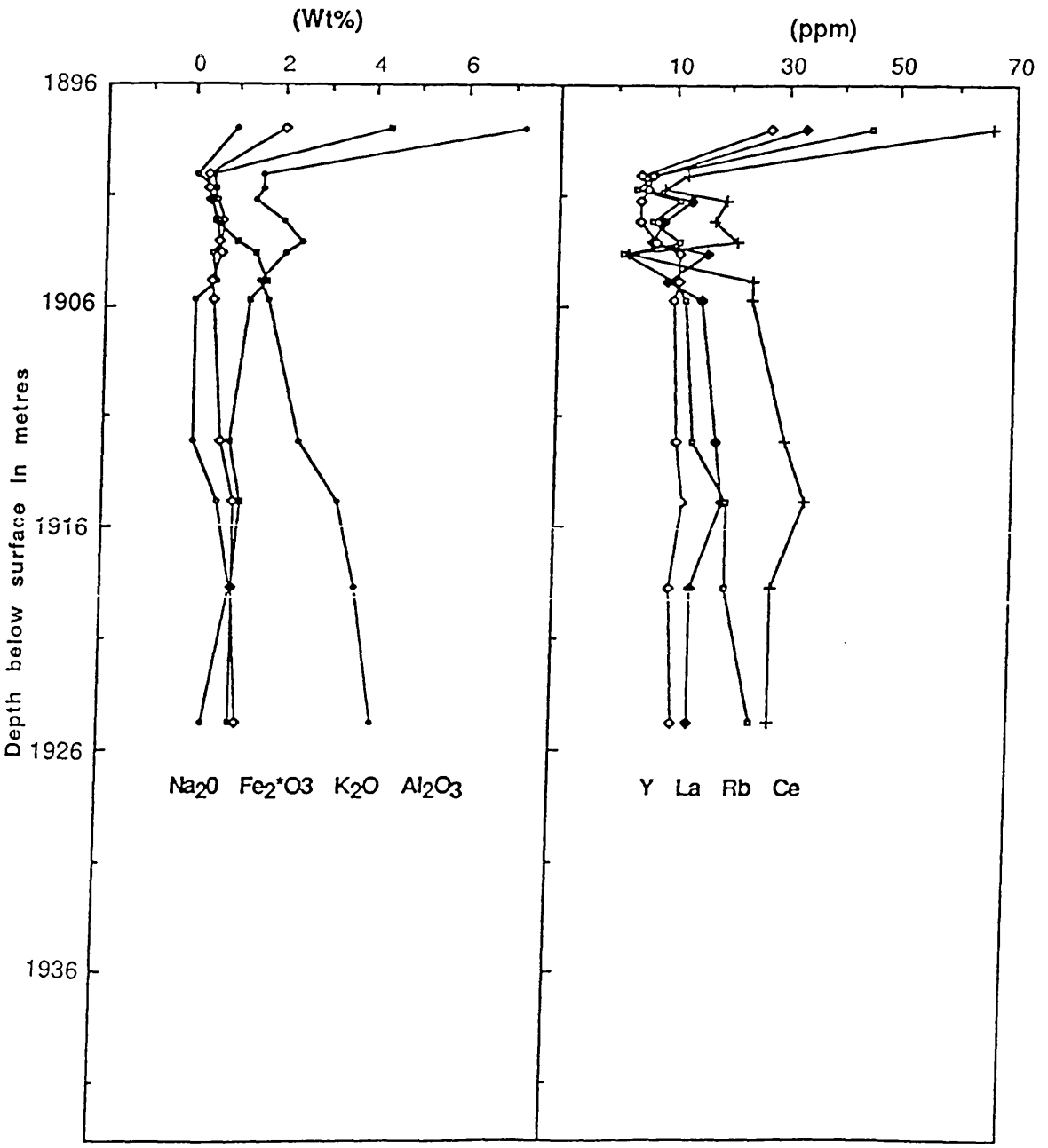

Fig. 5.32a Diagram showing variation in chemical composition and the concentration of major and trace elements with position in the Bahi Sandstone Formation (A2-32 borehole). The uppermost (glauconite-bearing) part of the formation is represented by the uppermost sample.

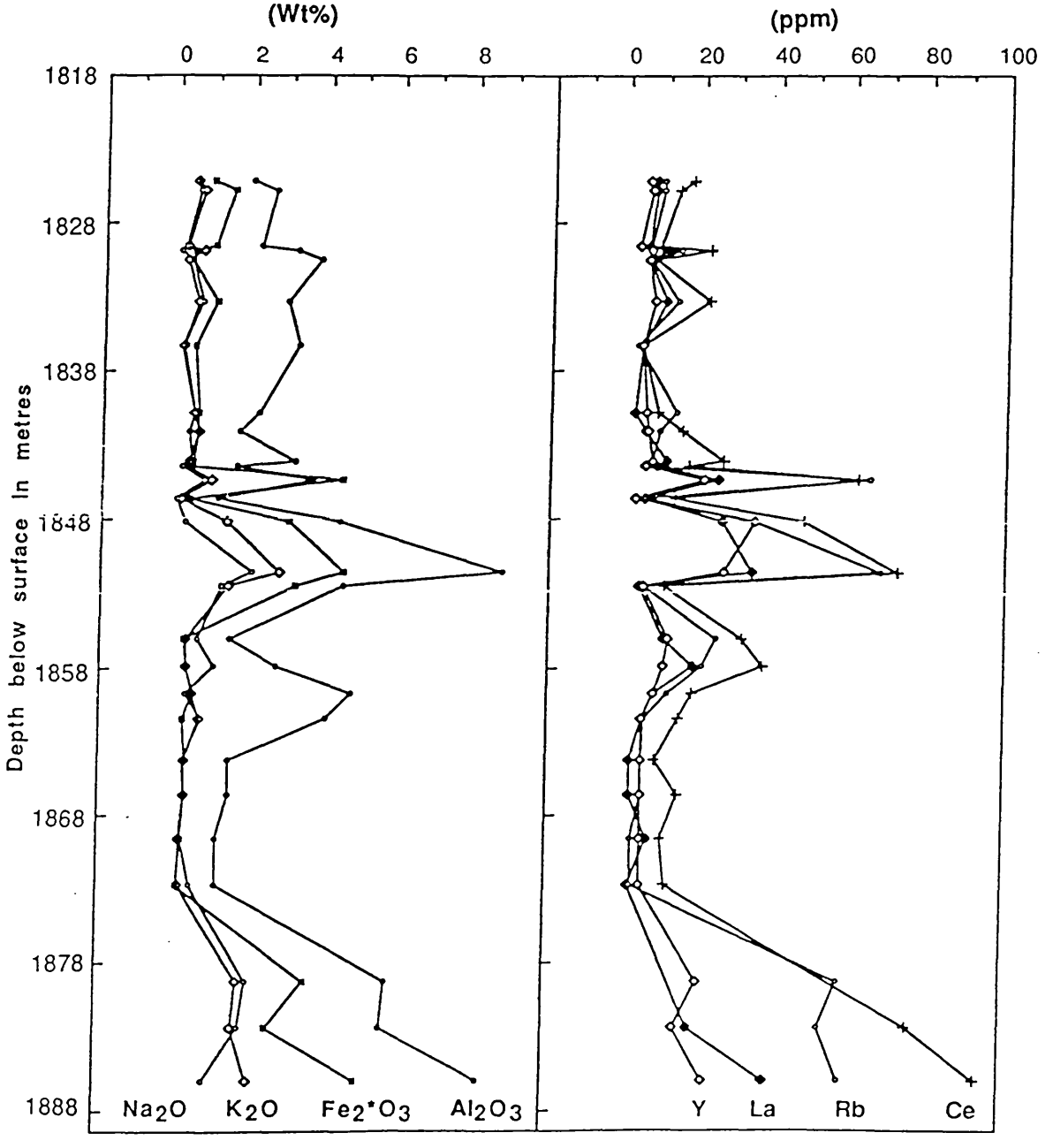

Fig. 5.32b Diagram showing variation in chemical composition and the concentration of major and trace elements with position in the Bahi Sandstone Formation (A4-32 borehole). The uppermost (glauconite-bearing) part of the formation is not represented.

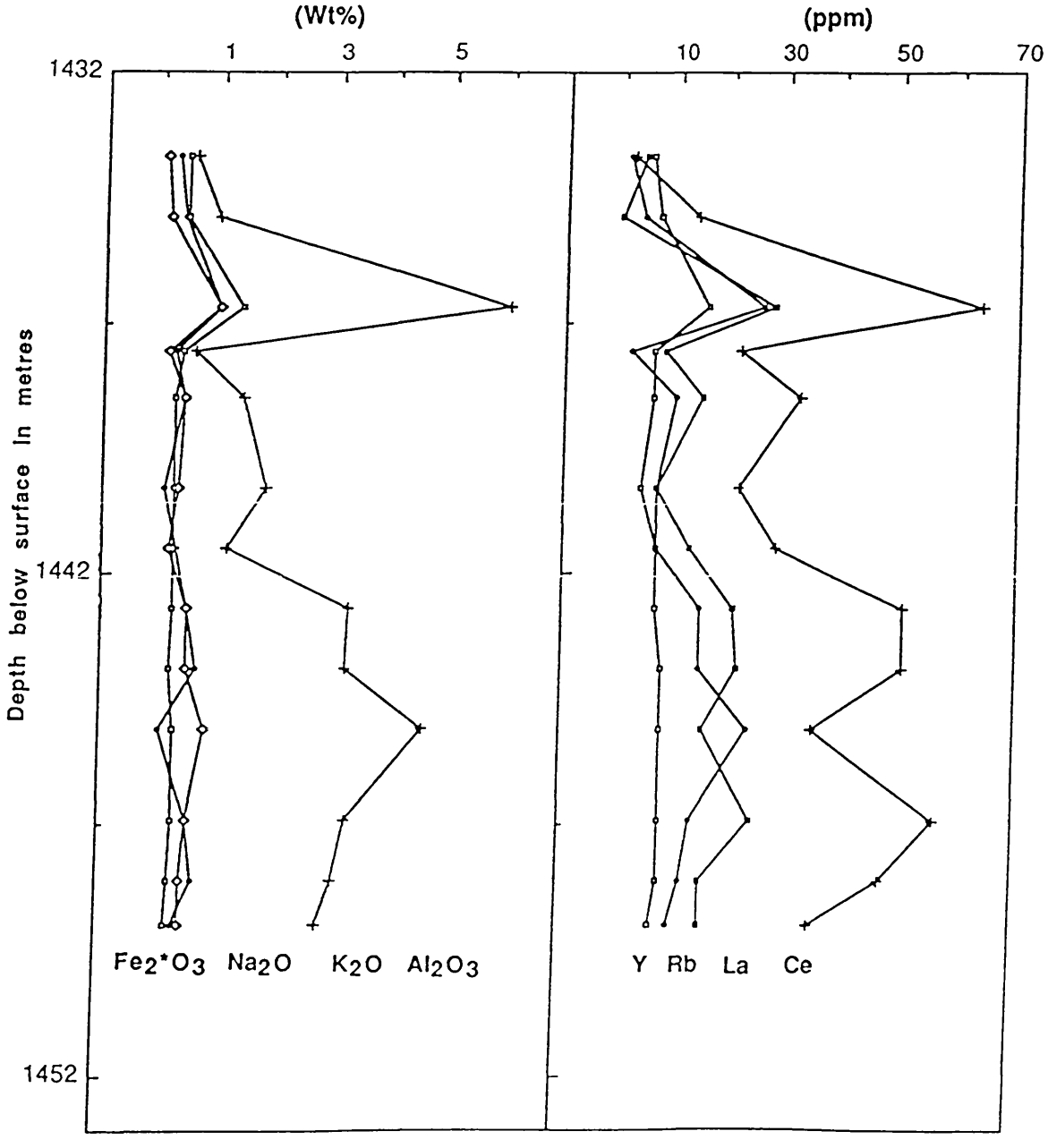

Fig. 5.32c Diagram showing variation in chemical composition and the concentration of major and trace elements with position in the Bahi Sandstone Formation (F6-32 borehole). The uppermost (glauconite-bearing) part of the formation is not represented.

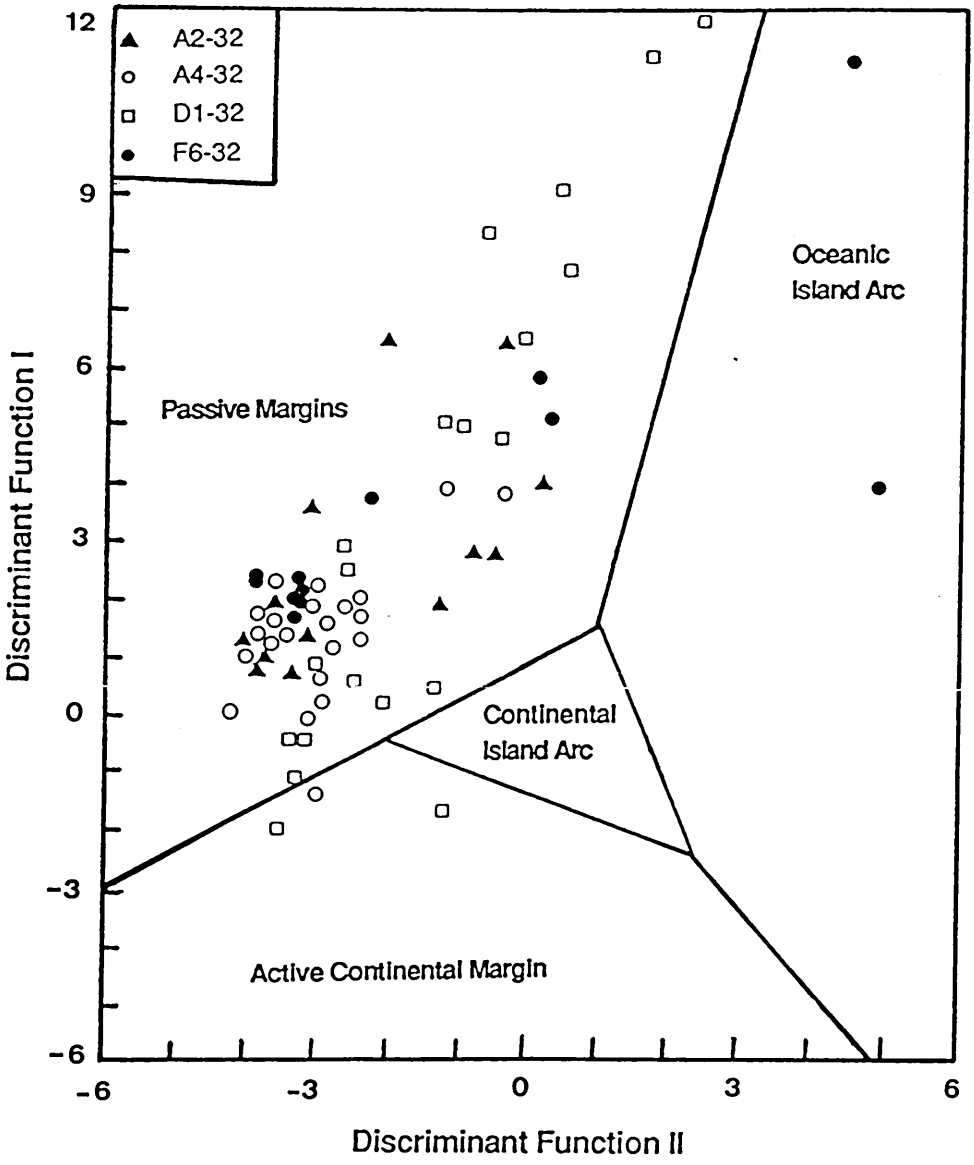

Fig. 5.33 Plot of discriminant scores along Function I versus Function II in the Bahi Sandstone Formation in the four boreholes, using Bhatia's (1983) fields of various tectonic setting. This suggests that the Bahi Sandstone Formation was derived from a passive continental margin.

Table 5.1 Chemical analysis (major & trace elements) of the Bahi Sandstone in the A2-32 borehole.

Sample (Wt %)	A2-1	A2-2	A2-3	A2-4	A2-5	A2-6	A2-7	A2-8	A2-9	A2-12	A2-13	A2-15	A2-17
SiO_2	80.06	71.13	68.54	64.28	77.55	68.10	94.40	78.50	85.45	94.14	92.46	92.00	91.18
TiO_2	0.64	0.06	0.04	0.03	0.06	0.09	0.19	0.13	0.15	0.16	0.19	0.19	0.18
Al_2O_3	7.24	1.53	1.54	1.37	2.02	2.43	2.04	1.51	1.68	2.41	3.29	3.70	4.11
Fe_2O_3	3.53	0.32	0.28	0.25	0.32	0.38	1.32	1.16	1.07	0.79	1.04	0.91	0.88
FeO	0.72	0.08	0.08	0.08	0.08	0.52	0.08	0.42	0.19	0.09	0.08	0.07	0.10
MnO	0.05	0.03	0.02	0.03	0.05	0.12	0.00	0.16	0.08	0.00	0.02	0.01	0.01
MgO	0.75	0.17	0.02	0.00	0.00	3.00	0.70	3.20	2.55	0.00	0.00	0.05	0.04
CaO	0.69	10.69	11.45	12.26	7.73	9.31	0.18	5.29	3.73	0.00	0.00	0.31	0.00
Na_2O	0.90	0.07	0.41	0.52	0.68	0.60	0.43	0.50	0.07	0.07	0.59	0.94	0.37
K_2O	2.02	0.32	0.30	0.35	0.53	0.55	0.61	0.43	0.46	0.69	0.98	0.95	1.11
P_2O_5	0.11	0.02	0.01	0.02	0.02	0.02	0.05	0.02	0.01	0.02	0.02	0.02	0.01
SO_3	-	14.16	15.66	14.97	9.09	5.92	-	-	-	-	-	-	-
H_2O	1.93	0.02	1.11	0.29	0.47	0.51	1.16	1.17	0.58	0.70	1.55	0.80	1.42
CO_2	0.93	0.06	0.39	3.37	0.42	7.25	0.42	8.01	5.67	0.30	0.00	0.57	0.08
Total	99.57	98.60	99.85	98.40	98.19	98.78	101.56	100.49	101.69	99.37	100.22	99.95	99.49
$Fe^*_2O_3$	4.33	0.41	0.48	0.39	0.45	0.96	1.41	1.63	1.28	0.89	1.13	0.99	0.99
(ppm)													
Ba	207	157	592	215	749	186	6	43	34	49	50	44	54
Ce	66	12	8	19	17	21	2	24	24	30	34	28	28
Co	7	0	1	0	0	2	nd	3	0	1	1	2	1
Cr	65	15	27	13	11	15	19	17	22	26	46	25	26
Cu	3	0	0	1	nd	20	4	4	0	10	0	nd	5
Ga	8	0	3	4	1	3	3	3	2	4	3	4	5
La	33	6	5	13	8	6	16	9	15	18	19	14	14
Ni	16	nd	nd	nd	nd	nd	1	nd	nd	3	2	3	5
Pb	7	6	3	3	2	2	4	4	6	4	6	2	5
Rb	45	6	3	11	6	11	1	10	12	14	20	20	25
Sr	119	543	41	425	665	285	57	53	60	54	57	62	56
Th	9	nd	0	0	nd	0	3	0	2	1	1	1	2
Y	27	4	5	4	4	7	11	11	10	11	12	10	11
Zn	19	9	13	17	9	26	36	22	39	28	103	23	46
Zr	637	89	34	70	93	99	235	164	145	175	167	169	131
U	3	1	2	1	1	1	2	1	3	0	1	2	2

nd: Not detected

Table 5.2 Chemical analysis (major & trace elements) of the Bahi Sandstone in the A4-32 borehole.

Sample	A4-1	A4-2	A4-5	A4-6	A4-7	A4-8	A4-9	A4-11	A4-12	A4-13	A4-14	A4-15	A4-16	A4-18
(Wt %)														
SiO_2	94.30	91.88	95.92	93.55	94.77	93.47	93.60	95.89	96.28	95.11	96.41	91.73	95.91	87.76
TiO_2	0.09	0.06	0.03	0.07	0.04	0.11	0.07	0.07	0.07	0.10	0.06	0.04	0.04	0.43
Al_2O_3	1.95	2.55	2.17	3.17	1.94	2.94	2.60	2.17	1.67	3.19	1.63	3.68	1.10	4.41
Fe_2O_3	0.67	1.08	0.80	0.17	0.12	0.96	0.38	0.50	0.27	0.39	0.15	0.88	0.11	2.94
FeO	0.21	0.33	0.16	0.18	0.23	0.06	0.06	0.09	0.07	0.05	0.08	0.10	0.28	0.11
MnO	0.04	0.06	0.02	0.01	0.03	0.01	0.02	0.01	0.01	0.00	0.02	0.02	0.00	0.03
MgO	0.00	0.14	0.00	0.00	0.00	0.00	0.00	0.00	0.00	0.00	0.00	0.03	0.00	0.23
CaO	0.05	0.00	0.00	0.00	0.01	0.01	0.04	0.08	0.00	0.00	0.00	0.31	0.17	0.59
Na_2O	0.41	0.53	0.15	0.01	0.33	0.64	0.07	0.46	2.08	0.37	0.13	0.77	0.10	0.30
K_2O	0.46	0.67	0.23	0.63	0.21	0.55	0.14	0.44	0.54	0.31	0.31	0.93	0.18	1.39
P_2O_5	0.02	0.01	0.01	0.02	0.01	0.02	0.02	0.01	0.02	0.02	0.02	0.01	0.02	0.44
H_2O	0.44	0.74	0.68	1.01	0.81	1.45	1.25	1.27	1.20	1.56	0.40	0.80	0.52	2.48
CO_2	0.63	0.87	0.91	0.24	0.31	0.16	0.31	0.31	0.22	0.02	0.17	0.57	0.50	0.13
Total	99.27	98.92	101.08	99.68	98.81	100.38	99.22	102.3	100.71	101.12	99.38	98.93	100.57	101.24
$Fe^*_2O_3$	0.90	1.45	0.98	0.37	0.36	1.03	0.45	0.60	0.57	0.45	0.42	4.45	0.39	3.06
(ppm)														
Ba	425	270	557	355	784	774	563	8336	662	2836	1514	192	5837	1149
Ce	17	13	8	22	7	22	4	8	15	26	17	62	13	11
Co	nd	nd	2	0	nd	1	1	2	1	1	nd	6	0	nd
Cr	12	30	7	8	18	15	9	10	14	16	15	76	20	16
Cu	nd	1	5	nd	8	nd	6	14	2	nd	nd	0	14	nd
Ga	3	3	2	3	2	4	1	3	2	3	2	9	1	2
La	7	7	5	10	5	10	4	2	5	11	8	25	5	4
Ni	0	0	nd	0	nd	nd	nd	7	0	nd	nd	21	nd	nd
Pb	0	1	4	2	2	5	nd	3	2	3	6	9	2	0
Rb	9	9	6	14	6	13	3	13	9	7	5	65	5	5
Sr	78	55	67	73	77	98	57	480	86	205	139	143	415	110
Th	nd	0	0	1	nd	0	nd	0	nd	0	2	5	nd	0
Y	5	6	3	6	5	7	4	5	6	7	5	21	3	5
Zn	8	16	6	13	10	12	6	12	11	7	14	28	9	16
Zr	42	46	31	51	55	62	51	78	78	128	57	229	68	47
U	0	1	2	3	1	2	1	1	2	2	1	2	2	2

nd: Not detected.

Table 5.2 continued.

Sample (Wt.%)	A4-19	A4-20	A4-21	A4-22	A4-23	A4-24	A4-25	A4-26	A4-27	A4-28	A4-30	A4-31	A4-32
SiO_2	79.15	87.08	95.89	93.66	92.00	92.20	98.22	97.26	98.30	99.13	87.34	87.81	81.78
TiO_2	0.76	0.45	0.05	0.07	0.14	0.17	0.05	0.07	0.06	0.17	0.43	0.46	0.79
Al_2O_3	8.76	4.51	1.69	2.73	4.86	4.07	1.48	1.52	1.18	1.20	5.79	5.69	8.30
Fe_2O_3	4.35	3.13	0.23	0.29	0.31	0.48	0.04	0.11	0.02	0.03	3.45	2.52	4.90
FeO	0.16	0.12	0.06	0.06	0.16	0.06	0.05	0.06	0.05	0.11	0.13	0.10	0.09
MnO	0.03	0.00	0.00	0.01	0.00	0.00	0.02	0.01	0.00	0.02	0.01	0.00	0.00
MgO	0.64	0.15	0.00	0.00	0.03	0.00	0.00	0.00	0.00	0.00	0.37	0.27	0.21
CaO	0.00	0.61	0.00	0.00	0.00	0.00	0.00	0.45	0.21	0.00	0.00	0.00	0.00
Na_2O	2.08	1.27	0.99	1.05	0.59	0.76	0.26	0.33	0.22	0.53	2.08	1.88	0.95
K_2O	2.80	1.42	0.20	0.35	0.53	0.72	0.34	0.36	0.27	0.21	1.84	1.68	2.11
P_2O_5	0.08	0.45	0.02	0.02	0.04	0.03	0.01	0.02	0.02	0.02	0.03	0.03	0.05
H_2O	2.40	1.83	0.14	1.03	1.22	0.24	1.10	1.36	0.50	0.42	1.28	1.65	1.70
CO_2	0.04	0.44	0.88	0.32	0.18	1.40	0.30	1.14	0.57	0.17	0.08	0.11	0.19
Total	101.25	101.46	100.15	99.59	100.06	100.13	101.87	101.68	101.25	102.01	102.83	102.2	101.07
$Fe^*_2O_3$	4.53	3.26	0.30	0.36	0.55	0.28	0.34	0.34	0.25	0.16	3.59	2.63	5.00
(ppm)													
Ba	50	75	469	528	765	2221	1879	2684	2587	3492	-	76	94
Ce	48	72	32	37	19	15	9	15	11	12	-	48	77
Co	5	4	nd	5	nd	nd	0	2	0	nd	-	1	1
Cr	125	62	21	38	19	20	20	22	16	16	-	56	56
Cu	nd	0	1	nd	21	3	nd	3	1	7	3	1	4
Ga	8	12	7	6	5	2	3	3	1	1	7	7	12
La	26	34	11	19	8	5	2	2	7	2	-	19	39
Ni	7	19	4	1	0	nd	nd	nd	nd	nd	8	3	6
Pb	3	8	3	2	1	5	2	3	2	0	8	7	9
Rb	35	68	25	21	12	6	5	5	3	3	58	53	59
Sr	80	190	131	156	120	181	145	225	186	230	100	68	160
Th	4	7	0	1	1	nd	nd	nd	nd	nd	4	5	9
Y	35	27	12	11	8	5	5	5	5	5	21	15	23
Zn	18	34	19	13	10	10	12	18	11	7	35	18	19
Zr	240	316	136	99	106	56	47	51	50	91	260	318	419
U	3	4	2	2	2	0	2	0	2	2	3	2	3

nd: Not detected

Table 5.3 Chemical analyses (major & trace elements) of the Bahi Formation in the D1-32 borehole.

Sample	D1-1	D1-2	D1-3	D1-4	D1-5	D1-6	D1-7	D1-8	D1-9	D1-10
(Wt %)										
SiO_2	77.79	66.70	54.32	57.58	93.14	90.39	83.52	97.29	95.56	62.79
TiO_2	0.41	0.06	0.09	0.22	0.07	0.06	0.17	0.09	0.03	0.13
Al_2O_3	9.79	1.15	1.86	4.44	1.34	1.25	1.74	1.18	1.15	2.43
Fe_2O_3	0.31	1.50	0.70	0.60	0.58	0.19	0.48	0.10	0.05	0.63
FeO	1.26	1.26	2.20	1.62	0.28	0.70	1.24	0.52	0.44	2.26
MnO	0.09	0.26	0.49	0.37	0.03	0.07	0.11	0.02	0.03	0.37
MgO	0.97	5.19	8.08	7.34	0.56	1.30	1.94	0.41	1.15	6.31
CaO	1.20	9.53	13.93	10.90	1.33	1.76	3.85	0.71	0.62	10.28
Na_2O	1.26	0.26	0.79	0.38	0.00	0.17	0.02	0.63	0.60	0.06
K_2O	2.53	0.39	0.48	1.20	0.29	0.30	0.41	0.11	0.09	0.65
P_2O_5	0.14	0.03	0.17	0.21	0.15	0.28	0.23	0.06	0.04	0.12
H_2O	2.23	0.31	0.32	1.52	0.67	0.14	0.29	0.44	0.22	0.61
CO_2	2.86	12.95	19.53	15.16	1.84	2.16	5.31	1.01	0.95	15.14
Total	100.84	99.59	102.96	101.54	100.28	98.77	99.31	102.57	100.93	102.13
$Fe^*_2O_3$	1.71	3.13	3.14	2.40	0.97	0.89	1.86	0.76	0.54	3.14
(ppm.)										
Ba	138	103	28	32	309	293	140	273	593	50
Ce	53	6	28	50	18	18	28	15	4	23
Co	14	3	10	9	6	6	5	0	2	6
Cr	31	19	28	105	22	10	16	15	10	20
Cu	3	nd	2	2	nd	1	3	2	3	6
Ga	9	2	2	5	3	2	1	3	1	3
La	29	2	9	1	10	8	10	6	4	13
Ni	11	nd	4	3	0	nd	3	1	nd	2
Pb	11	4	7	8	4	8	5	3	4	6
Rb	50	5	9	24	6	6	7	8	2	13
Sr	100	38	56	94	51	47	47	632	52	53
Th	5	nd	nd	0	1	1	0	1	nd	1
Y	22	9	12	16	10	12	15	4	6	13
Zn	33	11	10	16	10	12	12	9	15	10
Zr	353	38	54	88	53	47	190	93	36	71
U	3	2	2	3	2	2	2	2	2	3

nd: Not detected.

Table 5.3 continued.

Sample (Wt %)	D1-11	D1-12	D1-14	D1-15	D1-16	D1-17	D1-20	D1-21	D1-22	D1-23
SiO_2	75.81	90.44	69.98	72.42	57.40	66.18	63.97	63.48	60.49	57.79
TiO_2	0.03	0.06	0.76	0.66	0.54	0.60	0.84	0.85	0.96	0.93
Al_2O_3	1.32	2.67	13.11	11.45	9.33	10.93	14.30	13.76	16.11	15.85
Fe_2O_3	0.32	0.13	3.41	2.76	2.77	4.35	6.03	5.64	7.48	7.01
FeO	2.16	1.30	0.78	0.81	1.19	1.70	1.00	1.03	0.82	0.84
MnO	0.24	0.07	0.08	0.07	0.31	0.16	0.07	0.06	0.05	0.08
MgO	3.32	0.45	2.28	2.05	6.41	2.94	2.16	2.30	2.07	2.68
CaO	6.38	0.99	1.58	1.61	8.18	2.57	1.04	1.36	0.85	1.78
Na_2O	0.30	0.47	1.77	0.60	0.58	0.48	0.69	0.45	0.49	0.02
K_2O	0.18	0.51	4.42	3.83	3.12	3.73	4.81	4.64	5.52	5.45
P_2O_5	0.04	0.02	0.22	0.17	0.16	0.11	0.11	0.10	0.14	0.15
H_2O	0.19	0.91	3.47	3.36	2.26	1.16	4.15	4.60	4.18	4.68
CO_2	9.36	2.18	1.02	2.10	9.32	4.40	1.74	2.22	1.15	2.60
Total	99.65	100.20	102.88	101.89	101.57	99.31	100.91	100.49	100.31	99.86
$Fe^*{}_2O_3$	2.72	1.57	4.28	3.66	4.09	6.24	7.14	6.78	8.39	7.94
(ppm)										
Ba	105	516	194	187	-	-	99	107	-	-
Ce	7	16	6	69	-	-	87	85	-	-
Co	1	nd	18	7	-	-	nd	9	-	-
Cr	21	10	99	60	-	-	74	81	-	-
Cu	0	13	12	nd	-	-	2	2	-	-
Ga	2	1	18	16	-	-	20	21	-	-
La	7	7	35	30	-	-	45	41	-	-
Ni	nd	nd	32	18	-	-	30	23	-	-
Pb	1	3	7	6	-	-	14	9	-	-
Rb	4	10	103	94	-	-	135	141	-	-
Sr	32	70	159	154	-	-	155	153	-	-
Th	nd	1	6	6	-	-	11	11	-	-
Y	8	7	27	25	-	-	36	35	-	-
Zn	9	9	31	31	-	-	51	46	-	-
Zr	31	76	244	242	-	-	292	276	-	-
U	2	1	2	4	-	-	4	5	-	-

nd: Not detected.

Table 5.4 Chemical analysis (major & trace elements) of the Bahi Formation in the F6-32 borehole.

Sample	F6-2	F6-5	F6-6	F6-8	F6-9	F6-10	F6-11	F6-12	F6-13	F6-14	F6-15	F6-16	F6-17
(Wt %)													
SiO_2	52.64	46.33	84.49	97.64	93.65	95.94	96.98	95.67	93.97	91.80	93.72	94.05	94.78
TiO_2	0.04	0.00	0.26	0.11	0.13	0.17	0.11	0.15	0.15	0.16	0.11	0.05	0.14
Al_2O_3	0.50	0.98	6.03	0.84	1.74	1.85	1.16	3.40	3.21	4.60	3.27	3.08	2.80
Fe_2O_3	0.34	0.35	1.29	0.33	0.31	0.23	0.20	0.20	0.21	0.25	0.28	0.22	0.16
FeO	0.09	0.09	0.06	0.05	0.06	0.06	0.06	0.05	0.04	0.06	0.04	0.04	0.06
MnO	0.02	0.01	0.01	0.02	0.01	0.08	0.01	0.00	0.01	0.01	0.02	0.01	0.00
Mgo	4.42	3.36	0.20	0.00	0.00	0.27	0.00	0.00	0.02	0.00	0.00	0.00	0.02
CaO	17.40	25.69	1.14	0.00	0.70	0.82	0.19	0.00	0.00	0.00	0.04	0.00	0.31
Na_2O	0.29	0.38	1.03	0.54	1.21	0.10	0.30	0.55	0.70	0.18	0.57	0.70	0.37
K_2O	0.06	0.13	1.01	0.09	0.34	0.34	0.19	0.52	0.51	0.85	0.57	0.46	0.47
P_2O_5	0.34	0.13	0.45	0.03	0.04	0.03	0.03	0.06	0.06	0.08	0.05	0.05	0.06
SO_3	1.42	14.92	-	-	-	-	-	-	-	-	-	-	-
H_2O	1.50	1.04	2.64	1.11	1.05	1.08	0.57	1.97	1.49	1.76	1.46	1.50	1.02
CO_2	19.65	6.33	1.50	0.73	0.54	0.28	0.95	0.56	0.16	0.22	0.42	0.29	0.89
Total	98.71	99.82	100.11	101.49	99.78	100.71	100.75	103.13	100.53	99.97	100.55	100.45	101.08
$Fe^*_2O_3$	0.44	0.45	1.36	0.39	0.26	0.26	0.27	0.26	0.25	0.32	0.32	0.26	0.23
(ppm)													
Ba	30	28	80	32	46	46	52	65	68	65	100	54	56
Ce	2	14	64	22	33	22	29	51	51	36	57	48	36
Co	0	nd	1	2	nd	nd	nd	nd	nd	0	nd	nd	0
Cr	26	20	35	12	20	14	15	24	85	50	26	25	17
Cu	5	0	13	58	5	44	15	4	6	1	5	7	6
Ga	1	2	7	1	2	2	1	5	4	6	4	2	3
La	4	0	28	8	15	7	13	21	22	16	25	16	16
Ni	6	nd	13	nd	nd	nd	nd	nd	0	0	nd	nd	nd
Pb	2	7	16	3	8	8	6	14	12	15	12	6	12
Rb	1	4	26	2	10	7	7	15	15	24	14	12	10
Sr	513	165	351	88	229	150	193	446	416	688	368	373	499
Th	nd	1	11	1	5	3	2	26	6	8	5	2	3
Y	5	7	16	6	6	4	7	7	8	8	8	8	7
Zn	7	13	23	59	11	9	6	10	13	8	16	11	9
Zr	187	175	272	303	228	254	371	399	340	349	277	322	298
U	4	2	6	2	4	2	2	2	1	1	1	1	1

nd: Not detected.

Table 5.5 Major and trace elements, mean ($\bar{x}$) and standard deviation (σ) of the Bahi Sandstone Formation in the four boreholes.
n = number of samples.

Borehole	A2-32 n=13		A4-32 n=27		D1-32 n=20		F6-32 n=13	
	$\bar{x}$	σ	$\bar{x}$	σ	$\bar{x}$	σ	$\bar{x}$	σ
SiO_2	81.37	10.97	92.92	5.01	72.85	14.22	87.14	17.07
TiO_2	0.16	0.16	0.18	0.22	0.38	0.35	0.12	0.06
Al_2O_3	2.68	1.63	3.30	2.03	6.76	5.83	2.53	1.64
Fe_2O_3	0.94	0.86	1.09	1.43	2.25	2.53	0.33	0.29
FeO	0.20	0.21	0.11	0.06	1.17	0.57	0.06	0.02
MnO	0.04	0.05	0.02	0.02	0.15	0.14	0.02	0.02
MgO	0.81	1.24	0.08	0.15	2.30	2.37	0.64	1.46
CaO	4.74	4.94	0.09	0.18	4.02	4.20	3.55	8.17
Na_2O	0.47	0.29	0.63	0.58	0.50	0.43	0.44	0.26
K_2O	0.72	0.47	0.74	0.69	2.13	2.06	0.43	0.28
P_2O_5	0.03	0.03	0.06	0.12	0.13	0.07	0.11	0.13
H_2O	0.90	0.55	1.09	0.59	1.84	1.70	1.40	0.52
CO_2	1.88	2.95	0.42	0.31	5.60	5.66	1.34	2.52

Borehole	A2-32 n=13		A4-32 n=27		D1-32 n=16		F6-32 n=13	
	$\bar{x}$	σ	$\bar{x}$	σ	$\bar{x}$	σ	$\bar{x}$	σ
Ba	183.54	229.97	1506.69	1944.71	197.94	164.39	55.54	20.56
Ce	24.08	15.54	24.62	20.45	32.06	20.02	35.77	18.05
Co	1.38	1.94	1.23	1.80	6.00	5.18	0.23	0.60
Cr	25.15	14.99	28.35	26.75	38.81	33.24	28.38	19.75
Cu	3.62	5.75	3.50	5.41	3.19	3.95	13.0	17.58
Ga	3.31	1.93	4.12	3.22	6.81	7.44	3.08	1.98
La	13.54	7.50	10.85	10.06	16.06	14.64	14.69	6.26
Ni	2.31	4.42	2.62	5.60	7.94	11.34	1.46	3.84
Pb	4.15	1.72	3.23	2.69	6.25	3.30	9.31	4.52
Rb	14.15	11.58	17.85	20.38	34.44	50.03	11.31	7.63
Sr	190.54	217.10	152.12	102.08	118.31	144.63	344.54	173.02
Th	1.46	2.47	1.35	2.50	2.75	3.86	5.82	6.86
Y	9.77	6.04	9.38	8.19	16.06	10.05	7.46	2.85
Zn	30.00	24.66	13.73	6.53	19.69	14.05	15.00	13.94
Zr	169.84	150.15	113.54	102.99	136.50	109.84	290.38	67.79
U	1.54	0.88	1.77	0.95	2.56	1.03	2.23	1.54

Table 5.6 Unstandardised discriminant Function Coefficient used to calculate Discriminant Scores for the Bahi Formation.

Elements	Discriminant Function I	Discriminant Function II
SiO_2	-0.0447	-0.421
TiO_2	-0.972	1.988
Al_2O_3	0.008	-0.526
Fe_2O_3	-0.267	-0.551
FeO	0.208	-1.610
MnO	-3.032	2.720
MgO	0.140	0.881
CaO	0.195	-0.907
Na_2O	0.719	-0.177
K_2O	-0.032	-1.840
P_2O_5	7.510	7.244
Constant	0.303	43.570

Table 5.7 Discriminant Scores of the Bahi Sandstone Formation in the four boreholes.

A2-32

Sample	Dis. Fun. I	Dis. Fun. II
2-1	-3.139	1.316
2-2	-0.785	2.713
2-3	-0.487	2.682
2-4	0.172	3.951
2-5	-1.299	1.847
2-6	-0.373	6.310
2-7	-3.623	1.893
2-8	-2.060	6.392
2-9	-3.087	3.528
2-12	-4.055	1.270
2-13	-3.768	0.881
2-15	-3.361	0.676
2-17	-3.849	0.760

F6-32

Sample	Dis. Fun. I	Dis. Fun. II
6-2	4.460	11.085
6-5	4.860	3.534
6-6	0.297	4.926
6-8	-3.973	1.811
6-9	-3.512	1.591
6-10	-2.254	3.459
6-11	-3.729	1.813
6-12	-3.266	1.580
6-13	-3.156	1.855
6-14	-3.373	1.615
6-15	-3.320	1.624
6-16	-3.142	1.688
6-17	-3.313	1.529

A4-32

Sample	Dis. Fun. I	Dis. Fun. II
4-1	-3.803	1.605
4-2	-3.792	1.572
4-5	-4.063	1.085
4-6	-3.823	1.285
4-7	-3.766	1.152
4-8	-3.638	1.304
4-9	-3.097	-1.416
4-11	-3.728	1.335
4-12	-3.835	1.043
4-13	-3.708	1.263
4-14	-3.903	1.638
4-15	-3.023	0.862
4-16	-3.928	1.330
4-18	-1.234	3.687
4-19	-3.028	0.201
4-20	-0.414	3.515
4-21	-2.878	1.827
4-22	-3.132	1.928
4-23	-3.404	1.481
4-24	-3.318	1.348
4-25	-3.935	0.893
4-26	-3.684	0.849
4-27	-3.725	1.271
4-28	-3.806	1.068
4-30	-3.139	-0.264
4-31	-3.070	0.426
4-32	-4.323	-0.003

D1-32

Sample	Dis. Fun. I	Dis. Fun. II
1-1	-1.346	0.433
1-2	0.682	8.238
1-3	2.340	11.999
1-4	1.552	11.325
1-5	-0.447	4.755
1-6	-2.652	2.944
1-7	-1.040	4.994
1-8	-3.398	1.637
1-9	-2.596	2.506
1-10	0.362	9.034
1-11	-1.261	5.062
1-12	-3.029	0.857
1-14	-1.177	-1.733
1-15	-2.081	0.160
1-16	-0.149	6.515
1-17	-2.487	0.561
1-20	-3.203	-1.171
1-21	-3.214	-0.406
1-22	-3.503	-1.944
1-23	-3.312	-0.443

CHAPTER 6

GRAIN-SIZE ANALYSIS

6.1 Introduction

Many previous workers have used the grain-size distribution of clastic sediments to characterise depositional environments, to recognise the mechanisms of sediment transport and deposition and to differentiate between environmental settings (Folk & Ward, 1957; Passega, 1964; Mason & Folk 1958; Stewart, 1958; Friedman, 1961, 1967; Sahu,1964; Moiola & Weiser 1968; Passega & Byramjee, 1969; Visher, 1969; Folk,1974; Amaral & Pryor, 1977; Moshrif, 1980; Abu el-ella & Coleman, 1985; Darmoian & Lindqvist, 1988 and others).

Hitherto there have been no detailed grain-size analyses of the Bahi Formation. This has now been done to elucidate the following:

- To determine vertical and lateral texture variation within the Bahi Formation.
- To give a clear idea of the depositional environments of the formation.
- To throw light on the transporting agents of the sediment.

6.2 Procedures

A total of forty-five samples in the Bahi Sandstone in the A2-32, A4-32 and F6-32 boreholes have been analysed. These samples cover most of the succession, except for the uppermost part (a glauconite-bearing marine sequence) which has not been analysed owing to lack of available samples. In the laboratory samples were evenly crushed and checked using a binocular microscope to ensure that the grains were completely separated. The samples were dried and 50 grams were weighed and sieved using 1/2 ϕ sieve intervals for 15 minutes on a Ro-Tap shaker. Each fraction was weighed by a beam balance accurate to one hundredth of a gram and the frequences were then obtained.

From the grain-size analysis data, cumulative frequency curves were drawn on arithmetic probability paper using a ϕ scale. Grain-size statistical parameters - mean size, standard deviation, skewness and kurtosis - have been calculated following the procedures

outlined in Folk (1974). Table 6.1 shows the values of 5, 16, 25, 50, 75, 84 and 95 of the seven ϕ percentiles which have been obtained from cumulative frequency curves in order to calculate statistical grain-size parameters.

6.3 Cumulative curves

The most commonly used method of displaying the results of grain-size analysis is by plotting cumulative percentage against grain-size, expressed on a logarithmic scale. Krumbein (1934) suggested that this scale should be expressed in ϕ units ($\phi = - \log_2 d$, the negative logarithm to the base 2 of the particle diameter in millimeters) as a much more convenient way of presenting data than if the values are expressed in millimetres. This procedure has been used almost universally in recent work (Folk, 1974, 25).

The comparison of grain-size curves and the interpretation of separate populations is aided by the use of log-probability plots. The interpretation of the shapes of cumulative grain-size distributions in terms of sedimentary response to hydraulic conditions has attracted the attention of many geologists (e.g. Visher,1969; Freeman & Visher, 1975 and others). According to Visher (1969), a cumulative curve usually expresses three or four straight line segments which represent three populations. These populations are produced by the three modes of sediment transport: (1) surface creep, (2) saltation and (3) suspension. The point where a suspension population is truncated and joined to the next coarser distribution is close to 3.25ϕ or 100μ. The truncation of the saltation population occurs near 2ϕ or 250μ. At this size the material (washed load) is transported by rolling or sliding rather than saltation. The coarser straight line segment represents traction load or surface creep (Fig. 6.1).

Although the segmentation of the present cumulative curves is not exactly identical to those described by Visher, the nearest truncation point to 250 and 100μ may help to differentiate populations. The cumulative curve for each sample was first drawn separately, then the curves representing each borehole were compounded on the same plot. Representative cumulative curves are given in figures 6.2a-c. It has to be borne in mind that the record reflected by the grain-size analyses has been affected by diagenetic changes in that some

grains have been enlarged by overgrowth and some reduced in size by pressure-solutioning. An additional problem in the grain-size distribution studies is that the same sedimentary processes occur in a number of environments and thus textural results are similar. Bearing these constraints in mind, examination of the different segments in each cumulative curve leads to the following general observations:

- The suspension population represents about 10% of the distribution in most samples. This may also contain however small heavy minerals which really belong to the 'tractive' load.
- The saltation population is well developed: it represents more than 85% of the distribution.
- The traction population is usually very small and represents only about 1% of the distribution, except for a few samples where it represents more than 60% of the distribution.

This reflects two main modes of transportation of the Bahi sediment; a saltation load transport for most samples and surface creep or rolling transport for others.

6.4 Histograms

From the weight percentage data for the different grain-sizes, histograms have been constructed according to the Wentworth scale (1922): The class limits are again given in ϕ units to show the modality of the sediment (see figures 6.3a-c). The histograms show that most of the Bahi Sandstone in the A2-32 borehole is unimodal in distribution (Fig. 6.3a). In the A4-32 borehole most of the samples are unimodal (19 out of 22 samples), whereas the remaining samples, from the upper part of the section are bimodal (Fig. 6.3b): in the F6-32 borehole most of the samples are bimodal in distribution (Fig. 6.3c).

From these histograms, the Bahi sediment in the three boreholes shows vertical and lateral variation in the grain-size distribution from one borehole to the other. This variation may be related to changes in the energy of transporting agents and/or changes in the source of the sediment (See section 4.3 & 5.5).

6.5 Variation of grain-size parameters

The formulae of Folk and Ward (1957), and Folk (1974), have been used in this study,

to determine grain-size statistical parameters (mean size, standard deviation, skewness, kurtosis), because they cover most of the sediment distribution data for the Bahi samples especially in the tails of the distribution. Values for these parameters are given in table 6.2.

6.5.1 Graphic mean (Mz)

The best graphic measure for determining overall size is the graphic mean, given by the following formula (Folk, 1974):

$$Mz = \frac{\phi 16 + \phi 50 + \phi 84}{3}$$

Wentworth (1922) has a size scale which is converted into ϕ units which is used in interpreting the results of graphic mean diameter as follows:

Mz from -1.0 to 0.0ϕ,very coarse sand, 0.0 to 1.0ϕ, coarse sand,
1.0 to 2.0ϕ, medium sand, 2.0 to 3.0ϕ, fine sand,
3.0 to 4.0ϕ, very fine sand, 4.0 to 5.0ϕ, coarse silt,
5.0 to 6.0ϕ, medium silt, 6.0 to 7.0ϕ, fine silt,
7.0 to 8.0ϕ, very fine silt, >8.0ϕ, clay.

The mean size value of the Bahi sediment in the A2-32 borehole ranges between 3.13ϕ to 1.75ϕ (very fine to fine sand) in most of the samples. One sample has a value of -0.02ϕ (very coarse sand) in the upper part of the section. However, this section can divided into two parts according to the mean size value, the sediment in the lower part being very fine to fine sand and, in the upper part, very coarse sand (Fig.6.4a).

In the A4-32 borehole the mean size values range between 2.95ϕ to -1.50ϕ ((fine to very coarse sand). Here the Bahi Sandstone can divided into the following parts according to the mean size of the sediments. In the lowest part, the mean size value shows a coarsening upward pattern from fine into coarse and then very coarse sand followed by repetitive grading from medium to coarse sand. In the upper part the mean size values range from fine to medium into coarse and very coarse sand (Fig. 6.4b).

The mean size value in the F6-32 borehole ranges between 2.23ϕ and 0.43ϕ (fine to coarse sand). According to the grain-size values the Bahi Sandstone here can again be divided into two parts, the lower part coarsening upward from fine to medium into coarse sand and the upper part, also coarsening upward, ranging from fine to medium sand (Fig. 6.4c).

Generally, therefore, the overall mean size values of the three boreholes exhibits a coarsening upward trend from very fine sand into very coarse sand. This variation in mean size could be related to variation in the energy of transporting agents and/or change in the source of the sediment during deposition (See section 4.3 & 5.5).

6.5.2 Inclusive graphic standard deviation (σ_I)

Inclusive graphic standard deviation is a measure of sorting and is given by the following formula (Folk 1974):

$$\sigma_I = \frac{(\phi 84 - \phi 16)}{4} + \frac{(\phi 95 - \phi 5)}{6.6}$$

Folk suggested the following classification scale for sorting:

σ_I < 0.35ϕ, very well sorted, 0.35 to 0.50ϕ, well sorted,
0.50 to 0.71ϕ, moderately well sorted, 0.71 to 1.00ϕ, moderately sorted,
1.00 to 2.00ϕ, poorly sorted; 2.00 to 4.00ϕ, very poorly sorted;
> 4.00ϕ, extremely poorly sorted

Most of the samples in the A2-32 borehole are moderately to moderately well sorted (8 out of 11) and show uniform standard deviation values ranging between 0.50 and 0.79ϕ, with an average of 0.62ϕ. The remaining three samples of which two are from the upper part of the section sampled, are poorly sorted, ranging between 1.19 and 1.37ϕ, and one sample from the lowest part of the section is well sorted (0.38ϕ)-(Fig. 6.4a).

The samples from the A4-32 borehole are moderately to moderately well sorted (16 out of 22), and show uniform standard deviation values ranging between 0.60 and 0.98ϕ with an average of 0.79ϕ. The remaining samples are poorly to very poorly sorted and range from 1.03

to 2.09ϕ with an average of 1.31ϕ (Fig. 6.4b), whilst in the F6-32 borehole the samples are moderately sorted (10 out of 12), and show uniform standard deviation values ranging between 0.77 and 0.97ϕ with an average of 0.8ϕ, except for two samples from the upper and lowest part of the sampled section which are poorly sorted and range between 1.52 and 1.71ϕ with an average of 1.62ϕ (Fig.6.4c). Lateral and vertical variation of the sorting in the Bahi sediment from one borehole to another may reflect different sediment sources but may also reflect the nature of the transporting agents at the time of deposition (See Fig. 4.10 & 4.17).

6.5.3 Inclusive graphic skewness (SK_I)

Inclusive graphic skewness has been used as a measure of asymmetry in the distribution of the sediments and is given by the following formula (Folk, 1974):

$$SK_I = \frac{\phi16 + \phi84 - 2\,\phi50}{2(\phi84 - \phi16)} + \frac{\phi5 + \phi95 - 2\,\phi50}{2(\phi95 - \phi5)}$$

This is the most useful skewness measure available because it determines the skewness of the tails of the curve, not just the central portion. Symmetrical curves have SK_I = 0.0, excess fine material has (+) SK_I, excess coarse material has (-) SK_I. The more the skewness value departs from 0.0, the greater the degree of asymmetry (Folk, 1974, 47).

The following limits on skewness were suggested by Folk (1974):

SK_I +1.0 to +0.3, strongly fine skewed, +0.3 to +0.1, fine skewed,
+0.1 to -0.1, near symmetrical, -0.1 to -0.3, coarse skewed,
-0.3 to -1.0, strongly coarse skewed.

Values of inclusive graphic skewness in the A2-32 borehole, range from the strongly fine skewed to near symmetrical, with an overall range between -0.01 and +0.34 (Fig. 6.4a), whereas in the A4-32 borehole, skewness values range from strongly fine skewed to a near symmetrical curve, with an overall range between -0.07 and 0.56, except for one sample which

shows a strongly coarse skew -0.56, (Fig. 6.4b). In the F6-32 borehole, skewness values range from strongly fine skewed to strongly coarse skewed, with an overall range between -0.49 and +0.33 (Fig. 6.4c).

The overall average inclusive graphic skewness in the three boreholes shows strongly fine skewed to a near symmetrical distribution. This asymmetry in the sediment distribution, both laterally and vertically, may result from multiple sources for the Bahi sediment.

6.5.4 Graphic kurtosis (K_G)

Graphic kurtosis has been used to measure the ratio between the sorting in the tails of the distribution and the sorting in the central portion by using the following formula (Folk, 1974):

$$K_G = \frac{\phi 95 - \phi 5}{2.44\,(\phi 75 - \phi 25)}$$

If the central portion is better sorted than the tails the curve is said to be leptokurtic. If the tails are better sorted than the central portion the curve is said to be platykurtic (Folk, 1974).

The following limits were suggested by Folk (1974):

K_G	< 0.67, very platykurtic,	0.67 to 0.90, platykurtic,
	0.90 to 1.11, mesokurtic,	1.11 to 1.50, leptokurtic,
	1.50 to 3.00, very leptokurtic	> 3.00, extremely leptokurtic.

In the samples from the A2-32 borehole, graphic kurtosis is leptokurtic to very leptokurtic with a range between 1.134 and 2.596, except for three samples from the middle and lower part of the sampled section which are mesokurtic (Fig. 6.4a). In the A4-32 borehole, the samples are leptokurtic to very leptokurtic with ranges between 0.134 and 1.517, except for eight samples which are mesokurtic and one which is platykurtic (Fig. 6.4b). In the F6-32 borehole, most of the samples are mesokurtic with ranges between 0.907 and 1.092. Two samples however are very leptokurtic, two are platykurtic and one sample is very platykurtic (Fig.6.4c). Generally, the Bahi sediment in these boreholes is leptokurtic to very leptokurtic,

indicating that the central part of the samples are better sorted than the tails, whereas some samples are mesokurtic, showing similarity in sorting between the central and the tails portions of the sediment distribution curves. This indicates different degree of sorting and which may reflect multiple sources for the sediment and/or more than one mode of transportation.

6.6 Interrelationships between grain-size parameters

Scatter plots of inclusive standard deviation against inclusive graphic skewness, inclusive standard deviation against graphic mean size and median against inclusive standard deviation have been constructed in an attempt to recognise the depositional environment or environments for the Bahi sediment.

6.6.1 Plot of standard deviation against skewness

A plot of inclusive standard deviation against graphic skewness has been used by many workers to differentiate between river and beach sands (e.g. Friedman, 1961 & 1967; Moiola & Weiser, 1968 and others). Friedman (1967) showed that a plot of inclusive graphic skewness versus inclusive graphic standard deviation gives a good separation between beach and river sands. Beach sands tend to be better sorted than river sands and thus tend to have lower numerical standard deviation values (Friedman, 1961).

A plot of these two grain-size parameters for the Bahi samples in the three boreholes (Fig. 6.5), using Friedman (1967) and Moiola & Wieser (1968) boundary lines, shows that the majority of the samples are to be classified as river sands except for one sample from the A2-32 borehole which is to be classified as a beach sand. None of the analysed samples in the three boreholes includes the uppermost part of the formation which is known on mineralogical grounds to represent the initiation of a marine cycle (glauconitic sandstone).

6.6.2 Plot of standard deviation against graphic mean

A plot of standard deviation against mean size is also considered to be most effective in differentiating between depositional environments. Moshrif (1980) used a combination of the

"environmental boundaries" of Friedman (1961,1967) to differentiate between beach, dune and river sands. Applying these boundary lines to the Bahi samples from the three boreholes (Fig. 6.6a), most of them are to be classified as river sands, whereas a few samples from the A2-32 and A4-32 boreholes are to be classified as dune sands.

Applying Moiola & Wieser's framework (1968) for these parameters (standard deviation and mean size), shows, however, that all the analysed samples are to be classified as river sands (Fig.6.6b).

6.6.3 Median against standard deviation

Stewart (1958) used a scatter plot of standard deviation against median to differentiate between river processes, wave processes, and slow deposition in quiet water.

Stewart's diagram (Fig. 6.7), shows that wave processes are responsible for most of the samples in the Bahi Sandstone in the A2-32 borehole, and the river processes for most of the samples in the A4-32 borehole, except for two samples which fall on the wave processes side. Seven samples in the F6-32 borehole fall on the river processes side and one sample falls on the wave processes side. The remaining samples from the three boreholes fall outside both fields. They fall close to the river processes field, however , and their plot position may not be particularly significant. This suggests that the Bahi sediments were deposited under the changing mechanical conditions which would be expected as a fluvial regime passed, by degrees, into a littoral one.

6.6.4 Linear discriminant functions

Sahu (1964) established four discriminant functions depending on the graphic parameters of Folk & Ward (1957) which also differentiate between environments. He recognised aeolian, beach, shallow agitated marine, fluviatile and turbiditic sediments by studying samples from known modern environments. It was felt that the results of these analyses could be used as a basis for differentiation between ancient environments of deposition with respect to the Bahi samples.

1) To distinguish between aeolian and littoral processes equation (1) may be used.

$$Y_{\text{Aeolian:Beach}} = 3.5688(Mz) + 3.7016(\sigma_I) - 2.0766(SK_I) + 3.1135(K_G) \quad \ldots\ldots(1)$$

If the Y1 result is less than (-2.7411), it would indicate aeolian deposition and if greater it would indicate a beach environment.

2) To distinguish between beach and shallow agitated marine environment; equation (2) may be used.

$$Y_{\text{Beach:Sh.marine}} = 15.6534(Mz) + 65.7091(\sigma_I) + 18.1071(SK_I) + 18.5043(K_G) \quad \ldots\ldots(2)$$

If the Y2 result is less than (65.3650), it would indicate beach deposition and if greater it would indicate shallow agitated water deposition.

3) To distinguish between a shallow marine environment and fluvial processes equation (3) may be used.

$$Y_{\text{Sh. marine:Fluvial}} = 0.2852(Mz) - 8.7604(\sigma_I) - 4.8932(SK_I) + 0.0482(K_G) \quad \ldots\ldots(3)$$

If Y3 is less than (-7.4190), it would indicate a fluvial (deltaic) environment: a greater value would indicate shallow marine deposition.

4) To distinguish between fluvial (deltaic) and turbidity current deposition equation (4) may be used.

$$Y_{\text{Fluvial:Turbidite}} = 0.7215(Mz) + 0.4030(\sigma_I) + 6.7322(SK_I) + 5.2927(K_G) \quad \ldots\ldots(4)$$

If Y4 is less than (9.8433), it would indicate turbidity current deposition and if greater it would indicate fluvial (deltaic) deposition.

These four discriminant functions have been calculated for the samples taken from the three boreholes. The values are given in Table 6.3 and the average values have been calculated (Table 6.4) showing the distribution of the different depositional environments indicated within the Bahi Formation.

For the Bahi Formation, Y1 suggests a beach environment for all three boreholes; Y2 indicates shallow agitated water deposition and Y3 indicates a fluviodeltaic environment for the A4-32 and F6-32 boreholes and shallow marine deposition in the A2-32 borehole whereas Y4 points to turbidity current deposition in the A4-32 and F6-32 boreholes and fluviodeltaic

deposition in the A2-32 borehole. These discriminant functions produced totally contradictory results and thus failed to differentiate effectively between depositional environments for the Bahi sediment.

6.7 CM Diagram

Passega (1957, 1964) stated that sample point patterns representing the variations in a deposit of two parameters, C and M, are characteristic of the depositional agent. The C is the one percentile diameter (in μ), an approximation of the maximum grain-size; and M is the fifty percentile particle diameter (in μ), the median. He stated that the CM patterns are a geological tool which can be used to analyse the depositional conditions in recent sediments and thus to enable a reconstruction to be made of the conditions of deposition for ancient sediment suites. The CM diagram illustrates the relationship between grain-size and the hydraulic conditions under which clastic deposits have accumulated. Passega (1964) subdivided the CM pattern by points N, O, P, Q, R, and S into five segments each of which corresponds to a particular sedimentation mechanism. This implies that clastic sediments of a certain grain-size are available under particular hydraulic conditions. The mechanisms of transportation are represented mainly by rolling (NO); rolling and suspension (OP); suspension and rolling (PQ); graded suspension (QR) and uniform suspension (RS). Pelagic suspension (T) represents the finest sediments (below 15μ). In 1969 Passega and Byramjee further subdivided the CM diagram into 9 classes as shown in figure 6.8. Data falling in classes I, II, III, and IX indicates that the grains have been transported by rolling while those falling in classes IV, V, VI, VII, and VIII indicate grains which have been transported by saltation. The CM technique is mostly applied at the lamina scale but in this study has been applied to all grain-size analysis samples even thought the value may be limited.

Figure 6.8 shows the distribution for the samples from the Bahi sediment in the three boreholes. Most of the samples in the A2-32 borehole fall within classes IV and V, indicating that they were transported by saltation, except for two samples which fall in classes I and II indicating that they were transported by rolling. In the A4-32 and F6-32 boreholes, most of the

samples fall in class I indicating that they were transported by rolling, except for two samples in F6-32 borehole which fall in class IV indicating that they were transported by saltation.

6.8 Conclusions

It has to be born in mind that grain diminution and overgrowth may modify the size frequency characteristics of the sediment. Also the cement may itself break down into grains. Nevertheless, the following general conclusions can be reached:

1: Cumulative-frequency curves show two main modes of transportation for the Bahi Sandstone; saltation load transport for most of the samples and surface creep or rolling transport for the others.

2: Histograms show that most of the Bahi Sandstone samples are unimodal for the A2-32 and A4-32 boreholes, with a few samples showing bimodality in the latter borehole, whereas in the F6-32 borehole the majority of the samples show a bimodal distribution.

3: Sediment distribution in the formation exhibits a coarsening upward trend ranging from very fine to very coarse sand, moderately to very poorly sorted, characterised by a strongly fine to strongly coarse skewness which varies from leptokurtic to very leptokurtic with some samples being mesokurtic. This variation could be related to variation in the energy of transporting agents and/or changes in the source of the sediment during the Bahi deposition.

4: Although all the analysed samples in the three boreholes have not covered the uppermost part (marine cycle), some samples from the lower part, on scatter plots of statistical grain-size parameters, show that they are to be classified as marine sands.

5: Sorting data plotted against mean size and skewness show that the Bahi Formation largely comprises river sands, with a few samples which are to be regarded as beach sands.

6: Sorting evidence plotted against the median shows that the process agent for the Bahi sediment is by means of river and wave systems.

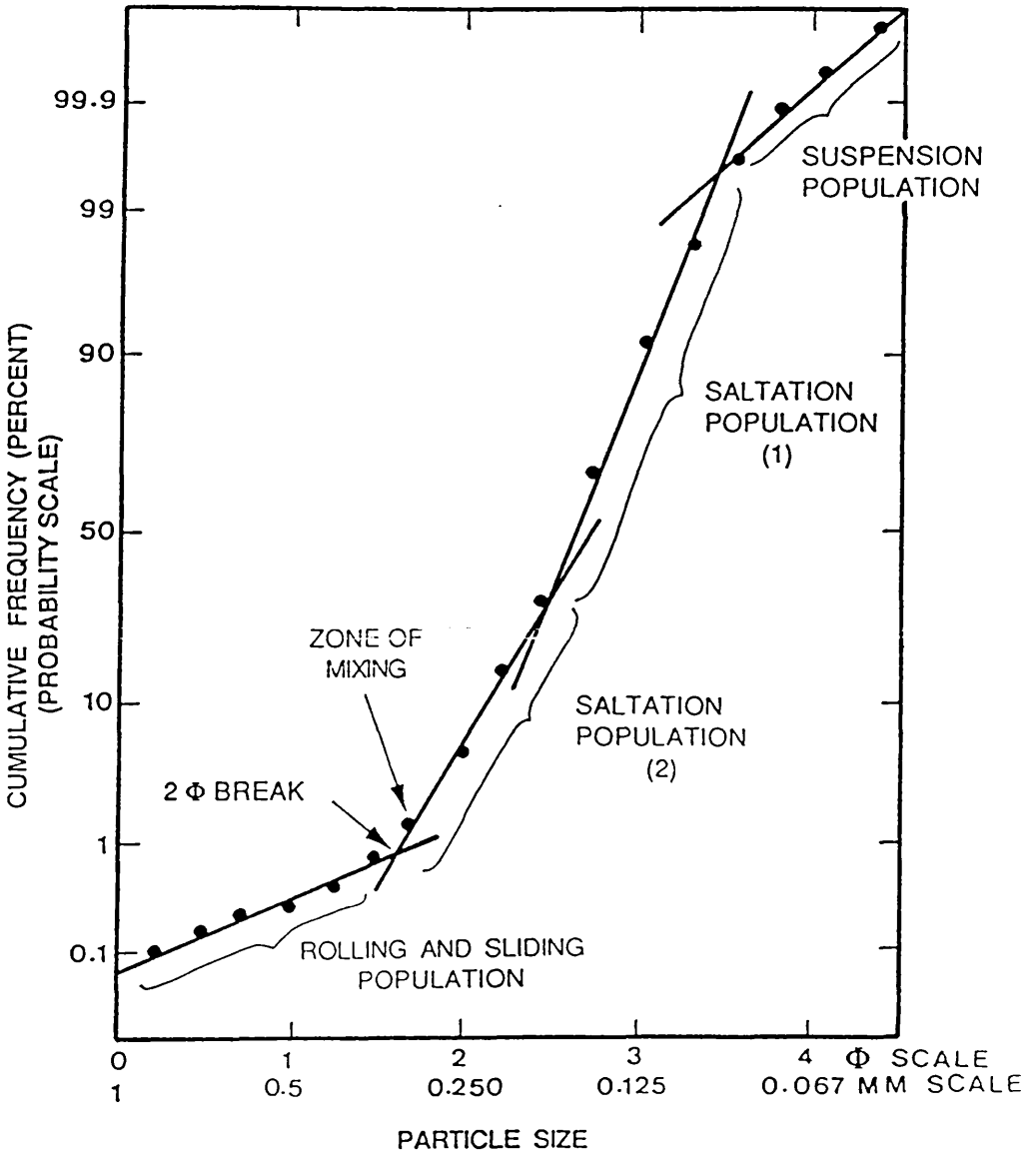

Fig. 6.1 Cumulative-frequency curve, showing the relationship between sediment transport dynamics with populations and truncation points in a grain-size distribution, after Visher (1969b, fig. 4).

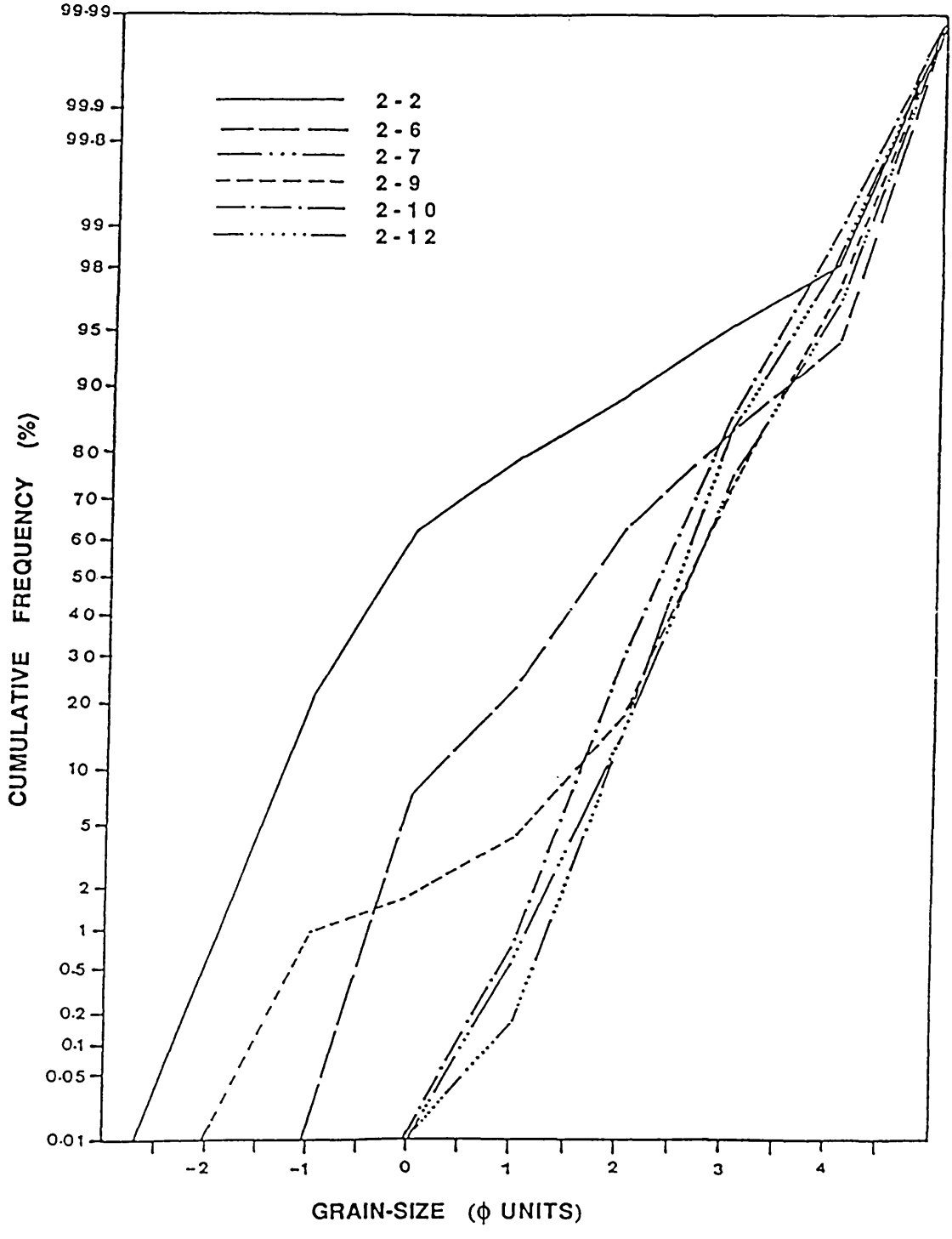

Fig. 6.2a Cumulative-frequency curves, showing grain-size distribution in the Bahi Formation (A2-32 borehole).

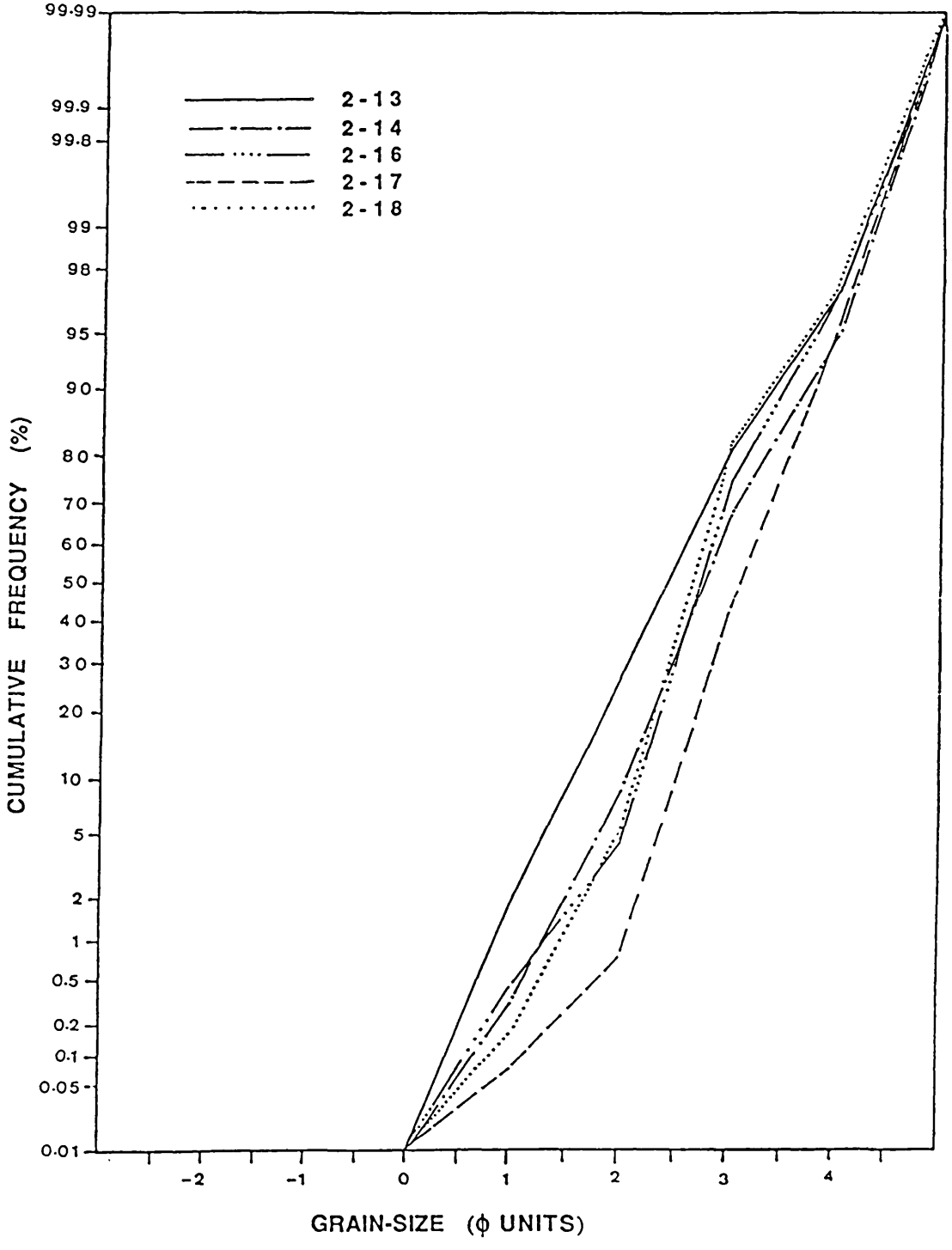

Fig. 6.2a continued.

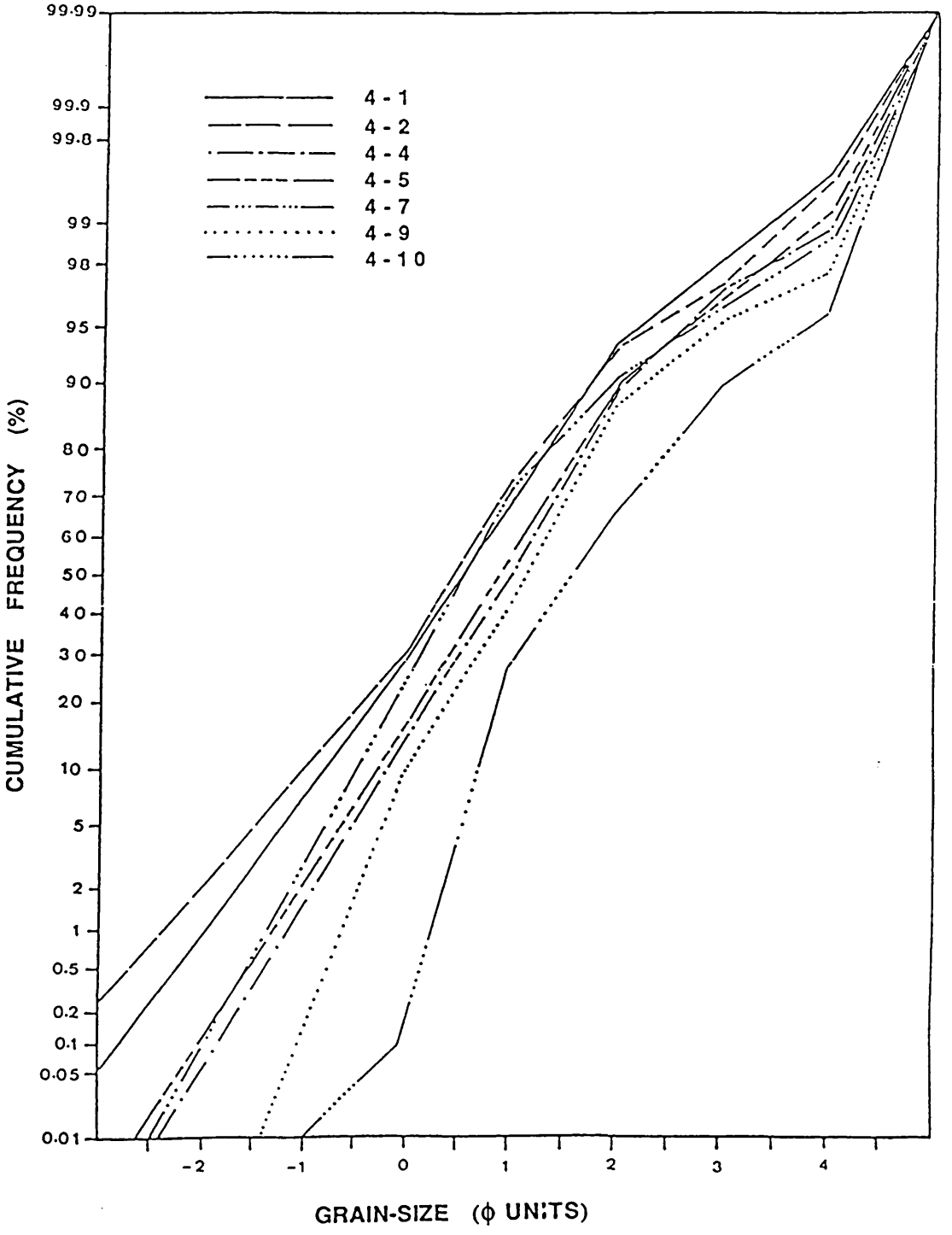

Fig. 6.2b Cumulative-frequency curves, showing grain-size distribution in the Bahi Formation (A4-32 borehole).

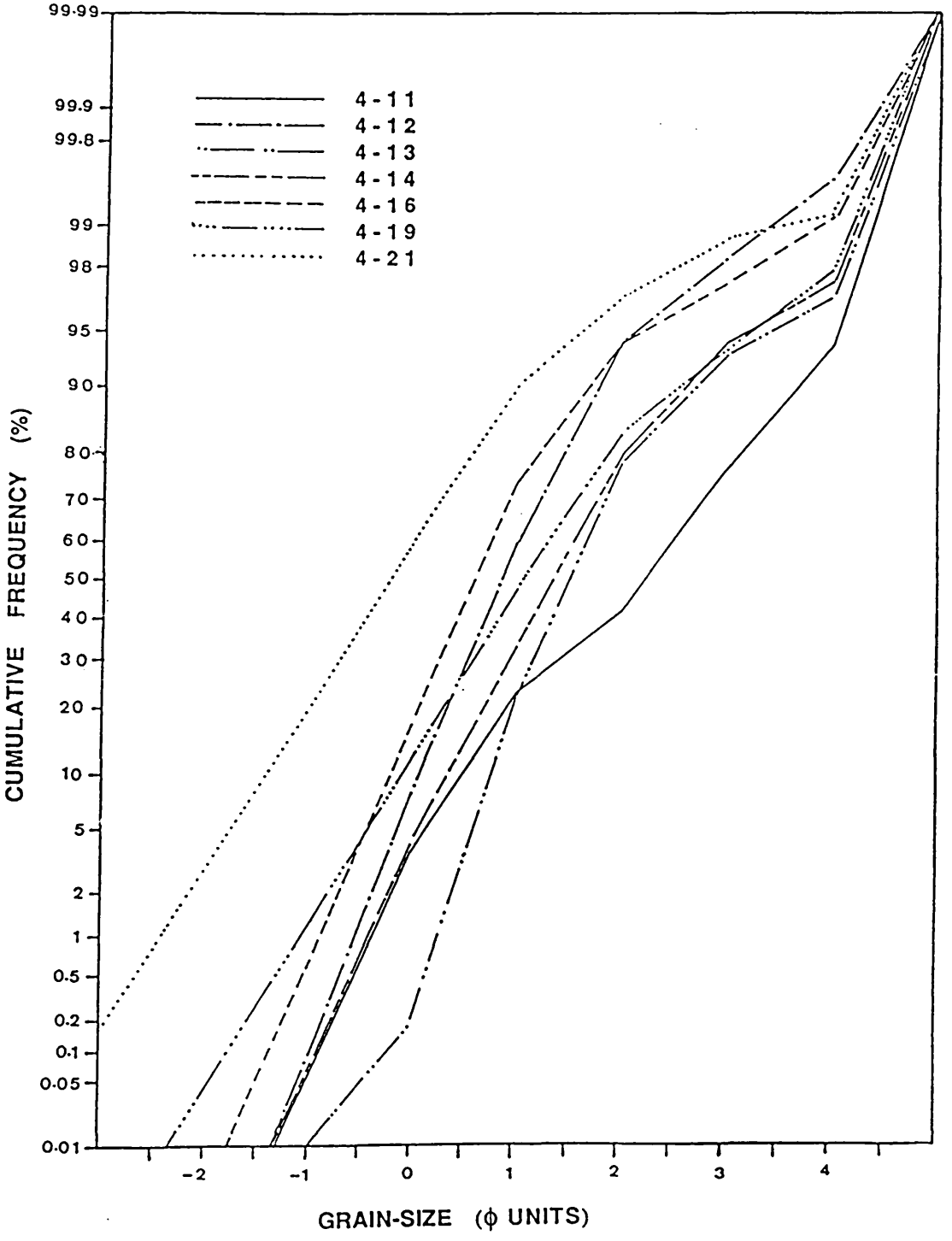

Fig. 6.2b continued.

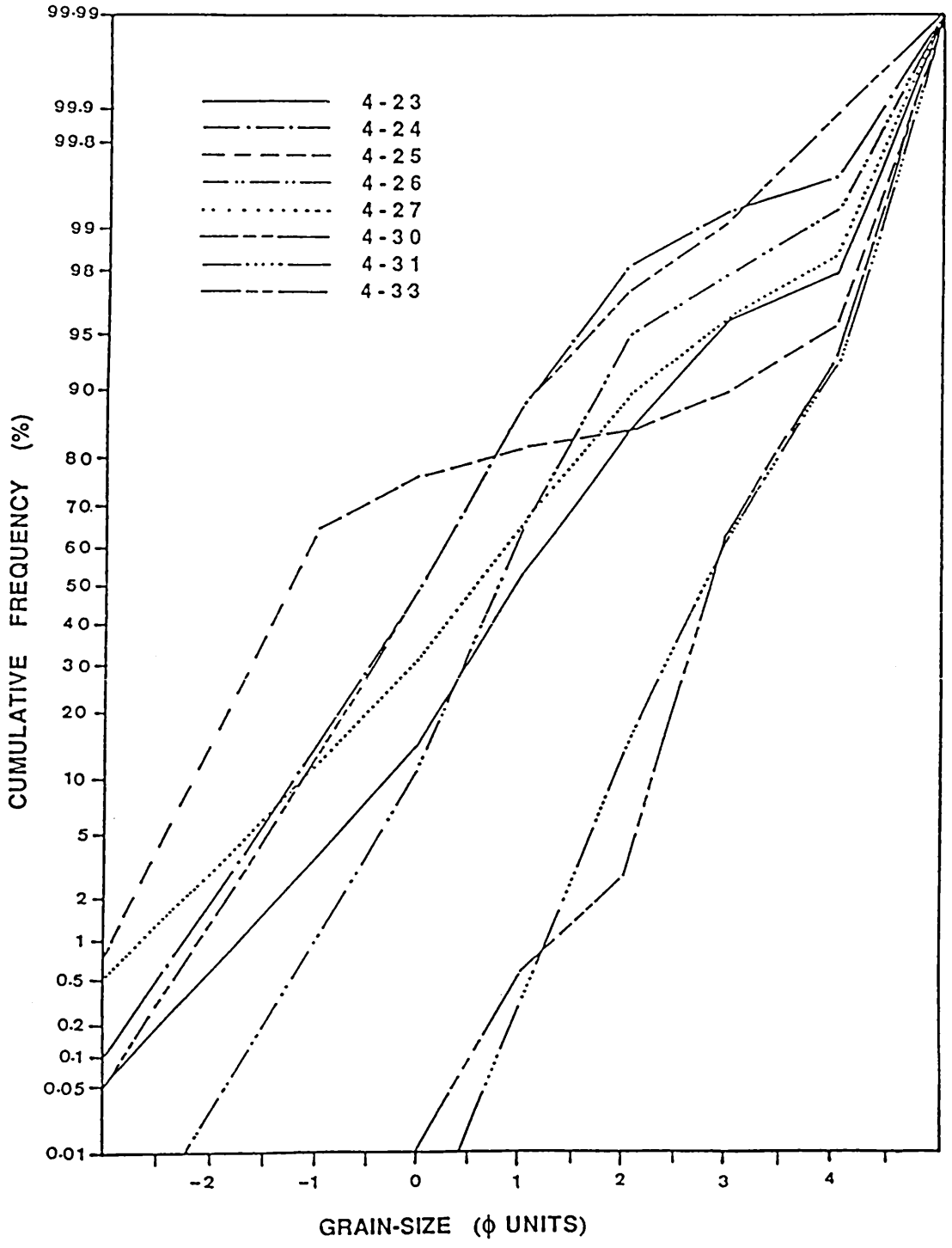

Fig. 6.2b continued.

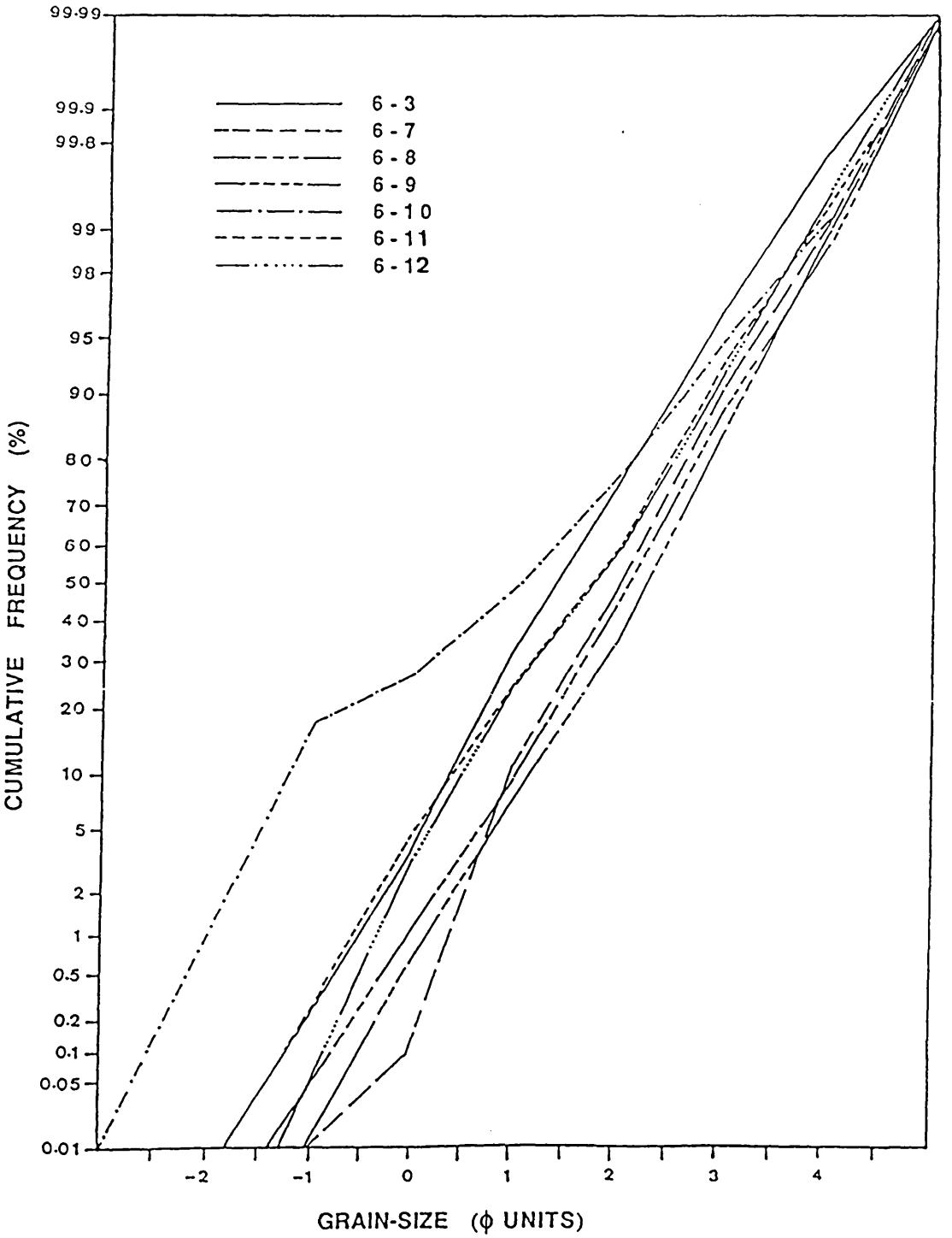

Fig. 6.2c Cumulative-frequency curves, showing grain-size distribution in the Bahi Formation (F6-32 borehole).

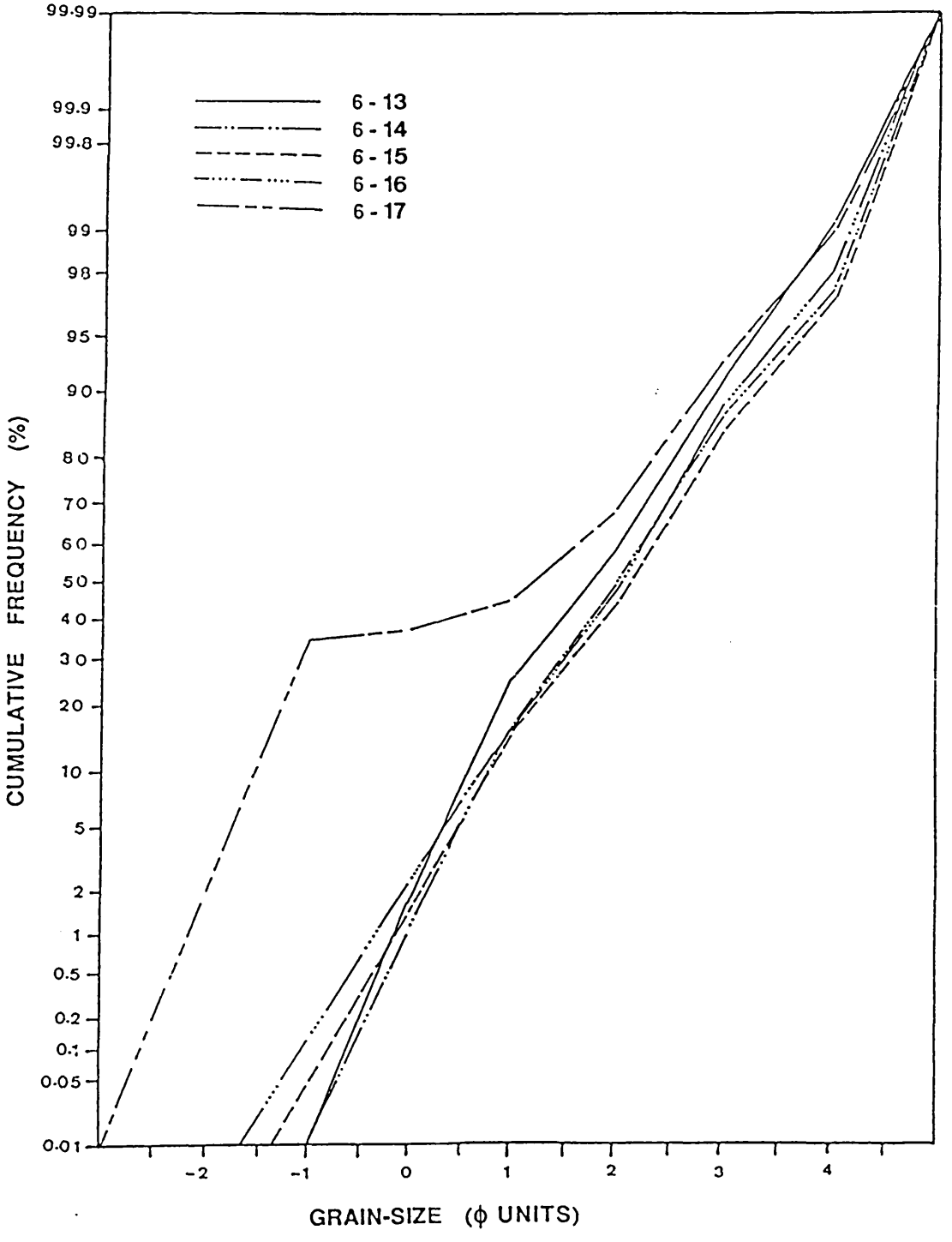

Fig. 6.2c continued.

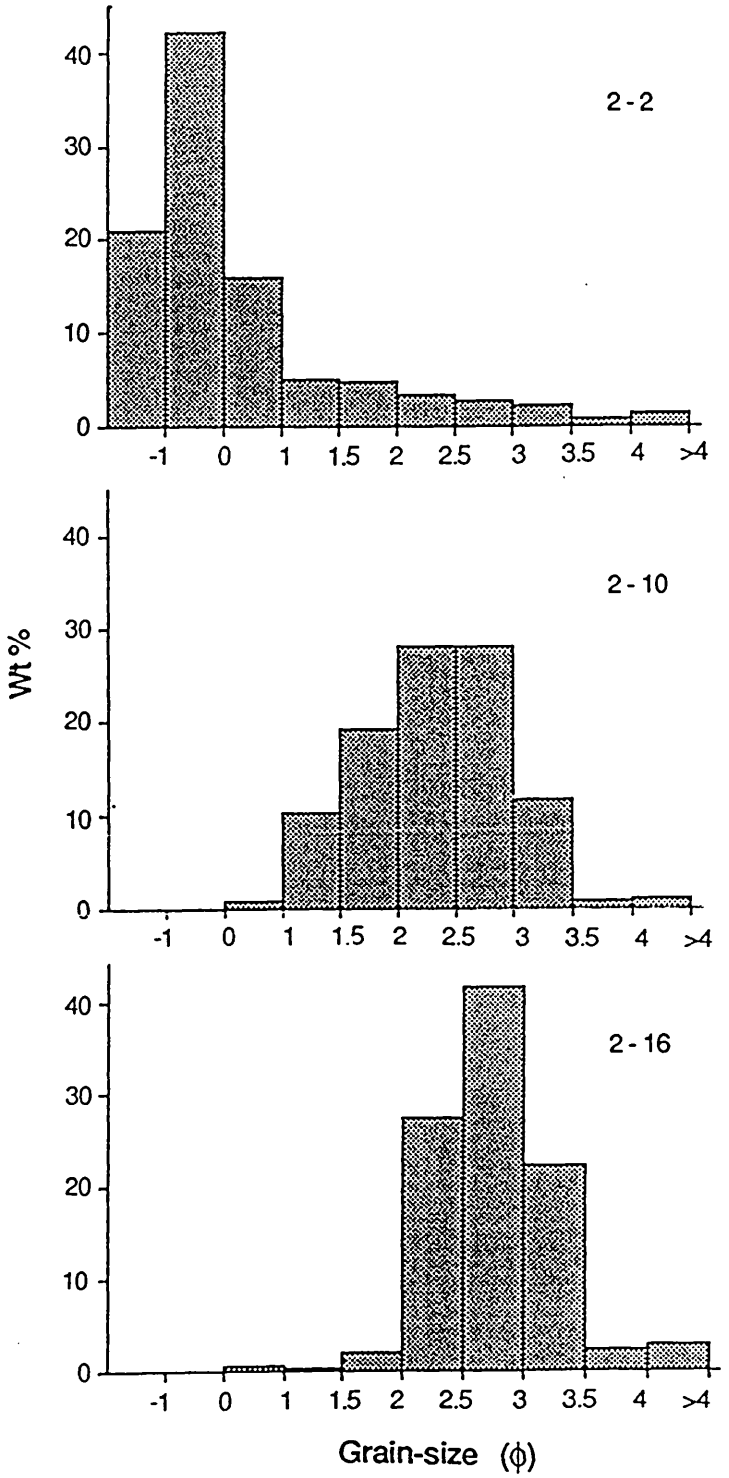

Fig. 6.3a Histograms, showing the grain-size distribution for three representative samples in the A2-32 borehole.

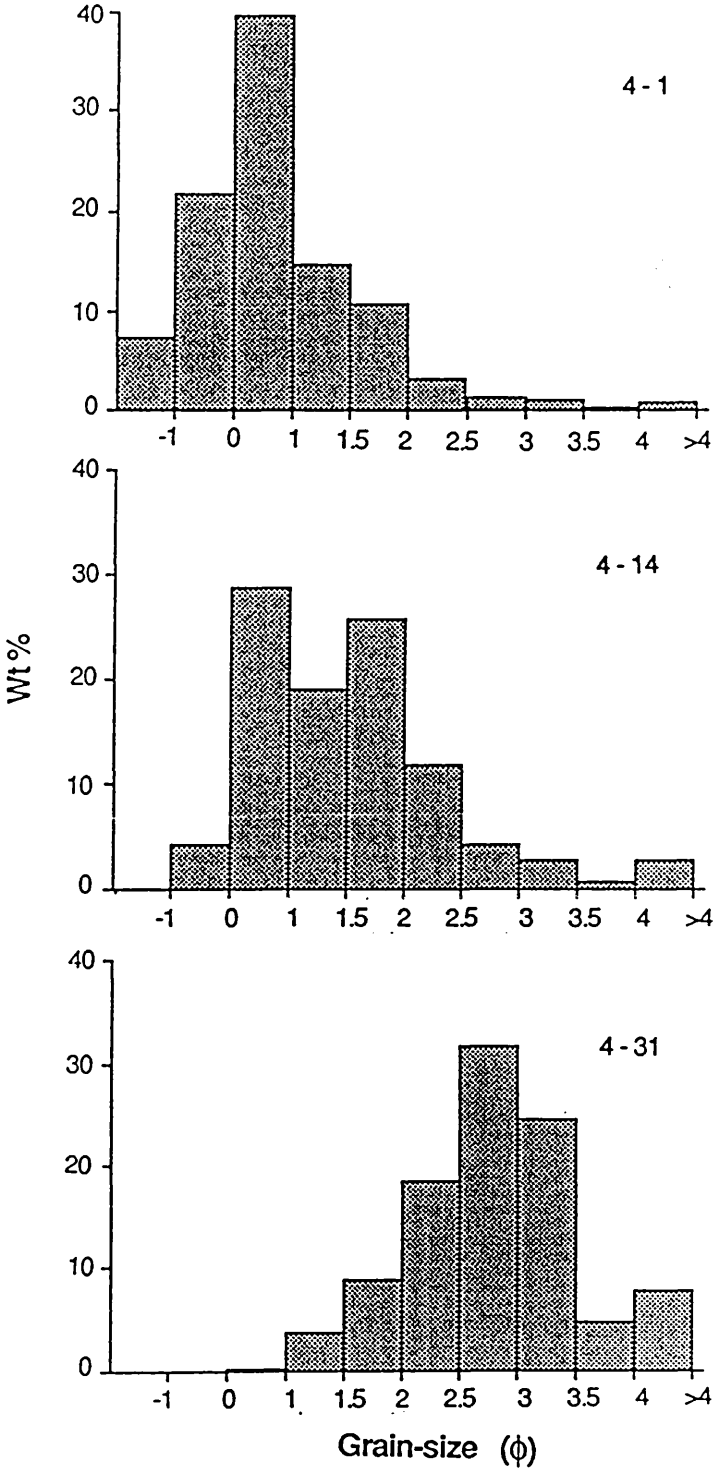

Fig. 6.3b Histograms, showing the grain-size distribution for three representative samples in the A4-32 borehole.

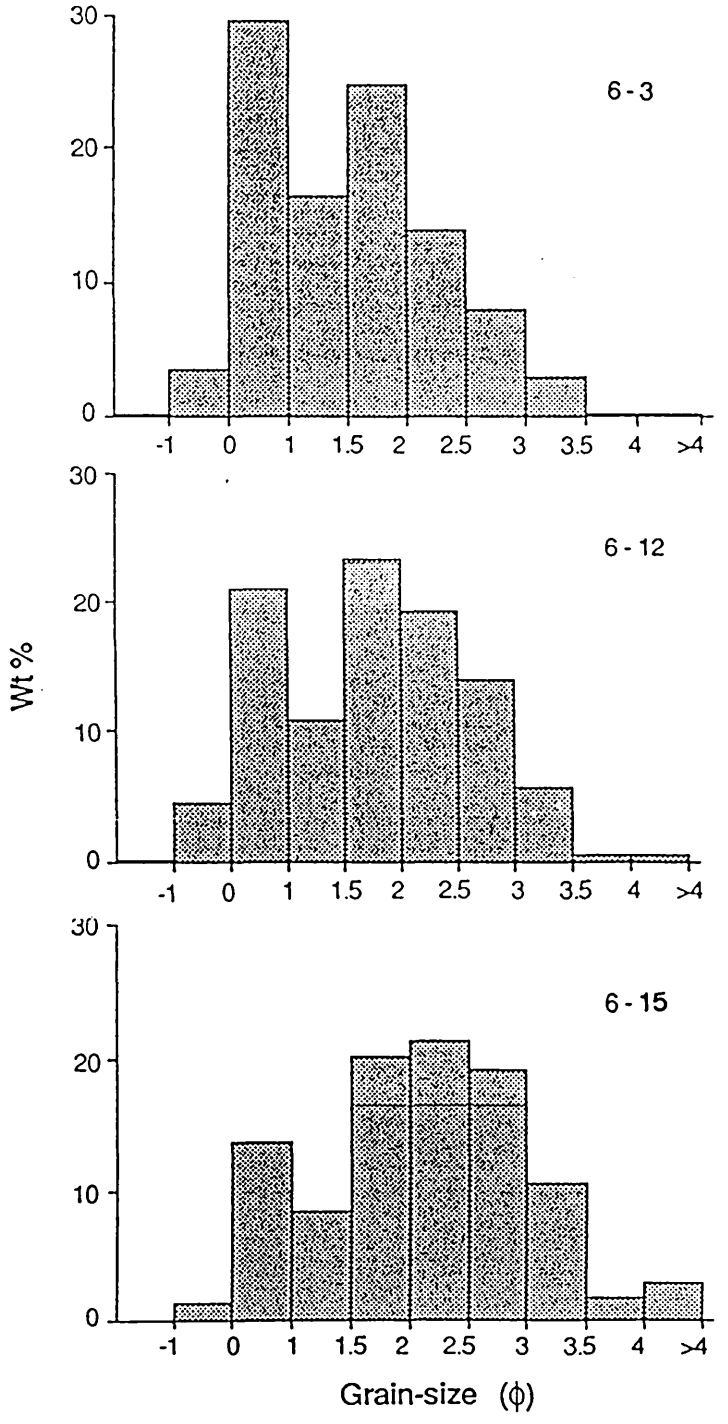

Fig. 6.3c Histograms, showing the grain-size distribution for three representative samples in the F6-32 borehole.

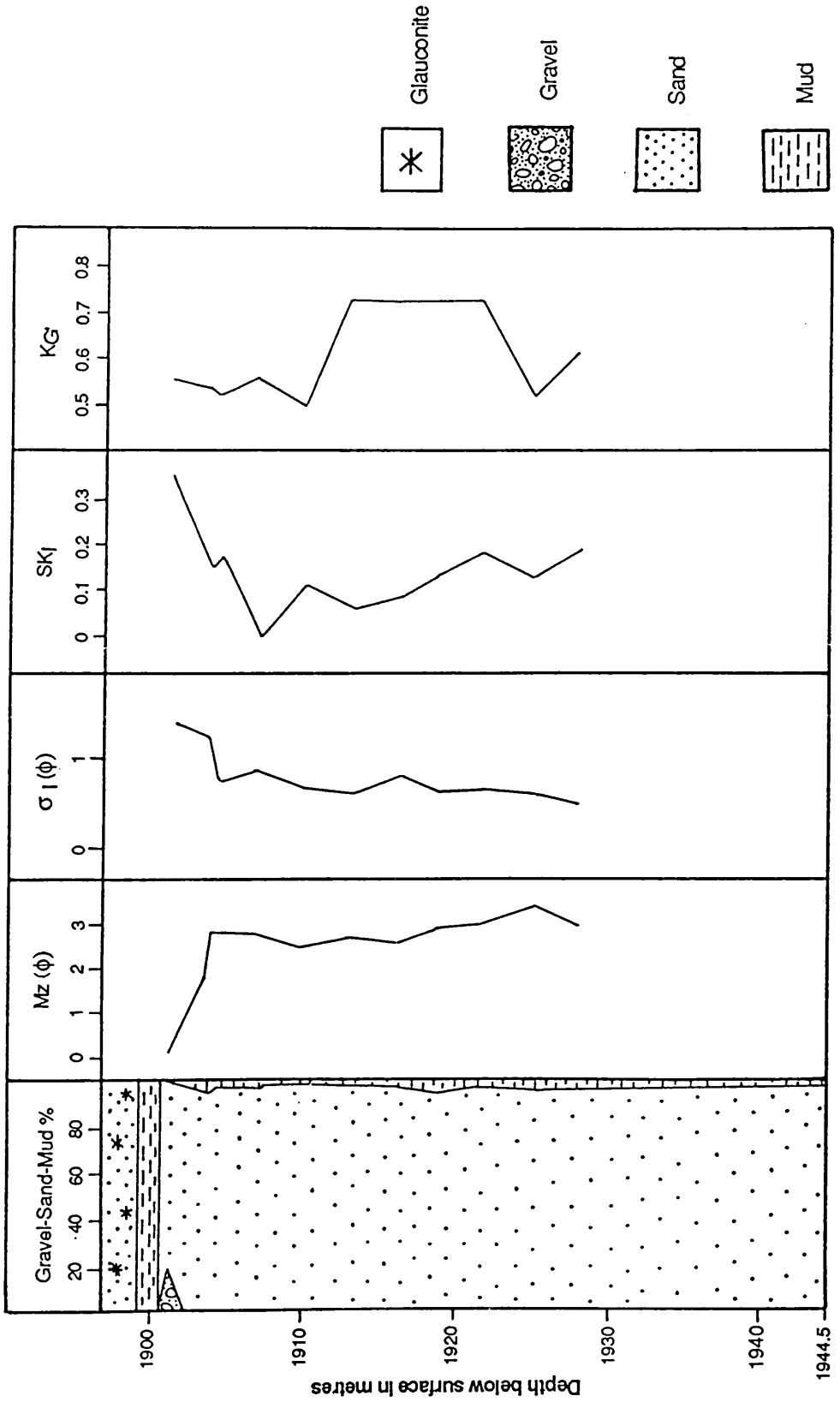

Fig. 6.4a. Vertical variation of gravel-sand-mud composition and grain-size parameters in the Bahi Formation (A2-32 borehole).

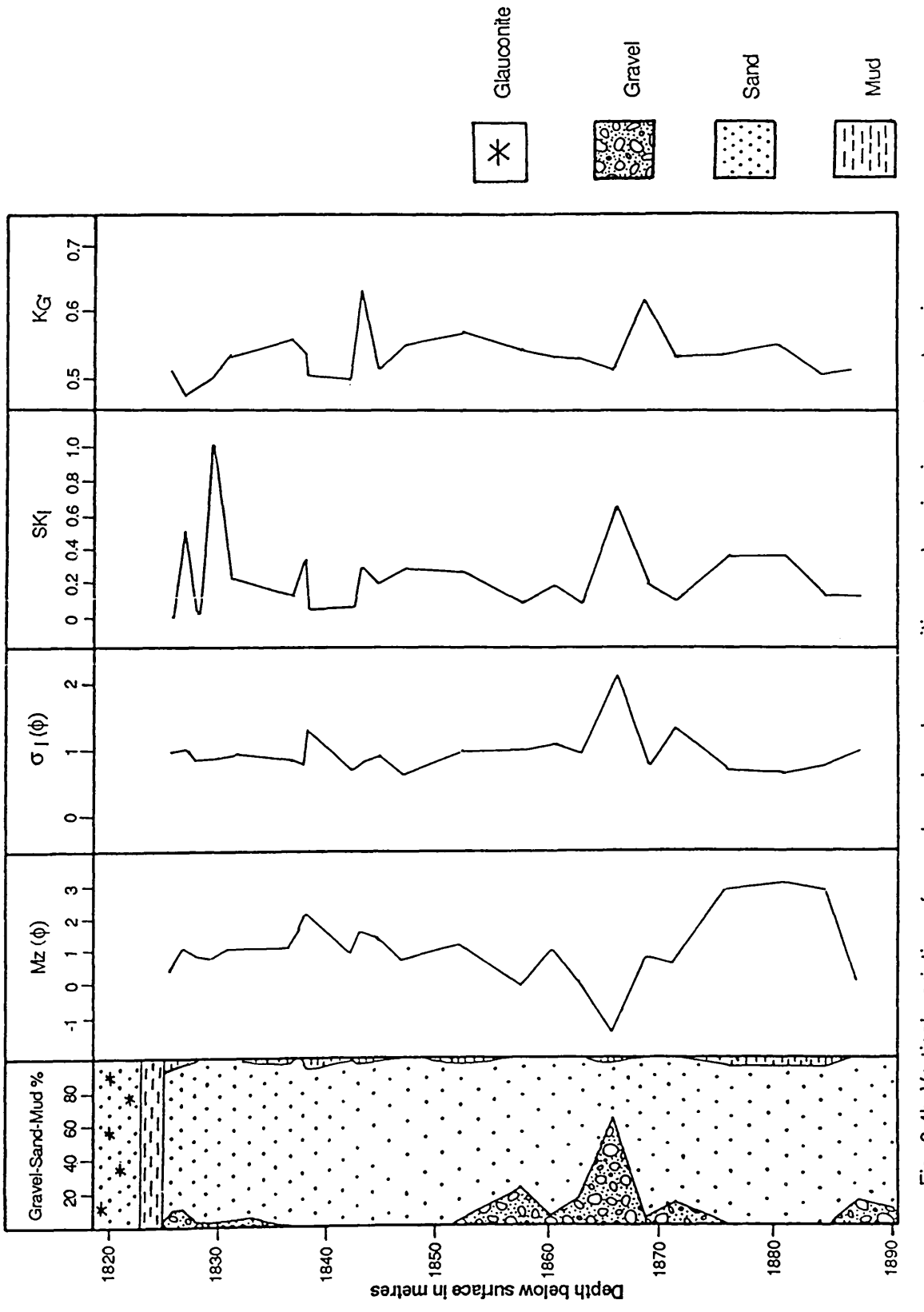

Fig. 6.4b. Vertical variation of gravel-sand-mud composition and grain-size parameters in the Bahi Formation (A4-32 borehole).

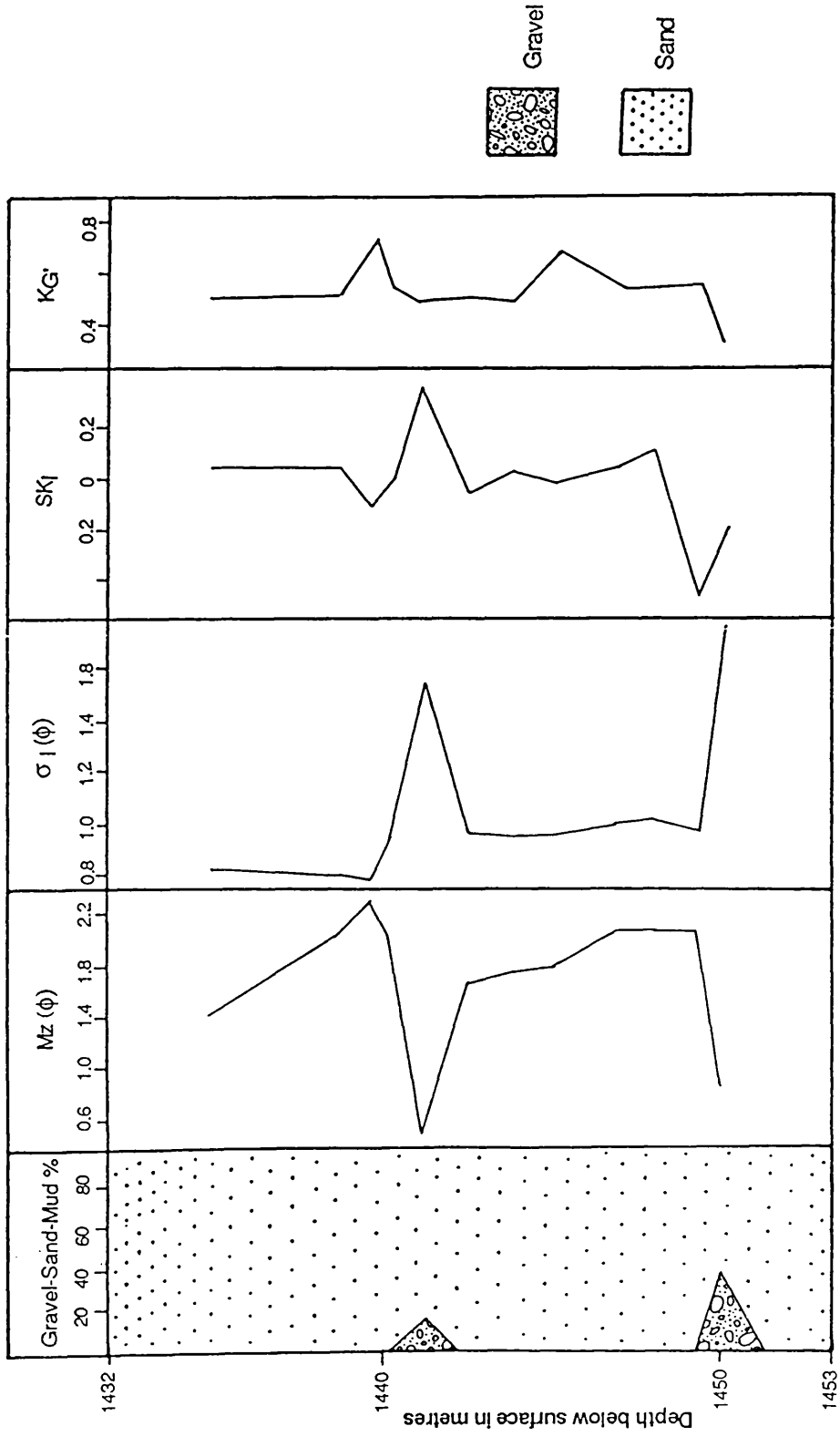

Fig. 6.4c Vertical variation of gravel-sand-mud composition and grain-size parameters in the Bahi Formation (F6-32 borehole).

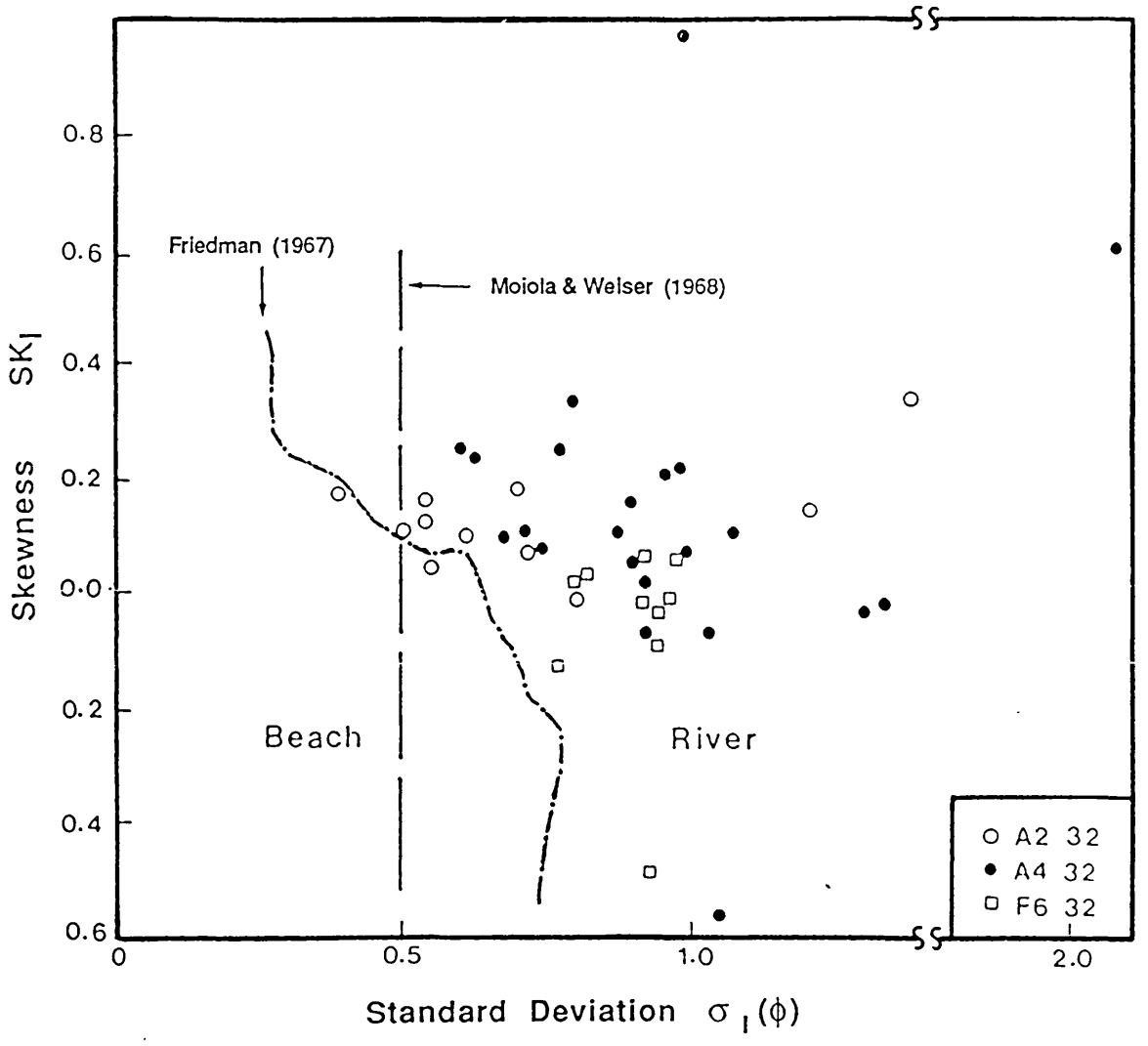

Fig. 6.5 Plot of inclusive graphic standard deviation against inclusive graphic skewness, showing the environment of deposition in the Bahi Formation in the boreholes studied, based on Friedman (1967) and Moiola & Weiser (1968).

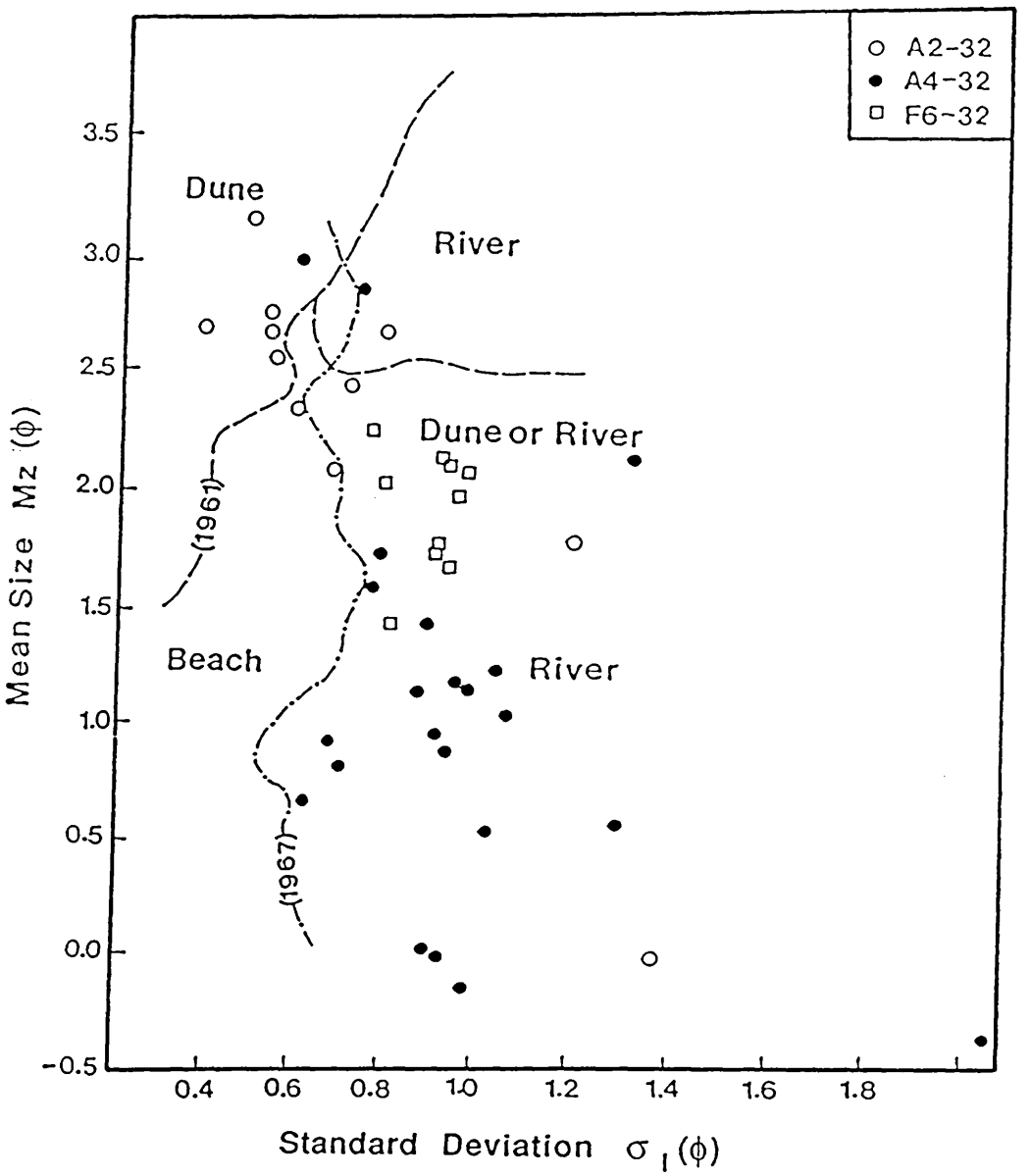

Fig. 6.6a Plot of inclusive graphic standard deviation against mean size, showing the environment of deposition in the Bahi Formation in the boreholes studied, based on Friedman (1961, 1967) .

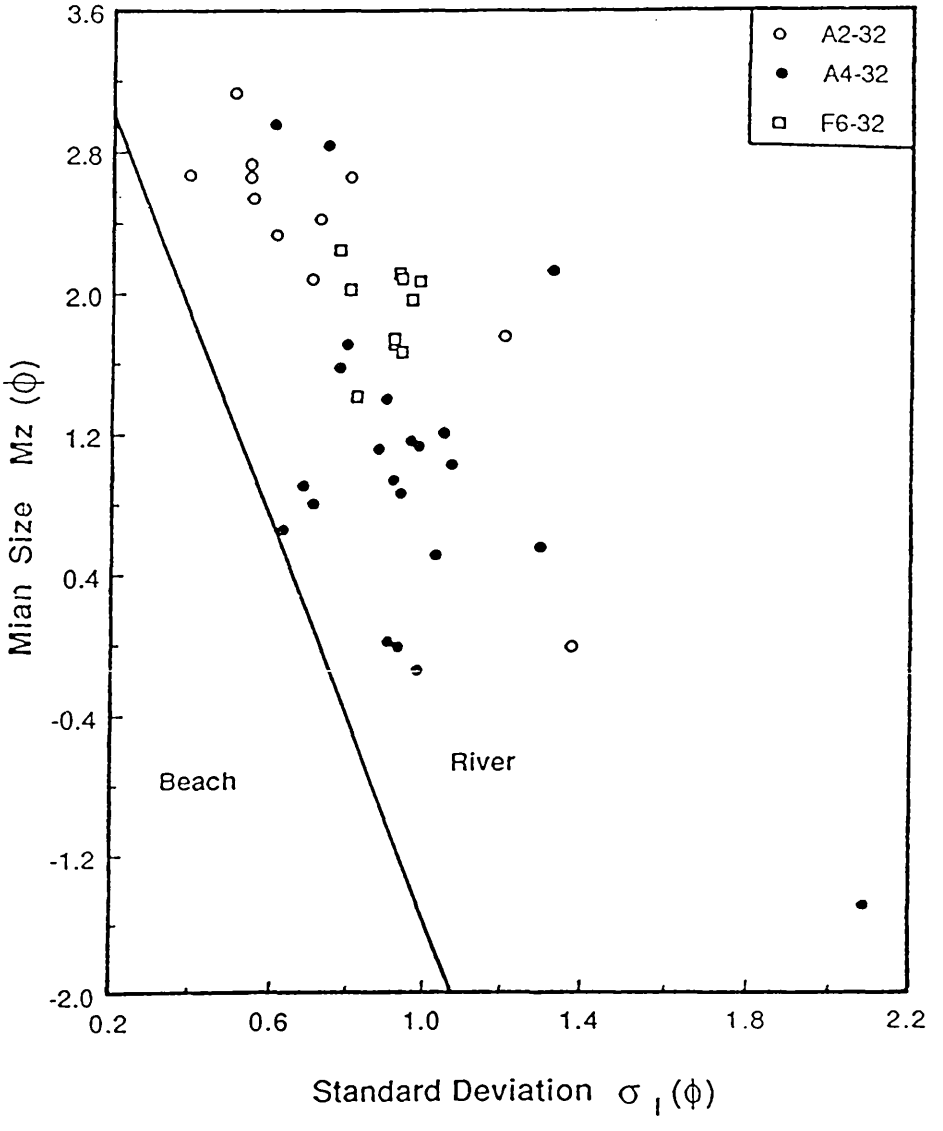

Fig. 6.6b Plot of inclusive graphic standard deviation against mean size, showing the environment of deposition in the Bahi Formation in the boreholes studied, based on Moiola & Weiser (1968).

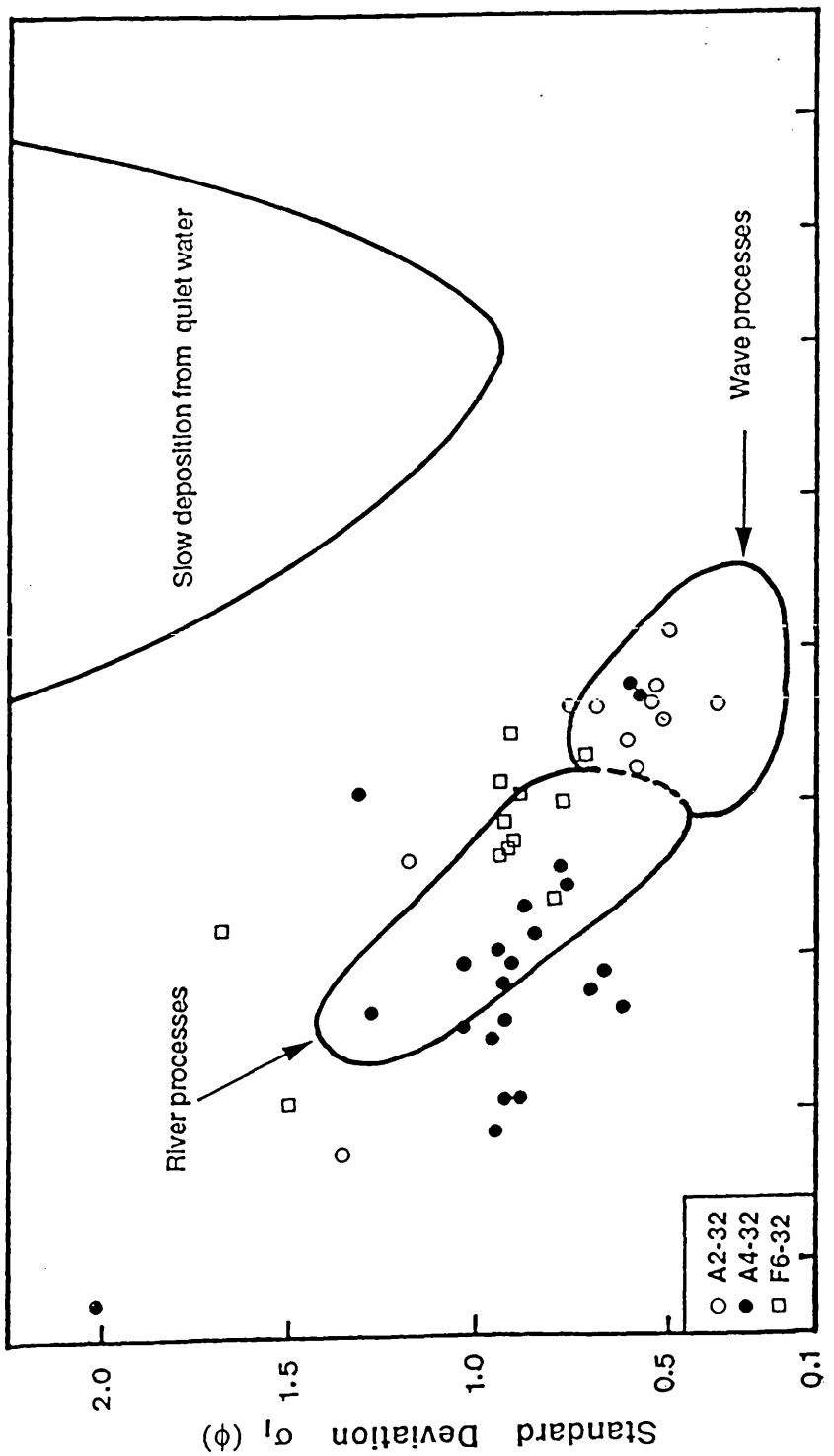

Fig. 6.7 Plot of inclusive standard deviation against median, showing the nature of deposition of the Bahi Formation in the boreholes studied, based on Stewart (1958).

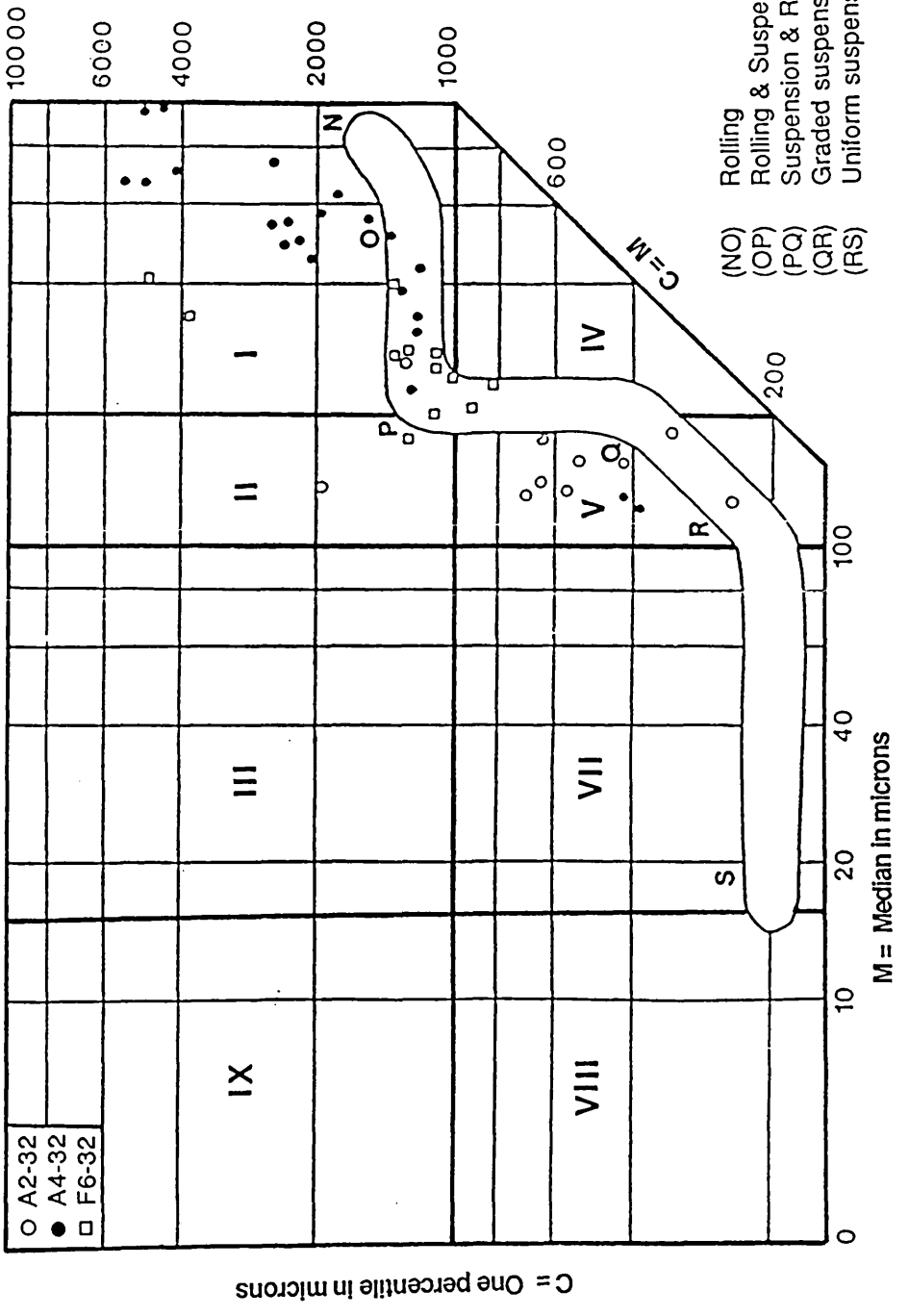

Fig. 6.8 Plot of C(1st percentile) against M (Median in diameter), showing the nature of transportation of the Bahi Formation in the boreholes studied, based on Passega & Pyramjee (1969).

Table 6.1 The seven phi percentiles for the analysed samples derived from grain-size data for the Bahi Sandstone in the A2-32, A4-32 and F6-32 boreholes.

Borehole	Sample	ϕ5	ϕ16	ϕ25	ϕ50	ϕ75	ϕ84	ϕ95
A2-32	2-2	-1.80	-1.20	-0.90	-0.30	0.75	1.45	2.90
	2-6	-0.10	0.66	1.00	1.65	2.50	3.00	4.05
	2-7	1.60	2.05	2.20	2.60	3.05	3.50	5.85
	2-9	1.10	1.90	2.15	2.60	3.05	3.45	3.80
	2-10	1.40	1.75	1.90	2.30	2.75	2.95	3.45
	2-12	1.70	2.02	2.20	2.55	2.85	3.05	3.60
	2-13	1.30	1.75	1.95	2.40	2.85	3.10	3.80
	2-14	1.80	2.20	2.40	2.75	3.20	3.00	4.02
	2-16	2.02	2.20	2.45	2.70	3.00	3.30	3.80
	2-17	2.35	2.65	2.80	3.10	3.50	3.65	4.02
	2-18	2.00	2.25	2.40	2.65	2.95	3.10	3.80
A4-32	4-1	-1.30	-0.52	-0.15	0.55	1.20	1.50	2.15
	4-2	-1.55	-0.65	-0.25	0.45	1.05	1.40	2.30
	4-4	-0.55	0.05	0.25	0.95	1.55	1.80	2.64
	4-5	-0.07	0.00	0.26	0.85	1.45	1.75	2.65
	4-7	-0.80	-0.25	0.00	0.55	1.15	1.55	2.70
	4-9	-0.20	0.30	0.60	1.15	1.70	1.90	2.95
	4-10	0.60	0.85	0.98	1.60	2.30	2.70	3.80
	4-11	0.15	0.75	1.10	2.20	2.95	3.40	4.50
	4-12	-0.12	0.25	0.45	0.88	1.35	1.60	2.15
	4-13	0.60	0.90	1.10	1.50	1.95	2.30	3.40
	4-14	0.10	0.60	0.80	1.35	1.90	2.25	3.30
	4-16	-0.40	-0.05	0.20	0.60	1.05	1.40	2.30
	4-19	-0.30	0.35	0.55	1.05	1.75	2.05	3.25
	4-21	-1.75	-1.10	-0.80	-0.20	0.45	0.75	1.70
	4-23	-0.80	0.05	0.35	0.95	1.70	2.05	2.95
	4-24	-1.60	-0.95	-0.65	0.05	0.60	0.85	1.55
	4-25	-2.85	-2.20	-1.90	-1.30	-0.05	2.00	4.00
	4-26	-0.35	0.15	0.35	0.75	1.25	1.50	2.10
	4-27	-1.65	-0.70	-0.25	0.60	1.40	1.75	2.85
	4-30	2.10	2.40	2.60	2.85	3.30	3.60	4.10
	4-31	1.70	2.10	2.30	2.80	3.30	3.60	4.10
	4-33	-1.45	-0.85	-0.60	0.05	0.60	0.85	1.70
F6-32	6-3	0.10	0.60	0.82	1.40	2.00	2.25	2.85
	6-7	0.75	1.20	1.45	2.00	2.50	2.85	3.30
	6-8	0.80	1.45	1.75	2.30	2.75	2.95	3.45
	6-9	0.65	1.30	1.55	2.10	2.60	2.85	3.45
	6-10	-1.50	-1.05	-0.25	0.05	1.85	2.30	3.00
	6-11	0.05	0.75	0.95	1.70	2.35	2.60	3.15
	6-12	0.20	0.75	0.98	1.72	2.37	2.65	3.20
	6-13	0.30	0.80	0.99	1.72	2.40	2.70	3.30
	6-14	0.50	0.98	1.30	2.00	2.62	2.90	3.65
	6-15	0.50	1.05	1.40	2.15	2.75	2.99	3.75
	6-16	0.40	1.00	1.35	2.50	2.60	2.85	3.50
	6-17	-1.75	-1.35	-1.15	1.20	2.20	2.50	3.20

Table 6.2 Statistical grain-size parameters (Mz, σ_I, SK_I ,K_G) for the analysed samples in the studied boreholes.

Borehole	Sample	Mz(ϕ)		$\sigma_I(\phi)$		SK_I		K_G	
A2-32	2-2	-0.02	(VCS)	1.375	(PS)	0.341	(SFSK)	1.243	(LK)
	2-6	1.75	(MS)	1.198	(PS)	0.141	(FSK)	1.134	(LK)
	2-7	2.72	(FS)	0.703	(MWS)	0.176	(FSK)	1.085	(MK)
	2-9	2.65	(FS)	0.797	(MSO)	-0.007	(NS)	1.229	(LK)
	2-10	2.33	(FS)	0.611	(MWS)	0.103	(FSK)	0.988	(MK)
	2-12	2.54	(FS)	0.545	(MWS)	0.042	(NS)	2.596	(VLK)
	2-13	2.42	(FS)	0.716	(MSO)	0.078	(NS)	2.277	(VLK)
	2-14	2.65	(FS)	0.536	(MWS)	0.116	(FSK)	2.467	(VLK)
	2-16	2.73	(FS)	0.545	(MWS)	0.163	(FSK)	2.432	(VLK)
	2-17	3.13	(VFS)	0.503	(MWS)	0.101	(NS)	0.978	(MK)
	2-18	2.67	(FS)	0.385	(WS)	0.168	(FSK)	1.341	(LK)
A4-32	4-1	0.51	(CS)	1.027	(PSO)	-0.066	(NS)	1.047	(MK)
	4-2	1.20	(MS)	1.049	(PSO)	-0.565	(SCSK)	1.213	(PK)
	4-4	0.93	(CS)	0.920	(MSO)	0.015	(NS)	1.005	(MK)
	4-5	0.87	(CS)	0.937	(MSO)	1.031	(SFSK)	1.134	(LK)
	4-7	1.13	(MS)	0.980	(MSO)	0.214	(FSK)	1.247	(LK)
	4-9	1.12	(MS)	0.877	(MSO)	0.102	(FSK)	1.173	(LK)
	4-10	1.71	(MS)	0.795	(MSO)	0.336	(SFSK)	0.993	(MK)
	4-11	2.12	(FS)	1.321	(PSO)	-0.019	(NS)	0.963	(MK)
	4-12	0.91	(CS)	0.681	(MWS)	0.092	(NS)	1.033	(MK)
	4-13	1.57	(MS)	0.774	(MSO)	0.249	(FSK)	1.647	(VLK)
	4-14	1.40	(MS)	0.897	(MSO)	0.154	(FSK)	1.192	(LK)
	4-16	0.65	(CS)	0.625	(MWS)	0.235	(FSK)	1.301	(LK)
	4-19	1.15	(MS)	0.962	(MSO)	0.207	(SFSK)	1.212	(LK)
	4-21	-0.15	(VCS)	0.985	(MSO)	0.064	(NS)	1.131	(LK)
	4-23	0.02	(CS)	1.068	(PSO)	1.103	(FSK)	1.119	(LK)
	4-24	-0.02	(VCS)	0.927	(MSO)	-0.073	(NS)	1.032	(MK)
	4-25	-1.50	(VCS)	2.087	(MSO)	0.559	((SFSK)	1.517	(VLK)
	4-26	0.80	(CS)	0.708	(MWS)	0.106	(FSK)	1.115	(LK)
	4-27	0.55	(CS)	1.294	(PSO)	-0.030	(NS)	1.117	(LK)
	4-30	2.95	(FS)	0.603	(MWS)	0.250	(FSK)	1.170	(LK)
	4-31	2.83	(FS)	0.739	(MSO)	0.074	(NS)	0.983	(MK)
	4-33	0.02	(CS)	0.902	(MSO)	0.052	(NS)	1.032	(MK)
F6-32	6-3	1.41	(MS)	0.820	(MSO)	0.033	(NS)	0.955	(MK)
	6-7	2.01	(FS)	0.798	(MSO)	0.024	(NS)	0.995	(MK)
	6-8	2.32	(FS)	0.770	(MSO)	-0.130	(CSK)	2.410	(VLK)
	6-9	2.08	(FS)	0.940	(MSO)	-0.033	(NS)	1.092	(MK)
	6-10	0.43	(CS)	1.519	(PSO)	0.327	(SFSK)	0.878	(PK)
	6-11	1.66	(MS)	0.944	(MSO)	-0.090	(NS)	0.907	(MK)
	6-12	1.70	(MS)	0.920	(MSO)	-0.016	(NS)	0.880	(PK)
	6-13	1.74	(MS)	0.920	(MSO)	0.059	(NS)	1.778	(PK)
	6-14	1.96	(MS)	0.957	(MSO)	-0.008	(NS)	0.978	(MK)
	6-15	2.06	(FS)	0.977	(MSO)	0.059	(NS)	0.986	(MK)
	6-16	2.11	(FS)	0.932	(MSO)	-0.487	(SCSK)	1.016	(MK)
	6-17	0.78	(CS)	1.713	(PSO)	-0.258	(CSK)	0.606	(VPK)

VFS = very fine sand
CS = Coarse sand
MSO = Moderatly sorted
FSK = Fine skewed
PK = PlatyKurtic
MK = Mesokurtic

FS = Fine sand
VCS = Very coarse sand
PSO = Poorly sorted
NS = Near symmetrical
VPK= Very platykurtic
LK = Leptokurtic

MS = Medium sand
MWS = Moderatly well sorted
CSK = Coarse skewed
SCSK = Strongly coarse skewed
SFSK = Strongly fine skewed
VLK = Very Leptokurtic

Table 6.3 The discriminant functions for the Bahi Sandstone in the studied boreholes, after Sahu (1964).

Borehole	Sample	Y1	Y2	Y3	Y4
A2-32	2-2	10.0958	153.0708	-18.1669	9.6231
	2-6	14.7992	145.2921	-12.7166	8.7902
	2-7	14.5383	98.2971	- 4.3690	9.0865
	2-9	15.6492	105.7983	- 4.7087	8.6266
	2-10	12.5706	81.1635	- 3.0547	7.7549
	2-12	18.1597	108.0879	- 1.9607	15.9727
	2-13	17.4493	115.0925	- 4.0797	14.5292
	2-14	17.9619	108.1147	-2.2101	15.8604
	2-16	18.0841	110.2260	-2.5006	16.0607
	2-17	14.9534	85.5886	-1.7690	8.2154
	2-18	13.8902	79.3454	-1.2979	10.2142
A4-32	4-1	5.6559	74.8758	- 8.7751	0.0006
	4-2	13.3058	103.3056	- 6.4746	3.9256
	4-4	9.5606	89.0892	- 7.1737	6.4344
	4-5	7.7364	110.9357	-12.4345	13.9320
	4-7	11.0366	107.7921	-9.0774	9.2452
	4-9	10.2693	91.5677	-6.8641	8.0129
	4-10	10.8361	92.7559	- 6.6454	9.0061
	4-11	17.0488	165.2633	-14.5444	7.1989
	4-12	7.9895	65.4987	- 4.2036	6.9302
	4-13	12.4171	98.8632	- 5.9405	11.7647
	4-14	11.3662	99.6305	- 7.3455	8.6800
	4-16	7.3283	64.1716	- 4.3238	9.0943
	4-19	10.8734	104.9869	- 8.7338	9.0110
	4-21	6.4441	83.4954	- 8.8020	6.7010
	4-23	11.1182	113.4246	-10.1526	7.8087
	4-24	6.4885	73.9899	-7.1257	5.3054
	4-25	14.3317	300.9133	- 41.2465	12.4654
	4-26	7.9620	68.0120	- 4.6280	7.3942
	4-27	11.8660	139.7419	-14.3087	9.8700
	4-30	14.8325	95.2660	-3.5135	7.0621
	4-31	15.0259	99.6751	- 4.2867	7.9626
	4-33	6.1739	73.7496	-7.3276	6.1516
F6-32	6-3	10.4258	84.5232	-5.6038	6.5650
	6-7	12.5786	92.1535	-5.0749	7.1347
	6-8	17.9266	116.1075	-3.8058	13.7281
	6-9	14.1730	110.2758	-6.9325	7.4164
	6-10	12.1455	180.6322	-21.6565	8.0937
	6-11	12.2337	99.6942	-6.8492	5.7514
	6-12	11.9731	98.2210	-6.8093	6.1175
	6-13	14.7628	116.9430	-7.1377	11.4049
	6-14	13.4466	108.8126	-7.3779	6.9056
	6-15	13.8324	114.2808	-8.0157	7.4868
	6-16	14.9201	100.0874	- 4.5758	3.9712
	6-17	16.0729	211.4926	-24.1747	3.2133

Table 6.4 Environmental interpretation based on Sahu's (1964) linear discriminant functions.

Borehole Test used	A2-32 Y_{value}	 Y_{result}	A4-32 Y_{value}	 Y_{result}	F6-32 Y_{value}	 Y_{result}
(1) Aeolian:Beach	5.2865	beach	10.4394	beach	13.7076	beach
(2) Beach:Sh. marine	108.1886	Sh. marine	105.3184	Sh. marine	119.4353	Sh. marine
(3) Sh. marine:Fluvial	-5.1667	Sh. marine	-9.6683	Fluv. deltaic	-9.0011	Fluv. deltaic
(4) Fluvial:Turbidite	11.3394	Fluv. deltaic	7.9071	Turbidite	7.3157	Turbidite

CHAPTER 7

CONCLUSIONS

The Bahi Formation is a significant reservoir in the northwestern part of the Sirte Basin, consisting of interbedded sandstone, siltstone, conglomerate and shale. Sandstone and pebbly sandstone are the most common lithologies in the Bahi area. The formation forms the lowest part of Upper Cretaceous sequences.

The following general conclusions are based on the analysis of well-logs records in ninety wells and boreholes and from laboratory studies (petrography, geochemistry and grain-size) of the core samples from the Bahi Formation in the A2-, A3-, A4-, D1-, and F6-32 boreholes (see Figure 7.1).

A. Subsurface analysis:

1: In the western part of the Sirte Basin the Bahi Formation usually rests unconformably on Palaeozoic rocks (Cambro-Ordovician and Devonian) but in a few areas its lies directly on Precambrian igneous and metamorphic basement rocks. It is conformably overlain by various younger Upper Cretaceous formations which range in age from Cenomanian to Maastrichtian.

2: The Bahi Formation is commonly divisible into two parts, the upper part consisting of coarse to very coarse-grained, cross-bedded sandstones and the lower part consisting of fine to very fine silty sandstone. The uppermost part of the formation is characterised by the presence of glauconite.

3: In the boreholes the top of the Bahi Formation occurs between 1500 to 2500m below sea level. The thickness variations are controlled by penecontemporaneous faulting and palaeotopography of the pre-Upper Cretaceous surface. There is clear evidence that the formation is widely diachronous, being overlain by different Upper Cretaceous marine sequences of known age.

B. Petrographical investigations:

1: Petrographical studies show that the Bahi Formation is to be classified as a subarkose quartz arenite and that the most abundant minerals are detrital grains of mono- and polycrystalline quartz and feldspar.

2: Glauconite is found only in the uppermost part of the formation.

3: Carbonate (calcite & dolomite) and anhydrite cements are present only in the upper part of the formation and are evidently absent lower down. This almost certainly results from downward percolation from the overlying formations. Quartz overgrowths and haematitic cements are present throughout the formation.

4: Radially-arranged flakes and filamentous illite, 'books' consisting of stacked pseudo-hexagonal platy crystals of kaolinite and face-to-edge oriented flakes of chlorite dominate the authigenic clay mineral association throughout the formation.

5: Zircon, tourmaline, rutile and opaques are the dominant heavy minerals. There is a gross similarity in heavy minerals assemblages throughout the formation indicating a common source or sources. It is a mature assemblage and consists largely of multi-cycled grains originally deriving from metamorphic and plutonic terranes.

6: The framework mineralogy suggests that the Bahi Sandstone was derived largely from a craton interior containing pre-existing and multi-cycled quartzose sedimentary rocks.

C. Geochemical investigations:

1: The significance of the major and trace element distributions within the Bahi Formation show that the large amount of SiO_2 in most samples indicates a high degree of maturity, whilst a low content of SiO_2 in others is probably caused by enrichment of the sediment with carbonate, anhydrite and clay minerals.

2: The variation in K_2O and Al_2O_3 content is probably due to the variation in feldspar and clay mineral content both laterally and vertically.

3: Most of the trace elements are associated with the K-feldspar and/or clay minerals,

whereas some trace elements are associated with non-sheet silicates such as rutile and the opaques.

4: The relationship between trace elements shows that the Bahi sediment was derived primarily from a pre-existing sedimentary source or sources.

5: Discriminant function analysis indicates that the Bahi Sandstone was derived from a passive continental margin with a mature sandstone cover, i.e., a pre-existing cratonic sequence.

6: Variation in major and trace element distribution both laterally and vertically is related to specific lithofacies and probably results from variation in environmental conditions at the time of deposition.

D. Grain-size analysis

1: Grain-size analyses show that the Bahi Sandstone was transported by two main methods - saltation load and surface creep or rolling transport.

2: Histograms of grain-size distribution show that most of the Bahi sediment in the boreholes is unimodal whereas some samples have a bimodal distribution. All are moderately to very poorly sorted and show strongly fine to strongly coarse skewness and curves that are leptokurtic to very leptokurtic. This variation could be related to variation in the energy of transporting agents and/or changes in the source of sediment during Bahi deposition.

3: Scatter plots of statistical grain-size parameters show that most of the sediment is to be classified largely as river sand.

The depositional and source characteristics of the Bahi Formation can be summarised thus: The lower part of the formation was almost certainly deposited in a terrestrial environment. This assessment is based initially on the prevailing red colour, the ill-sorted, diverse nature of the sediments and the apparent absence of remains of marine organisms. Sedimentological and petrographical analyses confirm these observations and indicate a fluvial environment of

deposition. The presence of thick sequences of coarse to very coarse sandstone in the upper part of the formation, characterised by graded-bedding and cross-bedding is also suggestive of a fluvial origin dominated by channel-fill deposits. The presence of glauconite in the sandstone and shale of the uppermost part of the formation indicates a shallow marine environment and the initiation of a marine cycle.

It appears therefore that the marine transgression began to the north or northwest of the Sirte Basin and progressed southwards over a continental platform of low relief on which an alluvial plain had established itself in Cenomanian times. Regardless of local structural controls, the Bahi Formation everywhere reflects the same sequence of events but its relationship with overlying marine formations across the basin shows it to be extremely diachronous, as is to be expected.

Thus the bulk of the Bahi Formation is a diachronous, marginal cratonic alluvial deposit with only the uppermost glauconite-bearing part heralding the beginning of a marine incursion.

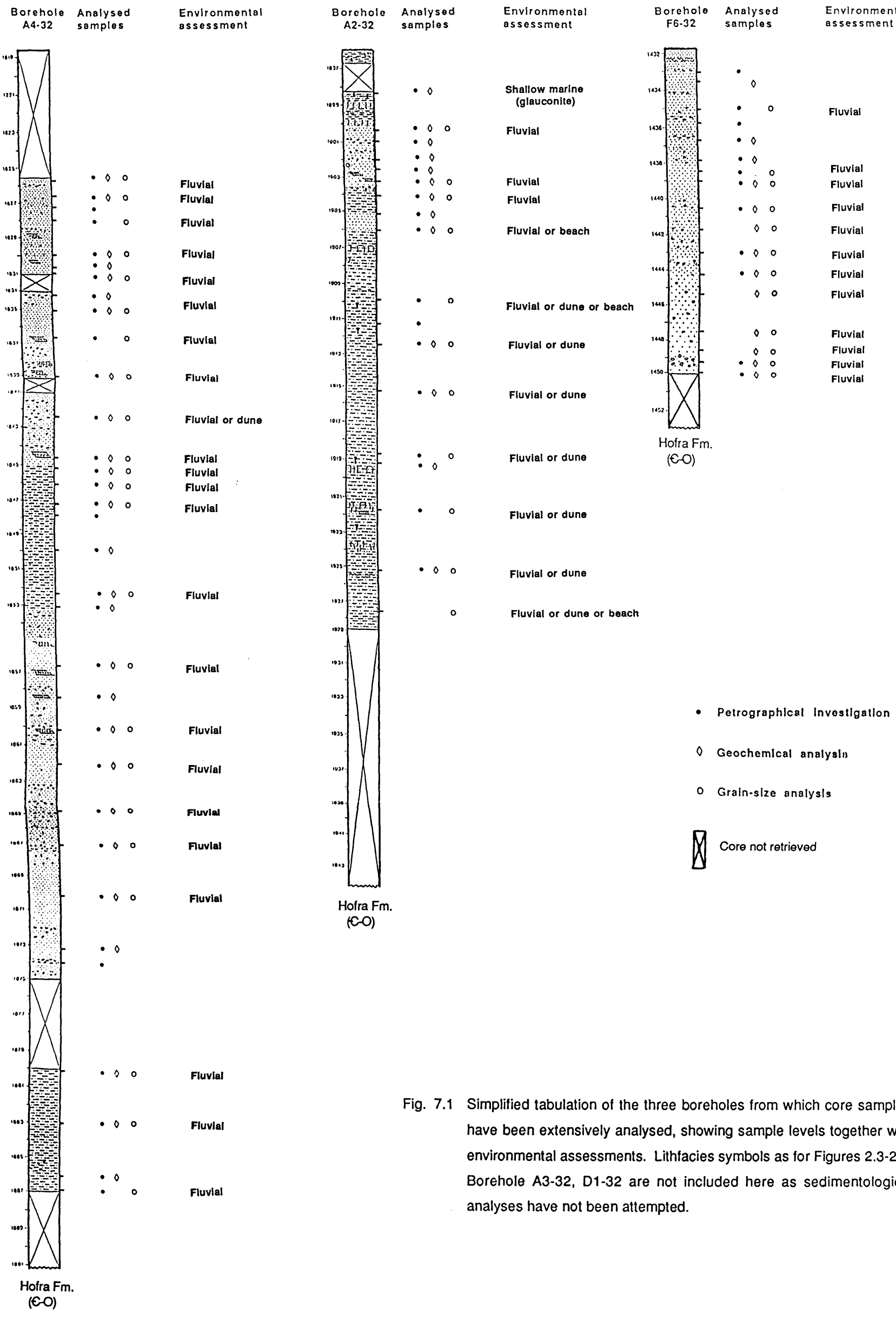

Fig. 7.1 Simplified tabulation of the three boreholes from which core samples have been extensively analysed, showing sample levels together with environmental assessments. Lithfacies symbols as for Figures 2.3-2.5. Borehole A3-32, D1-32 are not included here as sedimentological analyses have not been attempted.

REFERENCES

ABU EL-ELLA, R. & COLEMAN, J. M. 1985. Discrimination between depositional environments using grain- size analyses, **32**, 743-748.

AMARAL, E. J. & PRYOR, W. A. 1977. Depositional environment of the St. Peter Sandstone deduced by textural analysis. *J. Sedim. Petrol*, **47**, 32-52.

ARGAST, S. 1987. The chemical discrimination of clastic sedimentary components. *J. Sedim. Petrol.*, **57**, 813-823.

BAIRD, D. W. 1964. *Stratigraphy of the Bahi Sandstone, Sirte Basin, Libya. (internal report)*, Oasis Oil Co. Libya.

BARR, F. T. & WEEGAR, A. A. 1972. *Stratigraphic nomenclature of the Sirte Basin, Libya.* Petroleum Exploration Society of Libya. Grafiche Trevisan Castle Franco. Italy,179pp.

BASU, A., *et al* (4 authors). 1975. Re-evaluation of the use of undulatory extinction and polycrystallinity in detrital quartz in provenance interpretation. *J. Sedim. Petrol.*, **45**, 873- 882.

BELLINI, E. & MASSA, D. 1980. A stratigraphic contribution to the Palaeozoic of the Southern basins of Libya. *In* Salem M. J. & Busrewil M. T. (eds) 2nd Symposium Geology of Libya. *Univ. Libya , Fac. Sci.*, **1**, 3-19, Tripoli.

BHATIA, M. R. 1983. Plate tectonics and geochemical composition of sandstones. *J.Sedim. Petrol.*, **91**, 611-627.

BHATIA, M. R. & CROOK, K. A. W. 1983. Trace element characteristics of graywackes and tectonic setting discrimination of sedimentary basins. *Contribs. Miner. Petrol.*, **92**, 181-193.

BLATT, H. 1967. Original characterstics of clastic quartz grains. *J. Sedim. Petrol.*, **37**, 401-424.

_____ **& CHRISTIE, J. M.** 1963. Undulatory extinction in quartz of igneous and metamorphic rocks and its significance in provenance studies of sedimentary rocks. *J.*

Sedim. Petrol., **33**, 559-579.

_____ **MIDDLETON, G. & MURRAY, R.** 1972. *Origin of sedimentary rocks.* Prentice-Hall Englewood cliffs, New Jersey, 634pp.

BOKMAN, J. 1952. Clastic quartz particles as indices of provenance. *J. Sedim. Petrol.*, **22**, 14-17.

BRAMMALL, A. 1928. Dartmoor detritals: A study in provenance. *Proc. Geol. Assoc.*, **39**, 27-48.

BRUST, J. F. 1958. "Glauconite" pellets: Their mineral nature and applications to stratigraphic interpretations. *Bull. Am. Assoc. Petrol. Geol.*, **42**, 310-327.

BUTT, A. A. 1986. Upper Cretaceous biostratigraphy of the Sirte Basin, northern Libya. *Rev. Paléobiol*, **5**, 171-191.

CARROLL, D. 1970. Clay minerals: A guide to their X-ray identification. *Spec. Pap. Geol. Soc. Am.*,**126**, 75p.

CARVER, R. E. 1971. *Procedures in sedimentary petrography.* Wiley Interscience, 653pp.

CHEN, D. 1977. Table of key lines X-ray powder diffraction patterns of minerals in clays and associated rocks. *Dept. Nat. Resources, Indiana State Geol. Surv. Spec. Pap.* **21**, 67p.

CLIFFORD, H. J., GRUND, R. & MUSRATI, H. 1980. Geology of a stratigraphic giant: Messla oil field, Libya. *Bull. Am. Assoc. Petrol. Geol.*, **64**, 507-524.

CONANT, L. C., & GOUDARZI, G. H. 1967. Stratigraphic and tectonic framework of Libya. *Bull. Am. Assoc. Petrol. Geol.*, **51**, 719-730.

CONLEY, C. D. 1971. Stratigraphy and lithofacies of Lower Paleocene rocks, Sirte Basin, Libya. *In* Gray C. (ed) 1st Symposium Geology of Libya. *Univ. Libya, Fac. Sci.*, 127-140. Tripoli.

CONOLLY, J. R. 1965. The occurrence of polycrystallinity and undulatory extinction in quartz in sandstones. *J. Sedim. Petrol.*, **35**, 116-135.

DARMOIAN, S. A. & LINDQVIST, K. 1988. Sediments in the estuarine environment of the Tigris/Euphrates delta; Iraq; Arabian gulf. *Geol. J.*, **23**, 15-37

DECELLES P. G. & HERTEL F. 1989. Petrology of fluvial sands from the Amazonian foreland basin, Peru and Polivia. *Bull. Geol. Soc. Am.*, **101**, 1552-1569.

DEER, W. A., HOWIE, R. A. & ZUSSMAN, J. 1985. *An introduction to the rock forming minerals.* 5th ed, Longman, Hong-Kong, 528pp.

DENNEN, W. H. 1967. Trace elements in quartz as indicators of provenance. *Bull. Geol. Soc. Am.*, **78**, 125-130.

DESIO, A. 1959. *Lexicon of stratigraphy for Libya.* Petroleum Exploration Society of Libya, 157pp.

DICKINSON, W. R. 1970. Interpreting modes of graywacke and arkose. *J. Sedim. Petrol.*, **40**, 695-707.

_____ **& SUCZEK, C. A.** 1979. Plate tectonics and sandstone compositions. *Bull. Am. Assoc. Petrol. Geol.*, **63**, 2164-2182.

_____ **& Valloni, R.** 1980. Plate tectonics and provenance of sands in modern ocean basin. *Geology*, **8**, 82-86.

_____ **& *el al.*** (8 authors). 1983. Provenance of North American Phanerozoic sandstones in relation to tectonic settings. *Bull. Geol. Soc. Am.*, **94**, 222-235.

DURONIO, P. & COLOMBI, L. 1983. Mesozoic rocks of Libya. *Spec. Pap. Petroleum Exploration Society Libya*, S-1 - S-12.

DUTTA K. P. & SUTTNER L. J. 1986. Aluvial sandstone composition and paleoclimate, I. Framework mineralogy, *J. Sed. Petrol.*, **56**, 329-345.

FENNER, P. & HAGNER, A. F. 1967. Correlation of variations in trace elements and mineralogy of the Esopus Formation, Kingston, New York. *Geochim. cosmochim. Acta.*, **31**, 237-261.

FOLK, R. L. 1954. The distinction between grain size and mineral composition in sedimentary-rock nomenclature. *J. Geol.*, **62**, 344-359.

_____ 1974. *Petrology of sedimentary rocks.* Hemphill Publ. Co., Austin, Texas, 181pp.

_____ **& WARD, W. C.** 1957. Brazos river bar: A study in the significance of

grain-size parameters. *J. Sedim. Petrol.*, **27**, 3-26.

FRIEDMAN, G. M. 1961. Distinction between dune, beach, and river sands from their textural characteristics. *J. Sedim. Petrol.*, **31**, 514-529.

_____ 1967. Dynamic processes and statistical parameters compared for size frequency distribution of beach and river sands. *J. Sedim. Petrol.*, **37**, 327-354.

GILLEPSIE, I. & SANFORD, R. M. 1967. The geology of the Sarir Oil Field, Sirte Basin, Libya. *Proc. 7th World Petrol. Congr., Mexico*, **2**, 181-193, Elsevier Publ. Co.

GOUDARZI, G. H. 1980. Structure - Libya. *In* Salem M. J. & Busrewil M. T. (eds) 2nd Symposium Geology of Libya. *Univ. Libya , Fac. Sci.*, **3**, 879-891. Tripoli.

GRADER, G. W. 1968. *Play analysis of the Nubian Formation and basal Upper Cretaceous clastics, eastern Libya.* internal geological report, no. **17**, Esso Standard Inc. Libya.

GRAHAM, S. A., INGERSOLL, R. U. & DICKINSON, W. R. 1976. Common provenance for lithic grains in Carboniferous sandstones from Ouachita Mountains and Black Warrior basin. *J. Sedim. Petrol.*, **46**, 620-632.

GALEHOUSE, J. S. 1971. Point counting. *In* Carver (ed.) *Procedures in sedimentary rocks.* Wiley Interscience, New York, 385-407.

GRIM, R. E. & JOHNS, W. D. 1954. Clay mineral investigation of sediments in the northern Gulf of Mexico. *Clays and clay Miner.* Proc. 2nd nat. Conf., 81-103.

GUMATI, Y. D. & KANES, W. H. 1985. Early Tertiary subsidance and sedimentary facies, northern Sirte Basin, Libya. *Bull. Am. Assoc. Petrol. Geol.*, **69**, 39-52.

HAMMUDA, O. S. 1980. Sediments and palaeogeography of the Lower Campanian sand bodies along the southern Tip of Ad Daffah-Al Wahah ridge, Sirte Basin, Libya. *I n* Salem M. J. & Busrewil M. T. (eds) 2nd Symposium Geology of Libya. *Univ. Libya , Fac. Sci.*, **2**, 509-520. Tripoli.

HARDING, T. P. 1983. Graben hydrocarbon plays and structural styles. *Geol. Mijnborw,* **63**, 3-23.

HARVEY, P. K., TAYLOR, D. M., HENDRY, R. D. & BANCROFT, F. 1973. An accurate fusion method for the analysis of rocks and chemically related materials by

X-ray fluorescence spectrometry. *X-ray Spectrometry*, **2**, 33-44.

HEA, J. P. 1971. Petrography of the Paleozoic-Mesozoic sandstones of the southern Sirte Basin, Libya. *In* Gray C. (ed).1st. Symposium Geology of Libya, *Univ. Libya Fac. Sci.*, 107-125. Tripoli.

HEIMLICH, R. A., SHOTWELL, L. B., COOKRO, T. & GAWELL, M. J. 1975. Variabbility of zircons from the Sharon Conglomerate of northeastern Ohio. *J. Sedim. Petrol.*, **45**, 629-635.

HICKMAN, A. H. & WRIGHT, A. E. 1983. Geochemistry and chemostratigraphical correlation of slates, marbles and quartzites of the Appin Group, Argyll, Scotland. *Trans. Roy. Soc. Edinb: Earth Sci.*, **73**, 251-278.

HUTCHISON, C. S. 1974. *Laboratory handbook of petrographic techniques.* Wiley Interscience 527pp.

JAMES, R. H., ALAND, A. & GARY, B. G. 1974. The occurrence of glauconite in Monterey Bay, California, Diversity, origins and sedimentary environmental significance, *J. Sedim. Petrol.*, **44**, 562-571.

JOHNS, W. H., GRIM, R. E. & BRADLEY, W. F. 1954. Quantitative estimation of clay minerals by diffraction methods. *J. Sedim. Petrol.*, 24, 242-251.

KANTOROWICZ, J. 1984. The nature, origin and distribution of authigenic clay minerals from middle Jurassic Ravenscar and Brent group sandstones. *Clays and Clay miner.*, **19**, 359-375.

KLITZSCH, E. 1968. Outline of the geology of Libya. *In* Barr F. T. (ed) Geology and Archaeology of northern Cyrenaica, Libya.*Petrol. Explor. Soc. Libya.*10th Annual Field Conference, 71-78.

_____ 1971. The structural developments of parts of North Africa since Cambrian time. *In* Gray C. (ed) 1st Symposium Geology of Libya. *Univ. Libya, Fac. Sci.*, 253-262. Tripoli.

_____ 1981. Lower Palaeozoic rocks of Libya, Egypt and Sudan. *In* Lower Palaeozoic rocks of the Middle east, eastern and southern Africa and Antarctica *In* C. H. Holland

(ed.) *Lower Palaeozoic Rocks of the World*, Vol. **3**, 131-163.

KRAUSKOPF, K. B. 1967. *Introduction to geochemistry*. The Earth and Planetary Sciences, international series Mc Graw-Hill Co., New York, 721pp.

KRUMBEIN, W. C. 1934. Size frequency distribution of sediments, *J. Sedim. Petrol.*, **4**, 65-77.

KOGBE, C. A. 1980. The Trans-Saharan Seaway During the Cretaceous. *In* Salem M. J. & Busrewil M. T. (eds) 2nd Symposium Geology of Libya. *Univ. Libya , Fac. Sci.*, **1**, 91-96. Tripoli.

KUMATI, S. M. & ANKETELL, J. M. 1982. Structural analysis of western Sirte Basin, Libya. *Abstr. Bull. Am. Assoc. Petrol. Geol.*, **66**, 591.

KRYNINE P. D, 1946. The tourmaline group in sediments. *J. Geol.*, **LIV**, 65-87.

LEAKE, B. E. *et al* (9 authors). 1969. The chemical analysis of rock powders by automatic X-ray fluorescence. *Chem. Geol.*, **5**, 7-86.

LORING, D. H. 1982. Geochemical factors controlling the accumulation and dispersal of heavy metals in the Bay of Fundy sediments, *Can. J. Earth Sci.*, **19**, 930-944.

MACCHI, L. 1987. A review of sandstone illite cements and aspects of their significance to hydrocarbon exploration and development. *J. Geol.*, **22**, 333-345.

MACK, G. H. 1984. Exceptions to the relationship between plate tectonics and sandstone composition. *J. Sed. Petrol.*, 54, 212-220.

_____ **JAMES C. & THOMAS W. A.** 1981. Orogenic Provenance of Mississppian Sandstone Associated with Southern Appalachian-Ouachita Orogen. *Bull. Am. Assoc. Petrol. Geol.*, **65**, 1444-1456.

_____ **THOMAS W. A. & HORSELY C. A.** 1983. Cpomosition of Carboniferous Sandstones and tectonic framework of Southern Appalachian-Ouachita Orogen. *J. Sedim. Petrol.*, **53**, 931-946.

MASON, C. C. & FOLK, R. L. 1958. Differentiation of beach, dune, and aeolian flat environments by size analysis, Mustang Island, Texas. *J. Sedim. Petrol.*, **28**, 211-226.

MASSA, D. & DELORT, T. 1984. Evolution of the Sirte Basin (Libya) from Cambrian to

Cretaceous. *Bull. Geol. Soc. France*, **20**,1087-1096.

McBRIDE, E. F. 1963. A classification of common sandstones. *J. Sedim. Petrol.*, **33**, 664-669.

MEZZADRI G. & SACCNAI E. 1989. Heavy mineral distribution in Late Quaternary Sediments of the Southern Aegean Sea: Implication for provenance and sediment dispersal in sedimentary basins at active margins. *J. Sedim. Petrol.*, **59**, 412-422

MIKBEL, SH. R. 1977. Basement configuration and structure of west Libya. *Libyan J. Sci.*, **7A**, Tripoli.

_____ 1979. Structural and configuration map of the basement of east and central Libya. *N.Jb. Geol. Paläont. Abh*, **158**, 209-220. Stuttgart.

MOIOLA, R. J. & WEISER, D. 1968. Textural parameters: An evaluation. *J. Sedim. Petrol.*, **38**, 45-53.

MOSHRIF, M. A. 1980. Recognition of fluvial environments in the Biyadhi-Wasia Sandstones (Lower - Middle Cretaceous) as revealed by texture analysis. *J. Sedim. Petrol.*, **50**, 603-612.

MOUZUGHI, A. G. & TALEB, M. T. 1980. Tectonic map of Libya. *Petrol. Explor. Soc. Libya.*

MURRAY, R. C. 1964. Origin and diagenesis of gypsum and anhydrite, *J. Sedim. Petrol.*, **34**, 512-523.

NIGGLI, P. 1954. *Rocks and minerals deposits.* W. H. Freeman & Co. San Francisco, 559p.

PASSEGA, R. 1957. Texture as characteristic of clastic deposition. *Bull. Am. Assoc. Petrol. Geol.*, **41**, 1952-1984.

_____ 1964. Grain size representation by CM patterns as a geological tool. *J. Sedim. Petrol.*, **34**, 830-847.

_____ **Byramjee, R.** 1969. Grain-size image of clastic deposits. *Sedimentology*, **13**, 233-252.

PETTIJOHN, F. J. 1957. *Sedimentary rocks*, 2nd edn. Harper & Row, New York, 718pp.

_____ 1963. Chemical composition of sandstones - excluding carbonate and

volcanic sands. *Prof. Pap. U. S. Geol. Surv.*, 440-S, S1-S19.

_____ 1975. *Sedimentary rocks*, 3rd edn. Harper & Row, New York, 628pp.

_____ **POTTER, P. E., & SIEVER, R.** 1973. *Sand and sandstone.* Springer-Verlag, Berlin. Heidberg. New York, 618pp.

PITTMAN, E. D. 1972. Diagenesis of quartz in sandstones as revealed by scanning electron microscopy. *J. Sedim. Petrol.*, **42**, 507-519.

POMEYROL, R. 1968. Nubian sandstone. *Bull. Am. Assoc. Petrol. Geol.*, **52**, 589-600.

REINECK, H. E. & SINGH, I. B. 1980. *Depositional sedimentary environments.* Springer-Verlag, Berlin Heidberg, New York, 549pp.

ROSER, B. P. & KORSCH, R. J. 1986. Determination of tectonic setting of sandstone-mudstone suites using SiO_2 content and K_2O/Na_2O ratios. *J. Geol.*, **94**, 635-650.

_____ 1988. Provenance signatures of sandstone-mudstone suites determined using discriminant function analysis of major-element data. *Chem. Geol.*, **67**, 119-139.

READING, H. G. 1978. *Sedimentary environments and facies*, 2nd edn. Blackwell Sci. Publ., Oxford 615pp.

REYMENT, R. A. & DINGLE, R. V. 1987. Palaeogeography of Africa during the Cretaceous Period. *Palaeogeogr. Palaeoclim. Palaeoecol.*, **59**, 93-116.

SAHU, B. K. 1964. Depositional mechanisms from size analysis of clastic sediments. *J. Sedim. Petrol.*, **34**, 73-83.

SANFORD, R. M. 1970. Sarir Oil Field, Sirte Basin, Libya - Desert Surprise. *In* Halbouty, M. T. (ed). Geology of giant Petroleum Fields. *Mem. Am. Assoc. Petrol. Geol.*, **14**, 449-476.

SARKISYAN, S. G. 1970. Origin of authigenic clay minerals and their significance in petroleum geology. *Sedimen. Geol.*, **7**, 1-22.

_____ 1971. Application of the scanning electron microscope in the investigation of oil and gas reservoir rocks. *J. Sedim. Petrol.*, **41**, 289-292.

SCHULTZ, L. G. 1964. Quantitative interpretation of mineralogical composition from X-ray

and chemical data for the Pierre Shale. *Prof. Pap. U. S. Geol. Surv.* 391 - C, C1-C31.

SCHWAB, F. L. 1981. Evolution of the western continental margin, French-Italian Alps: Sandstone mineralogy as an index of plate tectonic setting. *J. Geol.*, **4**,11-15.

SENIOR, A. & LEAKE, B. E. 1978. Regional metasomatism and the geochemistry of the Dalradian metasediments of Connemara, western Ireland. *J. Sedim. Petrol.*,**19**, 585-625.

SMALE D. 1987. Heavy mineral suites of core samples from the Mckee Formation (Eocene-Lower Oligocene), Taranaki: implications for provenance and diagenesis. *New Zealand J. Geol. & Geoph.* **30**, 299-306.

STEWART, H. B. Jr. 1958. Sedimentary reflections of depositional environments in San Miguel Lagoon, Baja California, Mexico. *Bull. Am. Assoc. Petrol. Geol.*, **42**, 2567-2618.

THOREZ, J. 1976. *Practical identification of clay minerals.* B 4820 Dison, Belgium, 90pp.

UADDEN, J. A. 1914. Mechanical composition of clastic sediments. *Bull. Geol. Soc. Am.*, **25**, 655-754.

VAN de KAMP, P. C. & LEAKE, B. E. 1985. Petrography and geochemistry of feldspathic and mafic sediments of the northeastern Pacific margin. *Trans. Roy. Soc. Edinb. Earth Sci*, **76**, 411-449.

VAN de KAMP, P. C., LEAKE, B. E. & SENIOR, A. 1976. The petrography and geochemistry of some California arkoses with application to identifying gneisses of metasedimentary origin. *J. Geol.*, **84**,195-212.

VAN HOUTEN, F. B. 1980. Late Jurassic - Early Cretaceous regressive facies, northeast Africa. *Bull. Am. Assoc. Petrol. Geol.*, **64**, 857-867.

_____ 1983. Cretaceous rifting above a fixed mantle hotspot, Sirte Basin, north- central Libya. *Geology*, **11**,115-118.

VILLUMSEN, A. & NIELSEN O. B. 1976. The influence of palaeosalinity, grain-size distribution and clay minerals on the content of B, Li and Rb in Quaternary sediments from Eastern Jutland, Denmark. *Sedimentology*, **23**, 845-855.

VISHER, G. S. 1969. Grain size distributions and depositional processes. *J. Sedim. Petrol.*, **39**, 1074-1106.

VITANAGE, P. W. 1957. Studies of zircon types in Ceylon Precambrian Complex. *J. Sedim. Petrol.*, **65**, 2,117-128.

WEDEPOHL, K. H., (ed.) 1978. *Hand book of geochemistry* II/1-5. Springer-Verlage, New York.

WENTWORTH, C. K. 1922. A scale of grade and class terms for clastic sediments. *J. Geol.*, **30**, 377-392.

WEAVER, C. E. 1958. Geological interpretation of argillaceous sediments. Part I. Origin and significance of clay minerals in sedimentary rocks. *Bull. Am. Assoc. Petrol. Geol.* 42, 1455-1492.

WILLIAMS, J. J. 1972. The sedimentary and igneous reservoirs of the Augila Oil Field *In* Geology and Archaeology of northern Cyrenaica, Libya. *Petrol. Explor. Soc. Libya.* 10th Annual Field Conference, 197-205.

WILSON, M. D. & PITTMAN, E. D. 1977. Authigenic clays in sandstones; recognition and influence on reservoir properties and paleoenvironmental analysis. *J. Sed. Petrol.*, **47**, 3-31.

YOUNG, S. W. 1976. Petrographic textures of detrital polycrystalline quartz as an aid to interpreting crystalline source rocks. *J. Sedim. Petrol.*, **46**, 595-603.